INVERTED METAMORPHISM IN THE JUTOGH THRUST SHEET AROUND CHUR, HIMACHAL PRADESH

A THESIS

submitted in fulfilment of the
requirements for the award of the degree
of

DOCTOR OF PHILOSOPHY

in

EARTH SCIENCES

By

TAMAL KANTI GHOSH

DEPARTMENT OF EARTH SCIENCES
UNIVERSITY OF ROORKEE
ROORKEE-247 667, INDIA

JULY, 1995

CANDIDATE'S DECLARATION

I hereby, certify that the work which is being presented in this thesis entitled "INVERTED METAMORPHISM IN THE JUTOGH THRUST SHEET AROUND CHUR, HIMACHAL PRADESH" in fulfilment of the requirement for the award of the Degree of **Doctor of Philosophy**, submitted in the **Department of Earth Sciences** of the University, is an authentic record of my own work carried out during a period from July, 1989 to July 1995 under the supervision of Dr. D. K. Mukhopadhyay.
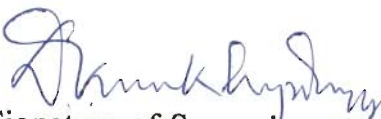
The matter embodied in this thesis has not been submitted by me for the award of any other degree.

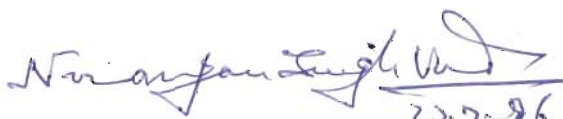(TAMAL KANTI GHOSH)

This is to certify that the above statement, made by the candidate, is correct to the best of my knowledge.

DR. D. K. MUKHOPADHYAY
Lecturer
Department of Earth Sciences
University of Roorkee
Roorkee 247667, U.P
INDIA

The Ph.D. viva-voce examination of Mr. TAMAL KANTI GHOSH, Research Scholar was held on 27.7.1996 .

Signature of Supervisor

Signature of External Examiner
23.7.96

ACKNOWLEDGEMENTS

TAMAL KANTI GHOSH

ABSTRACT

The rocks of the Jutogh Group representing the frontal part of the High Himalaya Crystalline thrust sheet is preserved in a Half klippe around the Chur peak (45 Km. south-east of Simla). In this area metamorphic index minerals, viz., garnet, staurolite, kyanite and sillimanite are present at successively higher topographic and structural levels depicting inverted metamorphic sequence. The metamorphic history of this inverted metamorphism has been elucidated from the sequence of deformation, microstructural and textural relations, mineral chemistry, garnet zonation patterns and geothermobarometry.

Four mappable lithological units in the Jutogh Group are recognized. These are lower carbonaceous schist, quartzite, upper carbonaceous schist and mica schist occurring at successively higher topographic and structural levels. At highest topographic and structural levels a granite body, called the Chur granite, is present. The Jutogh thrust which is a continuation of MCT separates the Jutogh Group from the underlying low-grade phyllites of the Chail Formation.

Structures from the Chur area can be grouped into early structures, structures related to ductile shearing and late structures. Early structures include folds of two generations (F_1 and F_2) which are tight to isoclinal, recumbent to gently plunging reclined/inclined folds with E or W trend of axis. S_1 penetrative cleavage is axial planer to F_1 folds. S_2 crenulation cleavage has sporadically developed during F_2 folding. A superimposed progressive ductile shearing modified and obliterated the early structures to varying extent and produced mylonites ranging from protomylonites through orthomylonites to ultramylonites with well developed mylonitic foliation. Late structures include a set of very open and upright folds and a set of subvertical fractures which cut across all early structures.

Four thrusts have been recognized from the study area which are the Chail thrust below the Chail Formation, the Jutogh thrust below the Jutogh Group, the Rajgarh thrust below the upper carbonaceous schist and the Chur thrust at the contact of the Chur granite. These thrust planes produce an imbricated structure which supports the view that MCT is a zone.

Garnet grade from the Chur area includes quartzite above the Jutogh thrust but below Rajgarh thrust. Above Rajgarh thrust mica schist belongs to staurolite grade. Near the vicinity of the Chur granite some of the mica schist samples contain kyanite and/or sillimanite.

Microstructural and textural evidences suggest that the major metamorphic index minerals are broadly synchronous with the F_1-F_2 foldings which is prior to the ductile shearing. During ductile shearing a low grade phase has been identified during which chlorite and biotite have crystallized.

Garnet is almandine rich with varying proportion of pyrope, spessartine and grossular components. From garnet grade to staurolite grade X_{Fe} increases and X_{Mn} and X_{Ca} decrease. In kyanite-sillimanite grades no such correlation is observed. X_{Mg} does neither vary with respect to grade nor with respect to X_{Fe}. In biotite, concentration of Al^{VI} is inversely proportional to Ti concentration. Chlorite in garnet grade is Fe-rich and in staurolite grade it is Mg-rich. Other minerals do not show any systematic variation in concentration with respect to metamorphic grade.

Growth zonation pattern is observed from garnet grade and also

iii

from staurolite grade. But in the staurolite grade the growth zonation pattern is gradually relaxed at successively higher topographic levels. In sillimanite grade reverse zonation patterns in Mn and Mg profile are observed near core. Single stage growth of garnet is suggested in garnet grade. Two stage growth to complex zonation pattern have been encountered in staurolite grade. In sillimanite grade the growth of garnet continued from kyanite grade to sillimanite grade.

Geothermobarometric calculation from matrix shows that pressure and temperature vary in unsystematic manner throughout the Jutogh Group of rocks. Structural distance from Jutogh thrust versus pressure and temperature plots show that there is no systematic variation of P-T data with reference to that thrust plane (Jutogh thrust) which is supposed to be the part of MCT. Also there is no systematic increase of temperature from the Jutogh thrust to the contact of the Chur granite. So the temperature and pressure condition is neither related with thrusting and consequent inverted geotherm near the vicinity of the thrust plane nor post-thrusting progressive T-P condition from the Jutogh thrust to the Chur granite has been predicted. These suggest the presence of pre-thrusting progressive metamorphism which is also supported by microstructural and textural relationship in the Chur area.

As the progressive metamorphism is pre-ductile shearing and pre-thrusting phenomenon the presence of inverted metamorphic sequence is the result of multiple thrust imbrication which brought up the higher grade rocks successively from deeper levels from an already metamorphosed terrain. Consequently the original isograds have been greatly dislocated due to later post-metamorphic thrust imbrication.

CONTENTS

6. GEOTHERMOMETRY AND GEOBAROMETRY   68

7. SUMMARY AND CONCLUSIONS   81

APPENDIX

All figures and tables are presented at the last of the respective Chapters.

CHAPTER - 1
INTRODUCTION

1.1 PRELUDE

The Himalayan mountain belt (Ca. 3000 Km long and 200-300 Km wide) represents continent-continent collision between the northward moving Indian plate and Northern Eurasian plate (Powell and Conaghan 1973; Le Fort 1975; Bird 1978). The Indus-Tsangpo Suture Zone (ITSZ) marks the site of this collision.

The location of the earliest contact between these two plates is in the Ladakh-Kohistan area in the NW Himalaya. But controversy still surrounds the timing of the initiation and completion of the collision between these two plates (Powell & Conaghan 1973; Molnar & Tapponier 1975; Patriach & Achache 1984; Besse et al. 1988). Klootwijk et al. (1992) suggested that the collision between the NW Greater Himalaya and southern Asia started at Cretaceous-Tertiary time (66 Ma) and completed at about 55 Ma ago when the velocity of the northward movement of Indian plate decreased dramatically from 18-19.5 cm/yr to 4.5 cm/yr. Post-collisional crustal shortening between the stable part of the Eurasian plate and the Indian plate is of the order of about 3000 Km (Besse & Courtillot 1988). A significant part of this shortening has been accommodated within the Indian indenter along the major thrust planes such as Main Central Thrust (MCT), Main Boundary Thrust (MBT), Main Frontal Thrust (MFT) and others.

The Himalayan orogenic belt is separated from the northern Tibetan Plateau by the Indus-Tsangpo valleys and in the south it is fringed by the low and nearly flat Indo Gangetic Alluvial Plain. Geologically Indus-

1

Tsangpo Suture Zone (ITSZ) demarcates the boundary between the Himalayan belt and the northern Trans-Himalayan zone of Eurasian plate. To the south of ITSZ the Himalayan range has been subdivided into four longitudinal lithotectonic zones (Fig.1.1): (1) High Himalaya Sedimentary Zone (HHSZ), (2) High Himalaya Crystalline Zone (HHCZ), (3) Lesser Himalaya Zone (LHZ) and (4) Sub Himalaya Zone (SHZ). The HHSZ is separated from the HHCZ by the South Tibetan Detachment System (STDS) which is north dipping normal fault (Burchfiel et. al. 1992). The rest three zones are bounded by three main thrusts viz., the Main Central Thrust, the Main Boundary Thrust and the Main Frontal Thrust respectively. Many workers have discussed about these different zones in detail (e.g. Gansser 1964,1974; Le fort 1975; Stöcklin 1980; Windley 1983, 1988). Fig.1.1 shows the distribution of different zones and the locations of main thrusts in the Himalaya.

1.2 METAMORPHISM IN THE HIMALAYA

In a broad sense, the metamorphism in the Himalaya is essentially of regional type (Fig 1.2) with minor contact metamorphic signatures. In this map the study area shows within the square. It is observed that the study area is under amphibolite facies metamorphism which is a continuation of the same facies of metamorphism in the HHCZ. The grade of metamorphism can be easily distinguished between HHCZ and LSZ where the metamorphism is of lower grade than that in the HHCZ. Within the Indus-Tsangpo Suture Zone high pressure metamorphism during Mid to Late Cretaceous is preserved in metaigneous blocks (Sinha Ray and Bhargava 1989; Honegger et al. 1989).

1.2.1 The High Himalayan Crystalline Zone

In the High Himalayan Crystalline Zone, a 25 to 30 Km thick pile of Crystalline rocks, exhibit$_\wedge^s$ polyphase metamorphism. In this zone two progressive metamorphic episodes (M_1 and M_2) are generally recognized (Le Fort 1975; Hodges & Silverberg 1988; Searle et. al. 1988; Hubbard 1989; Mohan et al. 1989; Searle & Rex 1989; Inger & Harris 1992 and many others). The M_1 phase is of lower intensity (chlorite to sillimanite grade) than M_2 phase (sillimanite-K felspar migmatitic gneisses). Occasionally a third phase of metamorphism (M_3) representing retrogression can be observed (Le Fort 1975; Kundig 1989; Searle & Rex 1989). Matcalfe (1993) identified three main phases of metamorphism (M_1, M_2 and M_3) and one last retrogression phase (M_4) from western Garhwal sector. The M_1 phase is considered to be of Barrovian type (Le Fort 1975; Hodges & Silverberg 1988; Searle and Rex 1989; Inger & Harris 1992) whereas the M_2 phase present in the upper part of HHCZ is Buchan type which was temporally coincident with the leucogranite magmatism (Windley 1983; Hodges & Silverberg 1988; Hubbard & Harrison 1989; Searle & Rex 1989). A brief discussion on the conditions of metamorphism from Central Himalaya, Eastern Himalaya and North-Western Himalaya follows.

From the Central Himalaya all the three metamorphic phases have been demonstrated by many workers (Le Fort et al. 1986; Hodges et al. 1988; Hodges & Silverberg 1988; Hubbard 1989; Pecher 1989; Arita et al. 1990; Purohit et al. 1990; Inger & Harris 1992; Matcalfe 1993). From Garhwal Himalaya Hodges and Silverberg (1988) described that the M_1 phase is of regional type and the M_2 phase in the upper part of the sequence of HHCZ as Buchan type. They identified an "erosion

controlled" uplift path after the M_1 phase of metamorphism. Hodges and Silverberg (1988) estimated the temperature and pressure during M_1 metamorphism at $>597^\circ C$ and >9.60 Kb respectively. The uplift and cooling path of the sequence after M_1 was interrupted by M_2 which is coincident with the generation of leucogranites in the upper part of HHCZ. The P-T condition of M_2 calculated by them was 3.17-5.23 Kb and $>600^\circ C$ respectively. Inger and Harris (1992) estimated P-T condition for M_1 in High Himalayan Crystalline Sequence of Langtang Valley as 9Kb and $710^\circ C$ respectively. They related (P= 5.8Kb, T= 760°C) M_2 with the sillimanite grade metamorphism and anatexis of metapelites at the upper part of the Main Central Thrust sheet. Pecher (1989) from Central Nepal and Kumaon, Arita et al. (1990) from North-Central Nepal and Matcalfe (1993) from Garhwal Himalaya also identified M_1 metamorphism as the event in the early stage of Himalayan Orogeny which was prior to the activation of MCT. Pecher (1989) calculated this phase of metamorphism reaching maximum temperatures of about $650^\circ C$-$700^\circ C$ and pressure of more than 8Kb. But Matcalfe (1993) estimated it from Garhwal Himalaya as $584^\circ C$ and 7.7Kb respectively. Pecher (1989) indicated that M_2 episode is marked in the upper part of the Tibetan slab by the appearance of sillimanite and the presence of tourmaline bearing leucosomes. Arita (1983) recognized two episodes of metamorphism from Nepal Himalaya. Arita et al. (1990) recognized two different cooling trajectories and inferred that the old one represented the main metamorphism of Barrovian type that had occurred prior to thrusting. The young cooling trajectory is indicative of the metamorphism related to thrusting from Oligocene to Miocene age. Purohit et al. (1990) also recognized M_1 and M_2 phases of metamorphism

4

as progressive ones and M_3 as a retrogressive phase with the formation of chlorite from biotite and garnet and sericite from sillimanite. Pecher (1989) recognized that M_3 retrogressive metamorphism present up and below the MCT in the basal part of Tibetan Slab. This M_3 caused the thermal accordance between both sides of the thrust. Though two phases of progressive metamorphism are generally recognized in HHCZ Gairola and Ackermand (1988) reported different picture identifying three phases of metamorphism from HHCZ of Garhwal Himalaya among which the first phase was the progressive one (their M_1) and the other two (their M_2 and M_3) were of retrogressive phases.

From the eastern Himalaya, Hubbard (1989) recognized that MCT separates chlorite-bearing schist from sillimanite-bearing magmatic gneiss in the overlying Tibetan Slab in Mt Everest region. She demonstrated an increase of temperature up-section in the MCT zone from $503°C$ to $717°C$ and a decrease in temperature to $577°C$ in the lower Tibetan Slab. She also recognized the presence of higher temperature in the upper Tibetan Slab than the lower one suggesting later resetting of thermobarometers by intrusion of large amounts of leucogranite at that structural level.

From the North-Western Himalaya, Searle and Rex (1989) and Staubli (1989) reported that M_1 metamorphism may be related to early (c. 40 Ma) Himalayan Barrovian event. Searle et al. (1988) reported from south of Zanskar valley (High Himalaya Zone) that M_1 is associated with the initial deformation phase D_1 following continental collision. Searle and Rex (1989), Staubli (1989) pointed out that the M_1 phase was a single prograde reaction series from chlorite grade through biotite, garnet, staurolite and kyanite grade to sillimanite bearing assemblage at moderate

to high pressure. M_2 phase of metamorphism in Zanskar Himalaya is associated with the MCT thrusting event (Searle & Rex 1989). However, Staubli (1989) calculated isothermal condition (500°-600°C) which were attained due to garnet-biotite exchange equilibria during later retrograde phase M_3. Pressure has been estimated by Staubli (1989) as 6-7.5 Kb. Pognante and Lombardo (1989) estimated the pressure temperature condition of M_1 metamorphism in rare metabasics which occurred at about 750°C and 12 Kb. In this area also, M_2 phase of metamorphism overprinted the M_1 phase of metamorphism during high-grade MCT related anatexis (Searle et al. 1988; Searle & Rex 1989).

In summary, the High Himalaya Crystalline Zone exhibits the complex metamorphic history which started progressively prior to MCT thrusting event but continued during MCT thrusting event and crustal anatexis at the upper part of HHCZ with intermittent retrogressive phase. The last episode is an extensive retrogression phase which reequilibrates the progressive equilibrium condition.

1.2.2 The Lesser Himalaya

In the lesser Himalaya the overall metamorphic condition varies from low (chlorite, no biotite) to medium (Biotite, garnet, kyanite and/or staurolite) grade which is confined to various autochthonous to para-autochthnous zones and to crystalline nappes. Metamorphism in the lesser Himalaya is often marked by chlorite + biotite or biotite + garnet assemblages. In the eastern Himalaya Acharyya (1979) suggested two deformational episodes from lesser Himalayan sequence. One is pre-Tertiary possibly contemporaneous to Gondwana sedimentation and later one is associated with the main Himalayan phase. Mohan et al. (1989)

identified three phases of metamorphism (M_1, M_2 and M_3) from Darjeeling-Sikkim region of eastern Himalaya being M_1 in lower greenschist facies, M_2 being upper greenschist to amphibolite facies and M_3 being the retrogressive metamorphism. They estimated temperature from $580°C$ for the garnet zone to a maximum $770°C$ for the sillimanite zone. The preferred values for pressure range from 5.0Kb to 7.7Kb respectively.

1.3 STATUS OF THE MCT

As mentioned earlier the MCT separates the Higher Himalaya crystalline rock from Lesser Himalaya (Gansser 1964; Le Fort 1975). But despite the geodynamic importance of the MCT its location is still debated. It was originally defined (Heim & Gansser 1939) from Kumaon as basal contact of crystalline nappe of high grade metamorphism over the lower grade metamorphic rocks of the Lesser Himalaya. Gansser (1964) marked the MCT throughout the Himalaya according to this definition. It defines lower tectonic boundary of the Higher Himalaya against the Lesser Himalayan sedimentaries and epi- and meso-metamorphics. Valdiya (1980a,b) redefined the MCT of Heim and Gansser (1939) and designated it as a subsidiary thrust called Munsiari thrust. He recognized another thrust plane called the Vaikrita thrust further north and marked it as the equivalent of the MCT.

Recent workers considered the MCT to be a zone of multiple thrusting called "Main Central Thrust Zone" (e.g. Arita 1983; Hubbard 1989; Matcalfe 1993; Searle et al. 1993). From Central Nepal, Arita (1983) identified the base of this zone as Main Central Thrust-I (MCT-I) and the upper limiting boundary of MCT zone was named as

Main Central Thrust-II (MCT-II). Along the MCT-II Himalayan gneisses overlie the MCT Zone.

1.4 INVERTED METAMORPHISM IN THE HIMALAYA

For more than a century ago Oldham (1883) observed that high-grade metamorphic rocks lie structurally and topographically over low grade metamorphic rocks all along the Himalaya. This now-famous inverted metamorphism is "one of the most problematic facts of the whole Himalayan range" (Gansser 1964). The inverted metamorphic sequences occur in the vicinity of the MCT and has been reported from the entire Himalayan range. But the exact location of inverted metamorphism with respect to MCT is still controversial. Comparing 12 critical subareas throughout the Himalaya Sinha-Roy (1981,1982) concluded that the MCT should be placed along the base of the inverted metamorphic zones. In Central Nepal the MCT cut across the inverted metamorphic sequence roughly following the kyanite isograd (Le Fort 1975; Pecher 1977). In the Kumaon Himalaya, Valdiya (1980) placed the MCT at the top of the inverted metamorphic sequence. To explain the cause of inverted metamorphism present in the Himalaya several but conflicting models have been proposed.

1.5 MODELS FOR INVERTED METAMORPHISM

Many models for the inverted metamorphism in the Himalaya have been proposed (Oxburgh & Turcotte 1974; England & Thompson 1984; Le Fort 1975; Graham & England 1976; Bird 1978; Scholz 1980; Arita 1983; Jaupart & Provost 1985; Pecher 1989; Pilgrim & West 1928; Ray 1947; Gansser 1964; Naha & Ray 1971; Frank et al. 1977; Hubbard

1989; Jain & Manickavasgam 1993). These models can be classified into two broad groups. One group of models explain^s inverted metamorphism as due to perturbation of geotherm^s during fast movement along the MCT. In these models the metamorphism ~~used~~ *is considered* to be syn- to post-kinematic with respect to the deformation related to the movement along the MCT. The "Hot-over-cold" model with or without shear heating is a typical example of such models. The other group of models invoke structural reasons such as recumbent folding, multiple thrusting and ductile shearing, as a cause for inverted metamorphic zonation. In these models metamorphism ~~used~~ *is considered* to be pre-kinematic with respect to the deformation episode that resulted in this feature. Some of the important models are described below.

1.5.1 Hot Over Cold Model

In the hot over cold model (Oxburgh & Turcotte 1974; England & Thompson 1984) the inverted metamorphism is the result of thrusting of hot continental crust over the cold one. As the rocks are bad conductor of heat, thermal equilibration is initiated during rapid thrusting. As a result rise of temperature is restricted at the upper surface of the foot wall side due conduction of heat from hot continental crust (hanging wall side) to colder block (foot wall side). So, within the foot wall side temperature rises gradually from the deeper level towards the upper surface of the foot wall block. Thus the temperature gradient is inverted in the foot wall block which consequently shows the inverted metamorphic sequence in addition to lower part of the hanging wall side across the thrust plane. It may be pointed out that reverse temperature gradient is observed near the thrust contact as the heat conduction may be operative only near the contact. Mohan et al. (1989) explained that the presence of inverted

9

metamorphic sequence in Darjeeling-Sikkim Himalaya may be due to the presence of thrusted hot slab over cold one in that area. Pecher (1989) suggested that in the Tibetan slab the inversion of metamorphism is due to quick and quasi-adiabatic uplift of that slab by transportation of the block along the MCT.

1.5.2 Shear Heating Model

Additional shear heating may also be responsible for increasing the temperature along and near the thrust contact (Le Fort 1975; Graham & England 1976; Bird 1978; Scholz 1980; Arita 1983). Le Fort (1975) first explained the inverted metamorphism as a result of shear heating along a thrust plane (Fig.1.3a). Near the thrust plane the temperature gradient is reversed thus daveloping the inverted metamorphic sequence. Fig.1.3b and Fig.1.3c describe the two situations where the shear heating is not considered (Fig.1.3b) and considered (Fig.1.3c). In the case of Fig.1.3b upper thrust sheet is rapidly emplaced and no shear heating takes place. So except for a very brief transient period no inverted geotherm is produced. After that within a short period normal geothermal gradient is recovered and thus ultimately the temperatures beneath the thrust are lower than the initial temperature at the base of the thrust. But if shear heating is considered (Fig.1.3c) temperature rises sharply with time from the initial value at the thrust plane and consequently strong inverted temperature gradient will be present beneath the thrust. This inverted temperature gradient may be the cause of inverted metamorphic sequence associated with the thrust plane. Arita (1983) explained the presence of inverted metamorphic sequence in Midland metasediments of central Nepal beneath the MCT as a result of shear heating along the MCT.

Matcalfe (1993) modified the original Le Fort's (1975) model and suggested that the inverted metamorphic sequence is a consequence of three different metamorphic phases: M_1 was tectonically inverted, M_2 evolved downward conduction of heat from the still hot slab above and M_3 followed the upper slab decompression.

1.5.3 Recumbent Folding Model

Large scale post-metamorphic recumbent fold can show the metamorphic inversion in its inverted limb (Ray 1947; Gansser 1964). Ray (1947) suggested from Darjeeling Himalaya that the recumbent folding might be the cause of inverted metamorphic isograds present in that area. From the Zanskar region Searle and Rex (1989) described that the whole sequence is folded into a large-scale recumbent fold developing inverted metamorphic sequence in that area.

1.5.4 Multiple thrusting Model

The inverted metamorphism has also been explained as a result of ductile shear displacement along MCT (Frank et.al 1977; Hubbard 1989; Treloar et.al. 1989; Jain & Manickavasagam 1993). In the north Pakistan Treloar et. al. (1989) explained that the metamorphism at south of the Main Mantle Thrust was during the main Himalayan shearing event. The peak of this metamorphism was synchronous with the development of the main phase of shear fabric development at some places and also continuous until after the crenulation of that fabric in others. Subsequent to the peak of metamorphism, the metamorphic sequence was disrupted and imbricated by late northward-dipping thrusts. As a result of this thrusting a number of imbricated metamorphic blocks with an overall upward-increasing metamorphic grade were stacked on top of each other

developing the inverted metamorphism of that area. Jain and Manickavasgam (1993) showed that ductile shear displacements along common close spaced S-C shear planes may have caused inversion of metamorphism across a Higher Himalayan shear zone in Zanskar Himalaya.

1.5.5 Other Models

Jaupart and Provost (1985) explained the inversion of metamorphism present in the Himalaya by proposing another model called "heat refraction". HHSZ consists of sedimentary rocks which have the much lower thermal conductivity than that of the crystalline rocks of HHCZ. Thrusts along the continental collision zones put sedimentary layers (HHSZ) over the crystalline basement (of HHCZ). This leads to heat refraction effects of significant magnitude into the HHCZ because sedimentary layers act as a barrier to transport the heat. So the higher temperature gradient is attained in the upper part of the crystalline rocks below the HHSZ. It causes the inversion of metamorphism within the crystalline rocks of Higher Himalaya.

However, Inger and Harris (1992) could not find any link between thrust faulting and inverted metamorphism in Langtang area of northern Nepal. They proposed the presence of polyphase metamorphism in that area, rather than recording a transient inverted geotherm.

1.6 SCOPE OF THE PRESENT INVESTIGATION

It is apparent that the inverted metamorphism is still an enigmatic problem. One of the major reasons for the uncertainty is that in many sectors the relationship between the time of metamorphism and

thrusting/ductile shearing is ambiguous. In an overthrust terrain post-thrusting temperature increase is much more significant in the root zone than in the frontal part (e.g. Shi & Wang 1987; Molnar & England 1990). Consequently in the root zone post-thrusting metamorphism may obliterate the earlier fabric to varying extent. In such areas unambiguous interpretation about the relation between deformation and metamorphism may be difficult. In the frontal part of the thrust sheet post-thrusting metamorphism may be less intense and such relationship may be unequivocal.

Around the Chur peak (3647m. ca 40Km SE of Simla) frontal part of the HHCZ´ thrust sheet occurs in a half-klippe (Fig.1.2). This area is about 150Km away from the root zone. One of the earliest detailed description of inverted metamorphic zones comes from this area (Pilgrim & West 1928). Therefore, an area of about 850 Km^2 between $77°15'N$ - $77°35'N$ and $30°43'E$ - $31°E$ around the Chur peak in Simla and Sirmour districts of Himachal Pradesh state was chosen for detailed investigation. The area falls under the Survey of India toposheet No. 53F/5, 53F/6, 53F/9, 53F/10.

Evolution of the inverted metamorphism has been worked out from detailed structural analysis, microstructural and textural relation, mineralogy and mineral chemistry, garnet zonation pattern and geothermobarometry.

FIGURES
CHAPTER - 1

FIGURE 1.1: Geological sketch map of the Himalaya showing different lithotectonic zones and major faults (After Gansser 1974).
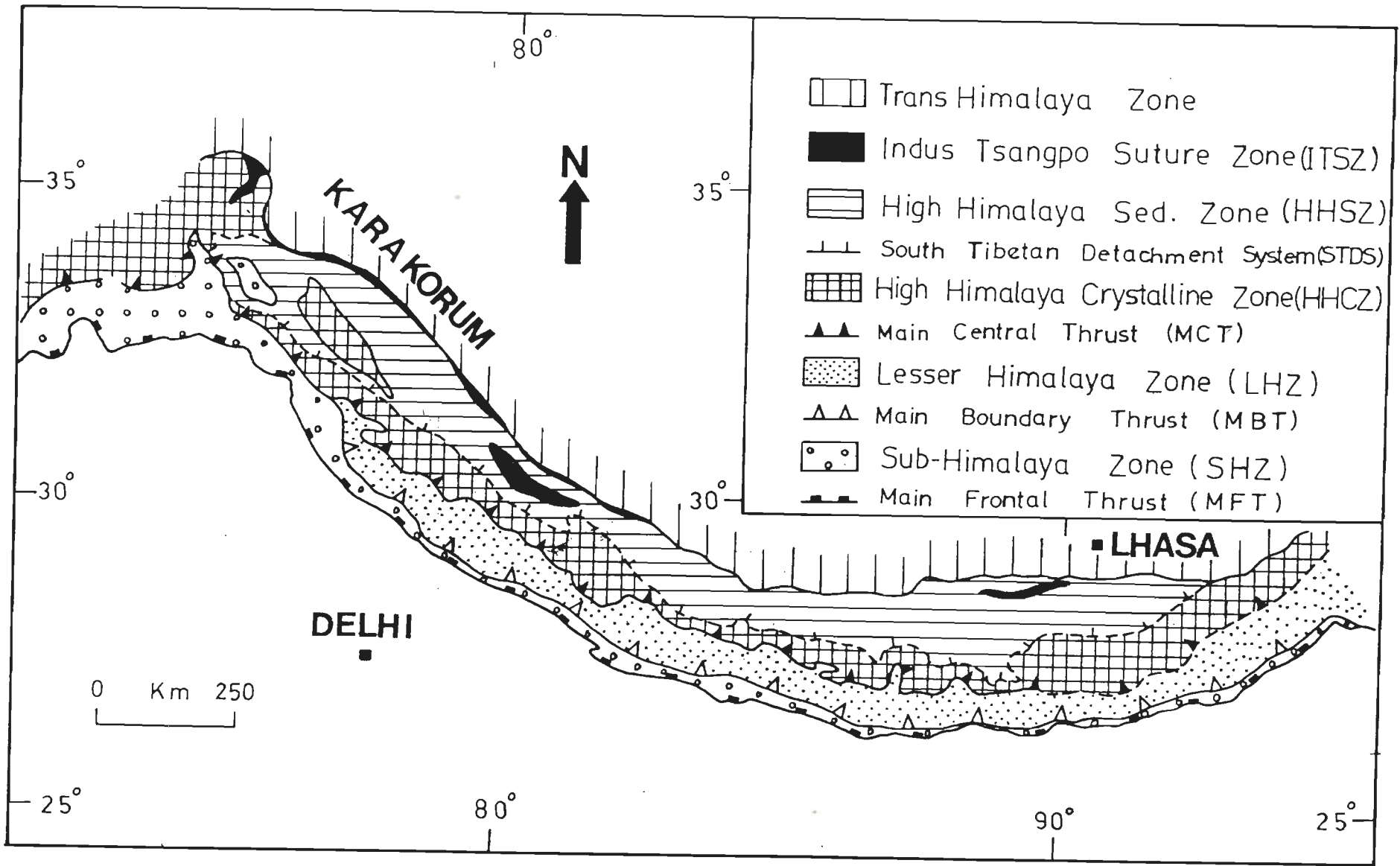
Fig. 1.1

FIGURE 1.2: Metamorphic facies map of the Western Himalaya (adapted from Sinha Roy & Bhargava 1989). The squared portion is the present atudy area.

N

INDEX

	NON METAMORPHIC
	ANCHIMETAMORPHIC TO LOWER GREENSCHIST FACIES
	GREENSCHIST FACIES
	AMPHIBOLITE FACIES
	BLUESCHIST FACIES
	MAJOR THRUST
	ACID PLUTONS

100 Km
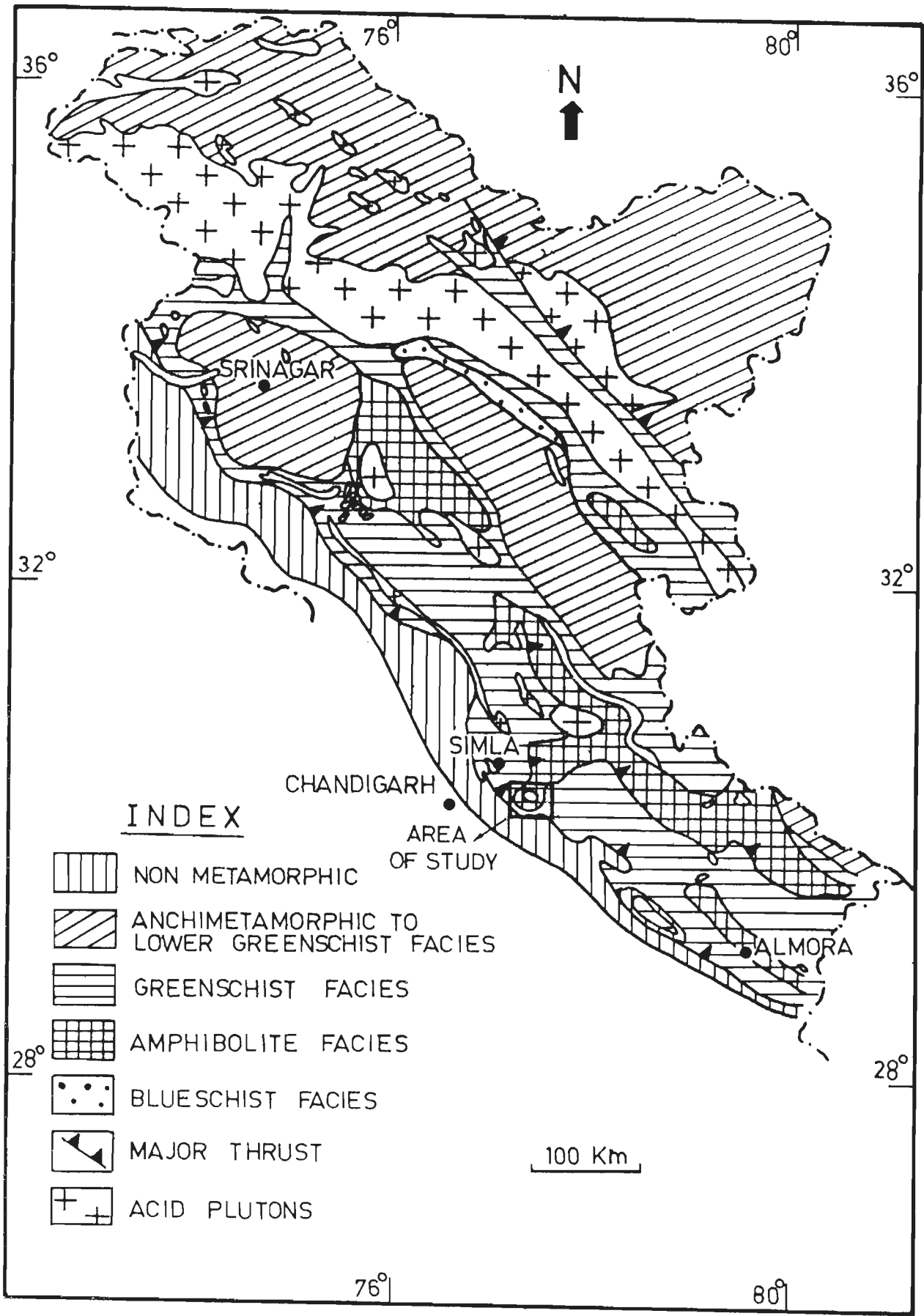
FIG. 1.2

FIGURE 1.3: SCHEMETIC DIAGRAMS OF MODELS TO EXPLAIN THE INVERTED METAMOPHISM IN THE HIMALAYA.

(a). Hot over cold model as explained by Le Fort (1975). Near the thrust plane (MCT) the temperature gradient has become inverted to produce the inverted metamorphic sequence.

(b). & (c). Two situations for the shear heating model. In (b) 30 Km thick thrust sheet is rapidly emplaced. As a result revarsal of thermal gradient is acheived during a very short period. Gradually normal temperature gradient is attained. But in (c) additional shear heating is added at the thrust. Due to shear heating the temperature progressively increases with time near the thrust plane. Below the thrust plane the reverse temperature gradient is attained which is enough to produce the inverted metamorphic sequence. Data calculated using the method described by Molnar et al. 1983. For all these models erosional effect is not considered.

a

S ... N

Pressure (kb)

topography

MCT

500°C
600°
700°
800°

Ky Sill

Zone of melting

500°
600°

0 ... 50 km

b

Temperature (°C)

200 ... 400 ... 600 ... 800 ... 1000

Depth (km)

Pressure (kb)

t_∞

t_0

1 2 3 5 10 20 30 50 MY

5

10

15

c

Temperature (°C)

100 ... 200 ... 300 ... 400

Depth (km)

Pressure (kb)

5 10 15 20 30 my.

5

10

15
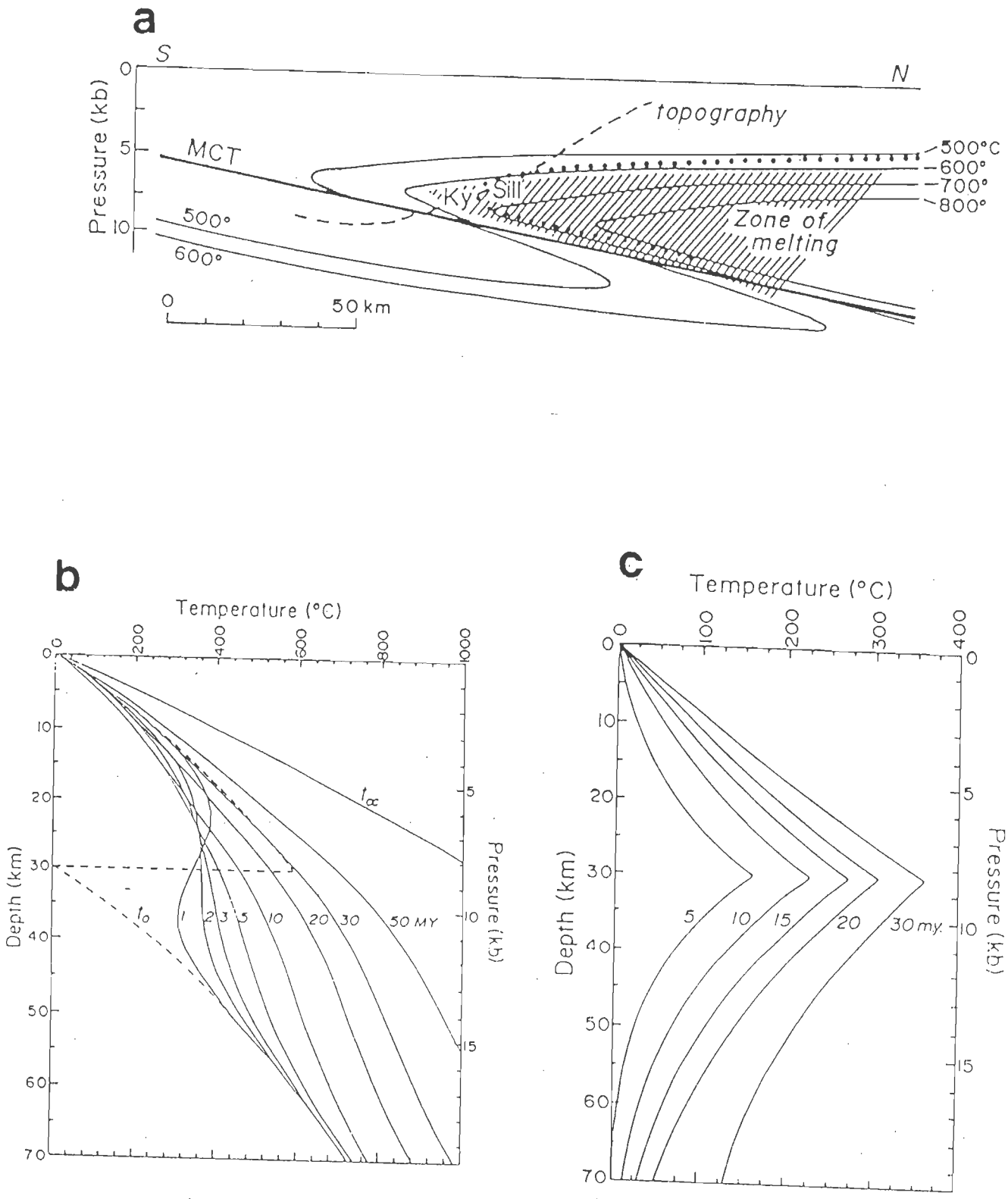
Fig. 1·3

CHAPTER - 2
GEOLOGY OF THE AREA

2.1 REGIONAL SETTING

The High Himalaya Crystalline Zone (HHCZ) consisting of high grade Precambrian rocks is a huge thrust sheet that can be traced along the entire Himalaya. The rocks of HHCZ have been broadly divided into two belts viz. inner crystalline belt and outer crystalline belt (Thakur 1980). The outer crystalline belt occurring as klippes and half-klippes represent the frontal part of HHCZ thrust sheet in the LHZ. Two separate lithotectonic units viz., the Jutogh Series and the Chail Series have been recognized in the outer crystalline belt (Pilgrim & West 1928). The Jutogh Series consists of medium to high grade metamorphic rocks where as the Chail series occasionally consists of the low grade metamorphic rocks. Fuchs (1981) considered the Chail series as a part of LHZ and is followed here. The Jutogh Series has been redefined by Srikantia et. al. (1975) as "Jutogh Group" to conform to the recent stratigraphic codes.

In the lower Himachal Himalaya the Jutogh Group is exposed in a half-klippe around the Chur peak. Around Simla about 45 Km NW of Chur peak the same Jutogh Group of rocks is exposed in a pear-shaped klippe. Thakur (1981) suggested that rocks of the Jutogh Group extended northward from the Chur area into Sutluj valley where it joins with the HHCZ.

In the Chur area a huge granite body called the "Chur granite" occupies the highest geographic and tectonic level (Fig.2.1). The Chail Formation of Lesser Himalaya (Fuchs 1981) underlies the Jutogh Group.

14

The contact between the Jutogh Group and the Chail Formation is marked by a pronounced thrust plane named "Jutogh Thrust" (Pilgrim and West 1928). At the base of the Chail Formation another major thrust plane called "Chail Thrust" marks the contact between the Chail Formation and underlying the Jaunsar Series.

There is a controversy whether Jutogh thrust is equivalent to MCT or not. Valdiya redesignated the originally defined MCT of Heim and Gansser (1939) as Munsiari thrust and considers Jutogh thrust to be its equivalent. Sinha-Roy (1982) considers Chail Thrust to be the MCT and Jutogh thrust as a subsidiary thrust above Chail thrust. However, Gansser (1964) recognized the Jutogh thrust as equivalent to MCT and is followed here.

2.2 PREVIOUS WORK

Pilgrim and West (1928) described in detail the geology of the Chur-Simla area and gave a classification of the rocks as given in table 2.1. They recognized two thrust planes from this area: Jutogh thrust at the contact between the Jutogh Group and the Chail Formation and Chail thrust at the contact between the Chail Formation and the Jaunsar Series. They also recognized a large scale recumbent fold whose limbs are identified by the two gently dipping carbonaceous schist bands. They suggested that the Chur granite is a laccolithic intrusion into the Jutogh Group. Garnet and staurolite zones were identified In the Jutogh Group, the staurolite zone occurring at a higher topographic level than the garnet zone. Pilgrim and West (1928) suggested that the contact metamorphism due to intrusion of the Chur granite superimposed on regional metamorphism, was responsible for the inversion of metamorphism in the

Chur area.

Naha and Ray (1970) and Ray and Naha (1971) recognized three phases of deformation and two phases of metamorphism in the rocks of the Jutogh Group around Simla. Naha and Ray (1970) showed that, in Simla area the first metamorphism postdates the large scale recumbent folding, formed during earliest phase of deformation but predates thrusting developed during second deformational episode. The weaker second phase of metamorphism is syn- to post-tectonic with respect to second phase of deformation but pre-tectonic to last phase of deformation (third deformation). Dubey and Bhat (1991) doubted on the presence of large scale recumbent folding in Simla area. Alternatively they opined that initiation of folding and thrust movements were simultaneous.

Das and Rastogi (1988) echoed the suggestions of Naha and Ray (1970) for the Jutogh metasediments in the north of the Chur area. They calculated the P-T condition suggesting the reactions responsible for the development of different grades. They divided the area in four zones viz. (a) garnet-chlorite, (b) staurolite-biotite, (c) kyanite-biotite and (d) sillimanite-garnet-biotite. The temperatures calculated from each zone are 540°C for garnet-chlorite zone, 560°C for staurolite-biotite zone, 640°C for kyanite-biotite zone and 650°C for sillimanite-garnet-biotite zone.

Kanwar and Singh (1979) mapped the southwest part (between Didag and Nohra) of the Jutogh Group and confirmed the structural interpretation by Naha and Ray (1970,1972) and Ray and Naha (1971).

Kishore and Kanwar (1984a,b) worked on the structural history of the Chur granite in Nohra-Haripurdhar section (southern part of Chur). On the basis of structural, petrological and geochemical study, they concluded that the Chur granite is not a single homogeneous body but

16

consists of foliated as well as non-foliated granites. The emplacement of granite took place in two pulses separated in time with the same source of magma. They suggested that the contact between the foliated granite and the Jutogh Group is discordant with the bedding planes of Jutogh metasediments.

Roy and Mukherjee (1976) have studied the relation between the metamorphism and deformation in western part of the Chur granite. They suggested that the first metamorphism reached upto the middle grade. The second phase of metamorphism was of lower intensity. Each progressive metamorphic episode was followed by a retrograde one. They suggested that the first metamorphism is syn- to post- first deformation episode while the second one completely postdates second deformation.

2.3 ROCK TYPES

Detailed field checking shows that the geological map prepared by Pilgrim and West (1928) is essentially correct with the following modifications (Fig 2.1).

Pilgrim and West (1928) recognized two rock types from the Jutogh Group: the carbonaceous schist bands representing two limbs of a large recumbent fold and Boileauganj quartzite. Extensive field checking and detailed geological mapping show that the two carbonaceous bands have separate identities: the band occurring at lower topographic level is termed as lower carbonaceous schist (LCS) and the band at higher topographic level is termed as upper carbonaceous schist (UCS). Between these two bands the rock is essentially quartzite with minor intercalations of mica schist. Above the upper carbonaceous schist band mica schist is the dominant rock type. Therefore, in the Jutogh Group four separate

17

rock units are present.

Pilgrim and West (1928) traced upper carbonaceous schist band upto Bagi in east and upto Thandidhar in north-west. But it may be extended beyond Bagi to further north and beyond Thandidhar to further east though it becomes very thin and sometimes appears as lenticular patches. Hence this band in northern side has been marked with dashed line (Fig.2.1).

Pilgrim and West (1928) also traced some fault planes in and around Rajgarh. But no such fault plane is present in that area.

2.3.1 Mica schist

Mica schist is one of the major rock units within the Jutogh Group. Thin layers of quartzose mica schist, amphibolite bands, calc-silicate and marble are present within the mica schist. The thickness of mica schist varies greatly from 100m to 2300m.

Mica schist is medium to coarse grained rock and is schistose in nature with a wide variation in colour and composition. The rocks rich in quartz and muscovite are dull gray whereas biotite rich rocks are dark gray in colour. On weathered surfaces mica schist looks brownish gray due to iron staining. Within the mica schist the schistosity is defined by parallel alignment of quartz and phyllosilicates like muscovite, biotite and chlorite. In the northern part it looks like phyllite. Quartz veins within the mica schist are common with varying size and orientation.

The mica schist unit comprises mainly of quartz, biotite, muscovite, garnet, opaques and occasionally staurolite, kyanite and sillimanite. Minor minerals present in mica schist are chlorite, epidote, tourmaline and zircon. Euhedral to elongated garnets of various sizes are

present ranging from <100 microns to about 4 cms. in diameter. Staurolites are not uniformly distributed throughout the area. Kyanites and sillimanites occur only near the granite contact. Opaques are mostly ilmenite and rarely magnetite.

2.3.2 Quartzite

Quartzite occurs between the two carbonaceous bands. The contacts between quartzite and upper carbonaceous band and between quartzite and lower carbonaceous band are sharp. In Rajgarh area quartzite directly overlies the Chail Formation. The thickness of the quartzite unit varies from place to place between 50m and 2000m.

Quartzite is essentially medium to fine grained rock with colour varying from gray to white. Most of the places quartzite is foliated. But quartzite is massive in the north-western part of the area, whereas in the other parts it is foliated one. It may be noted that in northern and eastern side quartzite is phyllitic in nature with finer grain size than rest of the area. Bedding planes in quartzite are well defined by alternate dark and light coloured bands of lithological layerings. Quartzite at some places is mica rich and at others, it is dominated by quartz. This type of compositional variation is neither gradational nor regular. Thin micaceous layers within quartzite can easily be recognized.

The quartzite is essentially composed of quartz, biotite, feldspar, muscovite and opaques. Garnet, chlorite, epidote, apatite and sphene are also present in minor proportions. With increasing proportion of muscovite and biotite, quartzite grades into micaceous quartzite. Sometimes biotite clots are aligned to form dominant mineral lineations in quartzite. Garnets are restricted within the micaceous layer which are

intercalated with quartzite. Retrograded chlorites are also confined to the micaceous layers.

2.3.3 Carbonaceous Schist

As mentioned earlier carbonaceous schist in the Jutogh Group is present as two separate bands: upper carbonaceous schist (UCS) and lower carbonaceous schist (LCS). The thickness for LCS varies from 35m to 1400m whereas the UCS is thinner with thickness ranging from 30m to 1300m. Carbonaceous schist includes some thin marble and calc-silicates bands sporadically.

Carbonaceous schist is fine to medium grained rock with gray to dark black colour. However on the weathered surfaces, colour becomes dark brownish due to iron staining. When the rock is enriched with graphite carbon particles it looks like coal. The rock is phyllitic to schistose in nature.

Quartz, muscovite, biotite, chlorite and opaques are the major minerals along with minor proportions of garnet, feldspar, tourmaline and epidote. Muscovite is the most dominant mineral which is often impregnated by fine grained carbon dust within the carbonaceous schist. Cubical pyrites of sufficiently large size have been easily recognized in the rock. Sometimes due to leached out pyrite crystals the rock shows vesicular structure. Retrograded chlorites are also present in carbonaceous schist.

2.3.4 Amphibolite

Amphibolite occurs as lenticular bodies within the mica schist. They are deformed metamorphosed mafic dykes and sills.

Amphibolite appears bottle green to moderately light green colour

20

in all outcrops. Grains vary in size from medium to fine.

Amphibolite is mainly composed of hornblende, quartz, plagioclase with minor amounts of garnet, epidote, apatite, sphene and opaque. In the southeast of Chur on Nohra-Haripurdhar road section, garnet porphyroblasts in amphibolite are as big as 6cm.

2.3.5 Marble and Calc-silicate rock

Marble is restricted in the southern part near Chauras, Telengana and south of Nohra and occur within the mica schist as thin lenticular and discontinuous bands. Irregular and patchy marble bodies are also present within the carbonaceous schist.

Pure marble looks milky white in colour which changes to dark gray colour with increasing proportion of carbon impurities. Grain size varies from medium to coarse. Contrasting colour bands defining original compositional variation marks the bedding planes in marble. Both foliated and non-foliated varieties of marble are present. In non-foliated variety granoblastic mosaic texture is shown by equant polygonal grains of calcite and other accessory minerals. In foliated variety calcite grains are elongated and inequant in shape and show preferred orientation along the foliation plane. Foliated marble is mainly restricted near the contact and within the carbonaceous schist.

Marble is composed dominantly of calcite. Other minerals such as quartz, muscovite, plagioclase, tourmaline, tremolite, epidote, sphene and opaques occur in minor proportion. In compositional banding the light coloured bands are dominated by calcite and quartz with occasionally plagioclase whereas the dark coloured bands are characterized by tourmaline, epidote and sphene.

In the Jutogh Group, marble grades into calc-silicate rock with increasing proportion of quartz and biotite. It is distributed as lenticular patches along the marble band in mica schist and in carbonaceous schist. Calc-silicate rocks are rarely seen in the northern and eastern part of the area.

Calc-silicate rock is dark gray to pale brown, medium to coarse grained rock. Bands of calcareous minerals are more weathered than those of silica rich bands. Calc-silicate also shows both granulose and foliated variety.

In addition to calcite, quartz also becomes a dominant mineral in calc-silicate rock. Other minerals like epidote, apatite, sphene and opaques also occur in varying proportion. In granulose calc-silicate rock, quartz and calcite mutually form mosaic texture. In foliated variety the foliation is defined by inequant calcite and quartz grains.

2.3.6 Chail Phyllite and Quartzite

The phyllites and quartzites are the dominant rock types in the Chail Formation. They are often interlayered and show varying thickness from one cm to more than one meter. Phyllites are fine to medium grained, gray to buff coloured cleaved rock. The Chail quartzite is medium to fine grained, pale green to light gray in colour.

The rocks of the Chail Formation are essentially composed of quartz, sericite and chlorites. Other minerals are feldspar, tourmaline, epidote and opaques. Occasionally biotite porphyroblasts are seen in Chail phyllite near Haripurdhar.

2.3.7 Chur granite

The Chur granite is surrounded by mica schist of the Jutogh

Group. The contact between the granite body and mica schist is sharp and concordant. Near the contact pegmatite veins are present. Xenoliths of mica schist are also present within the granite whose origin is uncertain. The Chur granite is gneissic near the margin but massive towards the centre. The gradation from gneissic to massive is gradual.

Granite is medium to coarse grained rock, with grayish white to dark gray colour. Towards the margin, the granite is foliated which is defined by preferred orientation of K-feldspar megacrysts and biotites flakes. The feldspar grains wrapped by the foliation to form augen gneisses. Near the contact biotite-rich granite is observed at some places. The size of K-feldspar phenocrysts varies from a few mm to more than 15 cms in length.

The Chur granite is composed of mainly of quartz, K-feldspar, plagioclase feldspar, biotite, muscovite, and rarely garnet, kyanite and sillimanite. Alumino-silicates are within the granite at some restricted localities. K-feldspar and plagioclase phenocrysts in the porphyritic granite occur in a groundmass consisting of quartz, biotite and muscovite imparting the rocks a porphyritic texture. The minor minerals present in the groundmass are zircon, apatite, epidote, sphene, tourmaline and opaques. At places, the granite is very fine grained showing equigranular texture containing very few feldspar phenocrysts. In deformed granite the phenocrysts are either broken or elongated to form lenses. In more intensely deformed granite the feldspar phenocrysts are broken into pieces and there is development of quartz ribbons. This type of rock is known as granite mylonite which shows varying grades from protomylonite through orthomylonite to ultramylonite.

FIGURE AND TABLE
CHAPTER - 2

FIGURE 2.1: Geological map of the study area (slightly modified after Pilgrim & West 1928). 1- Chur granite; 2- Mica schist; 3- Marble; 4- Upper carbonaceous schist; 5- Quartzite; 6- Lower carbonaceous schist; 7- Chail Formation; 8- Lesser Himalaya Rocks. 2-6 belong to the Jutogh Group. 7-8 belong to the Lesser Himalaya Zone.

N

GIRI R.

77° 20'
77° 25'
77° 30'
77° 35'

30° 55'
30° 55'

30° 50'
30° 50'

30° 45'
30° 45'

Chagdol
Habban
Phagu
Rohru
Rajgar
Daln
Churwadhar
Kol
Khairi
Nahog
Rampur
Bogdhar
Bharari
Didag
Chogtal
Nohra
Chauras
Charna
Bhawal
Harlpurdhar
Chandw
Bngl
Kupvi
Munalog
Saranh
Thundal
Pulwni
Khagna
Chaupal
Thandidhar
Dalenu
Sangrah

CHUR ▲ 3647m

0   Km   5

77° 20'
77° 25'
77° 30'
77° 35'

| 1 | 2 | 3 | 4 | 5 | 6 | 7 | 8 |
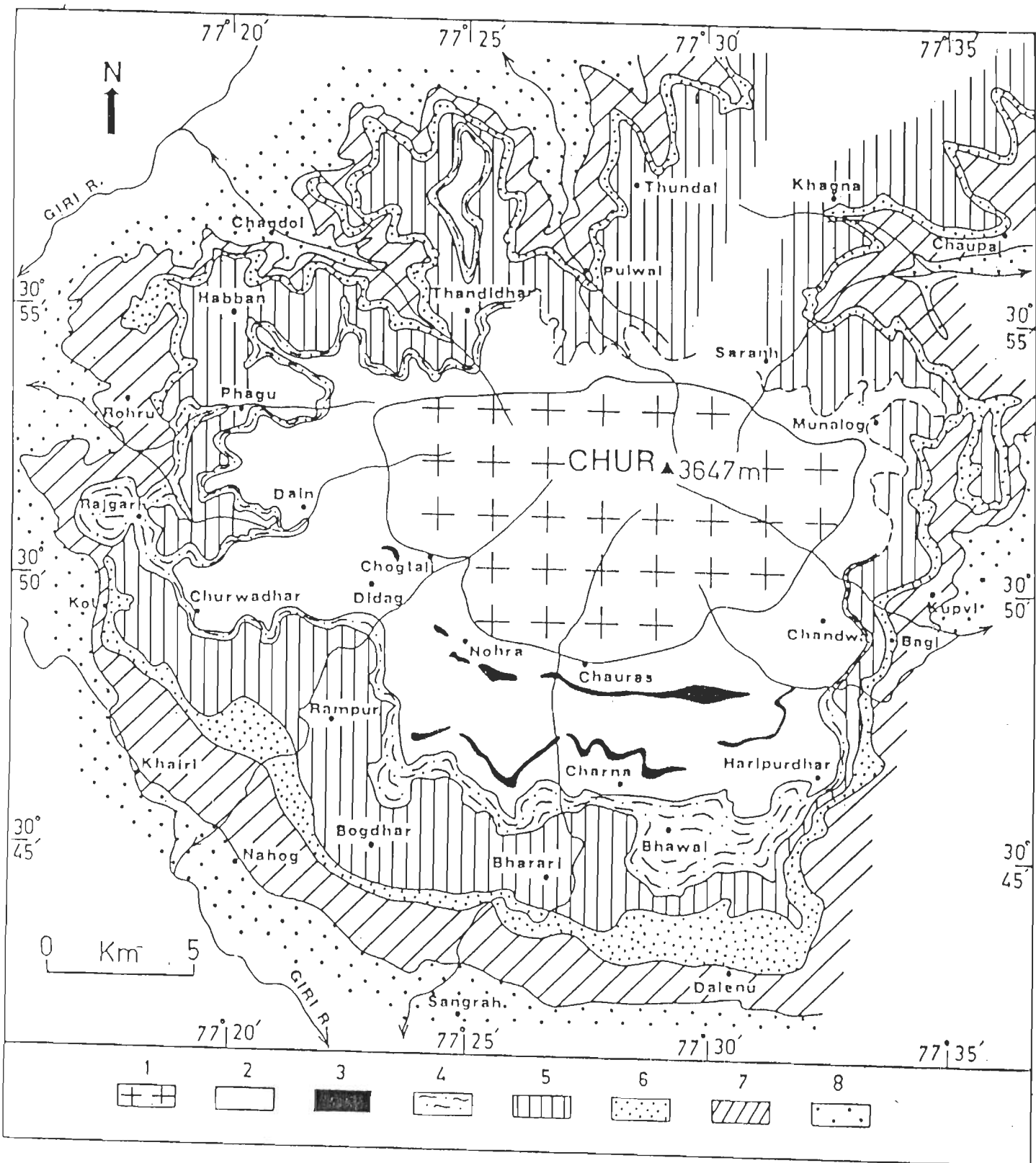
Fig. 2.1

TABLE - 2.1

CLASSIFICATION OF THE ROCKS OF SIMLA-CHUR PEAK AREA
(After Pilgrim and West, 1928)

Blaini Boulder Bed   Slate with pebbles   Upper Palaeozoic

-------------------- Unconformity --------------------

SIMLA SERIES
     Slates and micaceous sandstones   Lower Palaeozoic
     Limestones

-------------------- Unconformity --------------------

JAUNSAR SERIES
     Sub-schistose slates
     Micaceous slates and phyllites
     Phyllites and conglomerate   Late Precambrian
     Quartzites
     Slates with vein quartz

-------------------- Unconformity --------------------

CHAIL SERIES
     Schistose slates and quartz-schist
     Talcose flaggy quartzites and
     quartz schist
     Talc-schist   Late Precambrian
     Grey slates with interbedded
     lime stones

-------------------- Unconformity --------------------

     Intrusion of Chur granite into the
     Jutogh Series
     Intrusion of olivine dolerites into
     the granite and the Jutogh Series

JUTOGH SERIES
     Quartzite and schist
     Carbonaceous dolomitic lime stones
     Carboneceous slates and phyllites
     Quartzite and mica schist   Early Precambrian
     (Boileagunge quartzite)

CHAPTER - 3
STRUCTURES

3.1 SMALL-SCALE STRUCTURES

Structures observable in thin section to outcrop scale have been broadly classified into three groups: early folds, structures related to ductile shearing and the late structures.

3.1.1 Early Folds And Related Structures

The earliest diastrophic structure recognised in this area is a set of very tight to isoclinal folds (F_1) traced by stratification (S_0) (Fig. 3.1a). These folds are observed in all the metasedimentary rocks of both the Jutogh Group and the Chail Formation. The axial planes of the majority of the F1 folds have very gentle dips and the fold axes plunge either east or west. These folds are recumbent to gently plunging reclined/inclined in geometry. The F_1 folds are characterised by a well developed axial planar cleavage (S_1) which is the most dominant planar structure in this area. In the Chail phyllite and the Jutogh carbonaceous schist the S_1 is of the nature of slaty cleavage or phyllitic structure (cf. Davis 1984) but becomes schistosity in mica schist and amphibolite. Under the microscope, the S_1 in pelitic rocks shows all the variations from domainal cleavage to a cleavage defined by evenly dispersed mica flakes and inequant quartz grains with preferred orientation (Fig. 3.1b). In amphibolite and calc-silicate rocks amphibole prisms and elongated calcite grains define S_1 cleavage. Parallel to the hinges of F_1 folds a lineation, gives by the intersection of S_0 and S_1 surfaces, is commonly present. A mineral lineation defined by the preferred orientation of muscovite and

24

biotite in mica schist and inequant quartz grains in quartzite has also developed during F_1 folding.

The folds of the second generation (F_2) are traced by both the S_0 and S_1 surfaces. The F_2 folds are open to tight with the interlimb angle varying between 20° to 50°. In the mica schist the F_2 folds are often crenulation microfolds which are symmetric at the hinge zone and asymmetric at the limbs of the larger order F_2 folds. Majority of the F_2 fold axes are sub-horizontal to low plunging towards east or eastsoutheast and the axial planes usually have very gentle dip. Therefore, the F_2 folds are recumbent to gently reclined in geometry (Fig. 3.1c). The F_2 folds are common in the rocks of the Jutogh Group but they are absent in the Chail Formation. A crenulation cleavage (S_2) (Gray 1977) approximately parallel to the axial planes of the F_2 folds, have developed at places in the mica schist. In quartzite and marble the S_2 occurs as spaced cleavage (Davis 1984). The linear structure of the second generation is mainly pucker lineation which runs parallel to the F_2 fold axis. Sometimes the pucker lineation die out, bifurcate or converge. A lineation due to intersection between S_1 and S_2 has been observed in rare cases.

The F_1 and F_2 folds are tight to isoclinal, recumbent to reclined with gentle plunge towards east or west. They are mostly coaxial resulting in type-3 fold interference pattern (Ramsay, 1967) (Fig. 3.1d). At some places the axes of the F_1 and F_2 folds are at an angle (upto about 50°) and the F_1 folds become non-plane and noncylindrical. In many exposures neither the S_1 cleavage (and the F_1 linear structure) nor any overprinting relationship is present. In such cases it is virtually impossible to group a particular fold into either F_1 or F_2 generation. Since these folds are nearly coaxial in most cases and have similar geometry, they are grouped

together as "early folds" pre-dating the ductile shearing movement.

3.1.2 Structures in the Shear Zones

The ductile shear zones are often characterised by the development of mylonite microstructures including mylonitic foliation. Mylonite results primarily via ductile flow and crystal-plastic grain-size reduction (dynamic recrystallization and neomineralization) though brittle deformation in some minerals, such as feldspar, may occur (Bell and Etheridge 1973; Hobbs et al. 1976; Sibson 1977; White et al. 1980; Wise et al. 1984). In this area all the rock types of both the Chail Formation and the Jutogh Group as well as the Chur granite have been mylonitized to varying extent. All gradations from protomylonite through orthomylonite to ultramylonite (cf. Wise et al. 1984) have been observed. At the initial stage of the mylonitization quartz grains show strong undulose extinction (Fig. 3.2a). Recrystallization nearer to the grain boundaries of these deformed grains leads to the formation of core-and-mantle texture (Fig. 3.2b cf. White 1976). With increase in recrystallization the rocks acquire a 'pseudoporphyritic' texture with surviving deformed porphyroclasts in a fine-grained matrix (Figs. 3.2c). Where the grains are favourably oriented quartz-ribbon mylonite has developed (Figs. 3.2d). Porphyroclasts may or may not survive in a quartz-ribbon mylonite. The quartz grains in the ribbons are invariably recrystallized and show well formed subgrains. Finally, complete recrystallization obliterates the original fabric and the rock is composed of small polygonal relatively strain-free grains. The quartz-rich rocks, in such cases, become blastomylonite. The mica (muscovite and biotite)

grains also undergo similar sequence of deformation. The fine recrystallized micas are often smeared along mylonite foliaiton (Fig. 3.2c). In the ortho- and ultramylonites a mylonitic foliation (S_m) is usually very well developed (Fig. 3.2d) and obliterates the early cleavages to varying extent.

In the Jutogh Group the two carbonaceous bands are most intensely mylonitized. The Chail phyllite at the contact with the lower carbonaceous band and the Jutogh mica schist at the contact with both the upper carbonaceous band and the Chur granite are also highly mylonitized. The mylonitisation in the Chur granite is restricted to the margin i.e. near the contact with the surrounding mica schist.

In the ductile shear zones both compressional and extensional structures may be produced depending on the initial orientation of the layers/cleavage with respect to the shear zone wall (Ramsay and Allison 1979; Ramsay 1980; Mukhopadhyay 1989). In the area both these types of structures have been observed in the shear zones. S-C composite planar fabrics (Fig. 3.3a,b), folds on layering and crenulation folds on pre-existing cleavage surfaces (Fig.3.3c) or mylonitic foliation (Fig. 3.3d, 3.4a,b) and sheath folds are the common compressional structures. The extensional structures include extension crenulation cleavage (Fig. 3.4c) (Platt & Visser 1980; William & Price 1990); foliation boudinage, rotated boudinage (Fig. 3.4d) and pinch and swell structures. Besides these two types of structures, the other important feature developed in the shear zone is the repeated crenulations and crenulation cleavage development. Bell and Rubenach (1983) have shown that a cleavage can be progressively destroyed to completion through the development of crenulation cleavage and a new cleavage can form. In this area stages 1 to

27

6 of Bell and Rubenach (1983) have been repeated several, but unknown, times. Slaty cleavage (S_1) is crenulated and developed a crenulation cleavage (S_2). During progressive shearing, S_2 may be crenulated or form a differentiated crenulation cleavage by dissolution and transfer of quartz grains. With the recrystallisation of quartz grains, a mylonitic foliation may develop parallel to the differentiated layering. If this mylonitic foliation falls in the compression zone, it gets crenulated and a new cleavage develops. This process may continue throughout the progressive ductile shearing. All these features have been extensively developed in the two carbonaceous bands.

During progressive ductile shearing the early structures (F_1 and F_2) are largely modified and obliterated and new structures have developed. In the field often it is impossible to decide to which generation a particular fold belongs. And hence, all the folds in the shear zones have been grouped together as F_{sz}. In the shear zone the axial planes and the axes of folds (F_{sz}) show varying orientation. The folds formed in the early stage of the ductile shearing have been modified and repeatedly crenulated in the late stage. In the carbonaceous bands all the fold interference patterns, viz. type 1 (sheath fold; Cobbold & Quinquis 1980), type 2 and type 3 have been observed from outcrop scale (Fig. 3.5a) to thin section (Fig. 3.5b). The most common linear structure in the shear zone is the stretching lineation which is usually defined by quartz or mica-ribbons. The stretching lineation is usually very straight in outcrop scale but sometimes curved around the fold hinges.

In the "ideal" shear zone model (Ramsay & Graham 1970) a layer and a cleavage can not get back into the zone of contraction of the instantaneous flow field once it enters zone of extension (Ramsay 1980;

Ramsay & Huber 1983). However, several mechanisms have been proposed to account for superposed deformation in ductile shear zones (Bell 1978; Cobbold & Quinquis 1980; Platt 1983; Ghosh & Sengupta 1984,1987).

Gently-dipping small-scale thrusts are very common in the carbonaceous schist bands and adjacent rocks. In the hanging wall block the mylonitic foliaiton is usually subparallel to the thrust plane. But in the foot wall block the thrust planes often cut across the mylonitic foliation. A number of thin thrust sheets, each measuring less than a meter thick, ride over each other giving rise to imbricate or schuppen structures (Fig. 3.5c). In most of the cases the thrust planes dip at low angle (20°-30°) with sense of movement towards west or southwest.

3.1.3 Late Structures

The late structures are of two types: (i) A set of very broad-hinged upright warps (F_3) have affected all the structures of both the F_1-F_2 generations and in the shear zones. The effect of these structures is seen in broad undulations of the cleavage surfaces in outcrop to intermediate scales. (ii) Subvertical to steeply dipping fractures cutting across all the earlier structures represent the last episode of deformation in this area. They occur either as one set of subvertical fractures or as steeply dipping conjugate sets. At some places they show normal sense of displacement (Fig. 3.5d).

3.2 LARGE-SCALE STRUCTURES

The geometry of the large-scale structures have been interpreted based on the structural analyses of the orientation of the small-scale

structures. Structural data of main foliation and lineation, early folds and folds in shear zones have been plotted in the stereogram and analyzed.

3.2.1 Regional Variation in the Orientation of Foliation and Lineation

In most part of the area the penetrative cleavage is either S_1 or S_m which are sub-parallel to each other. In many instances it is impossible to distinguish between S_1 and S_m in the scale of hand specimen and outcrop. Although under the microscope they are easily distinguished from each other. Therefore, they have been plotted together as "main foliation" on stereograms. The synoptic stereogram of all the foliation planes gives a well defined point maximum (Fig. 3.6a). The modal foliation plane has a dip of $10°/N59°$. The synoptic stereogram of all the linear structures also show a point maximum corresponding to a plunge of $10°/N57°$ (Fig. 3.6a). This stereogram apparently suggests that in large scale there is a recumbent or low-plunging reclined fold with NE-SW axial trend of axes. The spread in the orientations of the foliations and lineations (Fig. 3.6a) could be an effect of F_3 folding.

3.2.2 Regional Variation in the Orientation of Fold Axes and Axial Planes

Early folds (F_1-F_2): The axes of most of the early folds are gently plunging approximately towards east (Fig. 3.6b). The spread in the orientation of the early fold is due to (i) F_1 and F_2 are not strictly coaxial and (ii) the primary spread is accentuated by superposition of the late folds (F_3). The axial planes of the early folds defines a point maximum that gives a gently dipping ($20°/N59°$) modal early axial plane. This suggests that the early folds in large-scale are tight to isoclinal, recumbent to gently plunging reclined/inclined with gentle plunge towards east.

30

Folds in shear zones: It has been mentioned earlier (section 3.1.2) that the two carbonaceous bands represents the most intensely deformed shear zones. The axial planes of the majority of folds in the shear zones have gentle dip. However, there is a wide scattering from this orientation (Fig. 3.6c). The hinge lines of these folds in general have gentle plunge but the variation in trend is extreme. With increasing shear strain the axial planes of folds should become subparallel to the plane of shear and the hinge lines should rotate towards the shear direction (Ramsay & Graham 1970; Ramsay 1980; Ramsay & Huber 1983). In this situation the fold axes should have a constant orientation. But Dennis and Secor (1987, 1990) have shown that in the shear zones the hinge lines of the crenulations may be perpendicular, parallel or oblique to the shear direction. Therefore, in a progressive shear, folds developing successively may have wide variation in trend. Some of the folds in shear zones are early folds (F_1-F_2). Rotation of the hinge lines of these folds may have also caused this spread.

3.2.3 Large-scale Thrusting

In the Simla-Chur peak area Pilgrim and West (1928) recognized two thrusts, viz., the Chail thrust and the Jutogh thrust on the basis of an assumed stratigraphic sequence. The Chail thrust separates the low-grade metamorphic rocks of the Chail Formation from the underlying sedimentary rocks of the LHZ. The Chail Formation in turn is separated from the overlying medium grade rocks of the Jutogh Group by the Jutogh thrust. These two thrust sheets, viz., the Jutogh thrust sheet and the Chail thrust sheet, have subsequently been recognized and mapped in much of the western Himalaya Virdi 1979, 1981; Thakur 1980; Srikantia

& Bhargava 1985).

The Chail thrust is not studied in detail here but a critical cross checking of the evidence given by the previous workers supports the presence of the Chail thrust.

In addition to the Jutogh thrust, well-established in the Simla area (Naha & Ray 1971), two new thrusts, viz., the Rajgarh thrust and the Chur thrust, have been recognized in the Jutogh Group. The Jutogh thrust is marked by the lower carbonaceous schist band as was originally suggested by Pilgrim and West (1928). The upper carbonaceous schist band marks the Rajgarh thrust and the contact between the Chur granite and the Jutogh mica schists marks the Chur thrust.

Jutogh Thrust: At the contact between the phyllites of the Chail Formation and the lower carbonaceous band of the Jutogh Group mark a significant break in the metamorphic grade. The lower carbonaceous schist contains both biotite and garnet porphyroblasts. Garnet is totally absent in the rocks of the Chail Formation. Except in a small area southeast of Haripurdhar biotite is also absent in the Chail phyllites. Chlorite and sericite are the most common minerals in these rocks. The biotite zone of the Barrovian sequence is therefore, missing, or truncated at the Jutogh-Chail contact.

The lower carbonaceous schist band shows the effect of intense ductile shearing. In this rock type the penetrative cleavage in a majority of the instances is a mylonitic foliation. Folds of different generations have been produced on the mylonitic foliation during the course of a progressive ductile shearing. The rocks adjacent to lower carbonaceous band are also mylonitised but intensity of the mylonitisation in general, decreases away from the lower carbonaceous band.

The F_1 folds are common in both the Chail and the Jutogh rocks. But the folds of the second generation (F_2) are absent in the Chail Formation. This suggests a structural discordance between the two rock groups. Further, this structural discordance also suggests that the pre-ductile shearing (i.e. early) deformations in these two rock groups are possibly unrelated.

Although the contact of the carbonaceous band with the adjacent rocks are parallel to the foliations, at some of the exposures the s-surfaces are truncated by the contact.

Small-scale thrusts are very common in the lower carbonaceous band and the adjacent rock types. They are rare away from the lower carbonaceous band. These thrusts sometimes reverse the order of occurrence of the rocks.

Rajgarh Thrust: The evidences shown for the Jutogh thrust are also common for Rajgarh thrust in many respects. The rock type, the effect of ductile shearing (mylonitisation) and small scale thrusting have been observed in both the carbonaceous bands. There is also a distinct structural and metamorphic discordance across the upper carbonaceous band.

Staurolite is present in the mica schists occurring just above the upper carbonaceous schist. This mineral has never been observed in the pelitic layers occurring within the Jutogh quartzite. The upper carbonaceous band, therefore, marks a transition from the garnet zone to the staurolite. Further, staurolite is very profusely developed in the mica schist in the western part but is rarely seen in the mica schists in the eastern part. This tentatively suggest that garnet-staurolite isograd is truncated by the upper carbonaceous band. However, since formation of

staurolite requires a restricted bulk chemistry no attempt has been made to draw this isograd.

The detailed microstructural studies indicate that the fabric development during ductile shearing is much more evident in Jutogh quartzite than in the Jutogh mica schists. The Jutogh quartzite as a whole may be considered as blastomylonite. The early fabrics are more commonly preserved in the Jutogh mica schists.

The most dramatic example of structural discontinuity is seen in the Rajgarh area where the lower and upper carbonaceous bands are not physically connected. Moreover, this area do not locate the hinge zone of a large isosclinal recumbent fold whose two limbs are supposedly represented by the two carbonaceous bands (Pilgrim & West 1928; Kanwar & Singh 1979). In normal tectonostratigraphic sequence, the upper carbonaceous schist is overlain by the mica schist and underlain by the quartzite which in turn in underlain by the lower carbonaceous schist and Chail phyllite respectively (Fig. 2.1). The occurrence of the upper carbonaceous schist over the Chail phyllite in the west of Rajgarh and discontinuous band of lower carbonaceous schist indicate a major structural discontinuity (Fig. 3.7). The geological cross section along NW-SE direction shows the truncation of the Jutogh thrust at the base of upper carbonaceous band (Fig. 3.8).

Chur Thrust: The central part of the Chur granite is coarse grained, massive and porphyritic in nature with randomly oriented K-feldspar phenocrysts (Fig. 3.9a) but it is strongly foliated near the margin (Fig. 3.9b,c). At the granite contact the K-feldspar megacrysts are broken into smaller fragments, become elliptical or lensoid-shaped giving rise to augen structure (Fig. 3.9b). In the foliated rocks the feldspar megacrysts

gradually diminishes with a well developed foliation traced by recrystallised quartz ribbons resulting typical granite mylonite (Figs. 3.9d). In the very well foliated granite, megacrysts are sometimes difficult to recognise and it looks like ultramylonite (Fig. 3.9c). The gradation from massive to foliated granite is perfectly gradual. But the effect of mylonitisation varies from protomylonite through mylonite to ultramylonite at different places all along the contact of the Chur granite.

The granite overlies the Jutogh mica schist with a razor-sharp contact. The contact and the foliation in both the granite and the adjacent mica schist are all strictly parallel. Nowhere any cross cutting relationship or apophysis has ever been observed from outcrop to map scale. The contact is always conformable with local foliation planes. Extensive petrographic studies of the surrounding mica schist of the Chur granite shows no contact metamorphic effect on the country rocks. Neither hornfelsic texture nor andalusite or cordierite have been observed. The mica schist adjacent to the granite contains kyanite and sillimanite indicating regional metamorphism.

All these features suggest that the two carbonaceous bands and the contact of the granite represent three separate thrusts within the Jutogh Group. Since the Jutogh thrust is truncated by the Rajgarh thrust, the former is older than the Rajgarh thrust. Thus around the Chur peak four thrusts can be recognized, viz. the Chur thrust, the Rajgarh thrust, the Jutogh thrust and the Chail thrust (Fig. 3.10). A general ENE-WSW cross-sections (Fig. 3.11) through Chur peak show that this area can be considered to consist of four thin imbricated thrust sheets. The shearing movement responsible for this was initially ductile as indicated by abundant meso-structures typically found in ductile shear zones. The

rocks deformed by early ductile shearing were later sliced up through brittle thrusts.

3.2.4 Map Pattern

The highest elevation in this area is around the Chur peak from where the topographic surface slopes away in all directions giving an inverted bowl type of topography. Except in the northeastern part of the area, the map pattern of all the lithological units are approximately semicircular about the Chur peak (Fig. 2.1). Each rock type is also more or less restricted to a particular attitude. From the area around the Chur peak a ridge extends in the northeasterly direction and the Jutogh/Chail rocks open out instead of closing giving rise to the half-klippe type outcrop pattern. This map pattern apparently suggests flat-lying or gently dipping s-surfaces in most of the area. The two carbonaceous schist bands occuring at two topographic levels were taken to represent two limbs of a huge recumbent fold. Although recumbent to gently plunging reclined folds are legion throughout the area no hinge zone corresponding to large scale recumbent fold is present. Further, the two carbonaceous schist bands have their separate lithotectonic statures. Within the Jutogh Group the thrust slices separated by the Jutogh thrust, Rajgarh thrust and the Chur thrust are structurally and topographically lying over each other. Thus the Chur thrust has the highest status in this area (Fig. 3.11).

FIGURES
CHAPTER - 3

FIGURE 3.1 EARLY FOLDS

(a). F_1 isoclinal recumbent fold defined by quartzo-feldspathic vein in quartz-biotite gneiss. Axial planar cleavage (S_1) cuts across the hinge. The fold show very high amplitude/wavelength ratio. Looking N25°. Location: Didag.

(b). S_1 cleavage in mica schist which shows uniformly distributed mica flakes. Base: 2 mm. Plane-polarized light. Location: 4 Km E of Pulwal.

(c). An asymmetric, gently-plunging, isoclinal reclined fold (F_2) defined by S_1 schistosity in mica schist. Looking N130°. Location: Nohra.

(d). Type-3 interference pattern due to coaxial superposition of F_2 folding on F_1 fold in impure marble. The F_1 fold is isoclinal whereas the F_2 fold is very tight. Looking: N16°. Location: 6 km SW of Nohra.
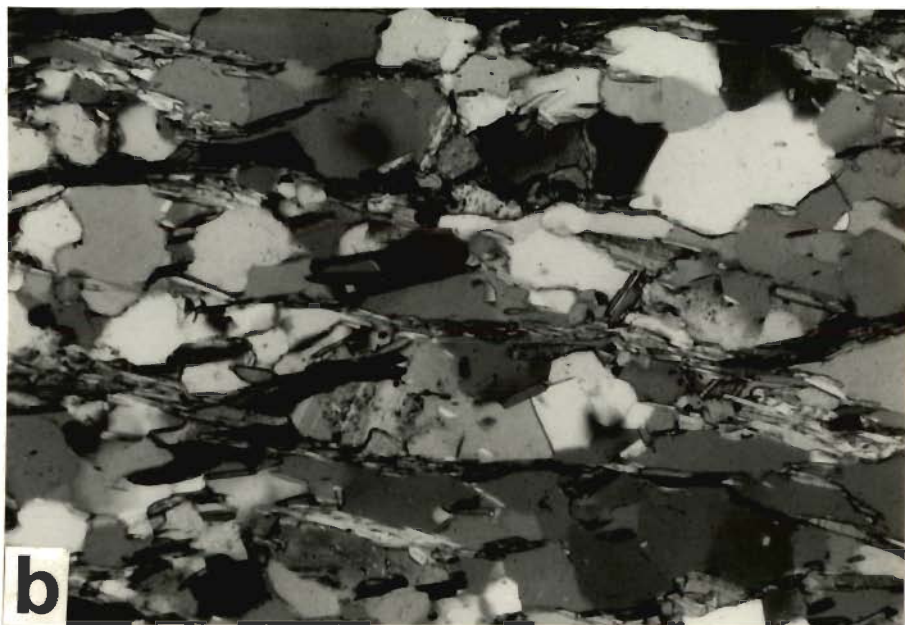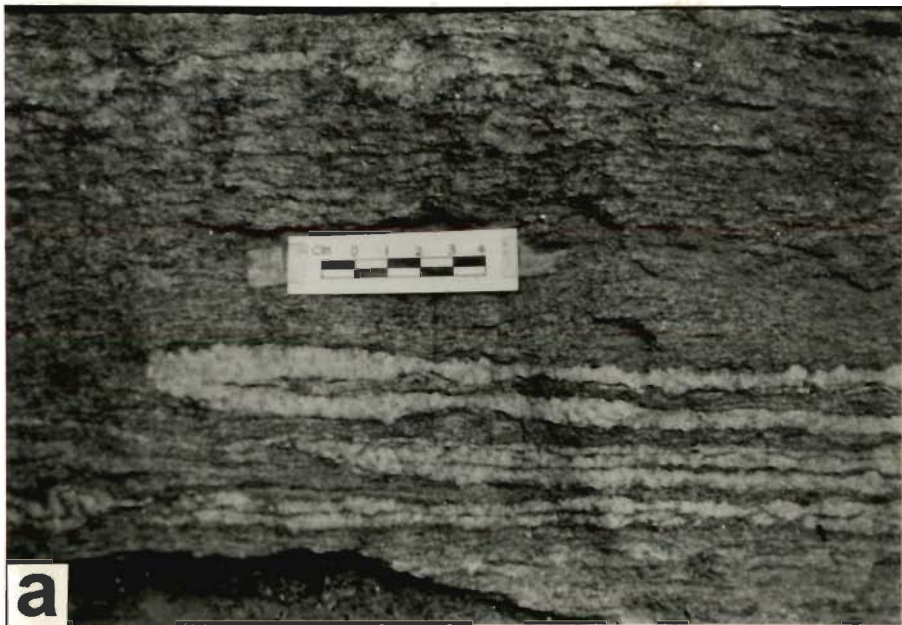
Fig. 3.1

FIGURE 3.2: MYLONITES AND MYLONITIC FOLIATION

(a). Protomylonite in quartzite showing original quartz grains with serrated grain boundaries and strong undulose extinction. Recrystallization and subgrain developement along the grain boundaries give core-and-mantle (e.g. mortar) texture. The rock is devoid of any cleavage surface. Base: 1.3 mm. Crossed nicols. Location: Bogdhar.

(b). Protomylonite in mica schist with surviving quartz porphyroclasts in a very fine-grained recrystallized matrix. Base: 6.5 mm. Crossed nicols. Location: 4 km W of Didag.

(c). Mica schist orthomylonite showing development of mylonitic foliation traced by quartz ribbons with few surviving quartz porphyroclasts. Base: 2 mm. Oblique nicols. Location: Thandidhar.

(d). Quartz-ribbon mylonite with very well developed mylonitic foliation in mica schist ultramylonite. Base: 8 mm. Plane-polarized light. Location: 4 km W of Didag.
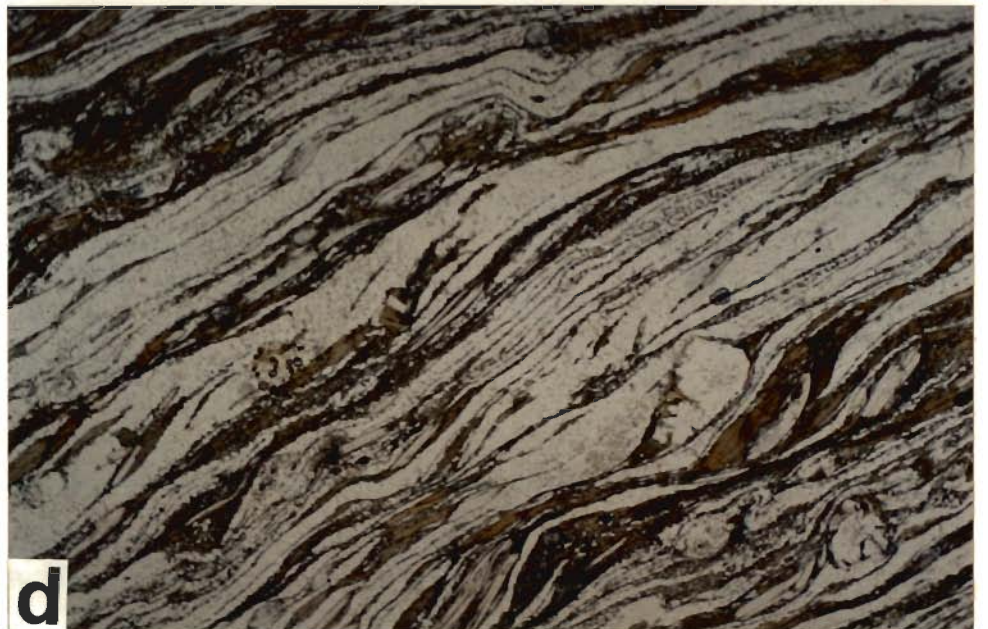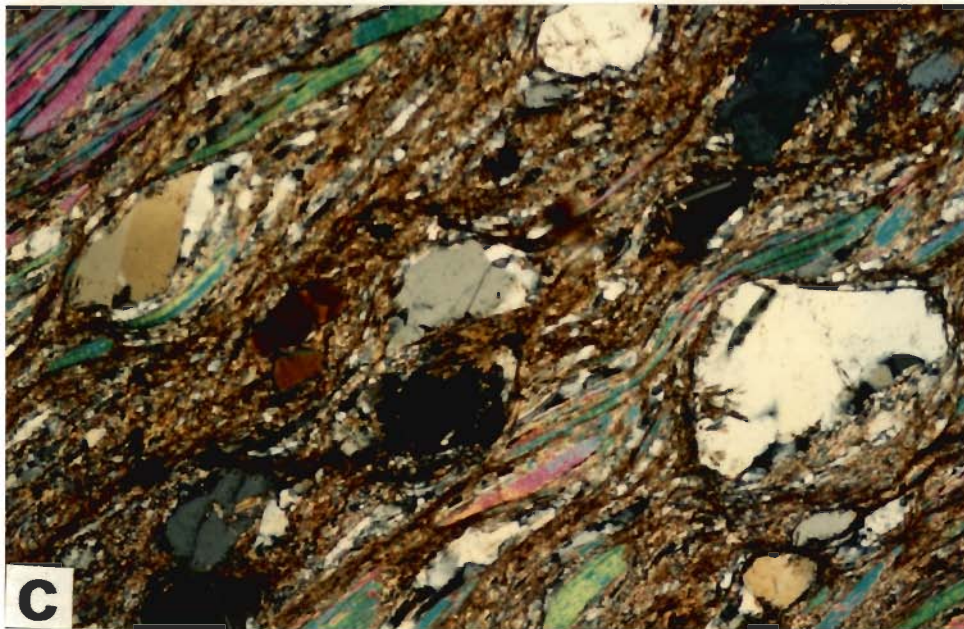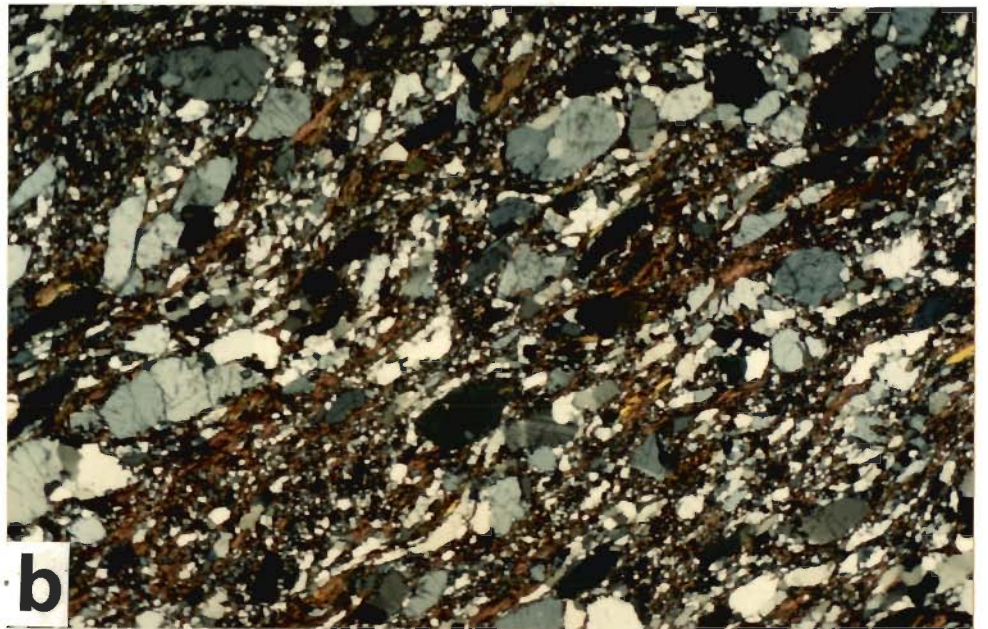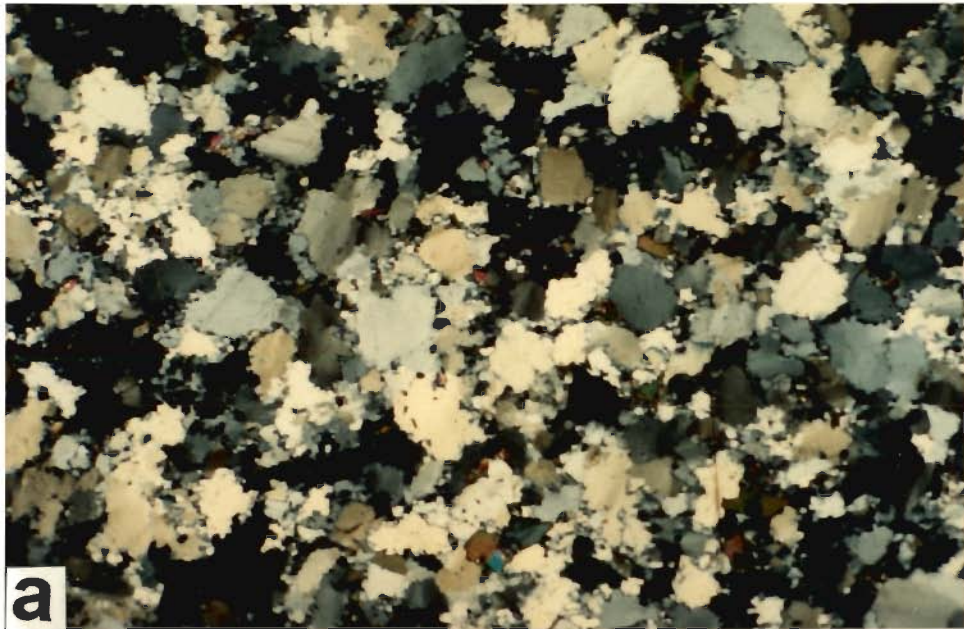
Fig.3.2

FIGURE 3.3: COMPRESSIONAL STRUCTURES IN THE SHEAR ZONES

(a). S-C structure in lower carbonaceous band. Looking N190°. Location: 2 km E of Kot.

(b). S-C structure in lower carbonaceous band in thin section   scale. Note that the s-surfaces are defined by a mylonitic fliation which sigmoidally curve into C-surfaces along which no new fabric has developed. Base: 8 mm. Oblique nicols. Location: 1 Km SE of Habban.

(c). The mylonitic folation is asymmetrically crenulated along with the ptygmatic fold traced by quartz vein in mylonitised mica schist. Looking N260°. Location: Didag.

(d). Asymmetric kinks on mylonitic foliation in mica schist at the contact with the granite. Looking N60°. Location: 1.5 Km E of Chogtali.
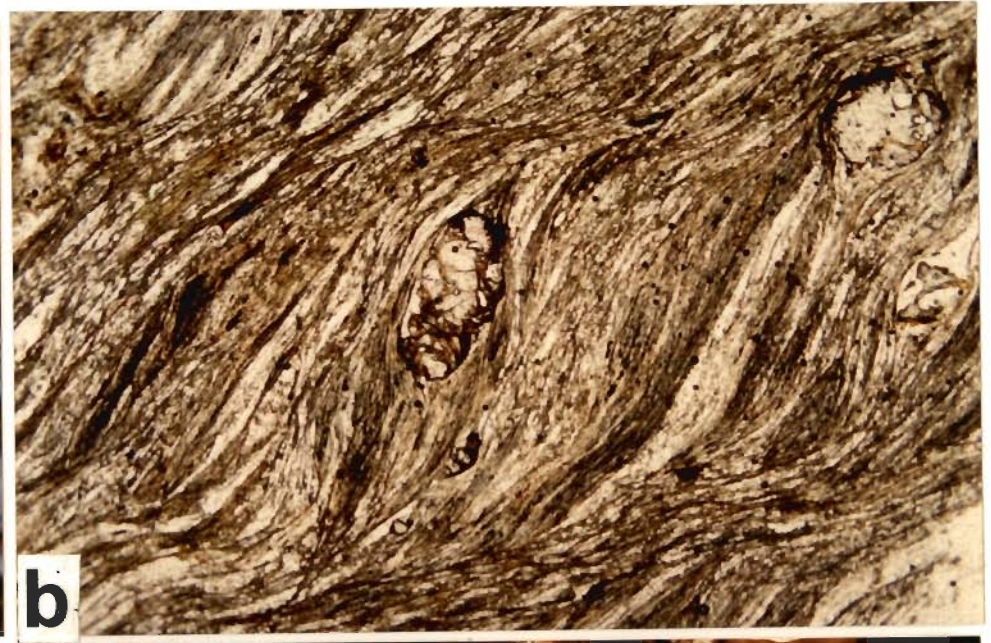
Fig.3.3

FIGURE 3.4: COMPRESSIONAL AND EXTENSIONAL STRUCTURES IN THE SHEAR ZONE

(a). Very tight fold in mica schst traced by recrystallised quartz ribbons. Note that the hinge is thickened and limbs are thinned. Base: 5.2mm. Oblique nicols. Location: Phagu.

(b). Crenulation fold on mylonitic foliation (quartz ribbon) in upper carbonaceous schist. Kink bands developed in the micaceous layers are axial planar to the crenulations. Base: 2mm. Plain polarised light. Location: 1.5 Km NNW of Bharari.

(c). Sigmoidally curved quartz ribbons within two subparallel extension crenulation cleavage surfaces in upper carbonaceous schist. Base: 2 mm. Oblique nicols. Location: 2 Km Sw of Haripurdhar.

(d). Rotated boudins traced by quartz vein in upper carbonaceous band. A shear foliation continues through the necking point. Location: 6 Km NE of Rajgarh.
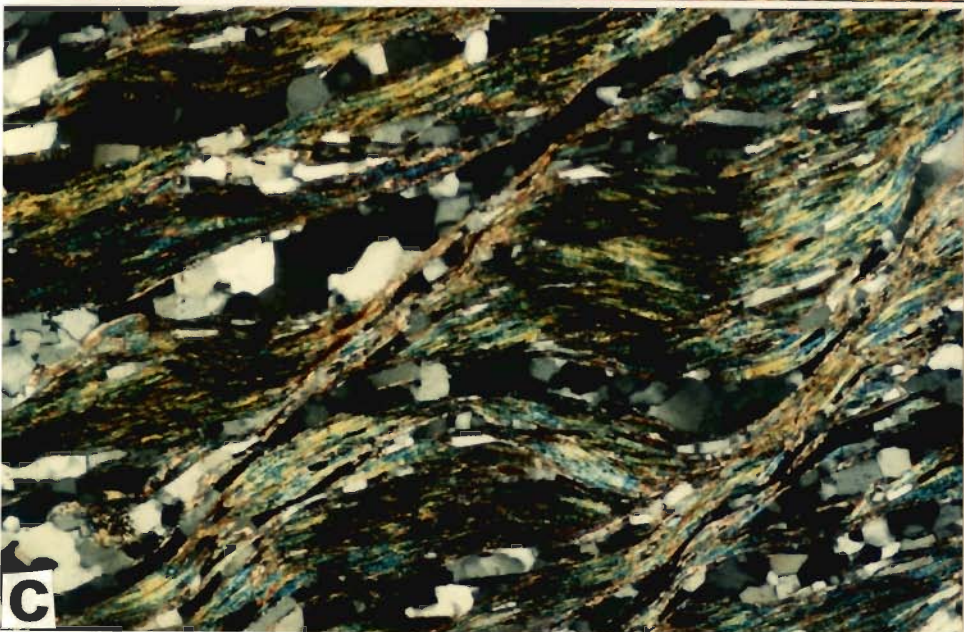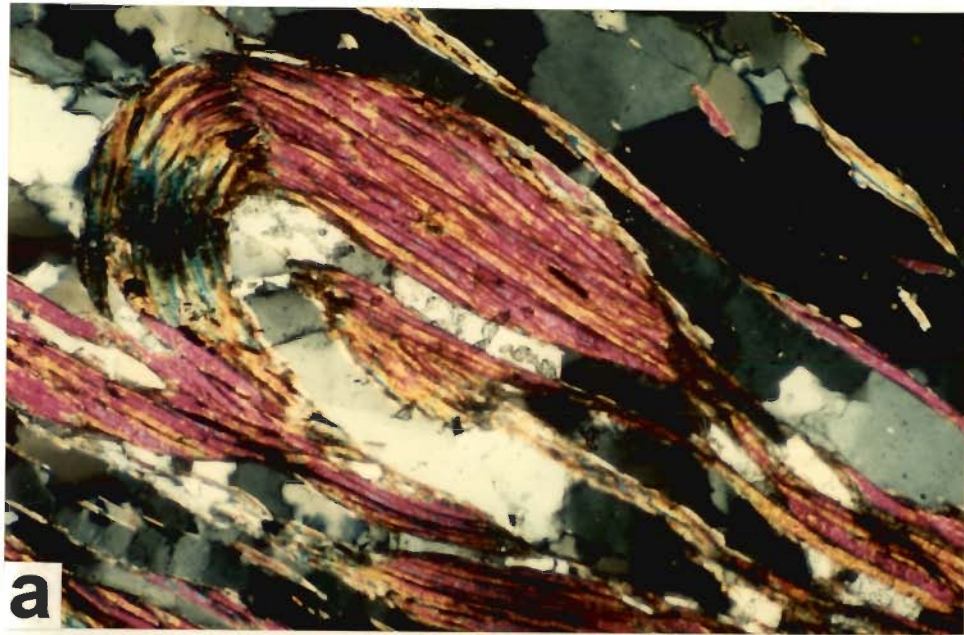
Fig.3.4

FIGURE 3.5: FOLD INTERFERENCE AND THRUST IMBRICATION IN SHEAR ZONES AND LATE STRUCTURES

(a). Elliptical cross-sectional view of a sheath fold in highly sheared mica schist. just below the granite contact. Looking N90°. Location: Nohra.

(b). Isoclinally folded quartz ribbon in mica schist refolded into open folds giving type-3 interference pattern. Note crenulations in mica-rich portions with axial planes parallel to both the early (bold line) and late (dashed line) axial planes. Base: 5.2 mm. Crossed nocols. Location: Churwadhar.

(c). Thrust imbrication in outcrop scale in quartzite at the contact with upper carbonaceous schist. The more prominant thrust planes have been emphasised. Looking N38°. Location: Churwadhar.

(d). Normal sense of displacement along steeply dipping fault planes in amphibolite occurring within mica schist. Looking N290°. Location: 2 Km W of Didag.
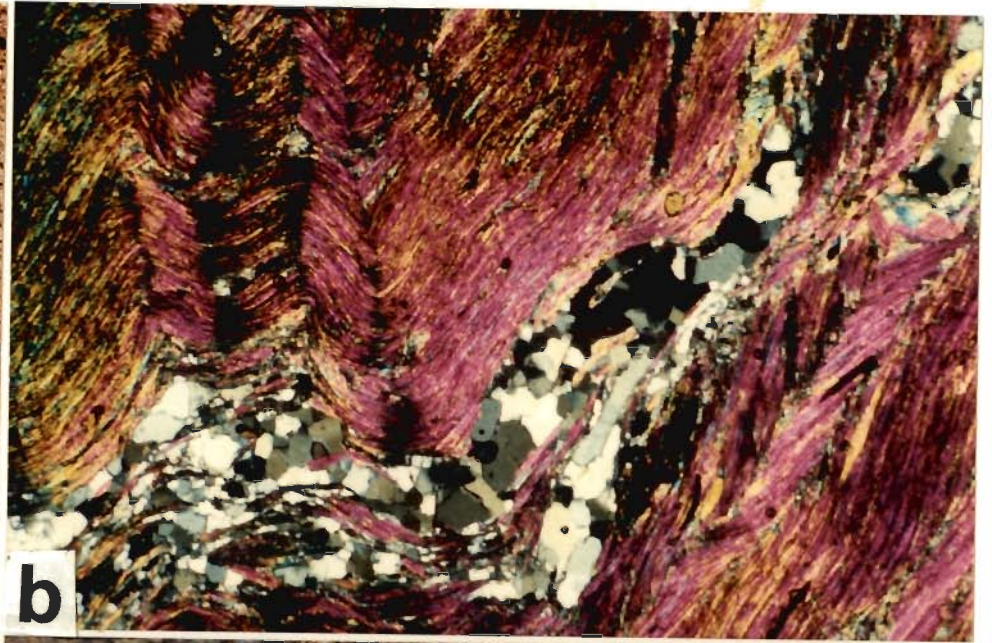
Fig.3.5

FIGURE 3.6:STEREOPLOTS OF FOLIATION AND LINEATION, AXIAL PLANES AND AXES OF EARLY FOLDS AND FOLDS IN SHEAR ZONES

(a). Synoptic stereograms of foliations (continuous contours) and lineations (dashed contours). Continuous cntours: 2086 poles to foliation, contours: 0.5-1-3-5-7% per 1% area. Dashed contours: 677 lineations, contours: 1-3-5-10-13% per 1% area.

(b). Orientations of small-scale early folds (F_1-F_2). Continuous contours: 139 poles to early (F_1-F_2) axial planes, contours: 1-3-5-8-11% per 1% area. Dashed contours: 185 early (F_1-F_2) fold axes, contours: 0.6-3-6-9% per 1% area.

(c). Synoptic stereogram for the orientatins of axial planes and axes of small scale folds in the two carbonaceouus bands. ~~Open circles:~~Dots: fold axes. Continuous contours: 217 poles of axial planes; contours: 0.5-2-3-5-6% per 1% area.

a

Modal
foliation

N

b

N

c
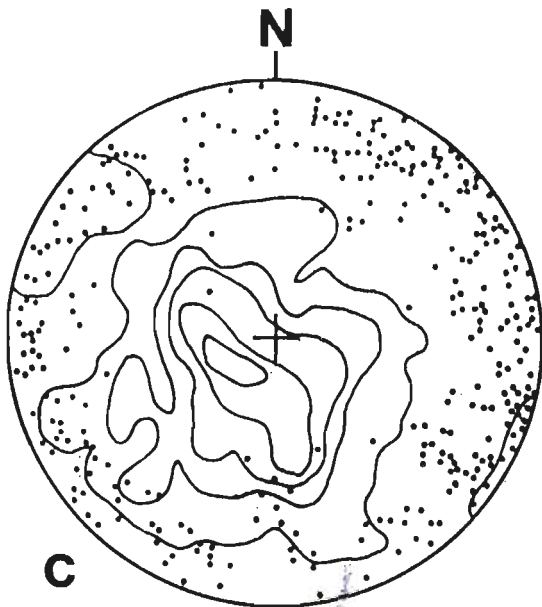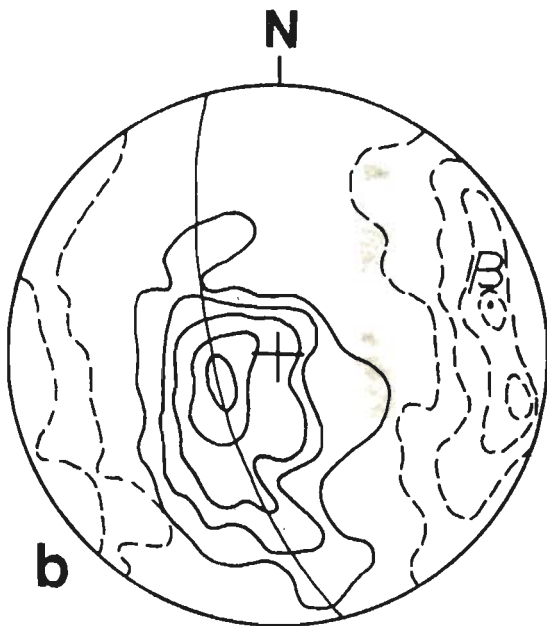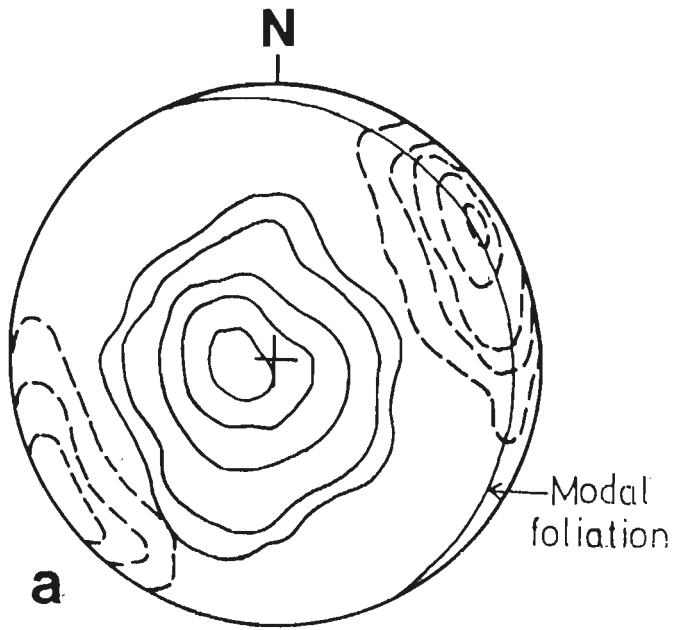
Fig. 3.6

FIGURE 3.7: Geological map around Rajgarh showing the discontinuous band of lower carbonaceous schist in the SW of Rajgarh. The upper carbonaceous schist is directly lying over the Chail phyllite in the west of Rajgah.
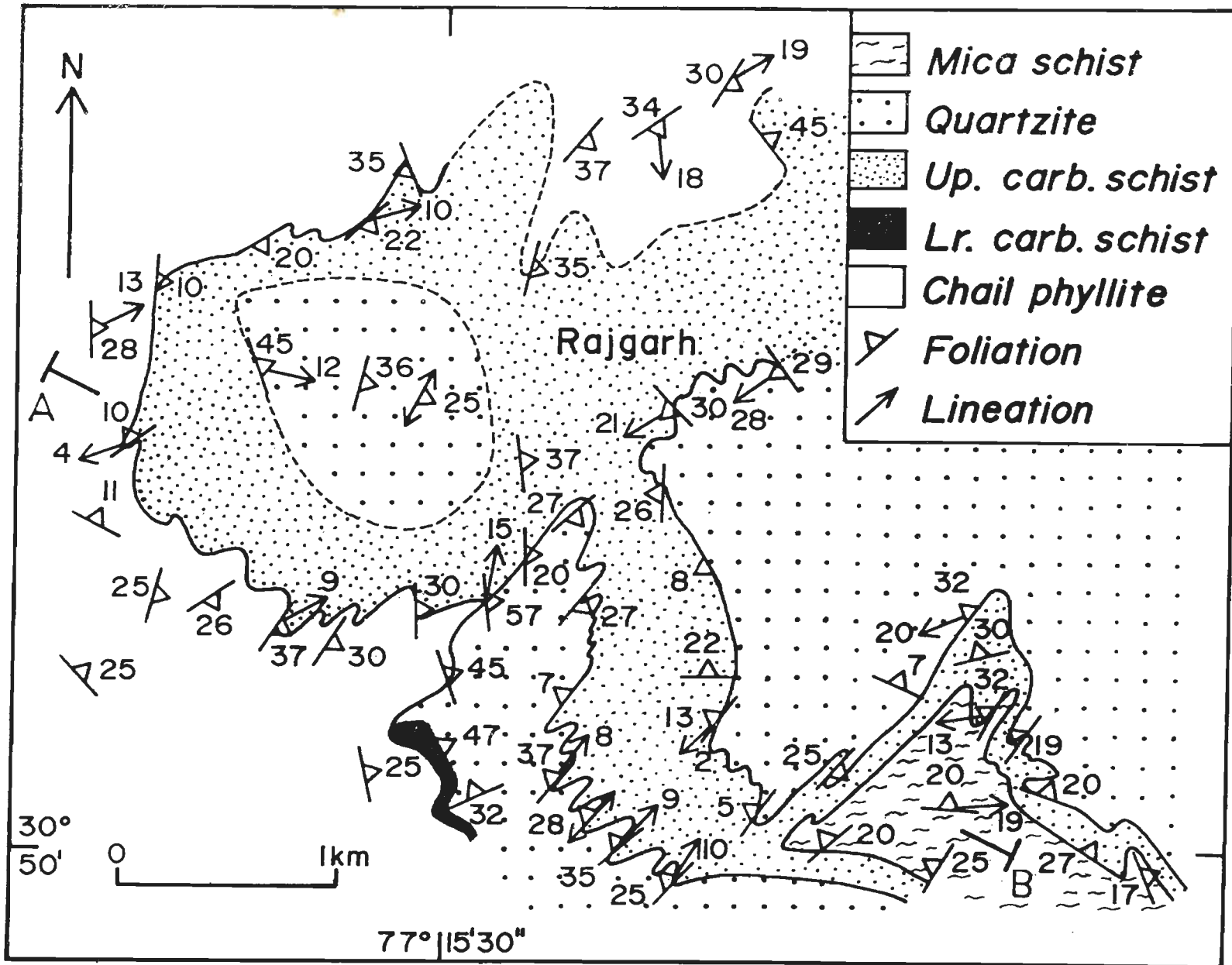
Fig. 3.7

FIGURE 3.8: Geological cross section along A-B (see Fig. 3.7) showing truncation of Jutogh thrust (JT) with the Rajgarh thrust (RT). Symbols as in Fig. 3.7.
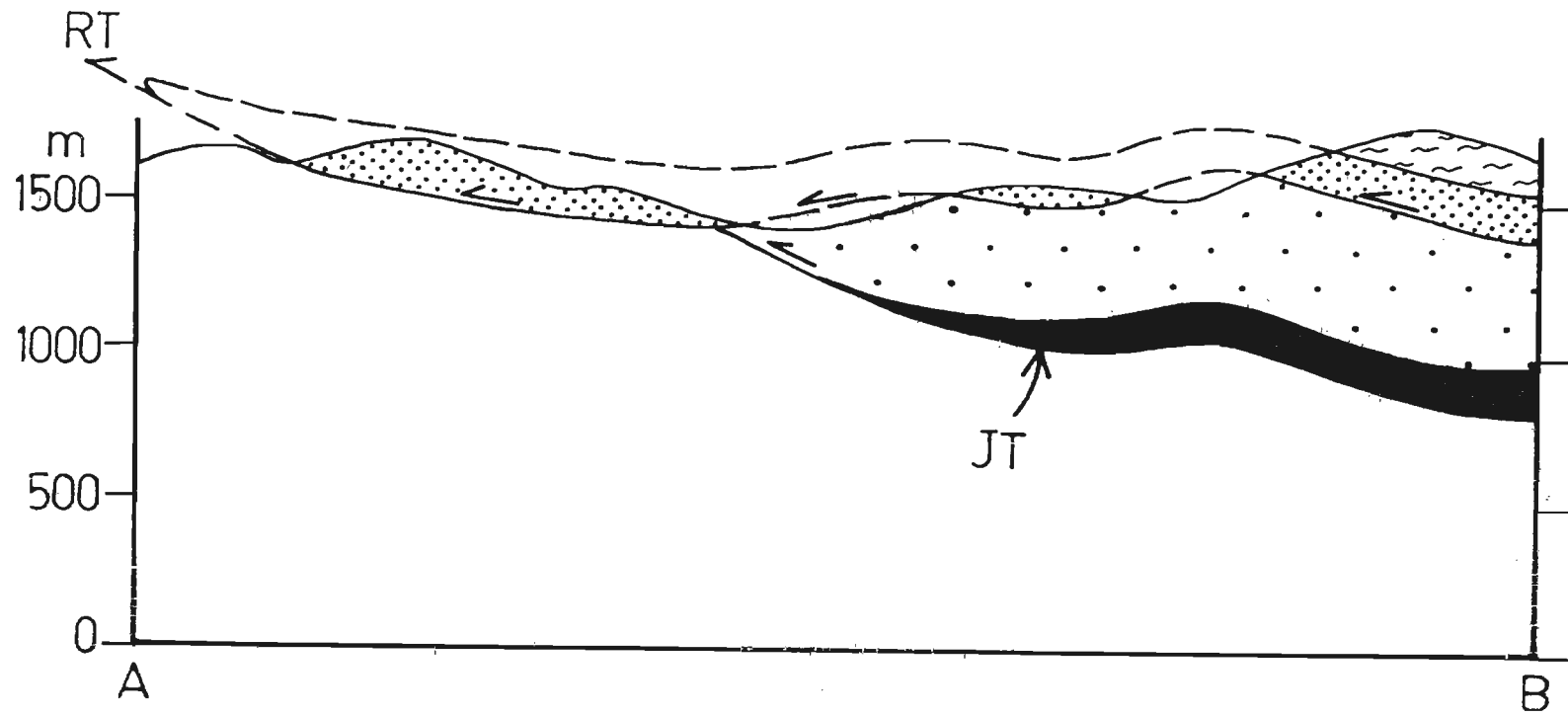
Fig. 3.8

FIGURE 3.9:GRANITE IN OUTCROP TO THIN SECTION SCALE

(a). Undeformed granite with large randomly oriented K-feldspar megacrysts in a coarse grained matrix defining porphyritic texture. Location: Chur peak.

(b). Deformed granite with preferred dimensional orientational orientation of elliptical K-feldspar megacrysts parallel to the mylonitic foliation. Location: Chogtali.

(c).Granite ultramylonite showing no surviving megacrysts within the matrix. Location: 2 Km east of Nohra.

(d).Mylonitic foliation defined by recrystallised quartz and mica (dark ribbons). Base: 5.2 mm. Crossed nicols. Location: 1 Km NE of Chogtali.

Fig.3.9

FIGURE 3.10 Geological map around the Chur peak showing the locatons of four thrust planes. CP=Chail Phyllite; LCS= Lower Carbonaceous Schist; Q= Quartzite; UPS= Upper Carboneceous Schist; MS= Mica Schist; G= Granite
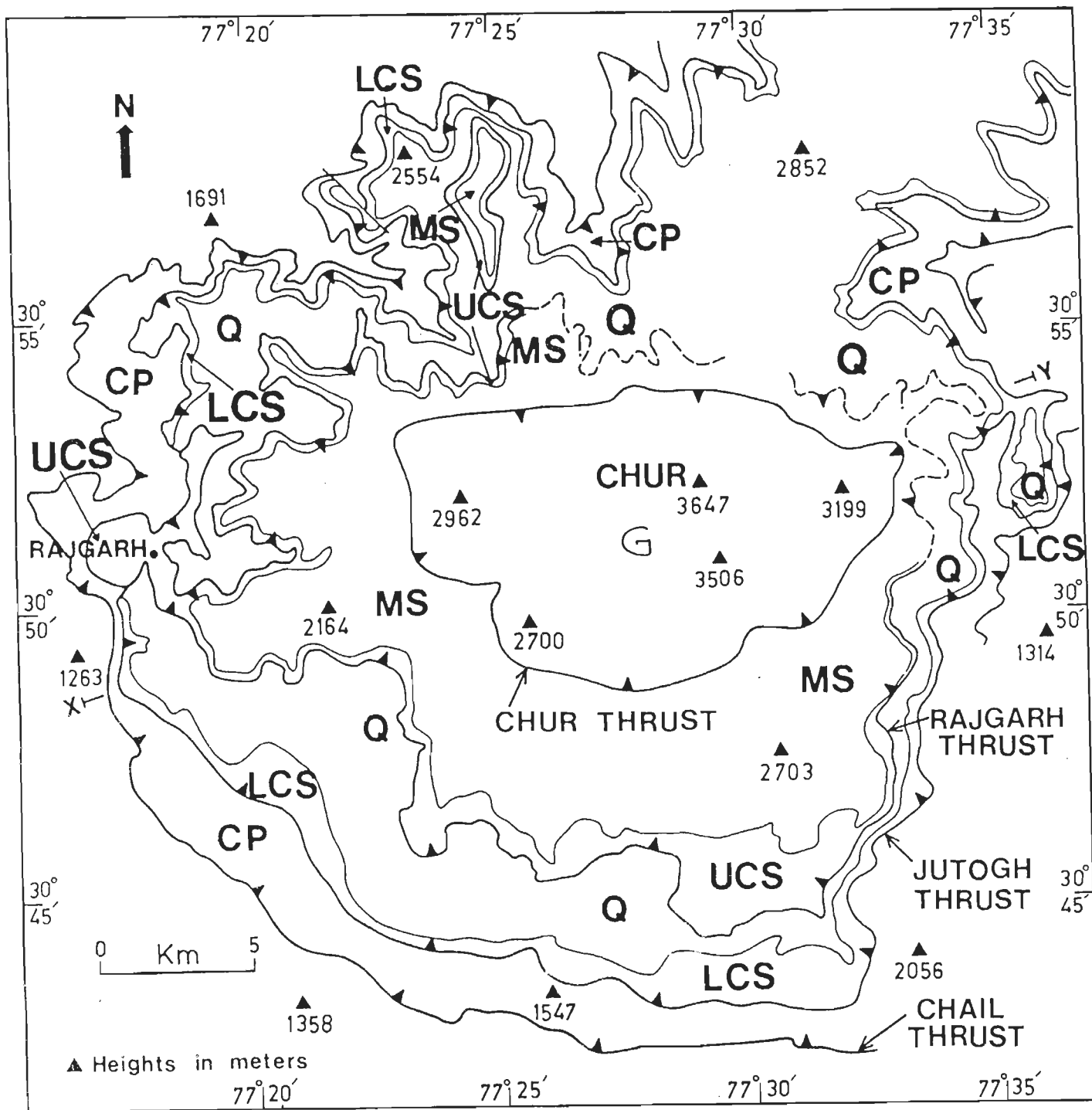
Fig.3.10

FIGURE 3.11 Generalised cross section along X-Y (Fig. 3.10) through the Chur peak showing imbrication of four thin thrust sheets. G: Chur granite; MS: Mica schist; Q: Quartzite; CP: Chail phyllite; LH: Lesser Himalaya Zone (LHZ).
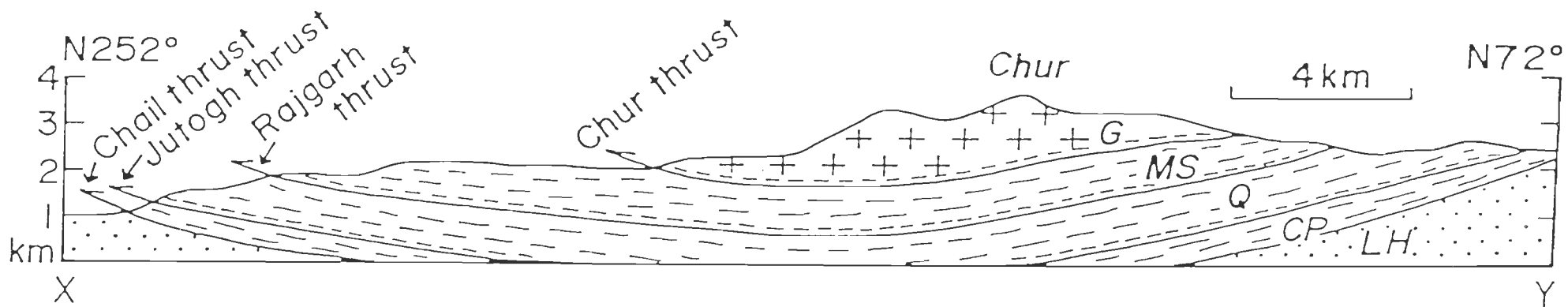
Fig.3.11

CHAPTER - 4
MICROSTRUCTURE AND TEXTURE

4.1 INTRODUCTION

The relationships between porphyroblast and matrix foliation have been used by many workers to decipher the temporal relationship between the episodes of metamorphism and deformation (Zwart 1962; Spry 1969). Excellent review on this subject has also been given by Vernon (1978, 1989).

The foliation present in the matrix is usually designated as S_e (e for external) and foliation present within the porphyroblast traced by oriented inclusion trails is referred to as S_i (i for internal). It is of paramount importance to characterize the external foliation (S_e) when a porphyroblast is designated as "pre-tectonic", "syn-tectonic" or "post-tectonic" it should be clearly stated to which fabric such relation is implied (Vernon 1978). In Chapter 3 it has been shown that there are three types of foliation (i.e. S_e) viz., S_1, S_2 and S_m related to F_1 folding, F_2 folding and ductile shearing respectively in this area. The S_m includes several generations of mylonitic foliations developed during a single progressive ductile shearing. Some of the important criteria used in this study have been summarized in Fig.4.1.

The temporal relationship between porphyroblasts and the matrix foliation has been much debated where the S_e or axial planes of folds swerve around porphyroblasts. This particular relationship has a critical importance in this area. Some workers (e.g. Misch 1971, 1972) suggest that matrix foliation is pushed apart by the gradually growing crystals which implies that such porphyroblasts are post-tectonic with respect to

matrix foliation. According to other group of workers the growth of such porphyroblasts is prior to the deformation which produced the foliation in the matrix i.e. S_e (Zwart 1962). This view is followed here for the following reasons.

(1) Perpendicular to the foliated surface, the compressive stress is maximum. Therefore, it is unreasonable to predict that syn-tectonic porphyroblast may grow and simultaneously pushesapart the foliation surfaces in that direction where compressive normal stress is maximum (Vernon 1978).

(2) The oriented internal foliations (S_i) (sometimes of several generations, e.g. Bell & Jhonson 1989) within the porphyroblasts is generally regarded as the incorporation of matrix foliation during the growth of porphyroblasts. If a growing prophyroblast pushes apart the S_e during growth the S_i should be rare.

(3) Numerical modelling (Ghosh 1977; Ghosh 1975; Ghosh & Ramberg 1976) shows that drag patterns in a deforming matrix swerve around a preexisting rigid inclusion.

(4) Another very convincing evidence comes from the Chur granite. The granite is strongly mylonitinised near the Chur thrust where augen-shaped K-feldspar megacrysts occur in a matrix that shows very well developed mylonitic foliation. The mylonitic foliation in the granite mylonite are always strongly deflected around the megacryst. Of course there is no doubt that the megacrysts are pre-kinematic with respect to the formation of the mylonitic foliation. Therefore, porphyroblast showing similar textural relationship should be treated as pre-kinematic with respect to the development of S_e.

4.2 MINERAL FORMATION IN RELATION TO DEFORMATION EPISODES

4.2.1 Chlorite

Some of the chlorite grains occur as flakes. They are evenly dispersed and aligned parallel to the S_1 foliation which suggests that they have formed syn-tectonically with respect to the S_1. Post-F_1 chlorites are those which overgrew and incorporated S_1 cleavage where S_i and S_e ($=S_1$) are continuous (Fig.4.2a,b). Where S_1 is involved in F_2 crenulation the S_i ($=S_1$) is either straight (Fig.4.2a) or crenulated (Fig.4.2b). Strong undulose extinction and kinked cleavage traces in these chlorite porphyroblasts suggest that they have been deformed by F_2 folding. However, in this case the crystallization does not probably outlast the second deformation.

Post-F_1 chlorite porphyroblasts are present as retrogression product from garnets which sometimes occur as relicts around which chlorite porphyroblasts grow (Fig.4.2c). At other places garnets in garnet grades are completely retrograded which make a "pool" of fibrous chlorite. In the staurolite grade retrograde chlorite is formed from staurolite, garnet and biotite, though the direct temporal relationship is not clear. However, since the staurolite is syn-tectonic with respect to post-F_1 (discussed later) and kyanite, sillimanite have been crystallized after that it may be possible that the crystallization of retrograde chlorites in staurolite grade started during pre-F_2 and outlasted it.

During ductile shearing the chlorites have been formed as relatively inclusion-free and are oriented parallel to the mylonitic foliation (S_m). It suggests the syn-tectonic growth of chlorite with respect to mylonitic foliation. But some of these grains show evidence of extensive post-

crystalline deformation and could also be relicts of syn-F_1 chlorite grains. Chlorite porphyroblasts in ductile shear zone also show that the S_i is continuous with S_e (Fig.4.2d). Typical "mica fish" structures are developed by some of those chlorites (Fig.4.3a). In some of the porphyroblasts the straight S_i are at high angle to and abut against the S_e (Fig.4.3b) indicating that they are pre-tectonic to the matrix foliation. But both the S_i and S_e are mylonitic foliation. The early mylonitic foliation in the matrix (now preserved as S_i) has been completely obliterated by a new mylonitic folation (S_e) which has been formed at a late stage of progressive shearing. In the pressure shadow zone against these porphyroblasts tiny flaky chlorites are oriented parallel to S_e ($=S_m$) (Fig.4.3c). These are syn-tectonic with respect to the mylonitic foliation present as S_e. Chlorites in the mylonitic matrix have also been crystallized along the S-fabric (Fig.4.3d). It suggests that the growth of these chlorites were at an early stage of ductile shearing.

In summary, the chlorite started forming syn-tectonically with respect to F_1 but ceased to grow before kyanite and sillimanite appeared. It again continued to grow during F_2 deformation and did not outlast it. Further, during ductile shearing the crystallization of the chlorite grains was extensive.

4.2.2 Biotite

Biotite is absent in the Chail Formation except at a small locality near Haripurdhar. It makes its first appearance at the Jutogh thrust and is present in all the rock types of the Jutogh Group and Chur granite.

Biotite has strong preferred dimensional orientations and define the S_1 cleavage suggesting that biotites are syn-tectonic with respect to the F_1

deformation. At some places in garnet grade cleavage traces of biotite porphyroblasts are at high angle to the S_1 (Fig.4.4a,b). Some of the biotite flakes are preserved in the Q-domain of the later cleavage (Fig.4.4c). These biotites are pretectonic to the F_1 deformation. Straight inclusions trails in some of these porphyroblasts are continuous with S_e ($=S_1$). These are late to post-tectonic with respect to F_1. At the hinge zone of F_2 crenulation biotites show signatures of post-crystalline deformation with kinking, bending and undulose extinction. These biotites are pre-tectonic with reference to F_2. Some of these biotites are however, sharply crystallized and S_2 crenulation cleavage is sometimes defined by these biotite flakes. Therefore the crystallization of biotite started growing syn-tectonically with F_1 but outlasted the F_2 deformation.

The biotites in the ductile shear zones show strong post-crystalline deformation. In such cases biotite porphyroblasts are broken into small pieces, recrystallized and distributed along the mylonitic foliation. Also the recrystallization of biotite occurred during ductile shearing. Some biotite porphyroblasts are oriented randomly in a ductile shear zone. Some of these biotites are deformed whereas the others are undeformed. The deformed grains indicate that they crystallized at the early stage of the ductile shearing but deformed during late stage of ductile shearing. The undeformed variety indicates that they have crystallized during the late stage of ductile shearing. Therefore recrystallization of biotite has taken place syn-tectonically with the progressive ductile shearing. Sometimes in ductile shear zone retrograde biotites are present near the rim of garnet porphyroblasts. These are randomly oriented and develop a "pool" of biotite flakes near garnet. These biotite have been formed during F_2 and outlasted it.

In conclusion biotite started forming during F_1 deformation and continued during F_2 outlasting the F_2 deformation. Crystallization of biotite also was present during ductile shearing at its early stage and late stage.

4.2.3 Garnet

Garnet porphyroblasts are present in all the rock types of the Jutogh Group but are completely absent in the rocks of the Chail Formation in this area. The size of garnets varies from as large as 3.5 cm to as small as 0.14 mm. The larger grains are subrounded to irregular in shape and smaller grains on the other hand are polygonal (Fig.4.5b,4.6b). The inclusions within the garnet are mainly quartz and ilmenite. Quartz and ilmenite inclusions within the garnet show random orientation (Fig.4.6c) as well as preferred orientation (Fig.4.5a,4.7a-d). Some of the garnet porphyroblasts have small (as compared to the grains in the matrix) unoriented inclusions and occur in a matrix with well developed S_1 foliation suggesting pre-tectonic growth of garnet with respect to the formation of S_1 foliation. Some garnet porphyroblasts have S-shaped inclusion trails (Fig.4.5a) which are continuous with Se which is S_1 cleavage. These porphyroblasts have syn-tectonic growth with reference to F_1 deformation. In some of the larger porphyroblasts unoriented quartz inclusions are present throughout the porphyroblasts giving a skeletal appearance. The included quartz grains are usually equant and coarse. These porphyroblasts are elongated along S_1 and are sometimes fractured and boudinaged suggesting syn-tectonic growth during F_1. Garnets with inclusion rich cores and relatively inclusion free rims have been observed (Fig.4.6c;4.7a,d) in the staurolite grade suggesting the two stage growth.

The inclusions present in the garnet cores are either unoriented (Fig.4.6a), spiral shaped (Fig.4.7a,b) or straight (Fig.4.7c,d). Though the matrix foliations where these garnets are present are mylonitic, from the grain size of those inclusions and type of foliation represented by inclusion trail it appears that the cores of these garnets are early- to late-tectonic with respect to F_1 and rims possibly overgrew post-dating F_1. The almost inclusion free porphyroblasts (Fig.4.8c) and some polygonal grains (Fig.4.6b) are contemporaneous with this post-dating phase of F_1. In a few thin sections the boundary between the core zone and the rim zone in garnet is marked by inequant quartz grains (Fig.4.8a) which confirms the two stage growth of garnet porphyroblasts during regional metamorphism. These garnets are fractured in outer portion showing effect of post crystalline deformation. The axial planes of F_2 microfolds and S_2 crenulation cleavage swerve around the garnet porphyroblasts suggesting pre-tectonic crystallization with reference to F_2 (Fig.4.5c).

The mylonitic foliation invariably swerves around the garnet porphyroblasts. Nowhere, the S_i in garnet is continuous with the mylonitic foliation ($S_m = S_e$). The axial plane of an isoclinal fold traced by the quartz ribbons in ultramylonites swerves around the garnet porphyroblasts (Fig.4.6c). Microfolds defined by mylonitic foliations abut sharply against garnets. But tightness of these microfolds decreases away from the garnet porphyroblasts (Fig.4.6b). Pressure-shadow zones (Fig.4.5d) are usually present where mylonitic foliation swerves the garnet grains. Garnets are broken into pieces in ductile shear zone and strewn along the mylonitic foliations (Fig.4.6d). The garnet porphyroblasts are, therefore, completely pre-tectonic with respect to ductile shearing but syn- to post-tectonic with respect to F_1 deformation.

In addition to quartz and ilmenite garnet occasionally incorporates chlorite, staurolite and sillimanite in garnet, staurolite and sillimanite grade respectively. The chlorites present within the garnet predict the formation of garnet from chlorite (Fig.4.8d). Staurolite is present near rim of the garnet suggesting the growth of garnet in the staurolite grade at the expense of staurolite during late stage (Fig.4.9a). Also sillimanite within the garnet predict the formation of garnet in sillimanite grade (Fig.4.9b). In staurolite grade muscovite inclusion within the garnet suggest$_{\wedge}$ the muscovite involving reaction to produce garnet.

4.2.4 Staurolite

The staurolite porphyroblasts are present sporadically only in the mica schist. They are absent in all other rock types. They are more common in the western part than the rest of the mica schist unit.

Staurolite has S-shaped or straight inclusion trails (S_i) which are continuous with the S_e ($=S_1$) suggesting syn- to post-tectonic growth with respect to F_1. The axial planes of F_2 microfolds and S_2 crenulation swerves around the staurolite porphyroblasts indicating pre-tectonic growth with respect to F_2. In the ductile shear zones the mylonitic foliations invariably swerve around the staurolite porphyroblasts (Fig.4.9d;4.10a). Strong undulose extinction and fracture are present in these grains which indicates the extensive post-crystalline deformation (Fig.4.10a). They are often boudinaged, broken into small pieces and are spread along the mylonitic foliation (Fig.4.10b). In the fracture zones retrograde chlorite and biotite have been formed. All these lines of evidence suggest that the staurolite porphyroblasts are completely pre-tectonic with reference to ductile shearing. Within the staurolite

44

porphyroblasts biotite flakes are sometimes present pointing to crystallization of staurolite involving biotite consuming reaction (Fig.4.10c).

4.2.5 Kyanite and Sillimanite

Kyanite and sillimanite have been observed in a few samples collected near the Chur granite body. Owing to their restricted occurrence and small grain sizes microtextural relations of these two minerals are relatively less certain. However, both kyanite and sillimanite show strong post-crystalline deformation with respect to mylonitization. At one place kyanite blades are sufficiently large to show that mylonitic foliation swerves around the porphyroblast (Fig.4.10d) similar to garnet and staurolite porphyroblasts. Kyanite sometimes shows straight S_i ($=S_1$) traced by fine biotite flakes (Fig.4.11a). This S_i is oblique to and abuts against S_e ($=S_m$). These features, together with strong post-crystalline deformation indicate that kyanite and sillimanite are pre-tectonic with respect to the ductile shearing. Sillimanite is present in the Jutogh Group as prismatic (Fig.4.9b) as well as fibrolite variety. Fibrolites are present around muscovite suggesting the crystallization of sillimanite involving muscovite consuming reaction.

4.2.6 Muscovite

Muscovite in the Jutogh Group of rocks is present throughout the area. Like biotites muscovites also have their strong preferred dimensional orientations and define the S_1 cleavage which suggests that muscovites are syn-tectonic with respect to S_1. Some of muscovite grains show strong bending and undulose extinction defining S_2 crenulation cleavage which suggest the post-crystalline deformation during F_2. Some

of the muscovite grains are recrystallized and define S_2 crenulation cleavage. These grains are syn-tectonic with respect to the S_2.

Strong post-crystalline deformation of muscovite is observed in ductile shear zones. These muscovites trace isoclinal folds with strong undulose extinction (Fig.4.11b). Mylonitic foliation swerves some of the pre-mylonitic muscovite porphyroblasts (Fig.4.11c). But mylonitic foliation is also defined by very small muscovite flakes suggesting the recrystallization of muscovite during ductile shearing also. In summary muscovite started crystallizing syn-tectonically with F_1, continued with F_2, outlasted it and again continued during ductile shearing.

Small muscovite flakes are present as inclusion within the garnet (Fig.4.5a) suggesting that muscovite was involved in garnet forming reactions.

4.2.7 Plagioclase

Plagioclase in the Jutogh Group is not present all over the area. In garnet grade plagioclases are absent from some of the localities. In staurolite grade staurolite bearing samples rarely contain plagioclase. But in sillimanite grade plagioclases are available abundantly. Mylonitic foliation clearly swerves around the plagioclase grains suggesting the crystallization of plagioclase during pre-ductile deformation (i.e. during F_1 and F_2) (Fig.4.11d).

4.2.8 Amphiboles

Amphiboles in calc-silicate rocks are tremolite-actinolite whereas in amphibolites they are hornblendes. Both the varieties usually define S_1 foliation and are therefore syn-tectonic with respect to F_1. Where F_2 crenulations is defined by S_1, amphibole prisms are bent, broken and

46

show undulose extinction suggesting deformation during F_2. Some of the amphibole grains cross cut the F_2 crenulation which suggests that the crystallization of amphiboles outlasted F_2 deformation. Hornblende in amphibolites present in the ductile shear zone shows strong post crystalline deformation. At places where ductile shearing is very intense recrystallization of hornblende is observed in amphibolite. The recrystallized grains are extremely fine-grained. No prismatic crystal which may be syn- to post-tectonic with respect to ductile shearing has ever been observed.

4.2.9 Other minerals

Quartz and calcite grains have crystallized during pre-ductile as well as post-ductile deformation. Crystallization of these minerals started at an early stage of the F_1 deformation, continued during F_1 and F_2 and ultimately outlasted the ductile shearing episodes. Tourmaline and epidote group of minerals are fairly common in the rocks of the Jutogh Group. When porphyroblastic these minerals are invariably syn-tectonic with early deformations (i.e. F_1-F_2) but pre-tectonic with reference to the ductile shearing. But small equant grains of tourmaline and epidote have however, crystallized syn-tectonically with respect to ductile shearing.

4.3 DISCUSSION

In the Jutogh Group of rocks the textural and microstrucatural relations suggest that the Barrovian index minerals such as chlorite, biotite, garnet, staurolite, kyanite and sillimanite started crystallizing prior to the ductile shearing (Tab.4.1). They are broadly syn-tectonic with respect to early deformation (F_1-F_2). Among those minerals chlorite and

biotite outlasted early deformation episode and continued growing during ductile shearing also. So the main phase of progressive metamorphic episode in the Jutogh Group is synchronous with the early deformation episodes which predated the progressive ductile shearing. During ductile shearing a low grade metamorphism commonly producing chlorite and less extensively biotite is generally recognized. The relationship between the crystallization of the main metamorphic minerals in relation to the deformation events has been shown in Table 4.1.

FIGURES AND TABLE
CHAPTER - 4

FIGURE 4.1: SOME OF THE PORPHYROBLAST-MATRIX RELATION SUGGESTING GROWTH OF PORPHYROBLAST IN RELATION TO DEFORMATION

(Modified after Zwart 1962; Vernon 1978, 1989)

(a). S_e swerves the porphyroblast. So the porphyroblast is pre-tectonic with respect to deformation during which S_e has been developed. Two stage growth of porphyroblast is suggested by inclusion-rich core and inclusion-free rim which suggests the static overgrowth.

(b). A porphyroblast is broken into pieces and strewn along the S_e foliation g pre-tectonic growth of that porphyroblast.

(c). External (S_e) crenulated foliation sharply abut against the porphyroblast which suggests that the porphyroblast is pre-tectonic with respect to S_e.

(d). Spiral S_i in the core with inclusion free rim in porphyroblast which is swerved by the S_e. Two stage growth is suggested. First stage is syn-tectonic with respect to S_i. Second stage is static overgrowth. But both stages are pre-tectonic with respect to deformation during which S_e has been developed.

(e). Straight S_i is oblique to S_e and not continuous with S_e. The porphyroblast is post-tectonic to S_i which represents the early foliation but pre-tectonic to S_e.

(f). Spiral S_i is continuous with the S_e. It suggests the syn-tectonic growth of porphyroblast with respect to deformation which developed S_e.

(g). S_e is continuous with S_i. But the crenulation of S_e is tighter than that of S_i which suggests the post-tectonic growth of porphyroblast with respect to S_e but syn-tectonic growth with respect to S_i.

(h). Straight S_i is continuous with S_e suggesting post-S_e growth of the porphyroblast.
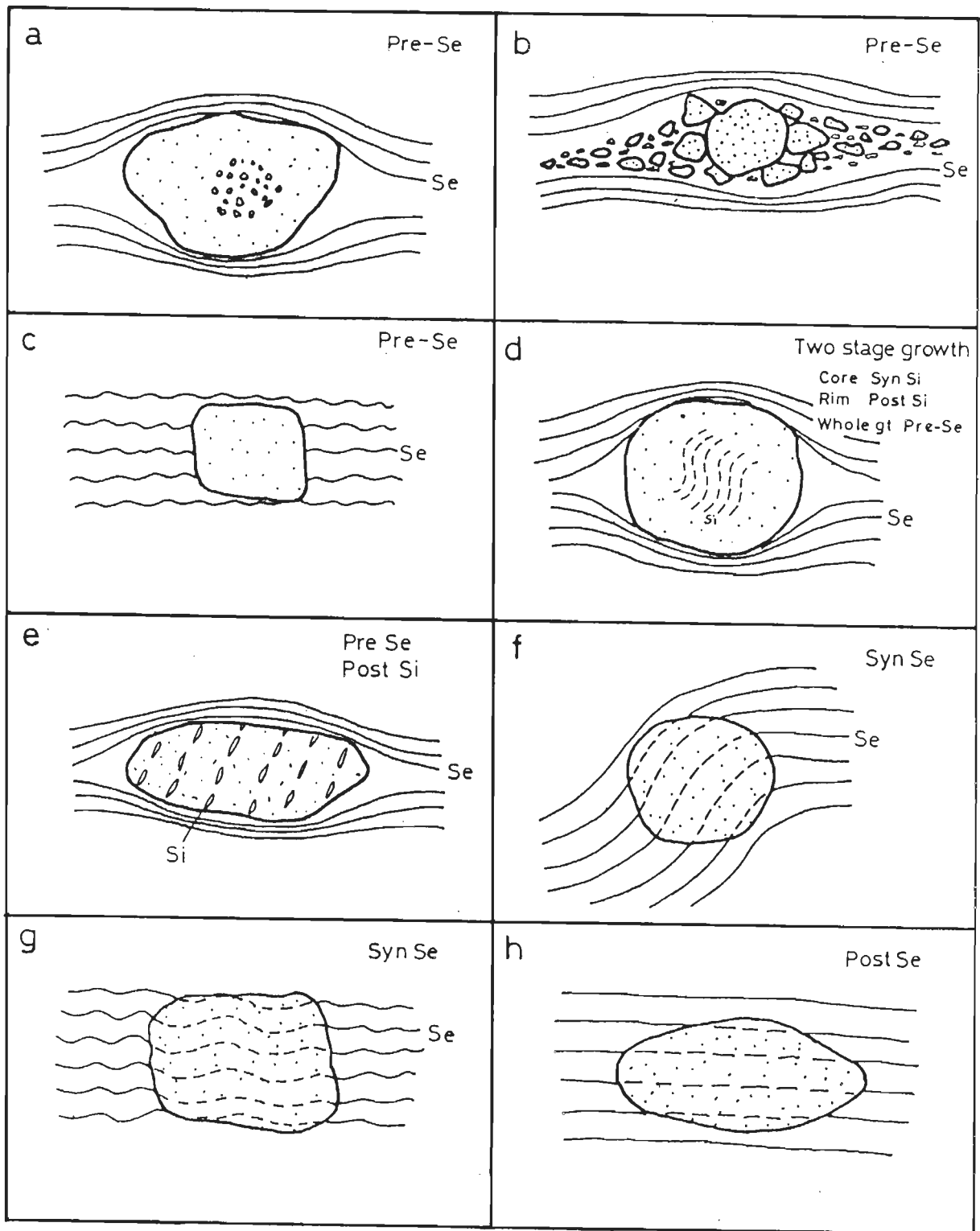
Fig: 4.1

FIGURE 4.2: CHLORITE PORPHYROBLASTS

(a). Chlorite porphyroblasts with straight S_i which is continuous with S_e ($=S_1$). The S_i in the matrix is involved in open F_2 crenulation (not shown in the photograph). These chlorites are post-F_1 but pre-F_2. Carbonaceous schist; Sample No. S-403; Crossed-Nicols; Base$=2$ mm.

(b). Crenulated S_i within chlorite is continuous with crenulated S_e ($=S_1$). The crenulation defined by S_i is more open than S_e. The chlorite porphyroblast shows kinked cleavage and strong undulose extinction. This chlorite is syntectonic with respect to F_2 deformation. Micaceous quartzite; Sample No. S-180; Crossed Nicols; Base$=2$ mm.

(c). Retrograde chlorite overgrowing garnet porphyroblast. S_i in the chlorite may be noticed. This retrogression was during post-F_1. Carbonaceous schist; Sample No. S-403; Oblique Nicols; Base$=2$ mm.

(d). Chlorite in ductile shear zone with slightly curved S_i trails which is continuous with mylonitic foliation in the matrix (S_m). S_i is traced by carboneceous matter and opaques. Carbonaceous schist; Sample No. S-244; Oblique Nicols; Base$=1.3$ mm.
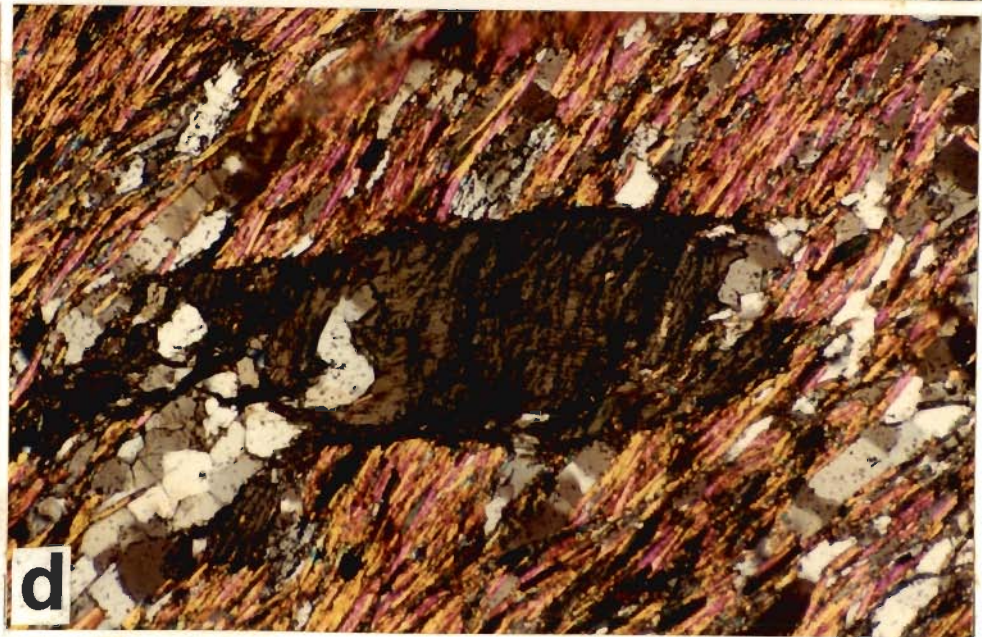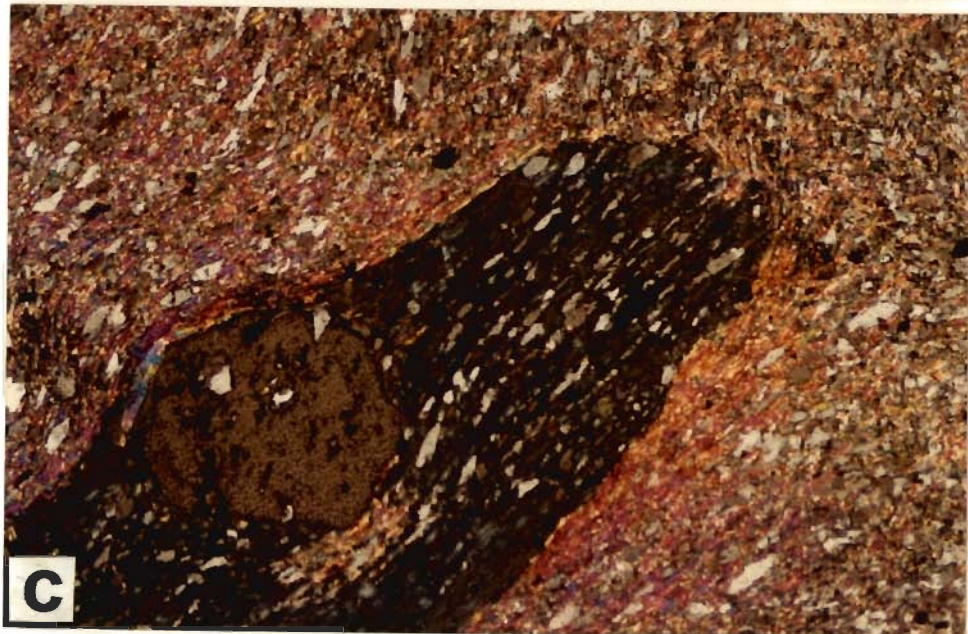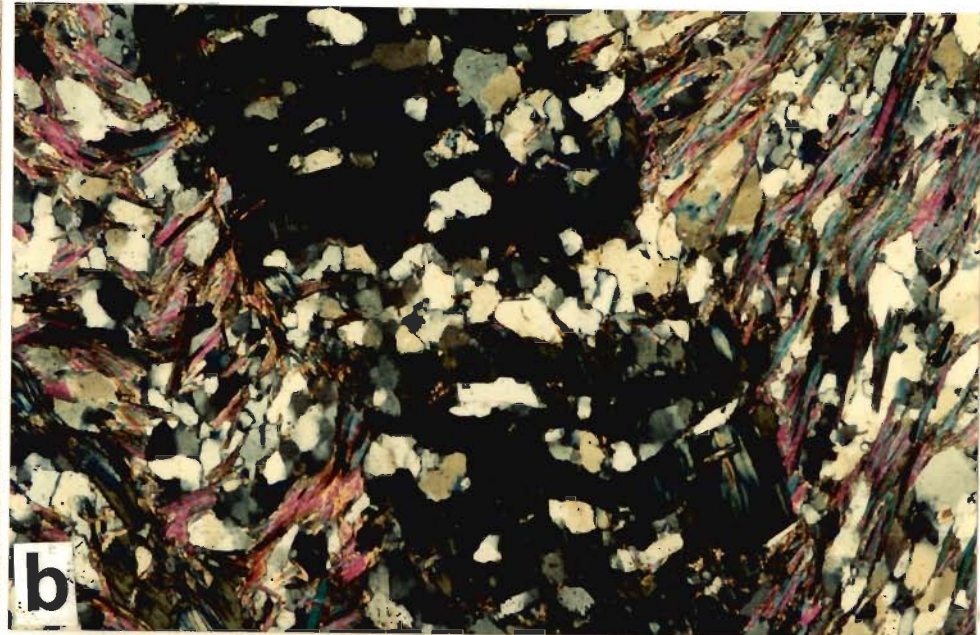
Fig.4.2

FIGURE 4.3: CHLORITE PORPHYROBLASTS

(a). Chlorite porphyroblast showing mica-fish type structure within mylonitic foliation. Lower carbonaeous schist; Sample No. S-459; Oblique Nicols; Base=2 mm.

(b). S_i is oblique to and truncated by the S_e. But both S_i and S_e are mylonitic foliation. This chlorite is post-tectonic to S_i but pre-tectonic to later mylonitic foliation (S_e). Lower carbonaceous schist; Sample No. S-459; Oblique Nicols; Base=2 mm.

(c). Straight S_i in chlorite is truncated by S_e both being the mylonitic foliation. The temporal relationship is same as (b). In the pressure-shadow zone between garnet and the chlorite porphyroblast small needles of syn-tectonic (to S_e) chlorite are alligned parallel to the matrix foliation suggesting syntectonic crystallization with S_e. Lower carbonaceous schist; Sample No. S-459; Oblique Nicols; Base=2 mm.

(d). Chlorite with ilmenite inclusion is developed along S-surface in S-C mylonite. This chlorite is syn-tectonic with respect to mylonitic folation. Mica schist; Sample No. S-607; Crossed Nicols; Base=1.3 mm.
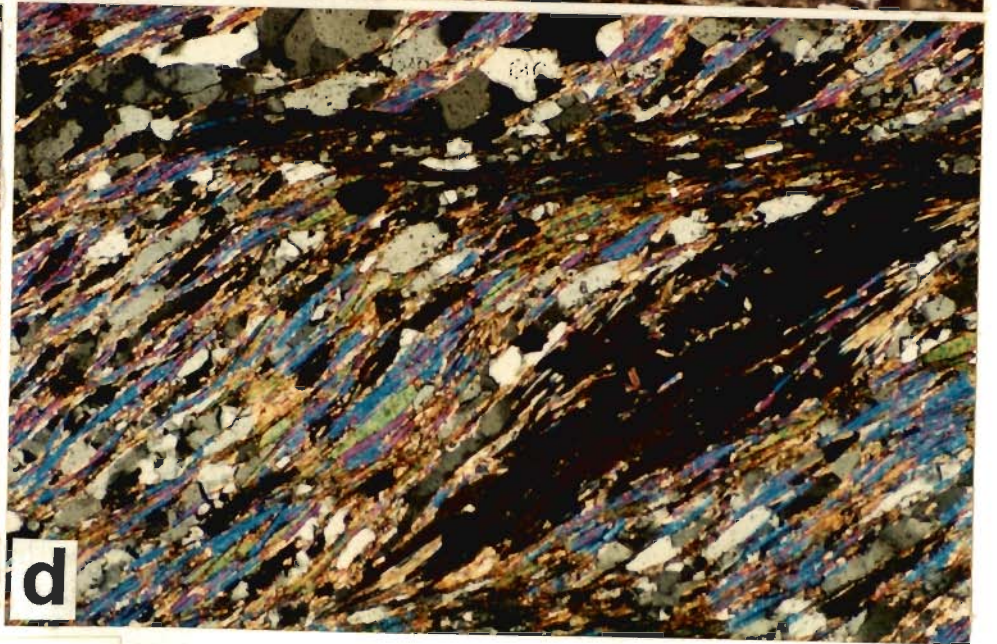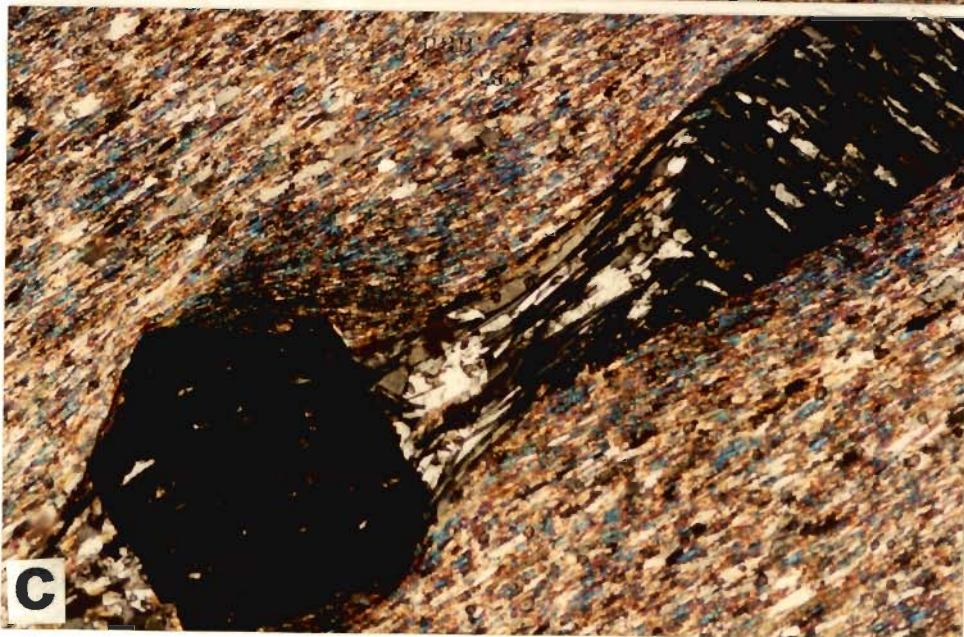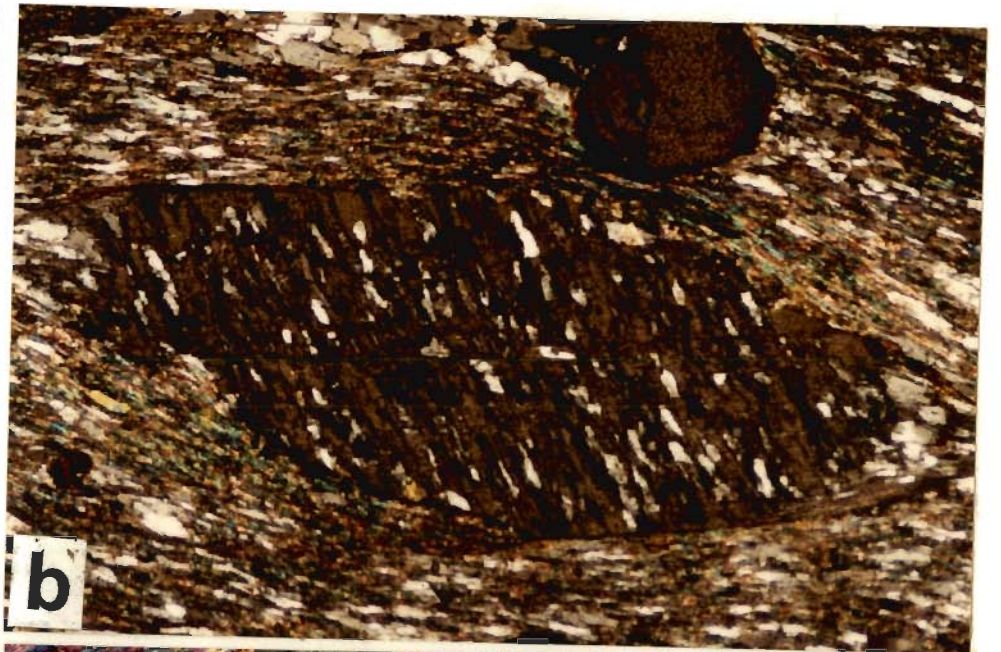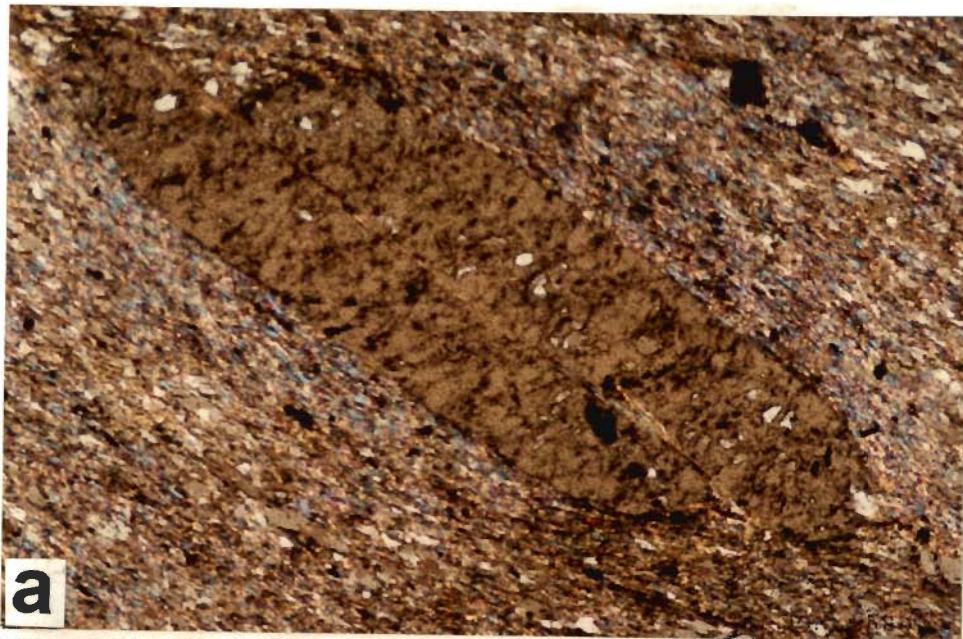
Fig.4.3

FIGURE 4.4: BIOTITE AND GARNET PORPHYROBLASTS

(a). Biotite porphyroblast, rich in quartz inclusion, is swerved by the S_1 foliation suggesting pre-teconic growth of biotite with respect to S_1. Mica schist; Sample No. S-749; Crossed Nicols; Base = 1.3 mm.

(b). Cleavage traces in biotite is at high angle to S_1 foliation. Mica schist; Sample No. S-749: Crossed Nicols; Base = 1.3 mm.

(c). Early cleavage (S_1) defined by muscivite and biotite is preserved in the Q-domain of the later cleavage suggesting the formation of biotite and muscovite prior to the S_1 as well as during S_1. Mica schist; Sample No. S-738; Crossed Nicols; Base = 1.3mm.

(d). Garnet and biotite porphyroblasts are swerved by the S_1 foliation. These are pre-tectonic to F_1 deformation. Mica schist; Sample No. S-839; Oblique Nicols; Base = 2 mm.
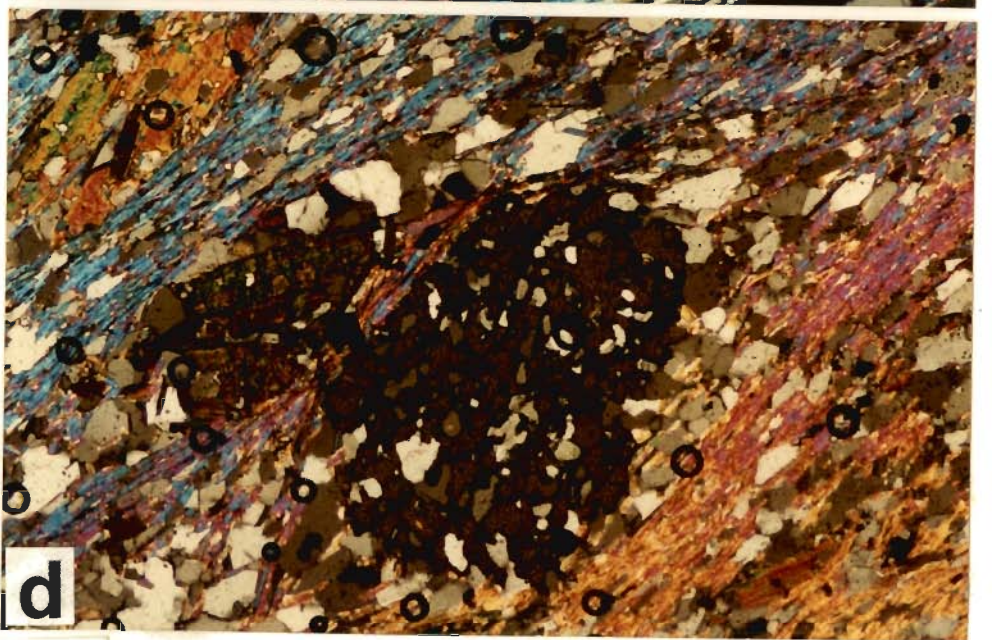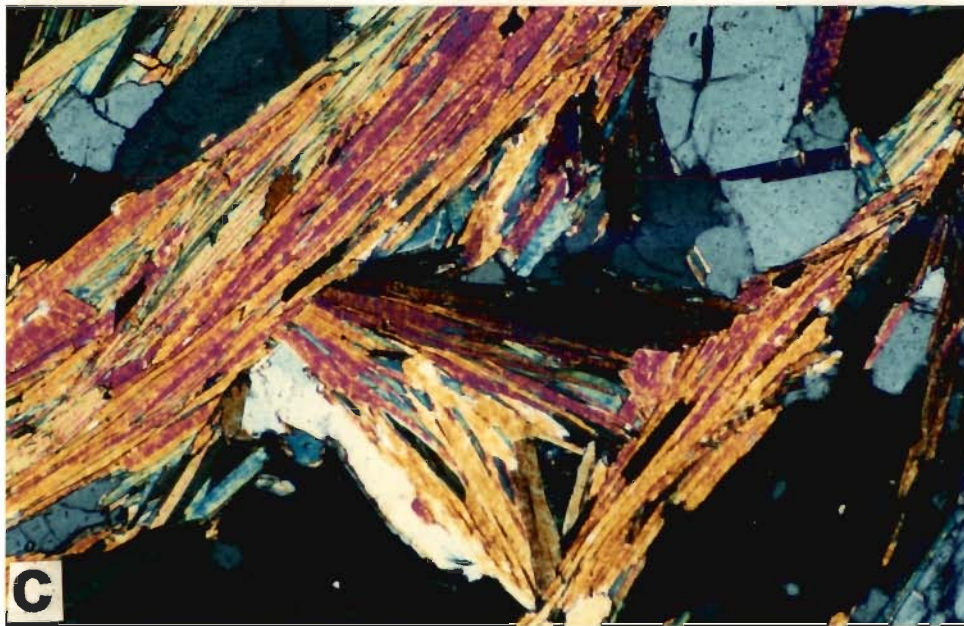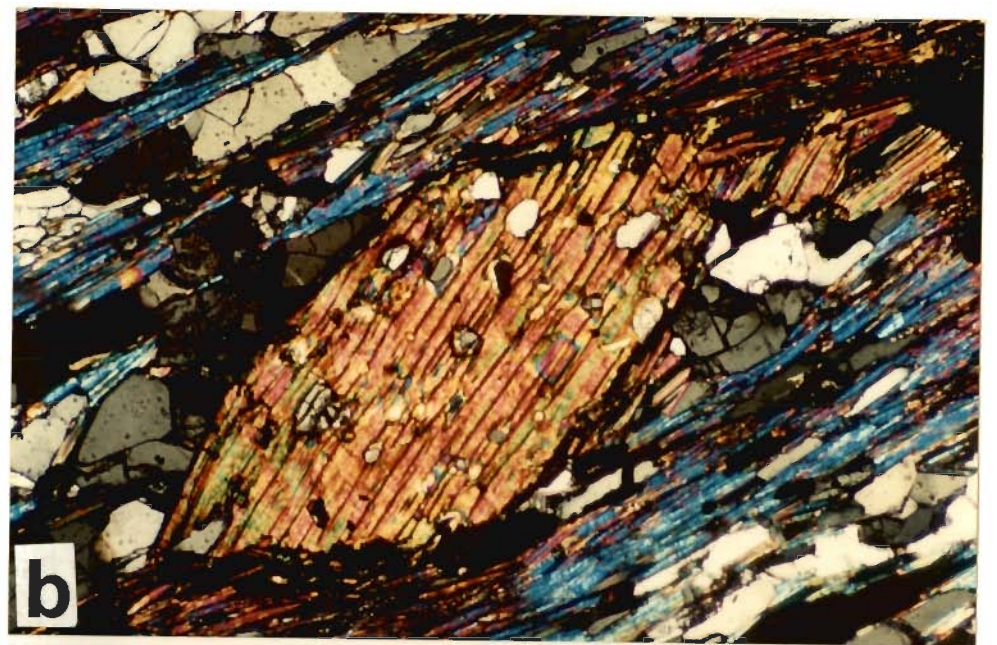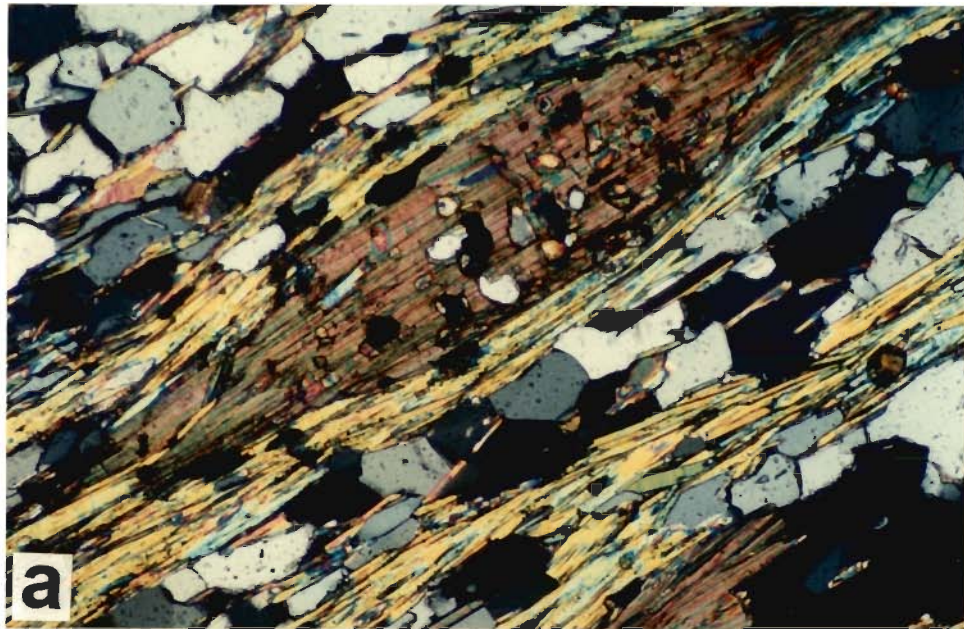
Fig.4.4

FIGURE 4.5: GARNET MICROSTRUCTURES

(a). S_i slightly curved in nearly rounded garnet porphyroblast is continuous with S_e. This garnet is syn-tectonic with respect to the S_e which is S_1. Micaceous quartzite; Sample No. S-16; Crossed Nicols; Base= 5.2 mm.

(b). ~~Tiny~~ P̸olygonal garnet porphyroblast with inclusion rich core and inclusion free rim. The S_e ($=S_1$)abut against the porphyroblast. This garnet is post-tectonic with respect to the F_1. Micaceous quartzite; Sample No. S-93/2, Plane Polerized; **Base**= 0.4 mm.

(c). The fractured garnet porphyroblast is swerved by the F_2-kinks. This garnet is pre-tectonic with respect to the F_2. Mica schist; Sample No. S-174; Oblique Nicols; Base= 6.5 mm.

(d). Almost inclusion free garnet porphyroblast is swerved by the mylonitic foliation. In the pressure-shadow elongated quartz grains and fine muscovite needles are noticeable. This garnet is pre-tectonic with respect to mylonitic foliation. Carbonaceous schist; Sample No. S-618; Crossed Nicols; Base= 5.2 mm.
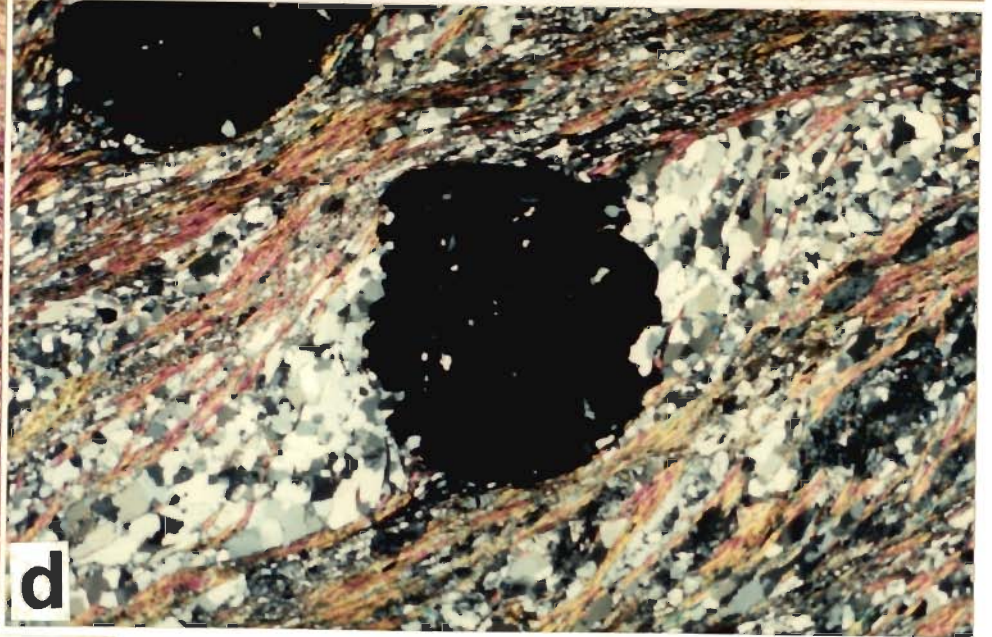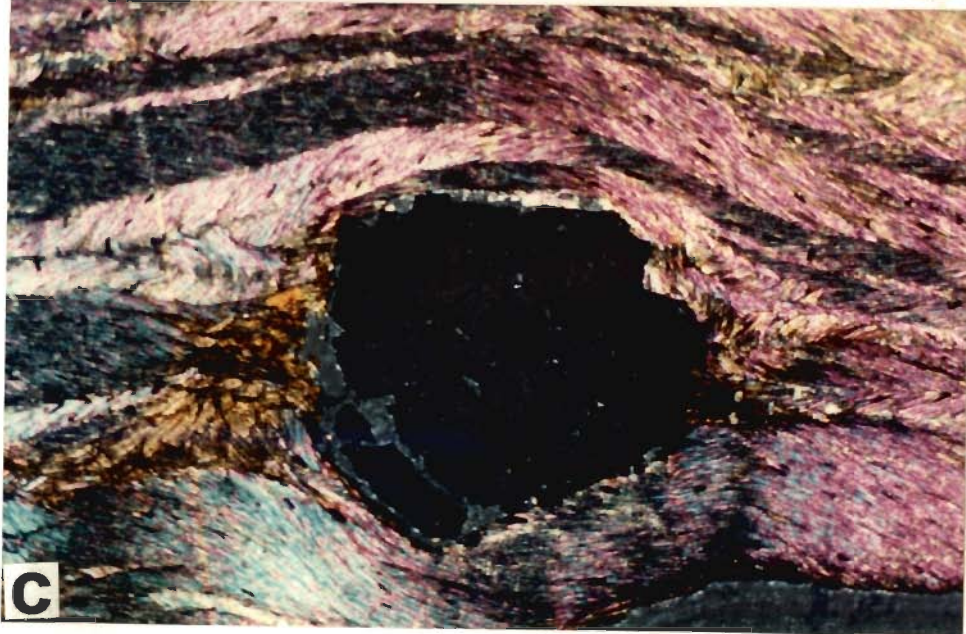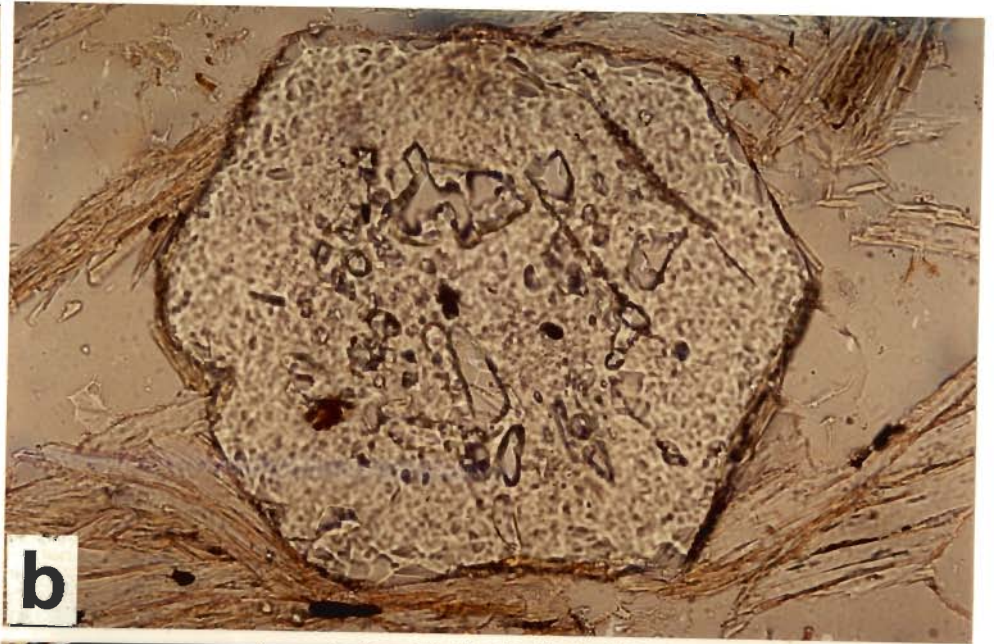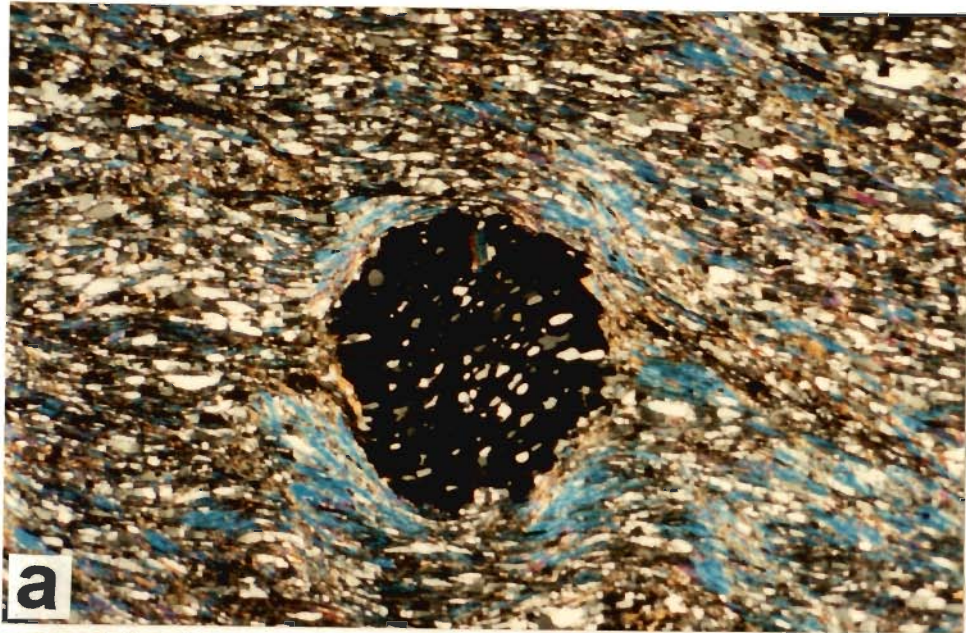
Fig.4.5

FIGURE 4.6: GARNET MICROSTRUCTURES

(a). Mylonitic foliation in the matrix (S_e) swerves around the garnet porphyroblast. The spiral shaped inclusion trail within the garnet (S_i) is not continuous with mylonitic foliation (S_e). This garnet is pre-tectonic with respect to ductile shearing. Mica schist; Sample No. S-44; Oblique Nicols; Base= 8 mm.

(b). Crenulated mylonitic foliation sharply abuts against the polygonal inclusion-free garnet porphyroblast. The wavelength of this crenulation gradually decrease away from the porphyroblast. The garnet is pre-tectonic with respect to the ductile shearing. Mica schist; Sample No. S-148; Oblique Nicols; Base= 5.2 mm.

(c). The axial planes of isoclinal folds defined by quartz ribbon swerving around the garnet porphyroblast. The garnet has its inclusion rich core and almost inclusion free rim. The inclusion rich core is pre-tectonic with respect to F_1 and inclusion free rim post-tectonic with respect to F_1. Mica schist; Sample No. S-119/2; Plane polerized; Base= 5.2 mm.

(d). Garnet porphyroblast is broken into small pieces and strewn along the mylonitic foliation during ductile shearing. Mica schist; Sample No. S-119/2; Oblique Nicols. Base= 5.2 mm.
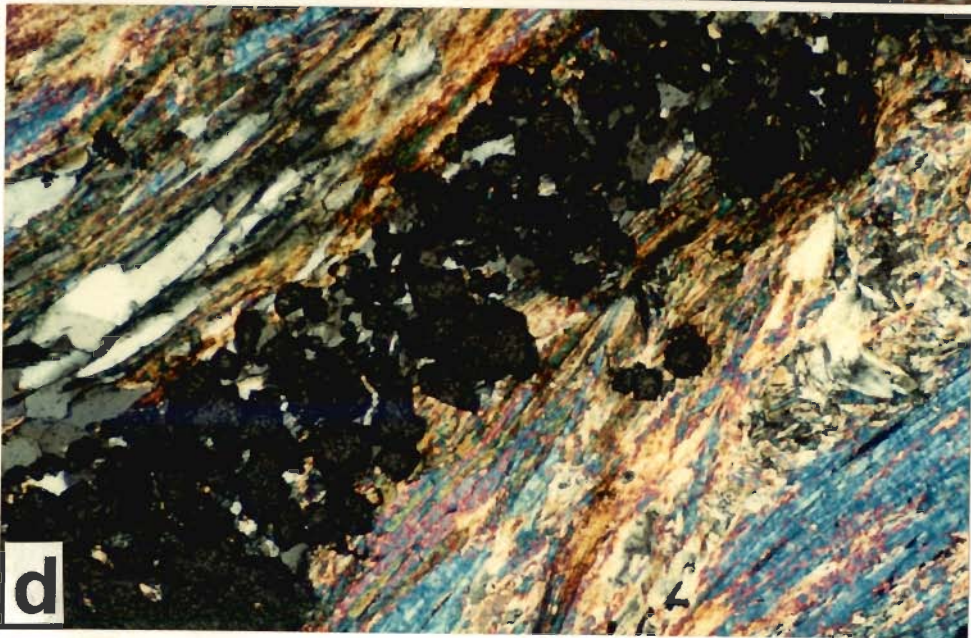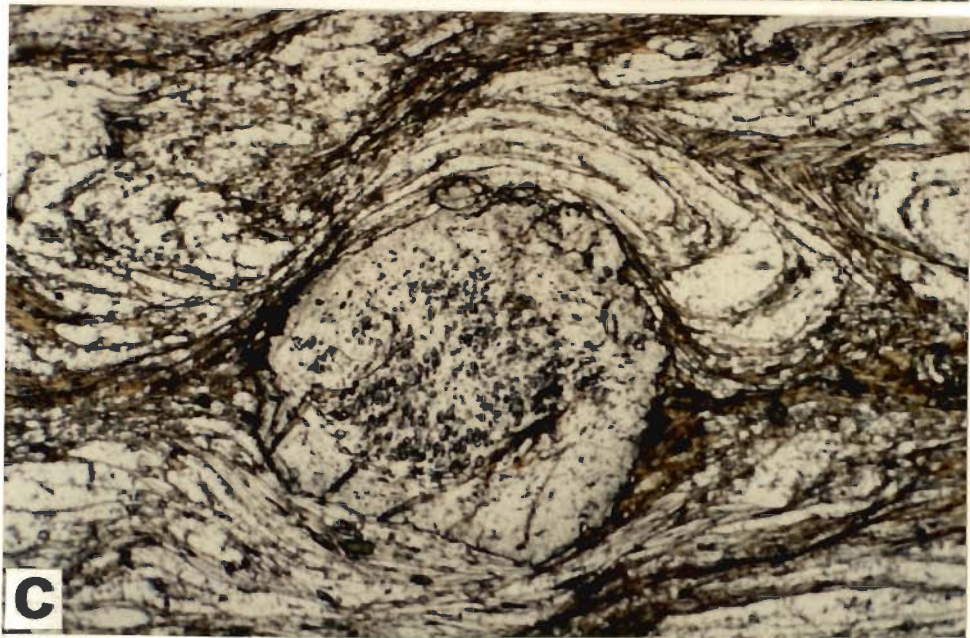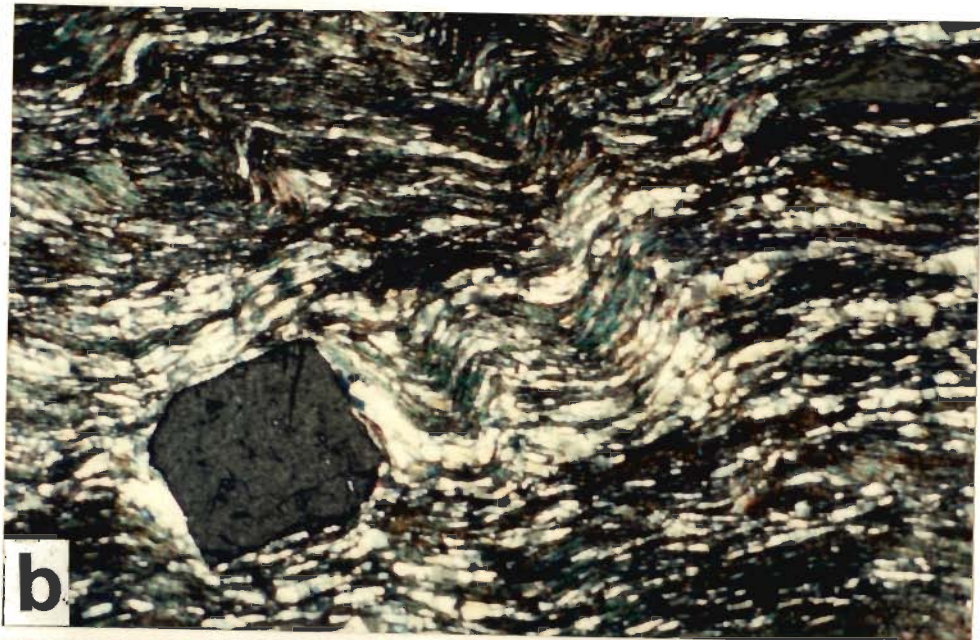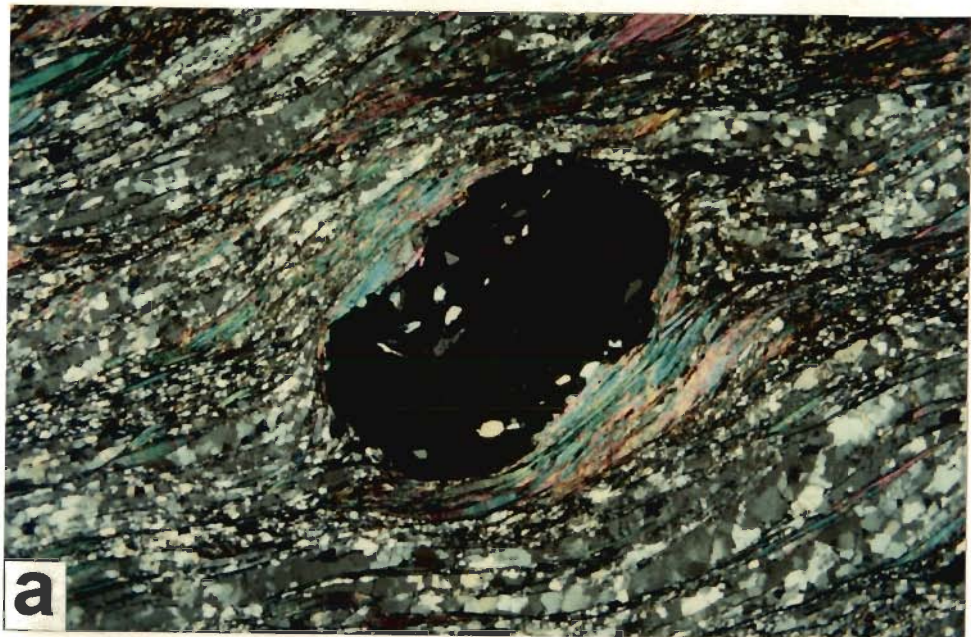
Fig.4.6

FIGURE 4.7: GARNET MICROSTRUCTURES

(a). Pre-tectonic garnet porphyroblast (with respect to mylonitic foliation) with spiral inclusion rich core and inclusion poor rim suggesting two stage growth. The core is syn-tectonic with respect to early foliation and rim is post-tectonic overgrowth. Note that one side of the porphyroblast has been consumed during retrogression. Mica schist; Sample No. S-365; Crossed Nicols; Base = 1.6 mm.

(b). Spiral shaped inclusion trail sharply abut against the S_2 external foliation which suggests that this garnet grew pre-tectonically with respect to F_2 but syn-tectonically with respect to S_1. Micaceous quartzite; Sample No. S-400; Plane Polarized; Base = 2 mm.

(c). Straight inclusion trail which is parallel to the S_e. It suggests the post-tectonic growth with respect to S_i but pre-tectonic growth with respect to S_e. Fracture has been developed due to later deformation. Mica schist; Sample No. S-881; Plane Polarized; Base = 2 mm.

(d). Straight inclusion trail in garnet core with relatively inclusion free rim. Mylonitic foliation (S_e) swerves the garnet which has pre-mylonitic growth in two stage. Mica schist; Sample No. S-59; Crossed Nicols; Base = 5.2 mm.
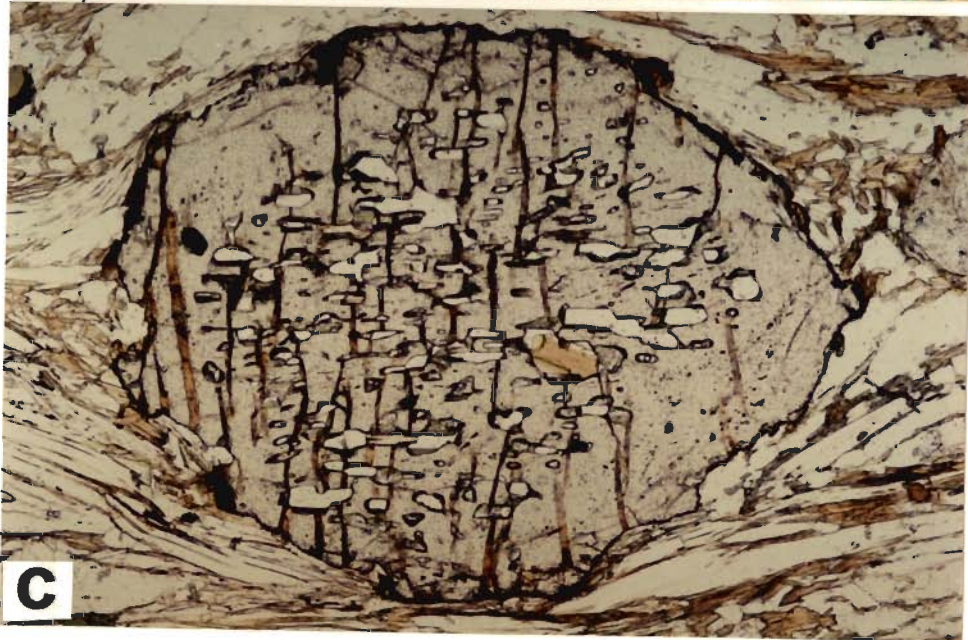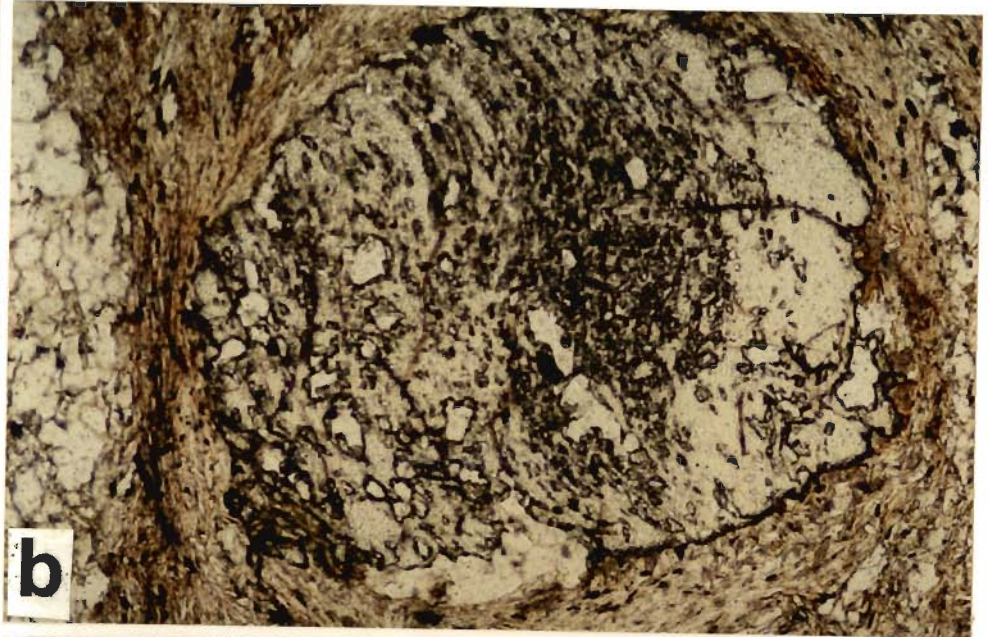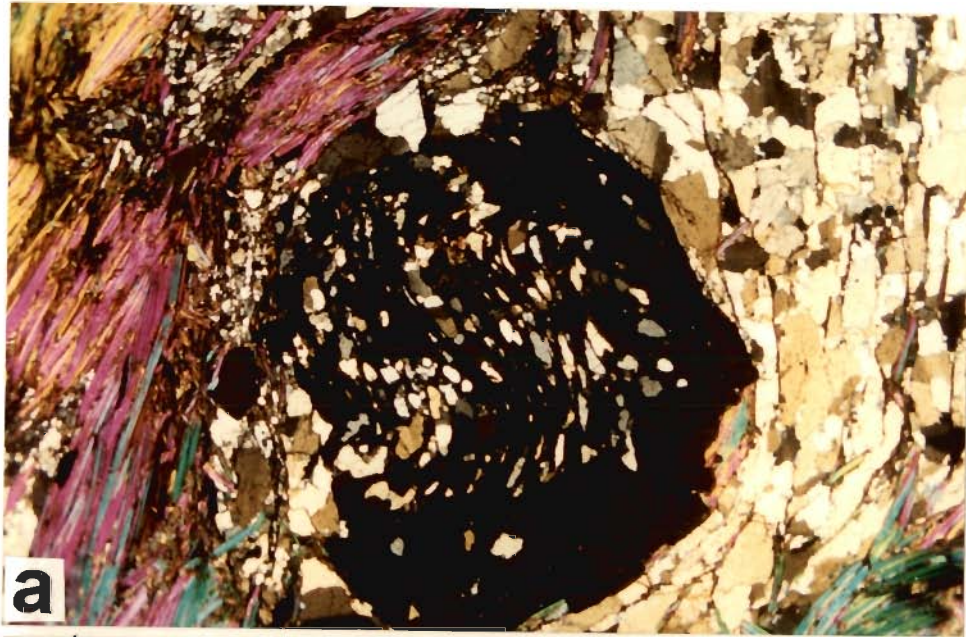
Fig.4.7

FIGURE 4.8: GARNET MICROSTRUCTURE

(a). Two stage growth of garnet marked by inequant quartz inclusions developed during the period between the growth of first and second stage. Mica schist; Sample No. S-676; Plane Polarized; Base=1.6 mm.

(b). Inclusion rich core and inclusion poor rim in garnet porphyroblast indicating two stage growth of garnet in staurolite grade. Mica schist; Sample No. S-119/2; Plane Polarized; Base=5.2 mm.

(c). Subrounded garnet porphyroblast is swerved by S surface in S-C developed during mylonitization. Well developed pressure shadow is present suggesting pre-mylonitic growth of this porphyroblast. Mica schist; Sample No. S-607; Crossed Nicols; Base=2 mm.

(d). Chlorite inclusion present in garnet suggesting the crystallization of garnet by chlorite breakdown reaction. Micaceous quartzite; Sample No. S-38; Crossed Nicols; Base= 0.4 mm
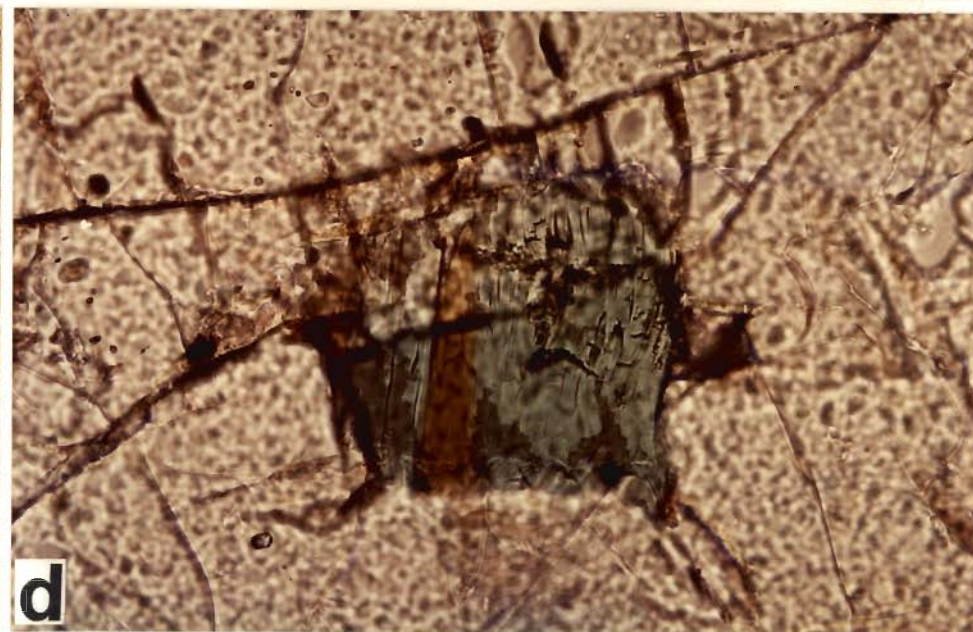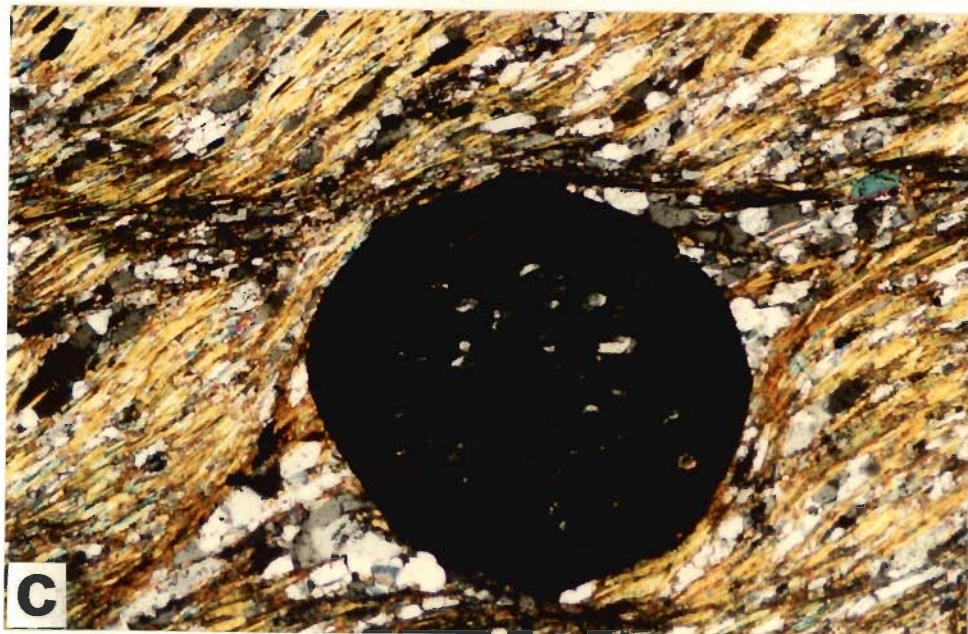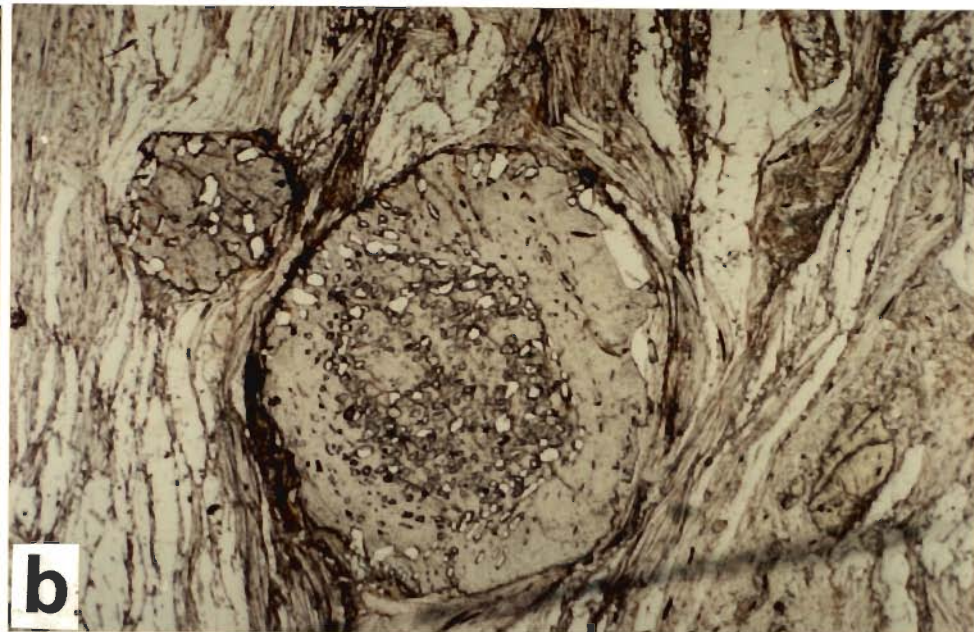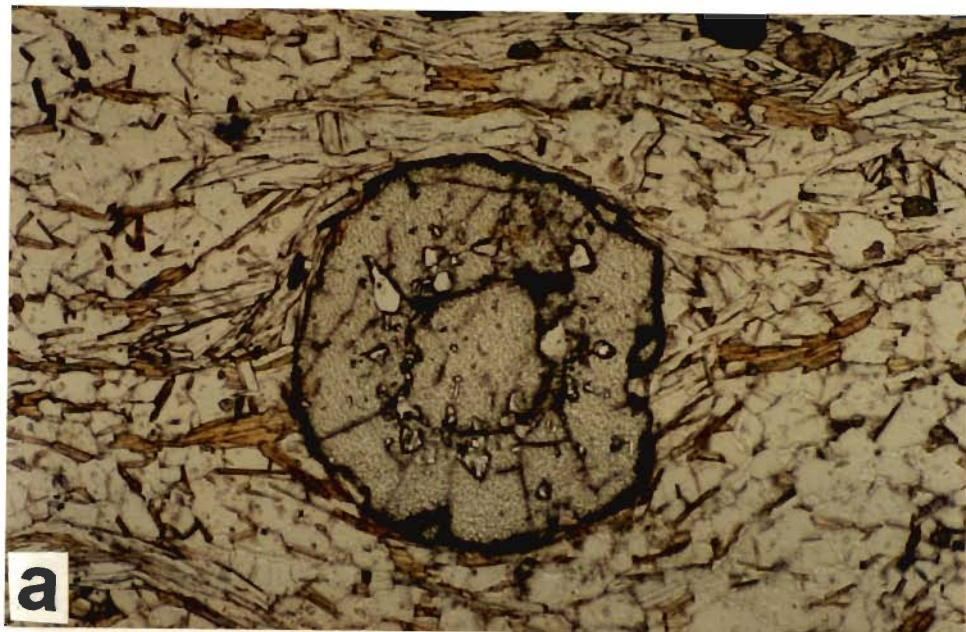
Fig.4.8

FIGURE 4.9: DIFFERENT INCLUSIONS IN GARNET OTHER THAN QUARTZ, ILMENITE AND CHLORITE, AND STAUROLITE GROWTH.

(a). Staurolite inclusion in garnet rim which suggest the late stage crystallization of garnet in staurolite grade by staurolite breakdown reaction. Note that fracture in staurolite is continuous with garnet suggesting post-crystalline deformation during mylonitization. S_e is mylonitic foliation (not shown in the photograph). Mica schist; Sample No. S-882; Plane Polarized; Base= 2 mm.

(b). Garnet has crystallized by sillimanite breakdown reaction incorporating sillimanite flakes as inclusions. Note the muscovite is also present as inclusion. Mica schist; Sample No. S-894; Crossed Nicols; Base= 2 mm.

(c). Muscovite inclusion present within garnet porphyroblast in staurolite grade indicates the formation of garnet by muscovite consuming reaction. Mica schist; Sample No. S-749; Crossed Nicols; Base= 2 mm.

(d). Staurolite porphyroblast is swerved by the mylonitic foliation (S_e) suggesting pre-mylonitic growth of staurolite. Mica schist; Sample No. S-107; Plane Polarized; Base= 5.2 mm.
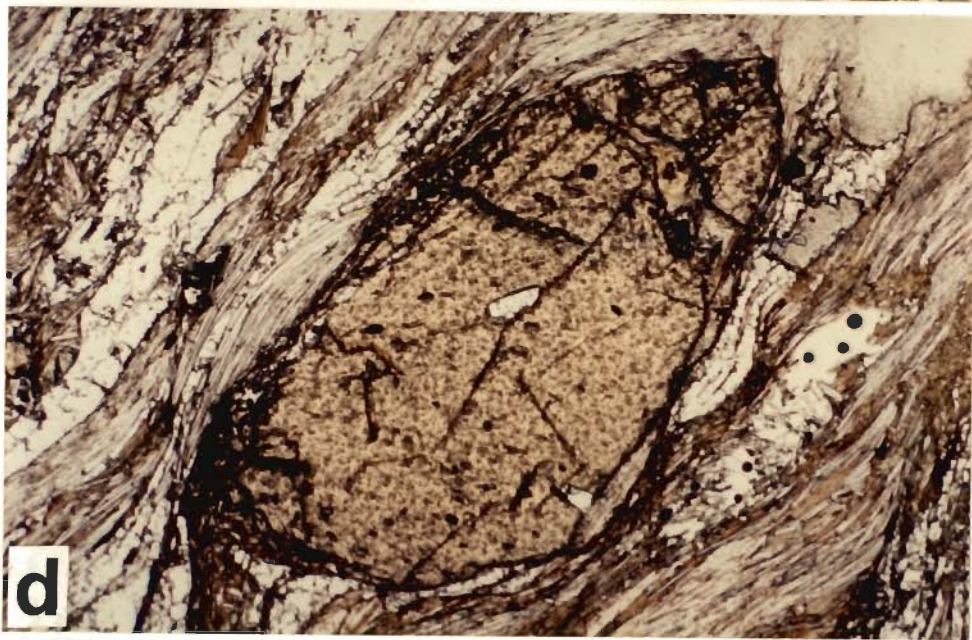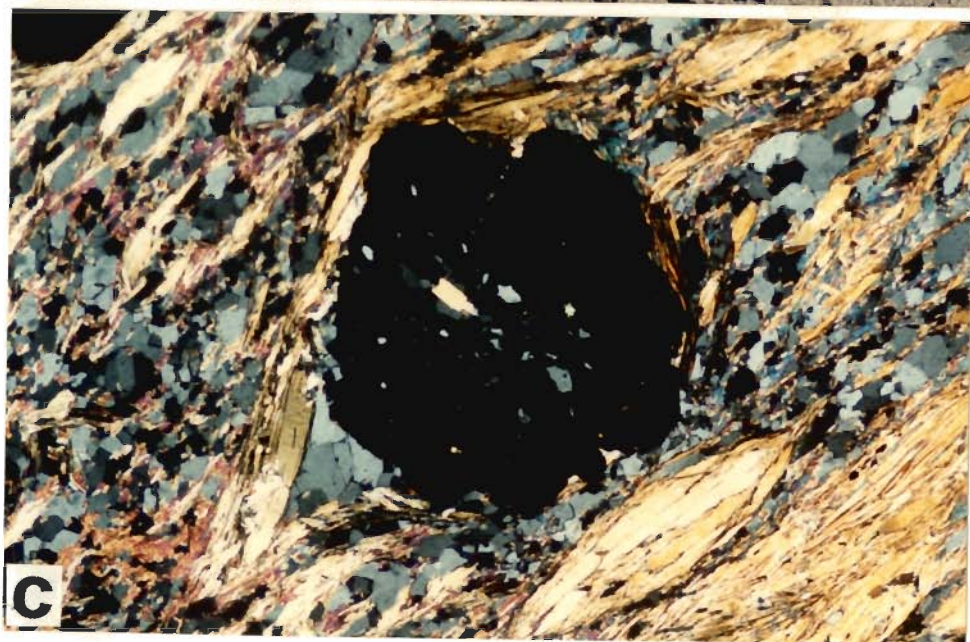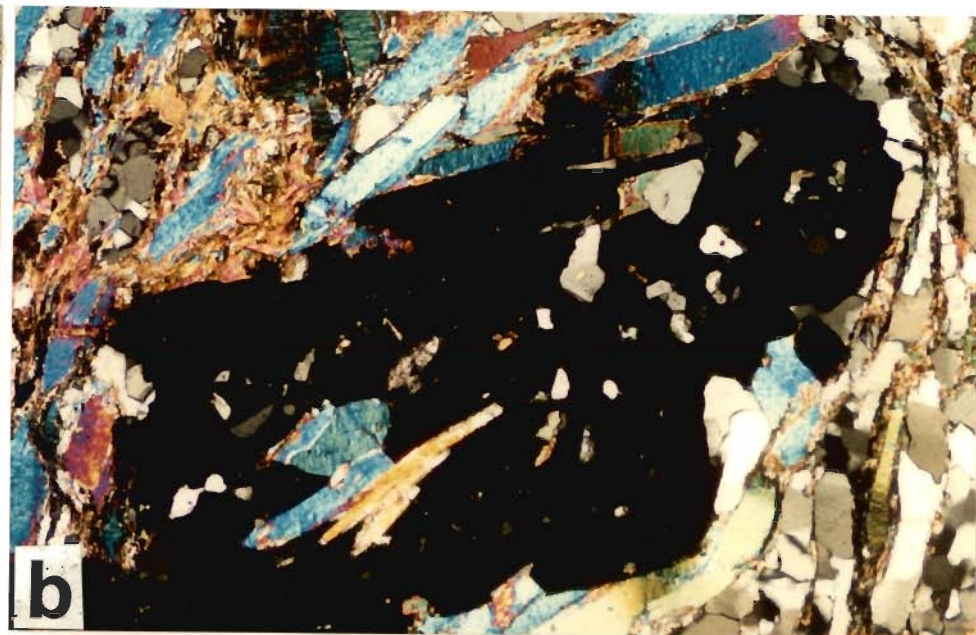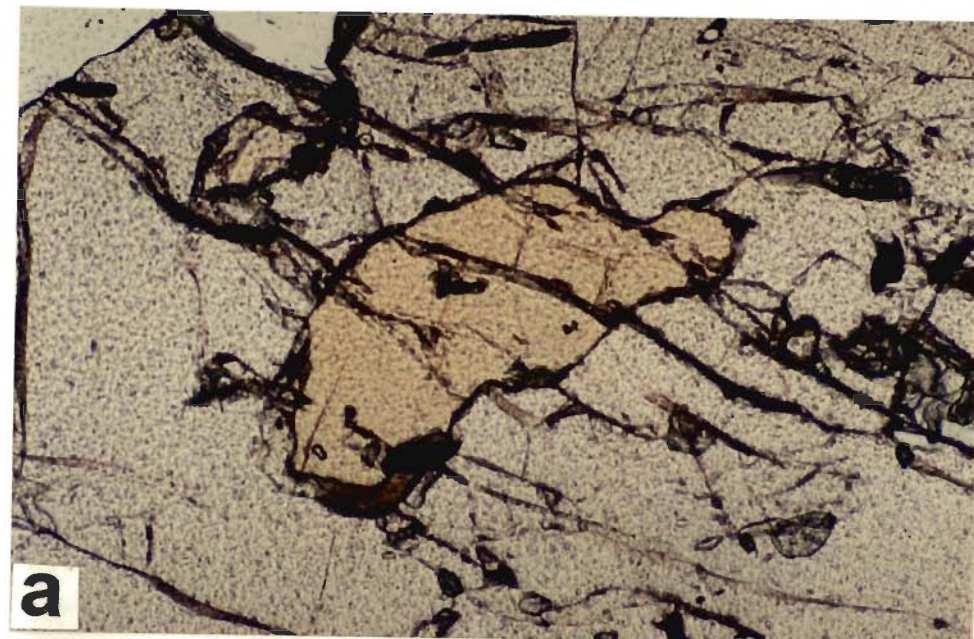
Fig.4.9

FIGURE 4.10: STAUROLITE AND KYANITE MICROSTRUCTURES

(a). Pre-tectonic staurolite porphyroblast showing strong undulose extinction and fractures due to post-crystalline deformation during ductile shearing. Mica achist; Sample No. S-858; Crossed Nicols; Base=8 mm.

(b). Staurolite is fractured and boudinaged during ductile shearing. Retrograde chlorite has been formed within the fracture zone aligned parallel to the swerved mylonitic foliation. Mica schist; Sample No. S-318; Crossed Nicols; Base=2 mm.

(c). Biotite inclusion in the staurolite which suggests the crytallization of staurolite by biotite involving reaction. Mica schist; Sample No. S-882; Crossed Nicols; Base=1.3 mm.

(d). Mylonitic foliation developed during ductile shearing swerving the kyanite porphyroblast suggesting pre-mylonitic growth of kyanite. Well developed pressure shadow is also present. Mica schist; Sample No. S-717; Crossed Nicols; Base= 2 mm.
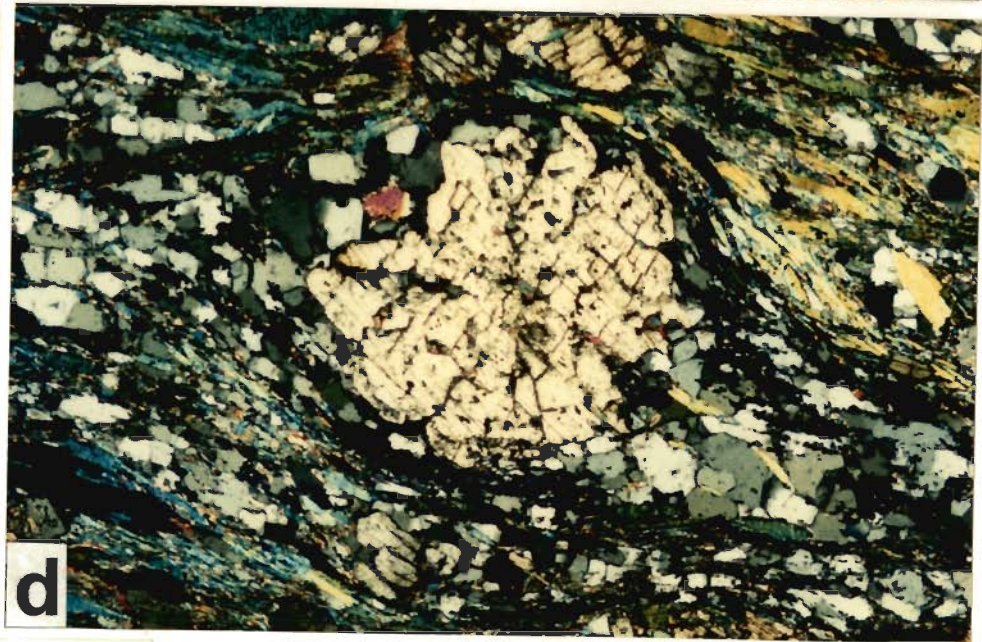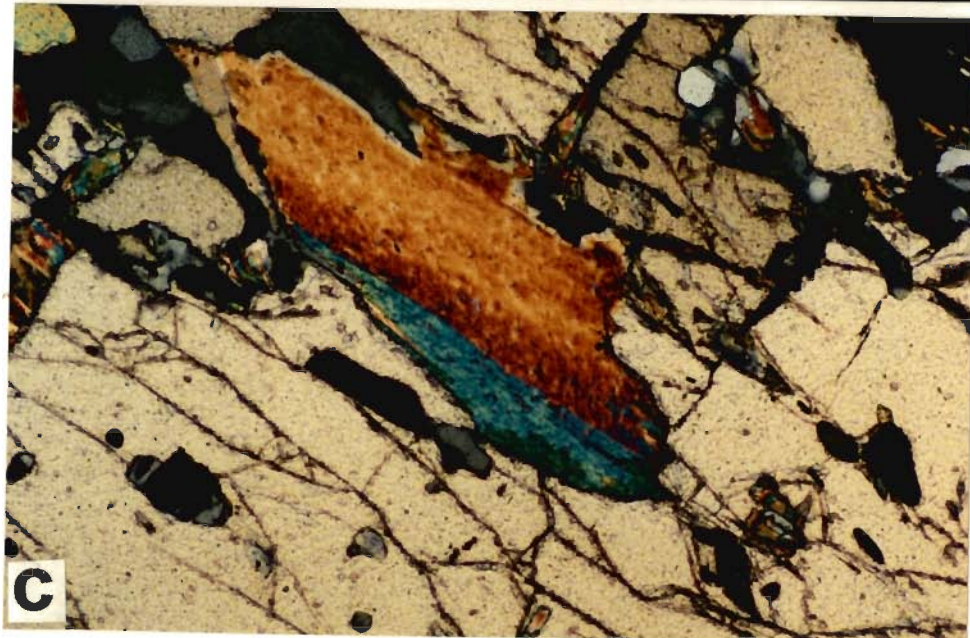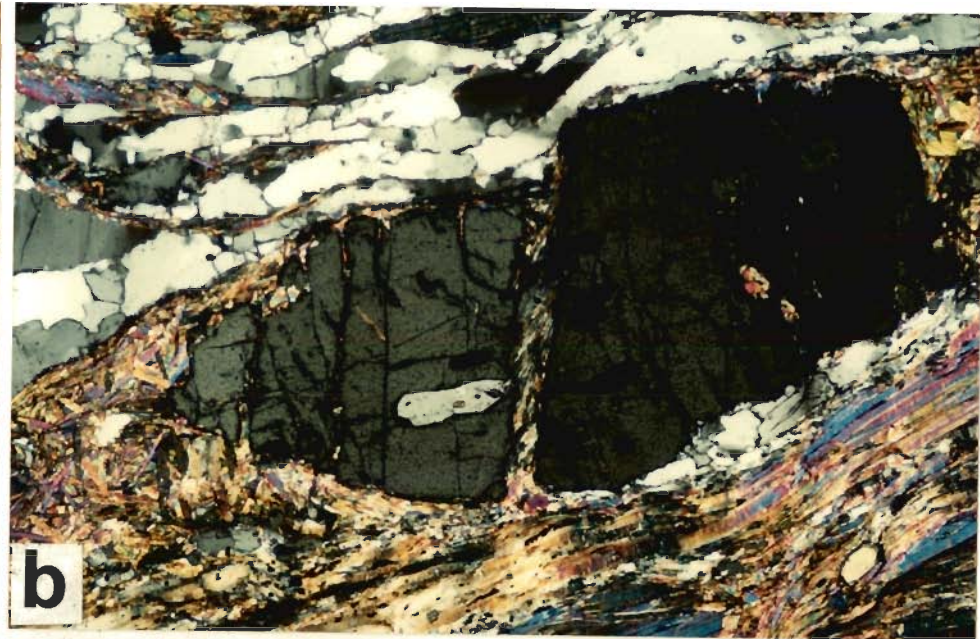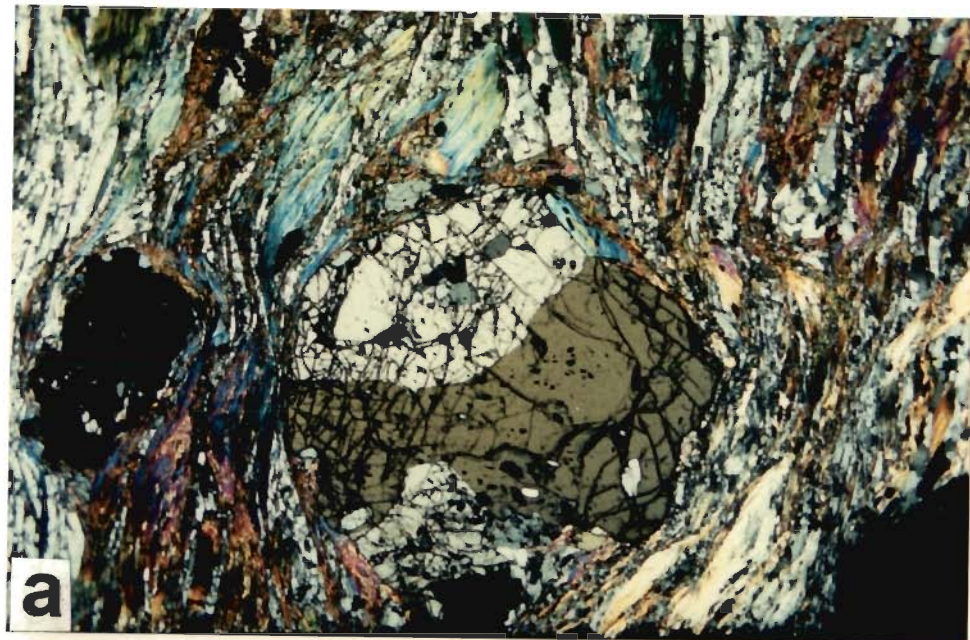
Fig.4.10

FIGURE 4.11: KYANITE, MUSCOVITE AND PLAGIOCLASE

(a). Straight S_i ($=S_1$) is defined by biotite flakes preserved in kyanite which is swerved by the mylonitic foliation (S_e). Kyanite has crystallized before ductile shearing. Mica schist; Sample No. S-717; Crossed Nicols; Base=1.3 mm.

(b). Muscovite flake is folded showing undulose extinction during ductile shearing. Matrix foliation is resulted during ductile shearing. Mica schist; Sample No. S-882; Crossed Nicols; Base= 5.2 mm.

(c). Muscovite "fish" is swerved by the mylonitic foliation. Ilmanite is present as inclusion. Mica schist; Sample No. S-62; Crossed Nicols; Base= 5.2 mm.

(d). Plagioclase porphyroblast is swerved by mylonitic foliation. The fracture developed within the plagioclase was due to post-crystalline deformation. Mica schist; Sample No. S-318; Crossed Nicols; Base= 5.2 mm.
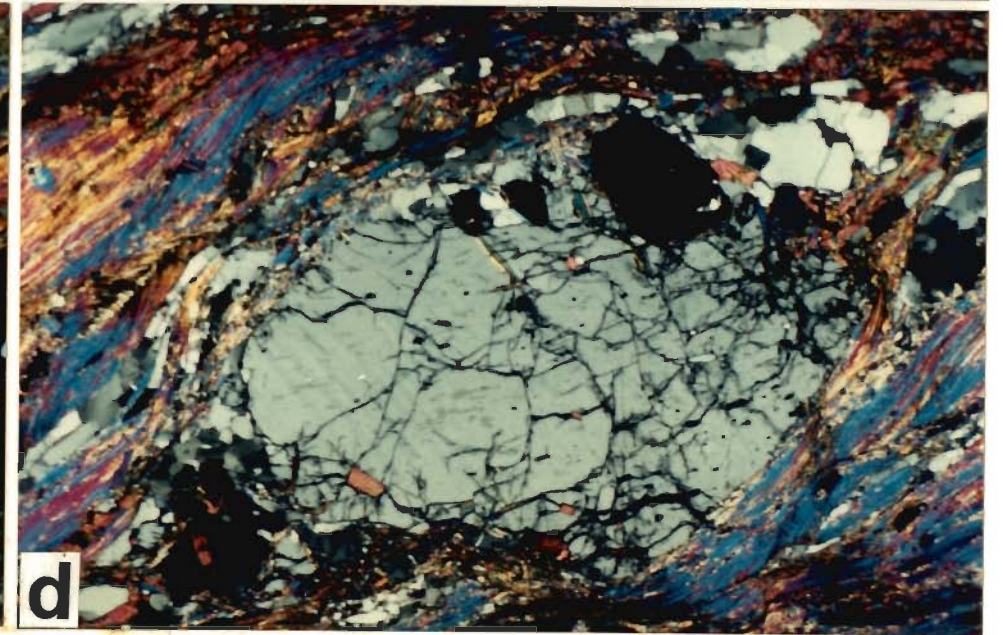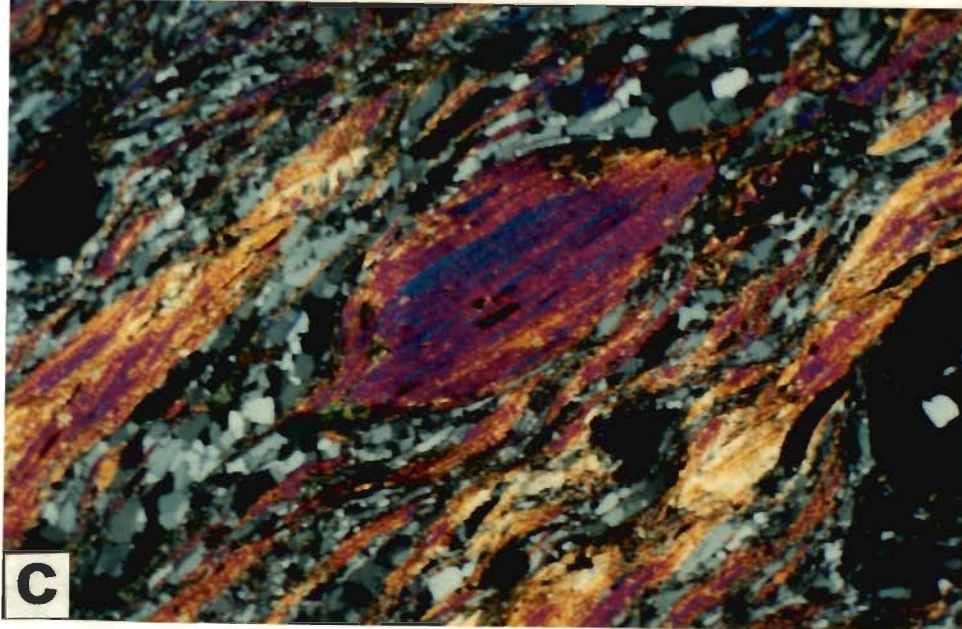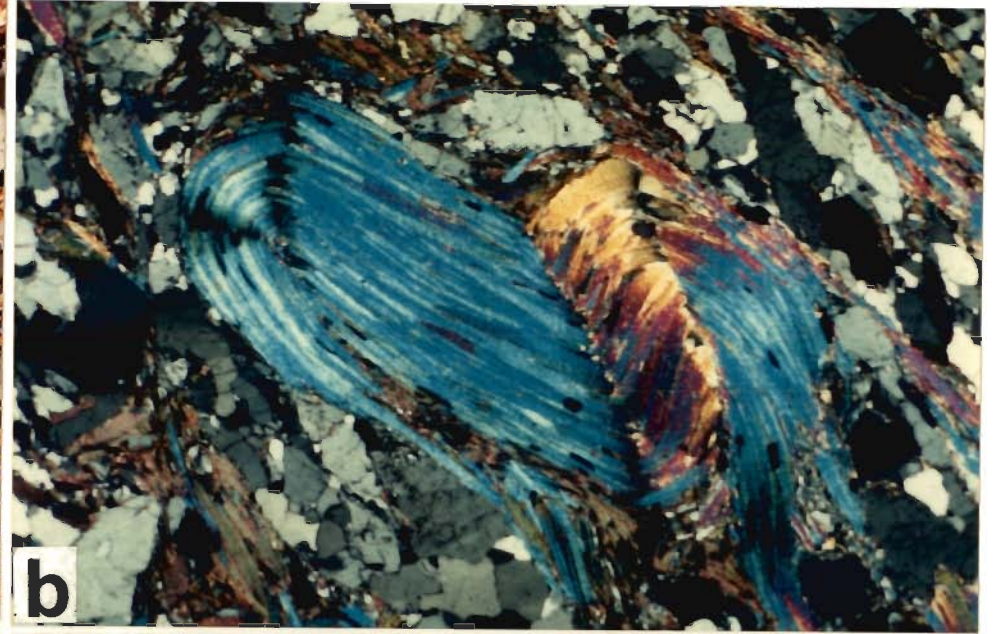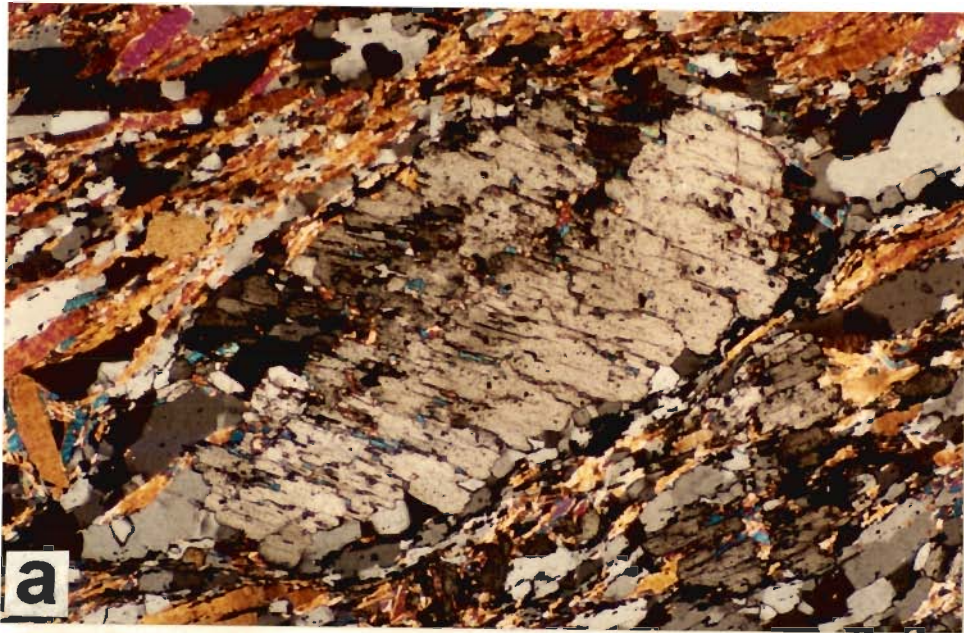
Fig.4.11

TABLE 4.1
TEMPORAL RELATIONS BETWEEN FORMATION OF MINERALS AND DEFORMATION EPISODES

|	F_1			F_2			Ductile Shearing
	Pre	Syn	Post	Pre	Syn	Post	
CHLORITE	————	——	--		·	·· ———	————————
BIOTITE	————						—————————
GARNET	————	————					
STAUROLITE			——---				
KYANITE			--—				
SILLIMANITE			--—				
MUSCOVITE	————						——————--
PLGIOCLASE	————						
QUARTZ	————						—————————
TOURMALINE	————						—————————

CHAPTER - 5
MINERALOGY AND MINERAL CHEMISTRY

5.1 INTRODUCTION

The rocks of the Jutogh Group have undergone Barrovian type metamorphism. As discussed in Chapter 2, the rocks are mainly pelitic and semipelitic with bands of marble, calc-silicate, carbonaceous schist and amphibolite. The index minerals of the Barrovian sequence from garnet to sillimanite appear successively at higher topographic and structural levels showing inversion of metamorphic grades within the Jutogh Group. It has already been established (Chapter - 4) that major metamorphic minerals are pre-kinematic to ductile shearing. In this chapter the mineral assemblages and mineral chemistry of major metamorphic minerals including garnet zoning patterns have been described.

5.2 DELINEATION OF METAMORPHIC ZONES

Four metamorphic grades are present within the Jutogh Group: garnet grade, staurolite grade, kyanite grade and sillimanite grade. Pilgrim and West (1928) and Naha and Ray (1970) reported that the highest grade of metamorphism attained by the rocks of the Jutogh Group in Simla-Chur area was upto staurolite grade. From the Chur area restricted occurrence of kyanite and sillimanite were reported by Roy and Mukherjee (1976) and Das and Rastogi (1988).

The quartzite of the Jutogh Group above the Jutogh thrust contain both biotite and garnet. The phyllites of the Chail Formation occurring below the Jutogh thrust contain only chlorite. In the Chail Formation

biotie is absent except in a small locality near Haripurdhar (Fig.2.1). However, garnet is totally absent in the Chail Formation. So the Jutogh thrust marks the boundary between chlorite grade rocks of the Chail Formation and the garnet grade rocks of the Jutogh Group. The quartzite containing garnet and biotite above the Jutogh thrust in the Jutogh Group is considered in the garnet grade. The Jutogh thrust marks a break in metamorphism where biotite isograd is missing except in a restricted locality within the Chail Formation.

Staurolite makes its first appearance in the Jutogh mica schist occurring above the Rajgarh thrust. So the mica schist above the Rajgarh thrust is in the staurolite grade. However, the staurolite is distributed very unevenly and it is more common in the western part than the rest of the area. Staurolite forms in Al-rich, Ca-poor true metapelites (Muellar & Saxena 1977; Yardley 1989). Consequently in the medium grade metamorphic condition pelitic rocks may not contain staurolite if the bulk chemistry does not favour the formation of staurolite. Mg-rich chlorite ($Mg > Fe$) is also another marker to identify the rocks of staurolite grade. Fe-rich chlorite ($Fe > Mg$) is stable below the temperature at which staurolite is formed by the chlorite break down reaction (section 5.6). But pure Mg-chlorite (clinochlore) can be stable at very high temperature (Mueller & Saxena 1977). However, Mg-rich chlorite can be stable together with staurolite, muscovite, quartz and/or biotite well within the medium grade rock (Winkler 1977). So the rocks with the presence of Mg-rich chlorite is also considered within staurolite grade.

Kyanite and/or sillimanite have been observed in a very few samples just near the contact of the Chur granite. Presence of only kyanite identifies the rocks of kyanite grade. Similarly presence of sillimanite

G1 0 2/3 2.

with or without kyanite is considered the rocks to be in the sillimanite grade.

5.3 MINERAL ASSEMBLAGES

For the purpose of textural and petrographic studies, about 500 thin sections from Jutogh metasediments have been studied. Representative mineral assemblages of those samples have been presented in the Table 5.1. It has been observed that the rocks from the Jutogh Group are dominated by pelites to semipelites in addition to calc-silicate and amphibolite.

The mineral assemblages in pelites and semipelites in different grades are described below.

5.3.1 Garnet Grade

Rocks in the garnet grade have mainly two type of assemblages. From quartzite the mineral assemblage is,

Quartz - Muscovite - Biotite.

From intercalated micaceous layer within quartzite the assemblage is

Quartz - Biotite - Muscovite - Garnet - Chlorite - Ilmenite ± Plagioclase (mostly oligoclase).

Epidote, sphene, apatite and tourmaline are present in minor proportion. Biotite and muscovite ratio in pelitic rock varies from place to place. Plagioclase is rare within the garnet grade. Both primary and retrograde chlorites are found in garnet grade.

5.3.2 Staurolite grade

In the staurolite grade the mineral assemblages are:

Quartz - Muscovite - Biotite - Garnet - (Mg-rich)Chlorite - Ilmenite $\pm$
Plagioclase,

Quartz - Muscovite - Biotite - Garnet - Staurolite - Ilmenite $\pm$ Plagioclase
and

Quartz - Muscovite - Biotite - Garnet - Plagioclase - Ilmenite.

In this grade also plagioclase is mostly oligoclase variety. Minerals present in minor amount are epidote, sphene, apatite and tourmaline.

5.3.3 Kyanite and Sillimanite grade

Both of these grades are described together because the mineral assemblages are same for both of the zones. Kyanite and sillimanite occur near the contact of .the Chur granite. Kyanite and sillimanite are also found in xenoliths within the granitic body (Loc:Near Chur Peak and W of Chur Peak), but is not considered here as the discussion includes only the Jutogh metasediments in the Chur area.

In the kyanite grade the mineral assemblage is,
Quartz - Biotite - Muscovite - Plagioclage - Kyanite $\pm$ Ilmenite.
For the sillimanite grade the assemblage is
Garnet - Biotite - Muscovite - Plagioclase - Sillimanite $\pm$ Ilmenite $\pm$
Kyanite.+ Quartz.

Sillimanite is present as mostly fibrolite and also as big flakes within the garnets.

5.3.4 Marble

Within the mica schist the pure marble and impure marble are present as bands. These are found to occur between Chogtali and Haripurdhar. The mineral composition of impure marble is
Quartz - Talc - Plagioclase - Tremolite - Epidote - Sphene - Opaques.

5.3.5 Basic rocks

The mineral assemblage in amphibolite is essentially,

Actinolite - Hornblende - Quartz - Plagioclase - Epidote - Garnet - Biotite $\pm$ Apatite $\pm$ Sphene $\pm$ Opaques.

5.4 AFM PLOTS

AFM projections, based on equilibrium mineral paragenesis and chemistry of the co-existing minerals, are presented for the individual metamorphic grades (Thompson 1957). These diagrams are very useful in the representation of mineral assemblages of metamorphic rocks derived from pelitic and semipelitic rocks which can be represented approximately by a system of six components: K_2O-FeO-MgO-Al_2O_3-SiO_2-H_2O (KFMASH).

Compositions of garnet, biotite and chlorite from the garnet grade are shown in Fig.5.2. In this grade garnet-biotite and garnet-biotite-chlorite co-exist. The `A' component in biotite has wider variation as compared to the garnet and chlorite. Mg/Fe ratio decreases from chlorite, through biotite to garnet. In this grade garnet-biotite-chlorite and garnet-biotite separately yield the crossing tie line relationship at very low angle which may be due to the analytical error. In the staurolite grade (Fig.5.3) primary chlorite does not coexist with staurolite but with garnet and biotite. Biotite has the most wide range of composition among all the minerals represented by AFM diagram in staurolite grade. But composition of staurolite has its least variation. Chlorite in staurolite grade is Mg-rich (Mg > Fe) than that in garnet grade. In this grade staurolite does not coexist with chlorite. In the kyanite and sillimanite

grade chlorite and staurolite are not present (Fig.5.4). The garnet composition in these grades is same as in staurolite grade. Biotite is more enriched in Al than that in staurolite grade.

5.5 MINERAL CHEMISTRY

5.5.1 Analytical procedure

Probe analyses were performed using a semiautomatic JEOL JXA-8600M electron probe X-ray microanalyzer with three channel wave length dispersive spectrometer (WDS) located in University Science Instrumentation Centre, University of Roorkee, India, operated at an accelerating voltage 15 KV and a sample current 20 nA. The beam size was 1 micron for garnet, staurolite, ilmenite, epidote, sphene and 10 micron for biotite, muscovite, chlorite and feldspar. The samples were well polished and then coated with carbon to a thickness of about 100A. Natural mineral standard (SPI standard, Canada) such as almandine, biotite, chlorite, plagioclase, sanidine, hematite, rutile were utilized. Wherever necessary multi-mineral standards were used in the analysis. ZAF correction regarding X-ray absorption, X-ray fluorescence effect, atomic number effect, back scatter and ionization penetration losses was applied to the raw data, and corrected using the software programme supplied by JEOL through DEC LSI-11/23 and 11/73 computers. Some of the analyses have also been carried out in Hokkaido University, Sapporo, Japan. The analytical condition was same as before.

Analyses were performed for coexisting minerals at rim part of the minerals except for the zoned minerals and used for calculation. For deducing the P-T condition 3 to 5 points were taken in 4 $micron^2$ area and

averaged to reduce the analytical error. This procedure was only followed in the case of garnet, biotite, muscovite and plagioclase. However plagioclase analyses were carried out only near the rim to avoid the effect of zoning in plagioclase. Mole fractions of different elements in garnet, biotite, muscovite, plagioclase have been calculated following the procedure as mentioned in table 6.1.

5.5.2 Garnet

Garnet from different metamorphic grades is characterized by almandine rich composition with varying proportion of spessartine, pyrope and grossular content. To account for the mineral chemistry of garnet only rim composition has been considered. It is observed that there is an overall increase of X_{Fe} from garnet grade (0.59-0.77) to staurolite grade (0.65-0.87). In the sillimanite grade X_{Fe} becomes little less (0.76-0.83). X_{Mn} decreases from garnet grade (0.04-0.18) to staurolite grade (0.005-0.09) (Fig.5.5a). Two samples viz., S-695 and S-616 from the staurolite grade show higher concentration (0.18 and 0.15 respectively) of X_{Mn}. In the sillimanite grade X_{Mn} is present in low concentration as well as high concentration (Fig.5.5a). X_{Ca} is more enriched in garnet grade (0.05-0.30) than that in staurolite grade (0.04-0.12) (Fig.5.5b). One sample from staurolite grade (S-320) shows high concentration of X_{Ca} (0.26). In sillimanite grade it ranges from 0.01 to 0.05. From garnet grade to staurolite grade X_{Fe} increases and X_{Mn} and X_{Ca} decrease. X_{Mg} does neither vary with respect to grade nor with respect to X_{Fe} (Fig.5.6a). X_{Mg} generally ranges from 0.05 to 0.12 irrespective of grade.

5.5.3-Biotite

Biotite does not show any major changes in composition in its octahedral site with respect to metamorphic grade. Naturally concentration of Fe increases with corresponding decrease of Mg in garnet and staurolite zones (Fig.5.6b). In garnet grade and staurolite grade X_{Fe} varies from 0.43-0.50 and 0.40-0.58 respectively. However in sillimanite grade it is about 0.43. X_{Mg} varies more widely in staurolite grade (0.27-0.46) than in garnet grade (0.33-0.39). In sillimanite grade it varies from 0.36 to 0.38. X_{Al} and X_{Ti} has no distinct correlation with respect to different grades (Fig.5.7a). Generally X_{Al} varies from 0.09 to 0.18 and X_{Ti} ranges from 0.01 to 0.06. But concentration of Al^{VI} is inversely proportional to the concentration of Ti in biotite. Also Mg/Fe in biotite does not change systematically with respect to zone. But Mg/Fe ratio shows that biotites from garnet, staurolite and sillimanite grade are mainly Fe rich. Biotites from S-738, S-616, S-858, S-321 and S-108 is Mg (Mg/Fe > 1) rich. There is no correlation between Mg/(Fe+Mg) in biotite and that in garnet according to grade (Fig.5.7b).

5.5.4 Muscovite

Muscovite does not show any variation in its composition with respect to grade. Generally Al in octahedral site decreases with increases in Fe (Fig.5.8a). X_{Al} in octahedral site restricted within the range from 0.88-0.94. X_{Fe} generally ranges from 0.02 to 0.06. One sample S-859 shows high concentration of Fe (X_{Fe}= 0.11) with low concentration of Al (X_{Al}= 0.84).

5.5.5 Chlorite

The chemical composition of chlorite varies from garnet grade to

staurolite grade (Fig.5.8b). In garnet grade X_{Fe} and X_{Mg} range from 0.51 to 0.55 and 0.44 to 0.48 respectively. But in staurolite grade chlorite is more rich in Mg than Fe. In this grade X_{Mg} ranges from 0.51 to 0.55 and X_{Fe} ranges from 0.45 to 0.48. Si, Al in tetrahedral site and Al in octahedral site do not show any correlation between garnet grade and staurolite grade. However, X_{Al} [$Al^{VI}/(Al^{VI}+Fe+Mg)$] of chlorite in both the grades is restricted within the range of 0.24 to 0.30.

5.5.6 Plagioclase

Plagioclase from the Jutogh Group of rocks is mostly of oligoclase composition. In oligoclase variety X_{Ca} varies from 0.10 to 0.25. But S-367, S-354 from staurolite grade and S-833 from sillimanite grade are albite (X_{Na}= 0.9, 0.92 and 0.92 respectively). S-38 and S-695 contain appreciable (X_K= 0.04 and 0.05 respectively) amount of potassium.

5.5.7 Ilmenite

Ilmenite is almost always pure with X_{Fe} [$Fe/(Fe+Mn)$] from 0.935 to 0.997 and X_{Mn} [$Mn/(Fe+Mn)$] from 0.003 to 0.065. There is no variation in mineral chemistry between ilmenite present in the matrix and as inclusion.

5.6 GARNET ZONING

Compositional variation within a single mineral grain is termed as chemical zoning (Tracy 1982). But all the elements present within a particular mineral need not necessarily show the chemical variation. Among the metamorphic minerals which show the chemical zoning, garnet is the most widely studied mineral because it invariably shows chemical zoning due to its refractory nature.

Two types of zoning may be observed in garnet (Tracy 1982): growth zoning and diffusion zoning. Growth zoning in garnet is produced by the continuous net transfer reaction and exchange reaction among the coexisting phases that are driven by changes in temperature and pressure during growth. The development of growth zonation pattern may be explained either as a result of fractionation of elements during growth (Hollister 1966; Tracy 1982) or as a result of partitioning of elements with the progress of garnet forming reaction. The difference between growth zoning and diffusion zoning is that, the growth zoning is developed due to garnet forming reaction and diffusion zoning is imposed on the pre-existing crystal that may or may not have been zoned (Tracy 1982). Diffusion zoning within the garnet may modify already zoned crystal into homogeneous one or an originally homogeneous crystal into zoned crystal. In the high grade garnets (sillimanite, K-feldspar grade) there is post-growth volume diffusion commonly during cooling which immediately follows the peak of metamorphism or during a later, lower grade remetamorphism (Tracy 1982). Spear (1991) reported that in amphibolite facies also the rim composition of garnet can be easily destroyed by diffusion.

Loomis (1983) listed and briefly discussed type of informations one may get from garnet zoning profile. One of the reasons to study the garnet zoning together with the inclusions of other phases is to explain the changes of bulk mineral assemblages during garnet growth (Loomis 1972a; Spear 1988). The composition of zoned crystals and their inclusions may also be used for calculating geothermometry and geobarometry (Spear & Silverstone 1983; Banno et al. 1986; St Onge 1987; Florence & Spear 1991). Garnet zoning profile also provides

information about the disequilibrium growth processes, helps to determine the rate of reaction that causes zoning in a crystal if the rate of diffusion is known.

5.6.1 Methodology

For the purpose to elucidate the zoning profile from the Chur area suitable garnets were chosen from pelites and pelitic layers within semipelites. Total 35 garnets have been analyzed. The analyses were performed from rim to rim along two perpendicular directions. In order to check the zoning pattern, profile should pass through the core of a grain. Since this cannot be ensured easily, the largest grain in one thin section has been chosen assuming that the core is exposed in such a grain. It has been observed that there is no substantial change of pattern comparing one direction with the other. So one profile from each garnet has been chosen.

Different textural types of garnets such as inclusion rich garnets, garnets with inclusions rich core and inclusion poor rim, inclusion poor garnets and the garnet with oriented inclusion trails from individual grade have been chosen. It has been observed that only in staurolite grade the zoning profiles are sometimes related with the garnet microstructure.

The garnets with more than about 1mm diameter are generally considered to ensure the least effect of diffusion due to sizes of garnets (Jiang & Lasaga 1990; Florence & Spear 1991). However, two garnets (S-765 & S-93/2) of smaller than 1mm have been taken into consideration because of the presence of characteristic zoning profile. The zoning profile from S-765 was considered because it retains the original growth zoning profile. The complete reverse zonation pattern in Mn is observed only in the garnets from S-93/2.

Representative zonation patterns of garnet grains from Jutogh Group are shown from Fig.5.9 to Fig.5.16. In each figure a photograph of the garnet is also shown.

5.6.2 Garnet zoning pattern in Garnet grade

Fig.5.9, Fig.5.10 and Fig.5.11 show the garnets and their respective zoning profiles from garnet grade. Fe is continuously enriched from core to rim in Fig.5.9b and Fig.5.10b. In Fig.5.11b Fe zonation pattern is erratic. Mg shows almost flat trend with little decrease near the rim in Fig.5.9b. In other cases Mg profiles are flat. Ca shows erratic trend in Fig.5.9b. In Fig.5.10b Ca profile is flat near core and trends downward near rim. In Fig.5.11b Ca increases near core and gradually decreases towards rim. Mn gradually decreases from core to rim of both garnets as in Fig.5.9b and Fig.5.10b though little increase in Mn near rim may be observed in Fig.5.9b. Completely reverse trend in Mn profile may be observed in Fig.5.11b.

The antithetic relations between Fe and Mn profiles in Fig.5.9b and Fig.5.10b suggest the continuous enrichment of Fe in expense of Mn. Chlorite is the major source of Mn at low temperature (Trzcienski 1977; Tracy 1982). As the temperature increases, garnets are formed by chlorite breakdown reaction (section 5.7.1). As a result chlorite is gradually depleted in the matrix which causes the decrease of Mn concentration and subsequent enrichment of Fe in the matrix. Gradual increase of Mn from core to rim in Fig.5.11b suggests that this garnet has been formed in a different environment where garnet was gradually enriched in Mn at the expense of Ca. Lack of any major break in all these profiles suggests that these garnets have grown in a single stage without any interruption

(Olimpio & Anderson 1978).

5.6.3 Garnet zoning pattern in Staurolite grade

In the staurolite grade the garnets show the profiles like in Fig.5.12b, Fig.5.13b, Fig.5.14b and Fig.5.15b. Garnet at the base of the mica schist unit near Rajgarh thrust shows bell shaped Mn-zoning profile (Fig.5.12b & 5.13b) with minor enrichment near rim (Fig.5.13b). The trend of Mn-zoning profile in garnet becomes more relaxed at higher topographic levels and nearer to granite contact (Fig.5.14b). Also Mn is more enriched near rim (Fig.5.14b). Garnets nearest to granite contact (Fig.5.15b) show flat profile of Mn. The antithetic relation between Mn and Fe profile is clearly observed near the upper carbonaceous -schist (Fig.5.12b, 5.13b). But no such relation is noted in higher topographic level as Mn shows flat trend near core though bowl shaped pattern in Fe is observed in those garnet (Fig.5.14b, 5.15b). Prominent undulation of Mn profile is also observed (Fig.5.12b) from staurolite grade rock at lower level (near upper carbonaceous schist). Bowl shaped Mg profile is observed prominently in Fig.5.13b and faintly in Fig.5.12b in lower level. Flat trend is observed from Fig.5.13b and Fig.5.14b and irregular trend in Fig.5.15b. In Fig.5.12b Ca concentration is depleted at the core with the gradual increase in concentration towards inner rim. Ca is again gradually depleted from the inner rim to rim. The garnet in Fig.5.12 has its inclusion rich core zone and inclusion poor rim zone. The bowl shaped profile of Ca corresponds to the inclusion rich core and depleted portion near rim corresponds to the inclusion poor inner rim. This garnet seems to have grown in two stages which is understood by inclusion rich core and inclusion poor rim zone. In other garnets Ca shows flat (Fig.5.13b),

erratic (Fig.5.14b) and flat near core with downward trend near rim (Fig.5.15b).

It may be observed that Mn-zoning profiles from staurolite grade vary systematically from the contact between upper carbonaceous schist and mica schist to the contact with the Chur granite. Mn enrichment near rim suggests the presence of rim resorption of garnet in staurolite grade at successively higher topographic levels. Karabinos (1983) suggested that the garnet gained a Mn rich rim by a resorption reaction in which garnet was deffussively depleted in Mg and Fe for the production of chlorite. But Robinson (1991) argued that the garnet was partially resorbed by the surface dissolution to produce an Mn-enriched retrograde assemblage of hydrous ferromagnesian silicates, mainly chlorite. Consequently rims of garnets were reset with the Mn-rich matrix to Mn-rich rim. However Jones (1994) reported flat chemical profile of low grade garnet from Leon region, France and interpreted it as the result of occurring this garnet in a shear zone reflecting increased rate of diffusion. Altogether, Mn profiles in garnets from staurolite grade suggest that the Mn zonation patterns have been partially modified at successively higher topographic level due to limited volume diffusion near rim. But Ca shows some original zoning profile even if the other divalent cations do not because of the slowest diffusion rate of Ca thus showing different trends in different garnets. Thus depletion of Ca at the inner rim in Fig.5.12b may be explained by the following continuous reaction at later stage:

$$St + Bio + Qtz + (Ca,Al)phase = Grt + Mus + H_2O \qquad [R\ 5.1]$$
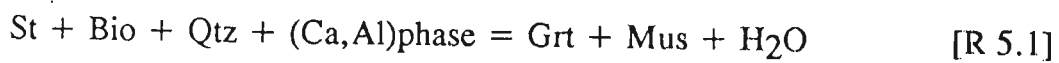
(Frost & Tracy 1991). The fluctuation of Ca like in Fig.5.14b has been reported by Anderson and Olimpio (1977). Crawford (1977) pointed out that reaction responsible for the formation of Ca zoning is different from

62

those controlling zoning of other elements. But Chakroborty and Ganguly (1991) argued that interdependency of zoning pattern of divalent cations must be present to maintain the stoichiometry of garnet. So for the garnet in Fig.5.14 complex method of pertitioning of elements is suggested which may be reflected by Ca zonation pattern. In Fig.5.15b Ca concentration is depleted near rim and uniform around core. It may be pointed out that the size of this garnet is more than 3.4mm showing flat trend of Mn and Ca and almost flat trend of Fe and Mg near core. Chakroborty and Ganguly (1991) suggested that concentration profile of different elements at garnet cores become progressively more homogeneous with increasing grain size, implying that the larger garnets grow earlier and thus have sufficient time to be effected by volume diffusion which gives the flat pattern near the core. So the flat patterns shown in Fig.5.15 suggests that this garnet started to grow at early stage, suffered the highest temperature within the staurolite grade and ultimately homogenized near the core.

In summary, the garnets from staurolite grade have their complex growth history. The increase of temperature towards the granite contact is clearly reflected by the different garnet zonation patterns in staurolite grade because the flattening of zoning trends is gradually extensive towards the granite contact. The reverse trends of Mn zonation profiles due to retrogression are also observed near rims.

5.6.4 Garnet zonation pattern in Sillimanite grade

Garnets showing the trend like Fig.5.16b are present within the sillimanite grade. In the garnet core Mg is enriched and Mn is depleted showing antithetic relationship. There is a slight increase of Mn at inner

rim. After that there is gradual decrease of Mn concentration upto rim. Fe and Ca show almost flat profiles across the core. But from inner rim to rim Fe increases with sudden decrease of Ca.

The same Mn-zoning profile like in sillimanite grade has been proposed by Miyashiro (1953) and Muller and Schneider (1971) as due to increase in temperature. The computer simulated profile from Frost and Tracy (1991) also show the similar zoning trend of Fe and Ca. The reaction as suggested by them is,

St + Mus + Qtz + An = Grt + Ky + Bio + H$_2$O   [R 5.2].
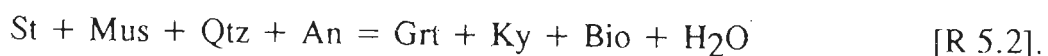
So the zoning profiles from the garnets of sillimanite grade (Fig.5.16b) suggest that garnet has been formed in kyanite grade and continued to grow at the early stage of sillimanite grade.

5.7 INFERRED METAMORPHIC REACTIONS

Metamorphic reactions have been based on mineral paragenesis, AFM topology and also from changes observed in mineral composition (Thompson 1976,1982; Winkler 1979; Turner 1981; Yardley 1989).

5.7.1 Garnet grade

In garnet grade garnet and chlorite coexist in between. Fe/(Fe+Mg) is more enriched in garnet and in biotite than in chlorite. Also it has been observed from this grade that $(Mg/Fe)^{Chl} > (Mg/Fe)^{Bio} > (Mg/Fe)^{Grt}$ (Fig.5.2). The garnet zonation pattern shows normal growth with decreasing of X_{Mn} and increasing X_{Mg} (Lal et al. 1987). From mineral chemistry and the co-existing mineral assemblage (see 5.3) following garnet forming continuous reaction is suggested (Spear 1991)

$$Chl + Mus + Qtz = Grt + Bio + H_2O \qquad\qquad [R\ 5.3].$$
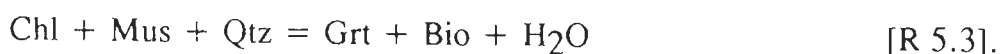
Frost and Tracy (1991) added the additional reactant phases of Ca,Al rich such as epidote and plagioclase [R 5.1]. Since chlorite has a stronger preference for Mg than the phases on the right-hand side of the reaction, this continuous reaction will cause the depletion of Fe in the remaining chlorite as the reaction proceeds (Yardley 1989).

5.7.2 Staurolite grade

As described in section 5.3.2 in the staurolite grade two main mineral assemblages are present. Staurolite also has restricted occurrence because the staurolite forms in a range of Al-rich, Ca-poor pelitic rocks (Yardley 1989 pp.67). Garnet zoning profile from this grade shows the retrograded nature at the rim. So it is concluded that staurolite has been formed by the garnet consuming discontinuous reaction,

$$Chl + Mus + Grt = St + Bio + Qtz + H_2O \qquad\qquad [R\ 5.4].$$
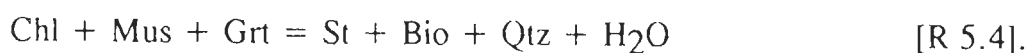
As the reaction proceeds phases from reactant side are gradually depleted. Chlorite being the least amount among others is consumed first and reaction is ceased. Ultimately the assemblage becomes without chlorite. Zoning profile suggests the possible continuous reaction at the last stage is

$$St + Bio + Qtz + (Ca,Al)phases = Grt + Mus + H_2O. \qquad [R\ 5.2]$$

5.7.3 Kyanite-Sillimanite grade

In the kyanite and sillimanite grades staurolite and chlorite are not present. The Al_2SiO_5 polymorphs was formed by the following discontinuous reactions:

$$St + Mus + Qtz = Al_2SiO_5 + Bio + Grt + H_2O \qquad\qquad [R\ 5.5]$$
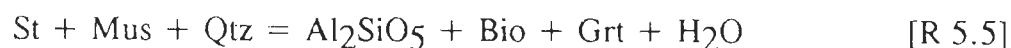
(Thompson & Norton 1968; Froese & Gasparrini 1975) and

$$Mg\text{-rich chlorite} + Mus + Qtz = Al_2SiO_5 + Bio + H_2O \qquad [R\ 5.6]$$

(Carmichel 1970).

From the texture it has been observed that garnet incorporates sillimanite flakes and muscovite. So in sillimanite grade garnet was formed by following continuous reaction:

Bio + Al$_2$SiO$_5$ + Qtz = Grt + Mus   [R 5.7]

5.8 DISCUSSION

From this area it has been observed that the major phase of metamorphism was prior to thrusting (Chapter 3). So the original positions of metamorphic isograds must have been greatly dislocated during thrusting. In this area though the positions of thrust planes have been identified along the contact between two different lithologies (Jutogh Thrust between the Chail formation and Lower Carbonaceous Schist, Rajgarh Thrust between Quartzite and Upper Carbonaceous Schist and Chur Thrust between Mica Schist and Granite) the thrust planes are also present in small scale which might slice the individual metamorphic isograd. The drawing of metamorphic isograd has not been attempted because in the above situation drawing of metamorphic isograds are tectonic artefacts that reflect the late thrusting phenomenon, rather than primary metamorphic features.

Single stage growth of garnet has been observed in garnet grade. But from two stage growth to complex zonation pattern have been noticed in staurolite grade. The effect of diffusion is more clearly observed at successively higher topographic levels. Within the staurolite grade the temperature increases gradually from lower levels to higher topographic levels because of the presence of inverted metamorphic sequence. So at the higher level the rocks have been cooled from higher temperature; thus

66

got more time to reach the closure temperature (Spear 1989) giving the more relaxed trend in zoning profile. Some of the garnets from staurolite grade near upper contact (topographically) of Upper carbonaceous schist show typical growth zonation pattern with bell shaped Mn profile with no resorption near rim in garnet grade and staurolite grade. In sillimanite grade garnet shows more relaxed trend due to limited volume diffusion.

FIGURES AND TABLE
CHAPTER - 5

FIGURE 5.1: Locations of the samples collected from Chur area to study different aspect.

Sample No. containing **staurolite** = S-48, S-54, S-59, S-62, S-107, S-119/2, S-134, S-164, S-177, S-318, S-321, S-851, S-858, S-882.

Sample No. containing **kyanite and/or sillimanite** = S-77/2, S-114, S-717, S-724, S-833, S-879, S-894, S-929.
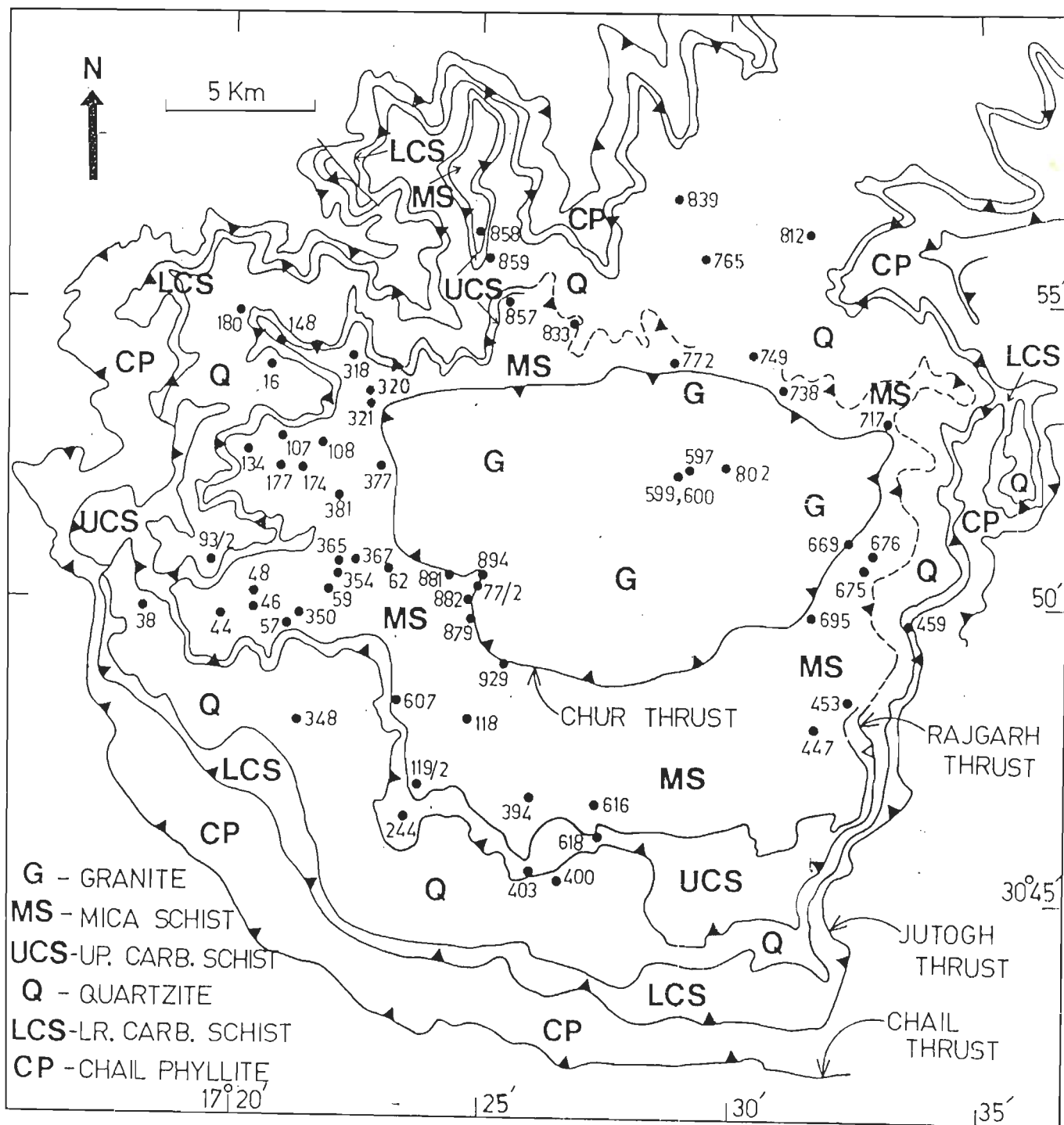
Fig. 5.1

FIGURE 5.2: AFM plot in garnet grade for different samples. Note that Fe concentration decreases from garnet through biotite to chlorite. The crossing tie lines at narrow angle may be because of analytical error.

A

+Mus
+Qtz

.8

.6

.4

GRT

CHL

.2

M

F

.2

BIO

O·5
F

1

O·5
F

O
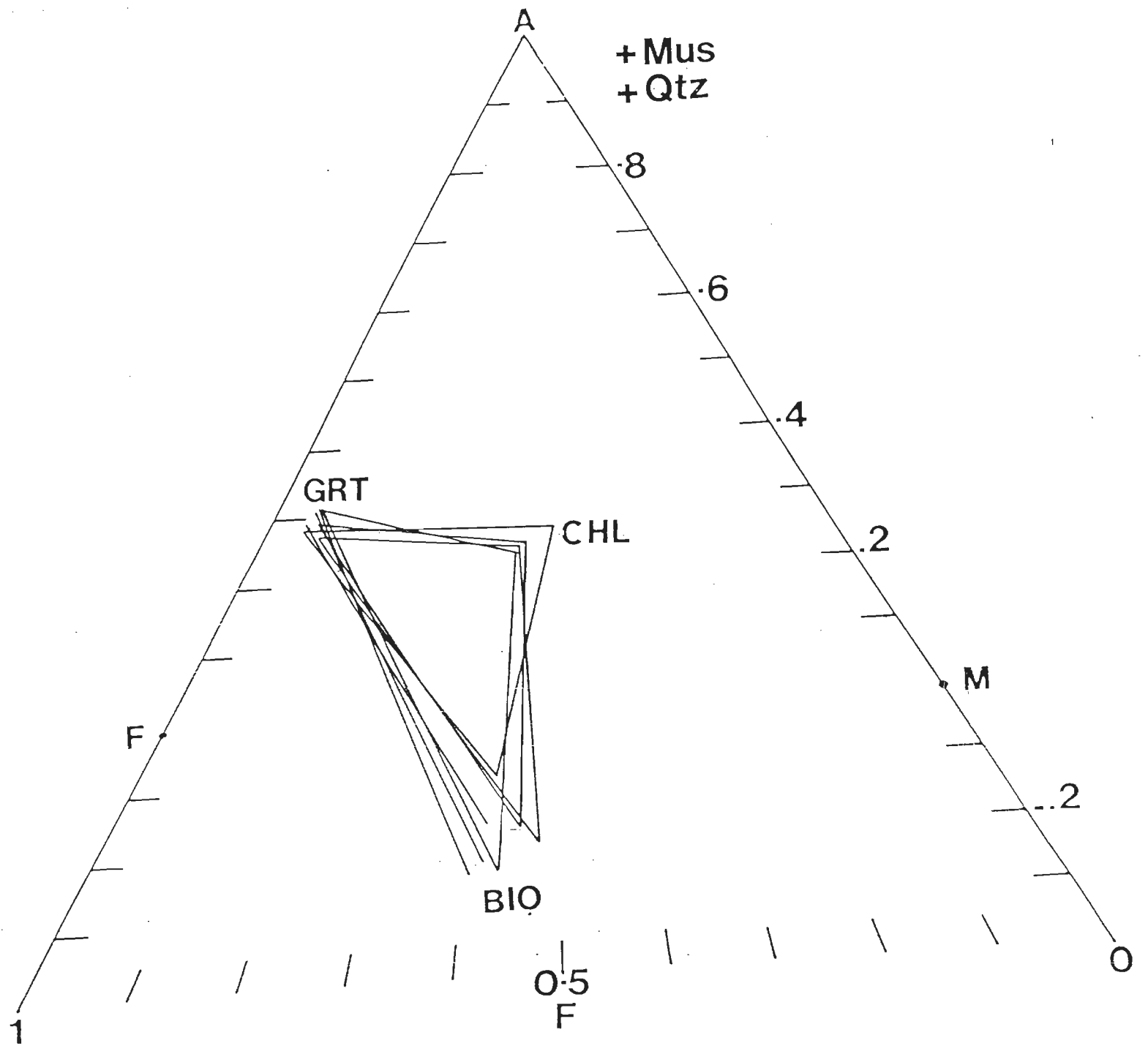
Fig.5.2

FIGURE 5.3: AFM plot in staurolite grade. There are two distinct assemblages; one with chlorite and another without chlorite. Also chlorite does not co-exists with staurolite. Composition of biotite has its wide variation.

A

+Mus
.8 +Qtz

ST

.6

GRT

.4

CHL

.2

M

F

-.2

BIO

1

O

0.5
F
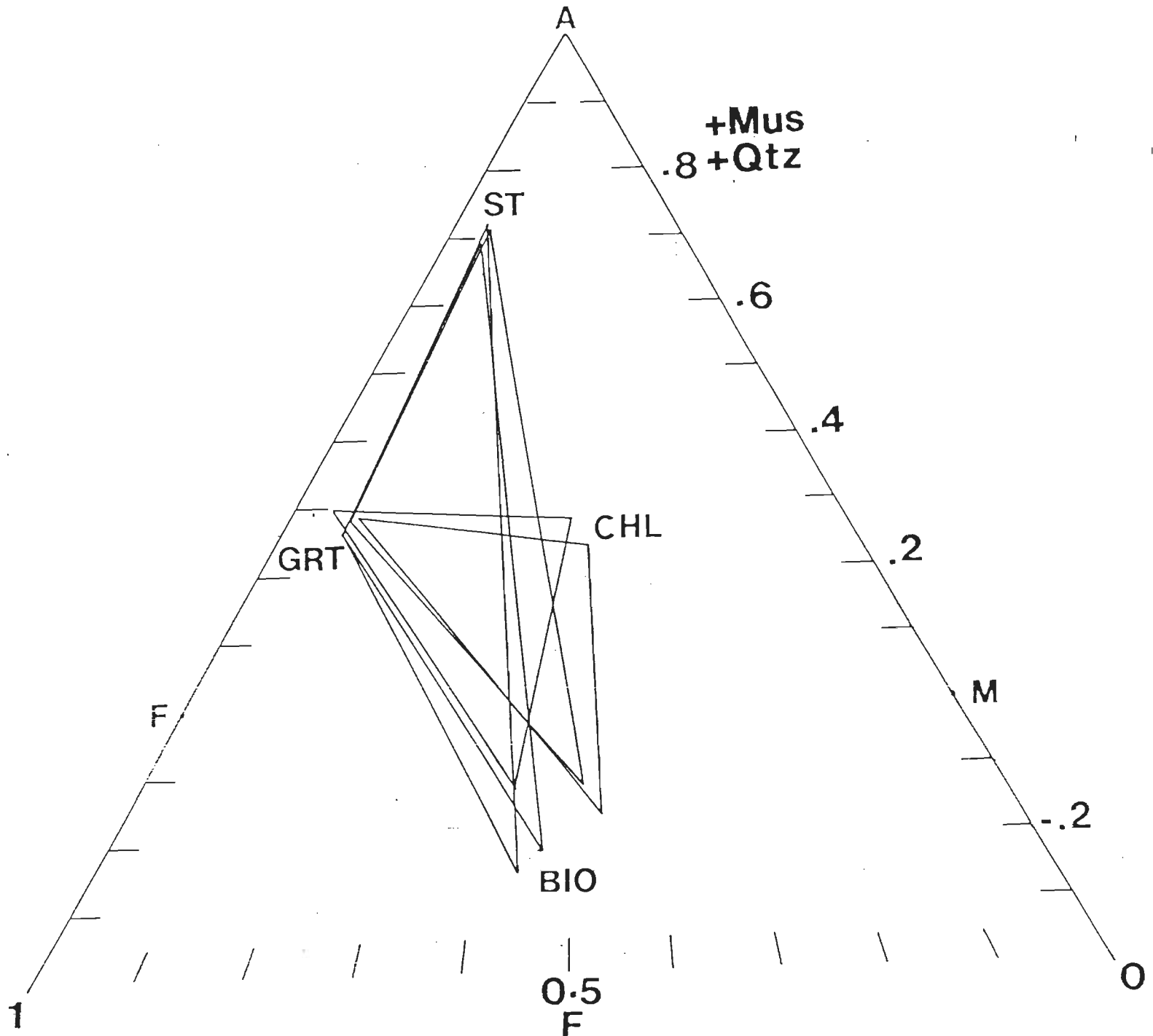
Fig.5.3

FIGURE 5.4: AFM plot in kyanite-sillimanite grade. In both the grades the mineral composition is same; thus are plotted in the same diagram. Note that biotie composition has changed from kyanite grade to sillimanite grade.

KY/SILL

+ Mus
+ Qtz

.8

.6

.4

.2

-.2

GRT

F.

.M

BIO

1

0.5
F

0
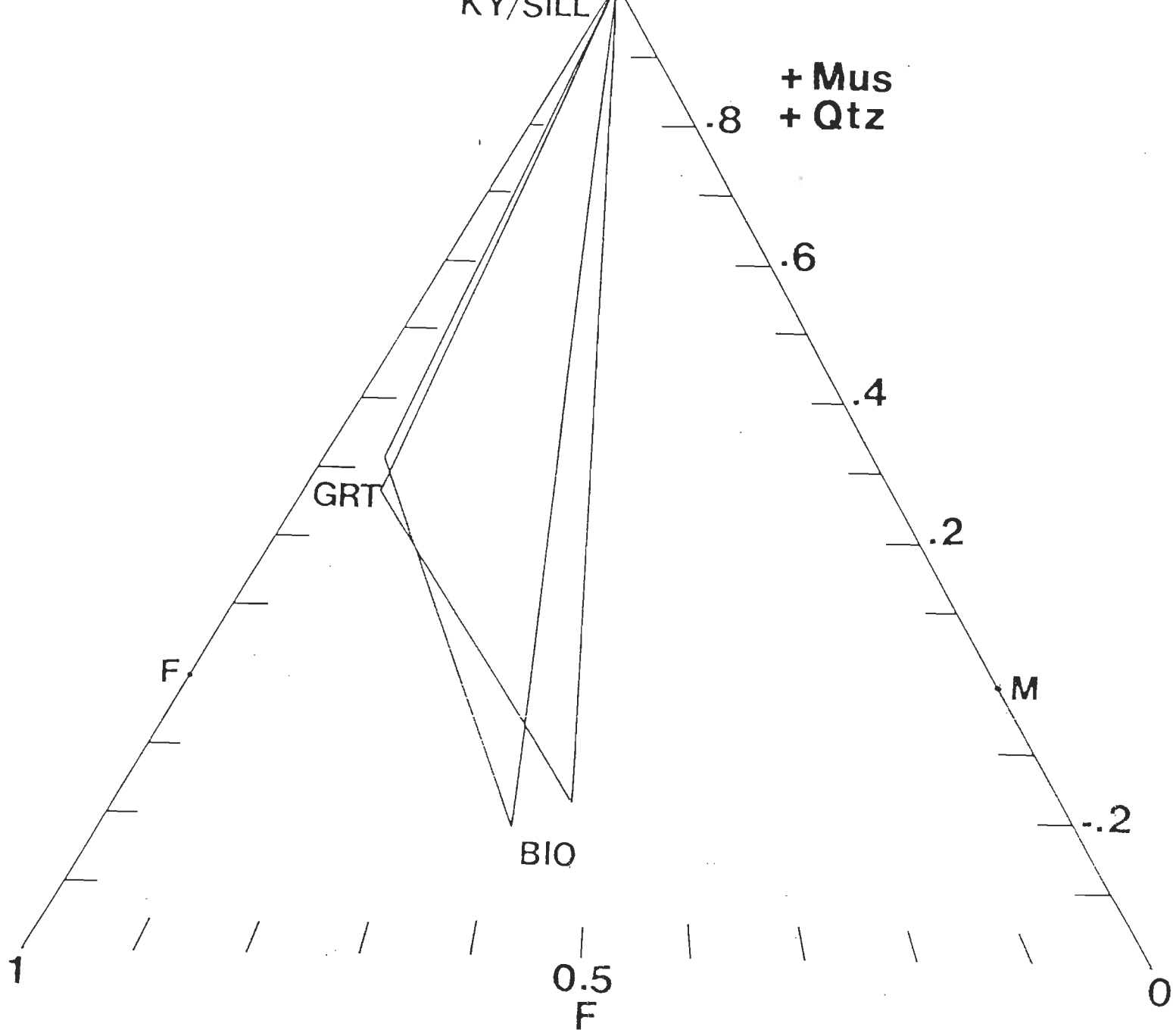
Fig. 5.4

FIGURE 5.5: VARIATION OF ELEMENTS IN GARNET

(a). X_{Mn} - X_{Fe} for garnets from different grades. With the increase of grade from garnet to staurolite X_{Mn} decreases and X_{Fe} increases. In kyanite-sillimanite grade there is no such correlation.

(b). X_{Ca} - X_{Fe} plot for gatnets from different grades. There this an approximate negetive corrilation between these parametres.

NOTE: From Figure 5.5 to Figure 5.8 the meaning of symbols are as follows.

Open Circle - Garnet Grade.
Open Square - Staurolite Grade.
Open Triangle - Kyanite-Sillimanite Grade.
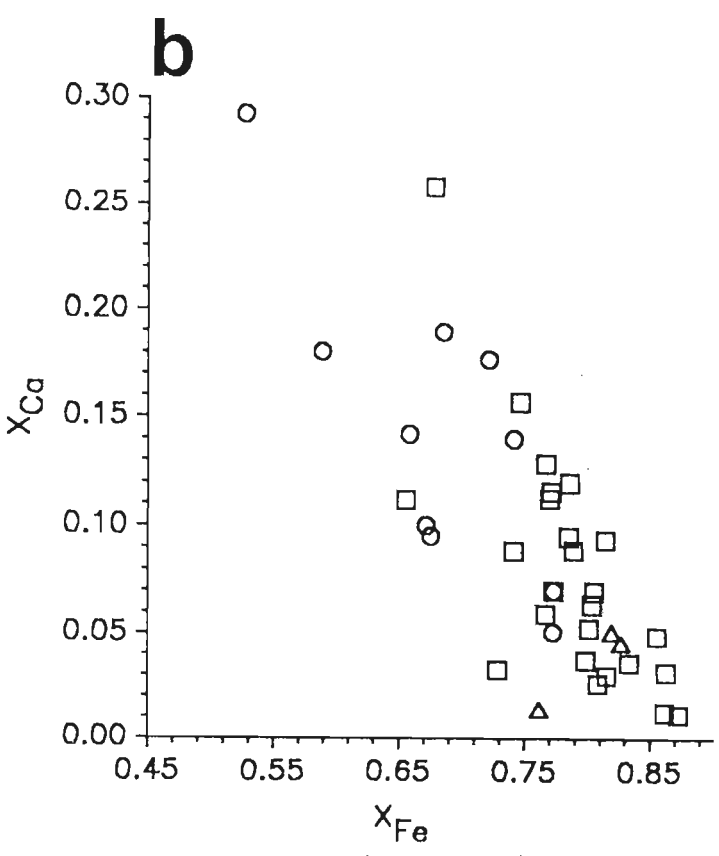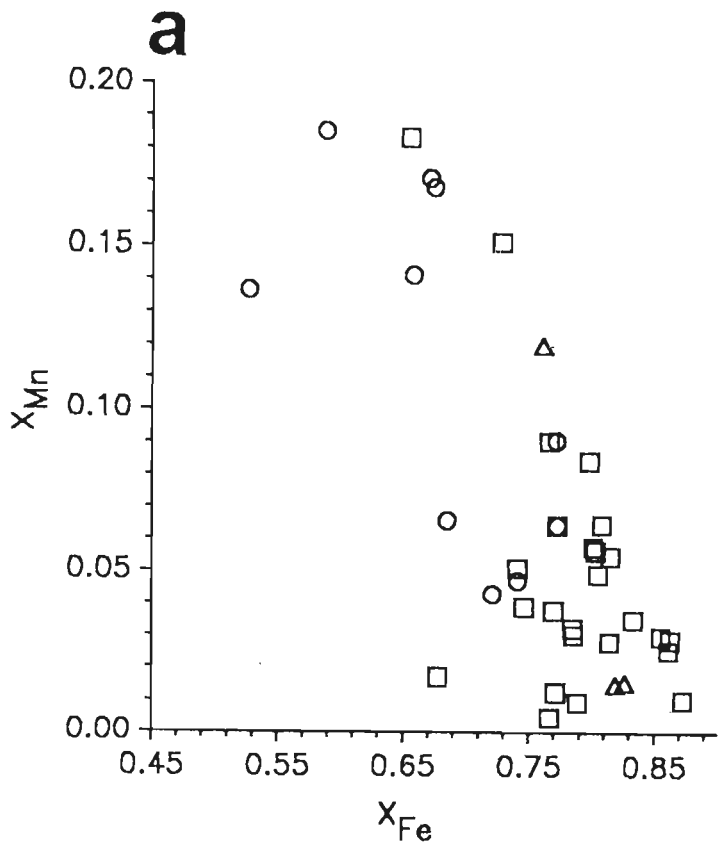
Fig.5.5

FIGURE 5.6: VARIATION OF ELEMENTS IN GARNET AND BIOTITE

(a). X_{Mg} - X_{Fe} plot for garnets from different grades.

(b). X_{Mg} - X_{Fe}. plot for biotites from different grades.
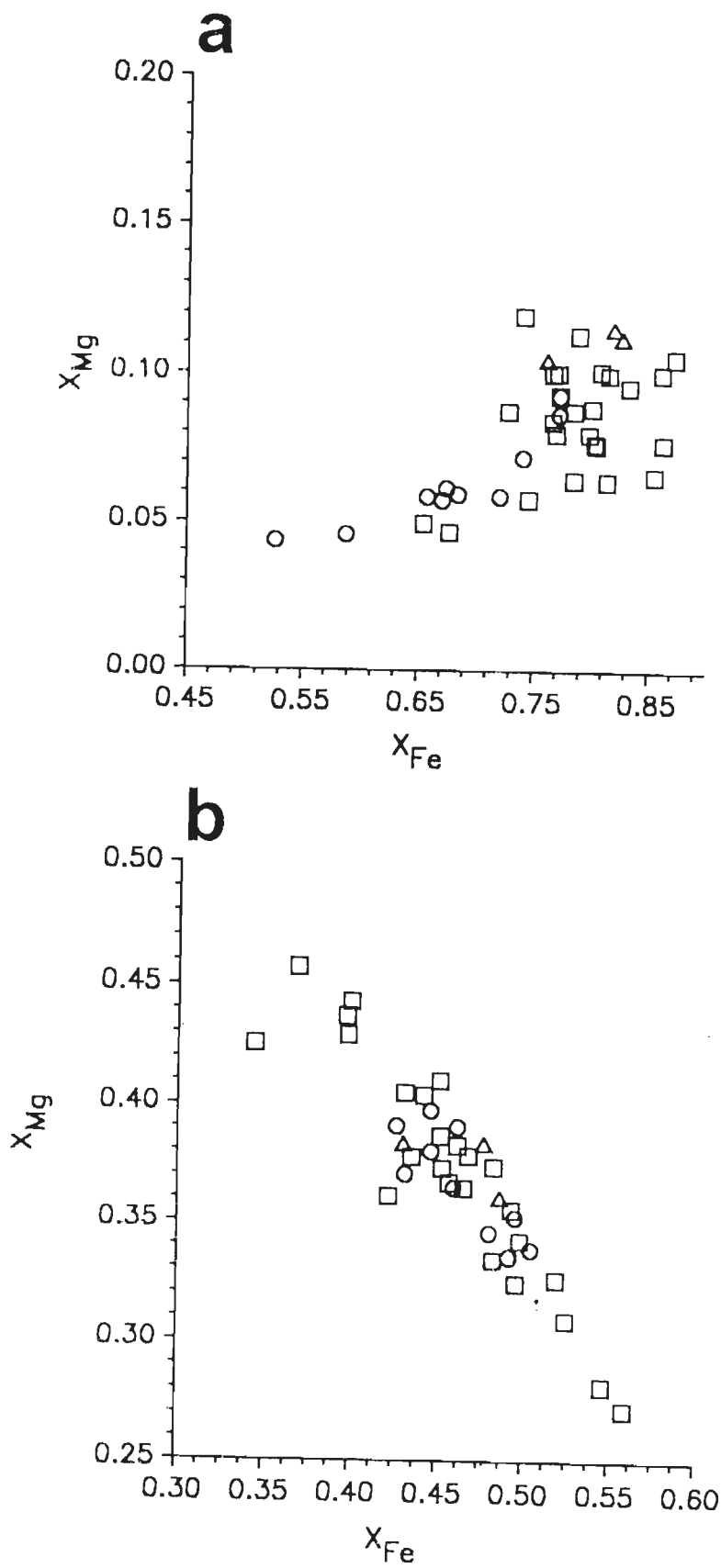
Fig.5.6

FIGURE 5.7: VARIATION OF ELEMENTS IN BIOTITE AND RELATION BETWEEN GARNET AND BIOTITE

(a). $(X_{Al})^{VI}$ - X_{Ti} plot for biotite showing negetive correlation. But there is no correlation according to grade.

(b). Between $Mg/(Fe+Mg)$ in biotite and that in garnet there is no correlation according to grade which suggests the $\ln K$ does not have a constant value. But both the values do not change from one grade to another.

Fig.5.7

FIGURE 5.8: VARIATION OF ELEMENTS IN MUSCOVITE AND CHLORITE

(a). $(X_{Al})^{VI}$ -(X_{Fe}) plot for muscovites. .

(b). X_{Mg} [Mg/(Fe+Mg)] in chlorite decreases with increase X_{Fe} [Fe/(Fe+Mg)]. Note that Fe rich chlorite is present in garnet grade where as Mg rich chlorite is present in staurolite grade.
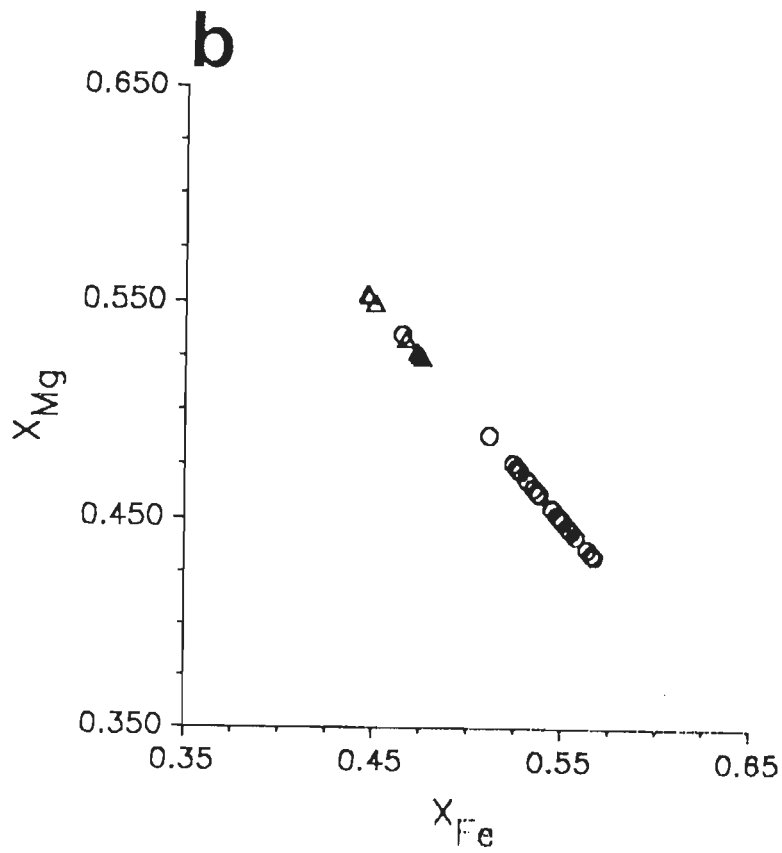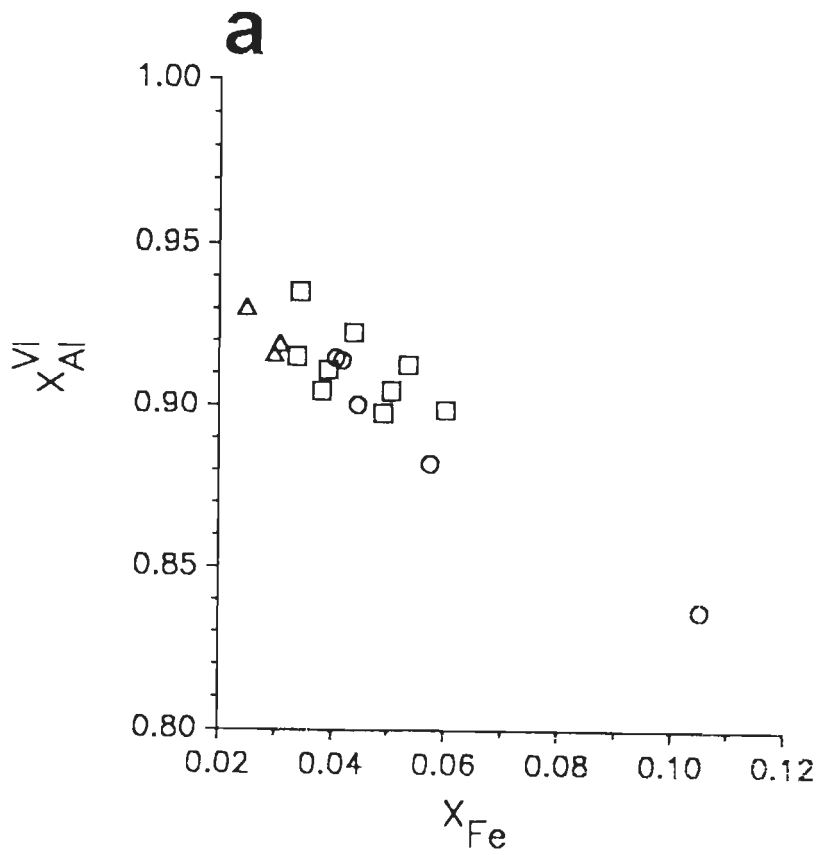
Fig.5.8

FIGURE 5.9: Zoning profile **(b)** for a syntectonic (to F_1) garnet **(a)**. Garnet Grade; Sample No. S-16; Base-
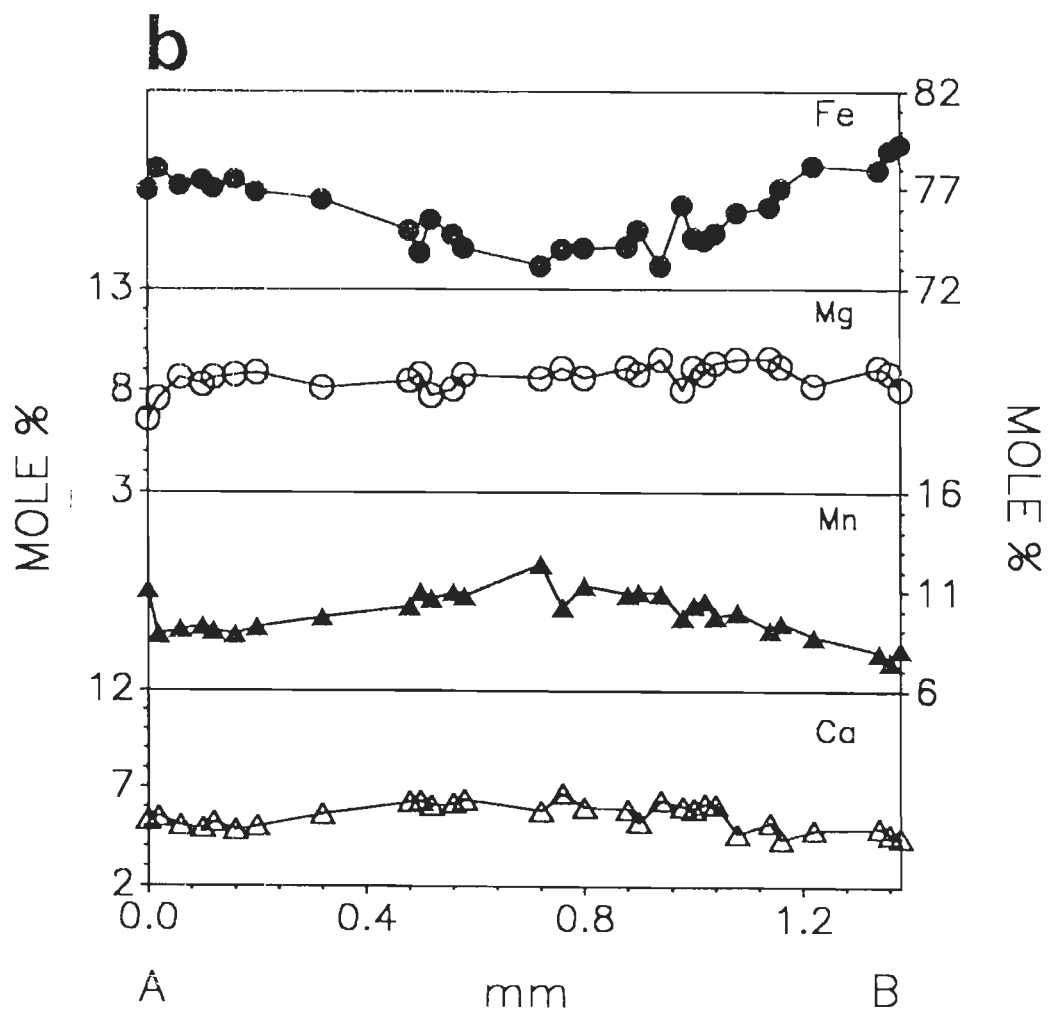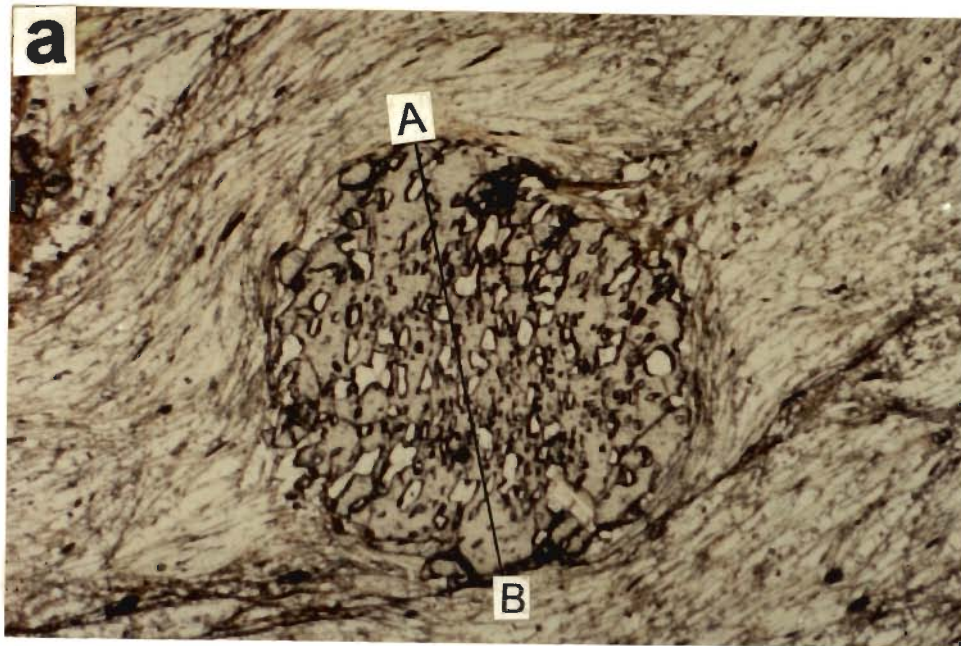
Fig.5.9

FIGURE 5.10: Inclusion rich garnet **(a)** is pre-tectonic with respect to S_e. Typical growth zonation pattern is clearly observed without any break in the profile **(b)** which suggests the single stage growth of this garnet. Antithetic relationship between Fe and Mn prevails in this garnet. Garnet Grade; Sample No. S-765; Base- 2 mm.
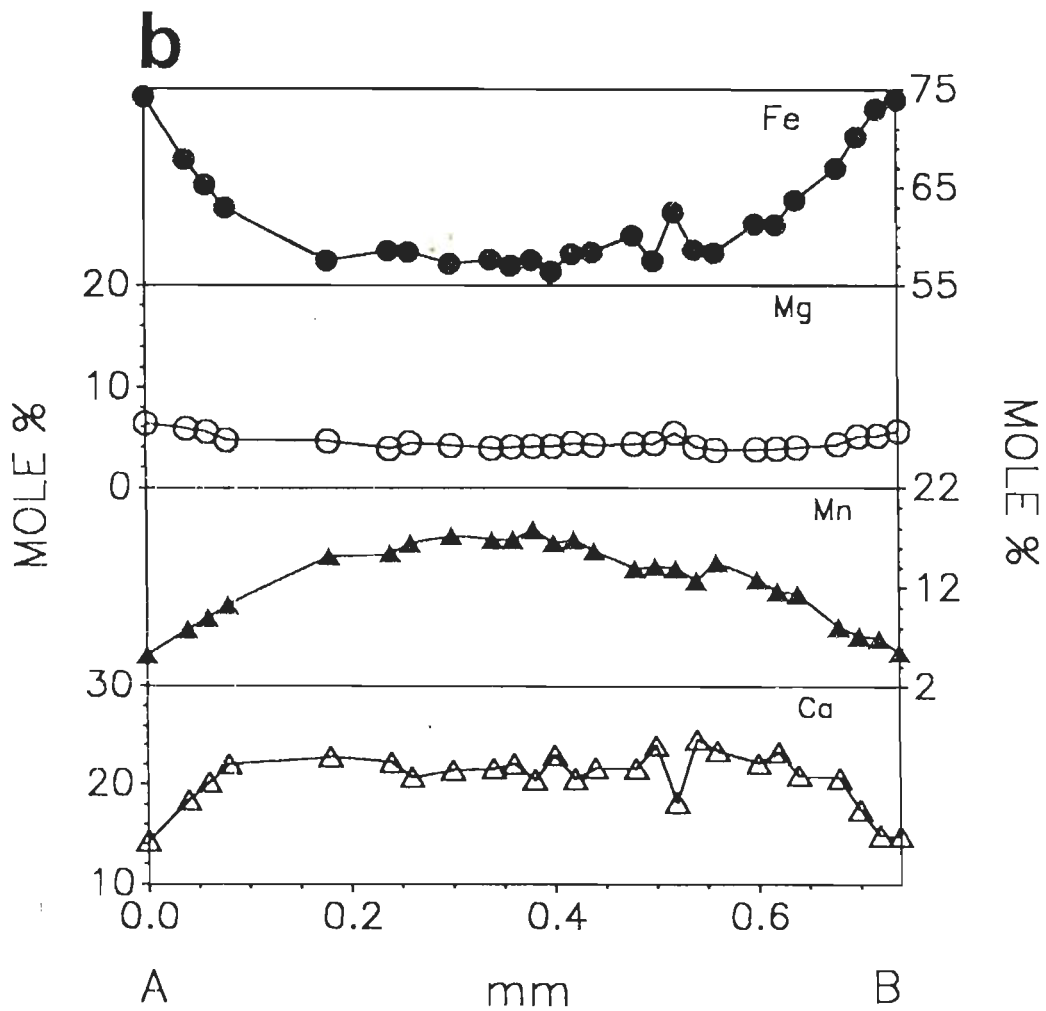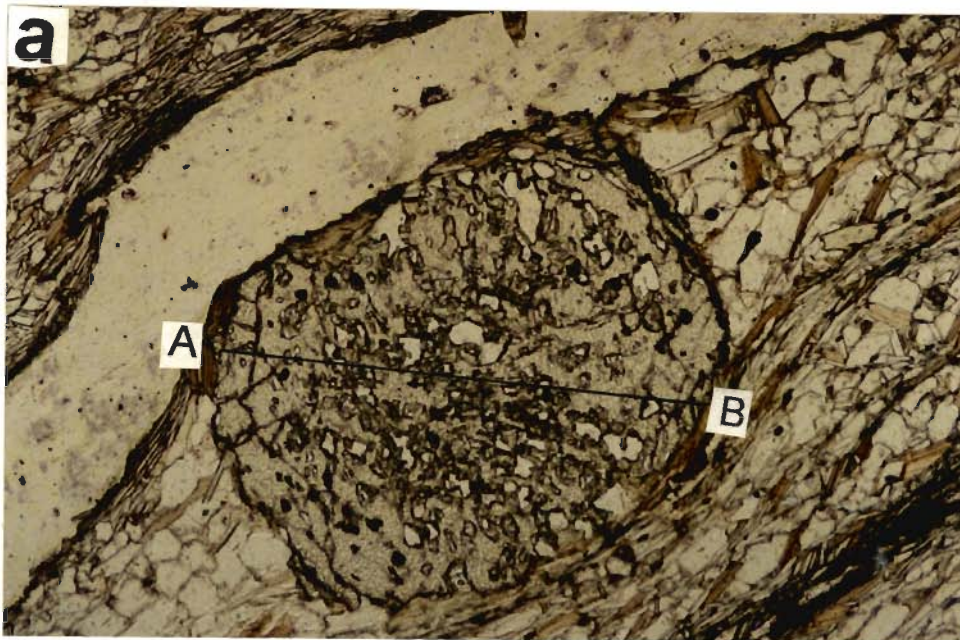
Fig.5.10

FIGURE 5.11: Small polygonal garnet (a) shows reverse zonation pattern of Mn (b). Note that antithetic relationship prevails between Mn and Ca in contrast to Fig.5.10 and Fig.5.11. Garnet Grade; Sample No. S-93/2; Base-0.4mm.
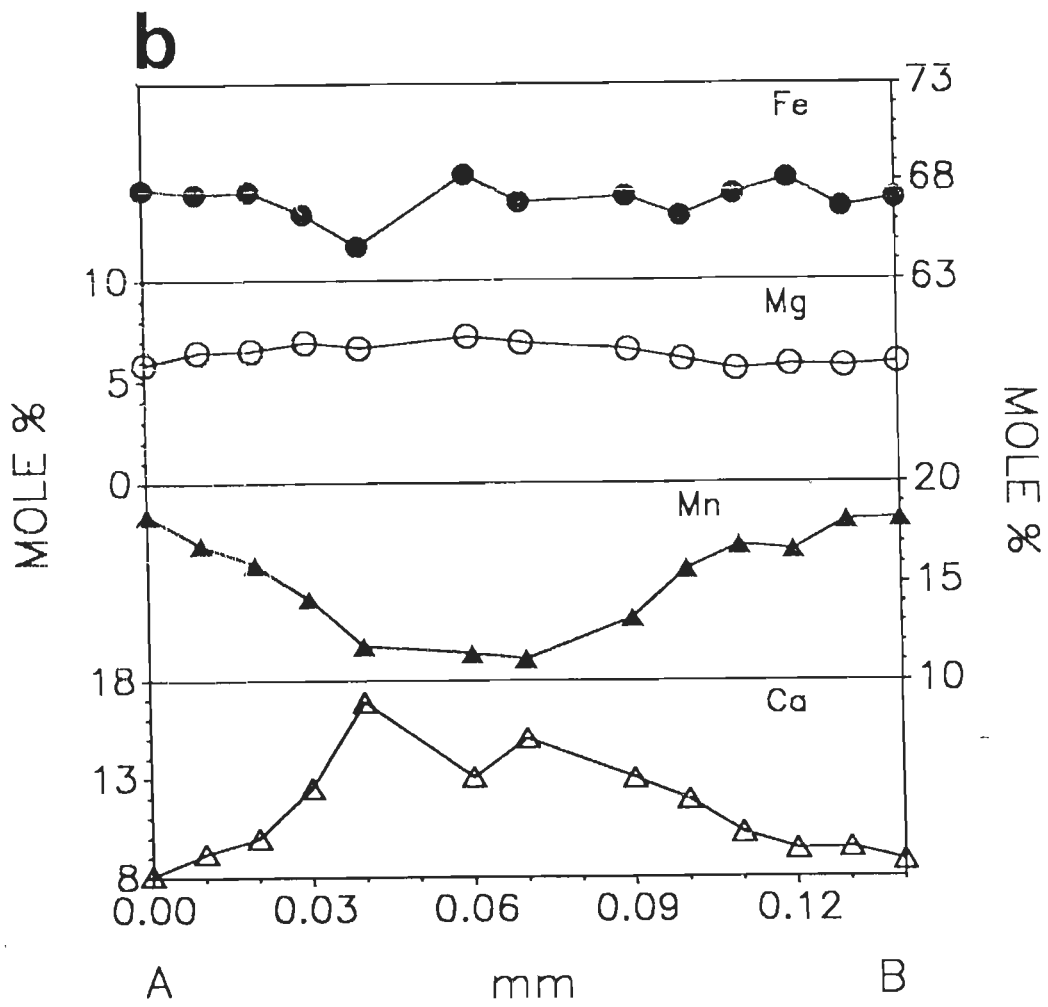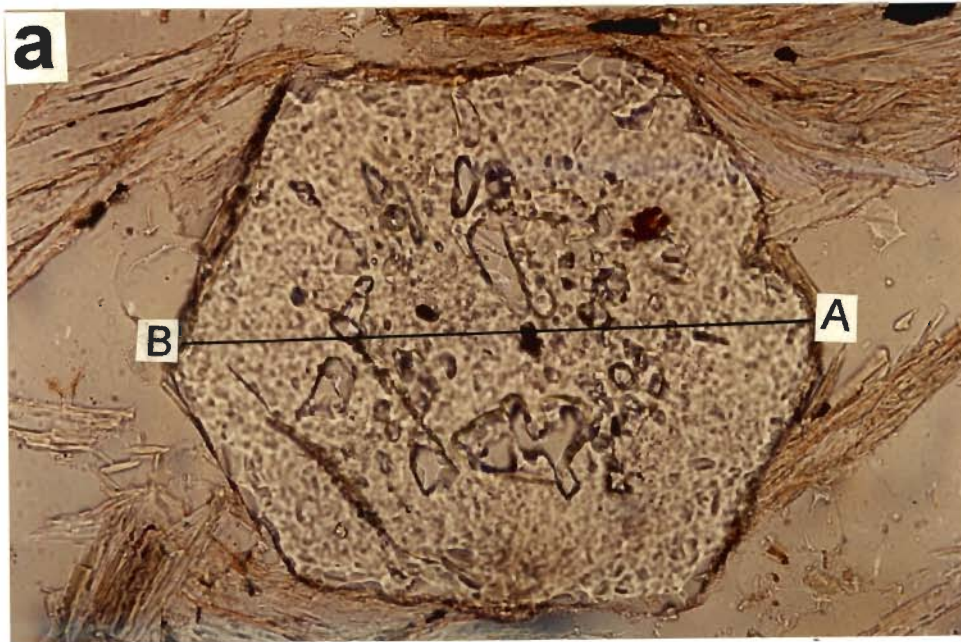
Fig.5.11

FIGURE 5.12: Pre-mylonitic garnet porphyroblast near the upper carbonaceous schist (a) showing growth zonation pattern (b) as Mn concentration is gradually decreased with the development of kinks. Ca shows bowl shape near core and bell shape near rim which may be compared with inclusion rich core and inclusion free rim. Staurolite Grade; Sample No. S-119/2; Base- 5.2 mm.
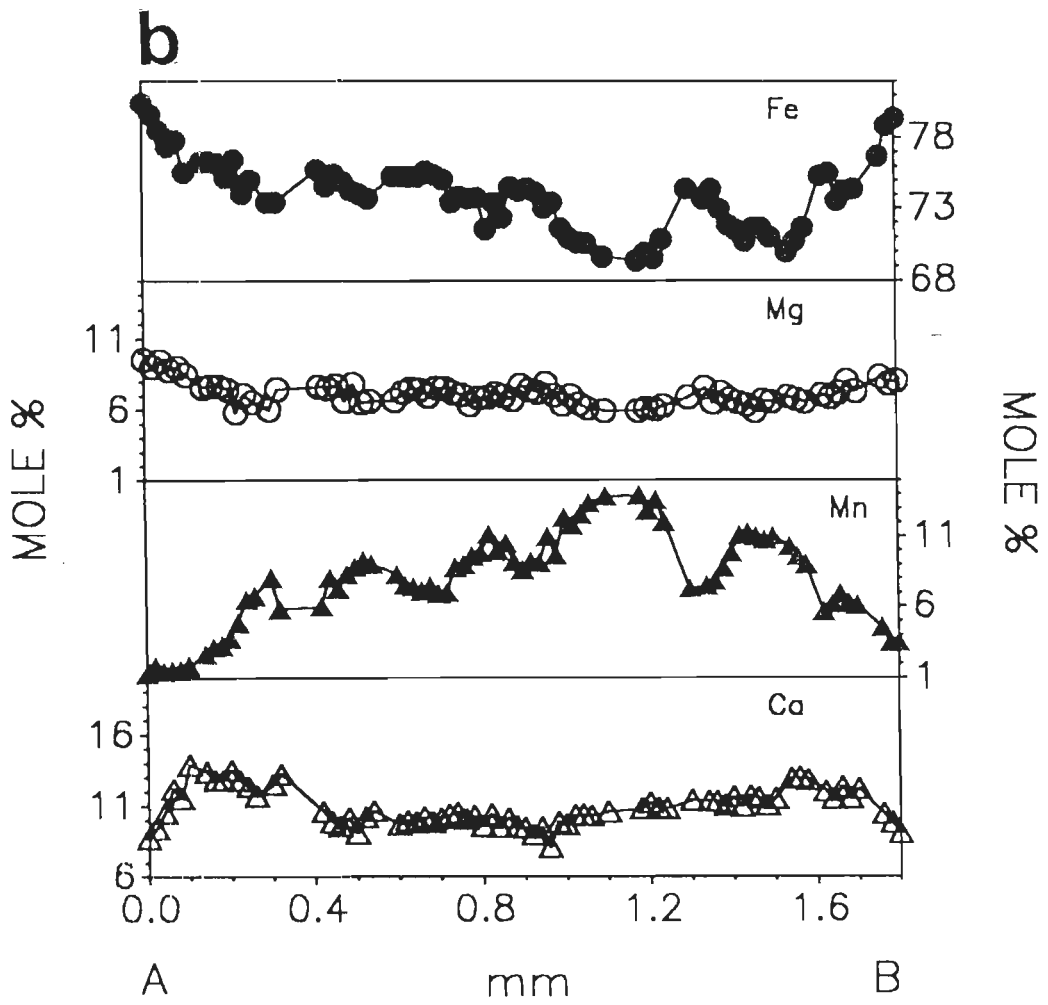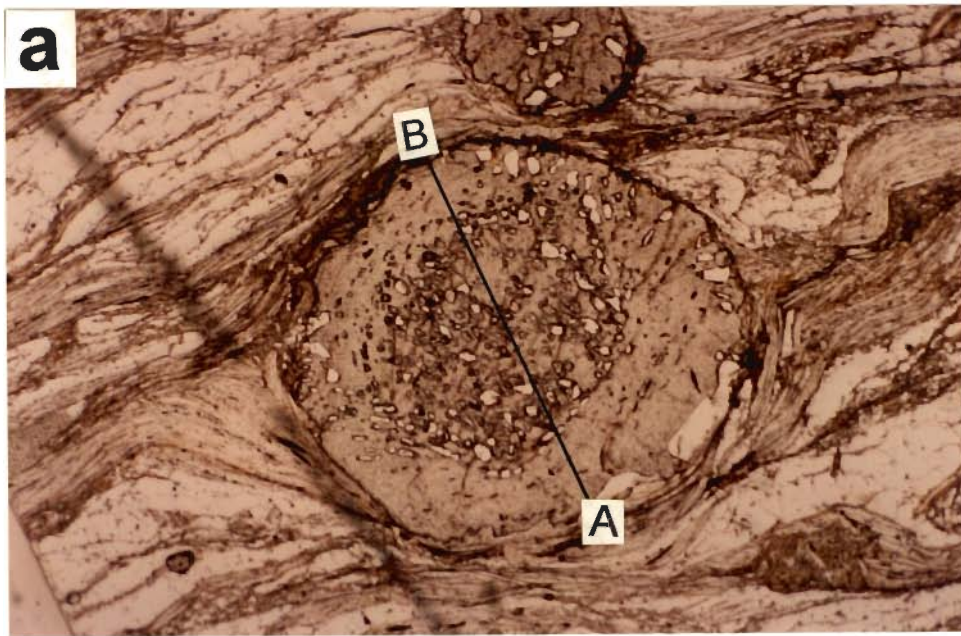
Fig.5.12

FIGURE 5.13: Pre-mylonitic garnet porphyroblast near the upper carbnaceous schist (a). Growth zonation pattern is observed (b) in Mn profile. But near rim enrichment of Mn is also observed suggesting minor rim resorption. Mg showas little bowl shaped pattern. Staurolite Grade; Sample No. S-119/1; Base- 5.2 mm.
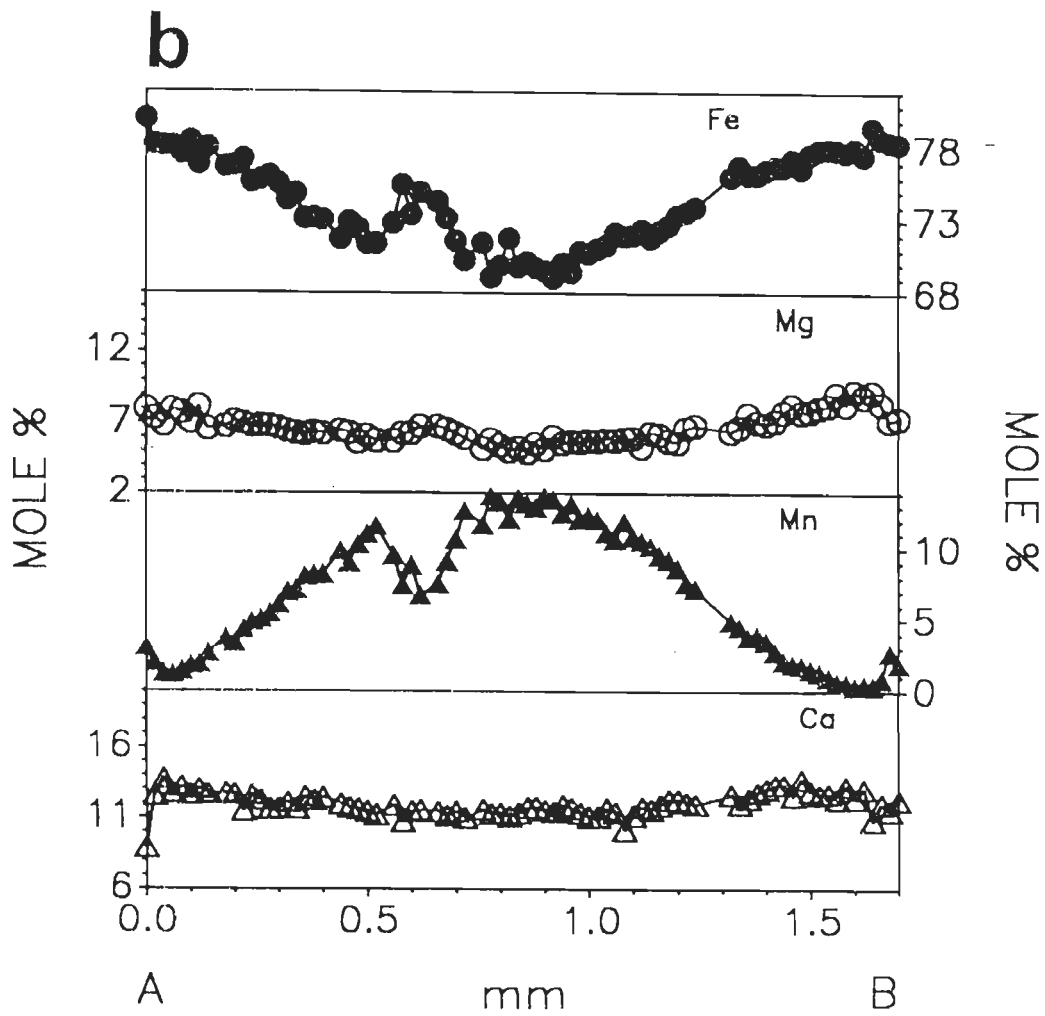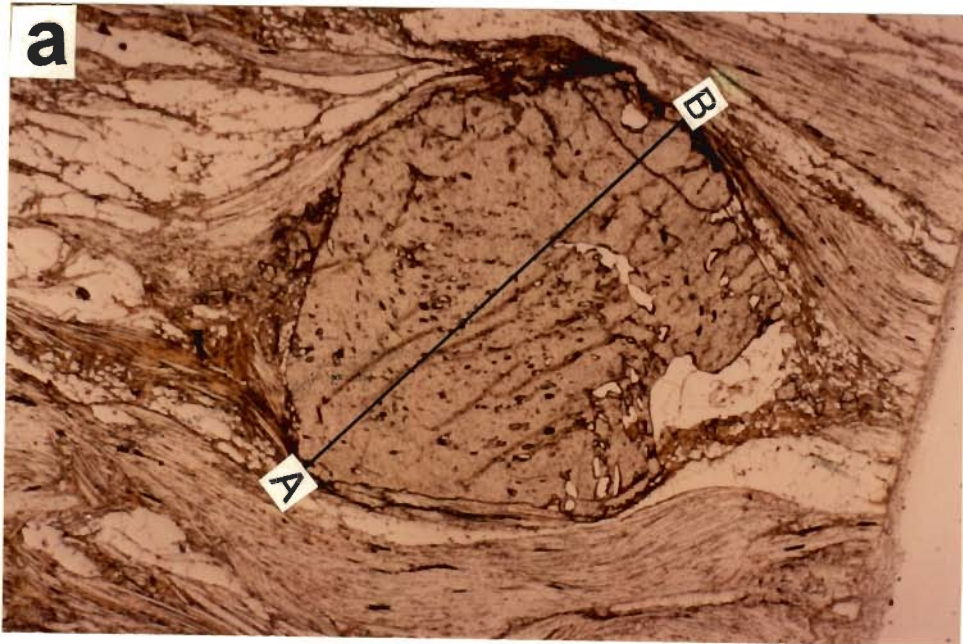
Fig.5.13

FIGURE 5.14: This garnet (a) with more relaxed trend in Mn profile (b) than the previous one Rim resorption is also more extensive as Mn is enriched more inside the garnet. This garnet is present within the mica schist nearer to the Chur granite at successively higher topographic levels. Staurolite Grade; Sample No. S-118; Base- 5.2 mm.
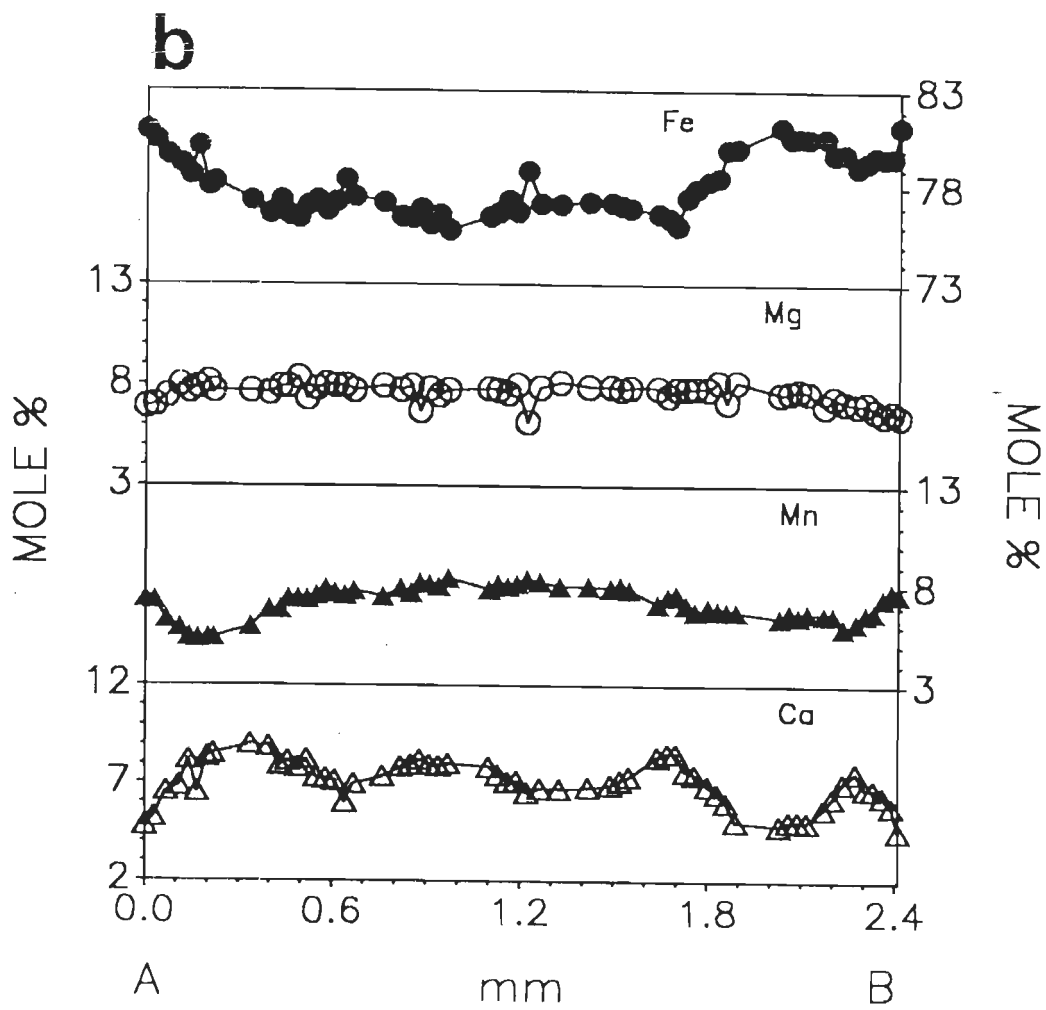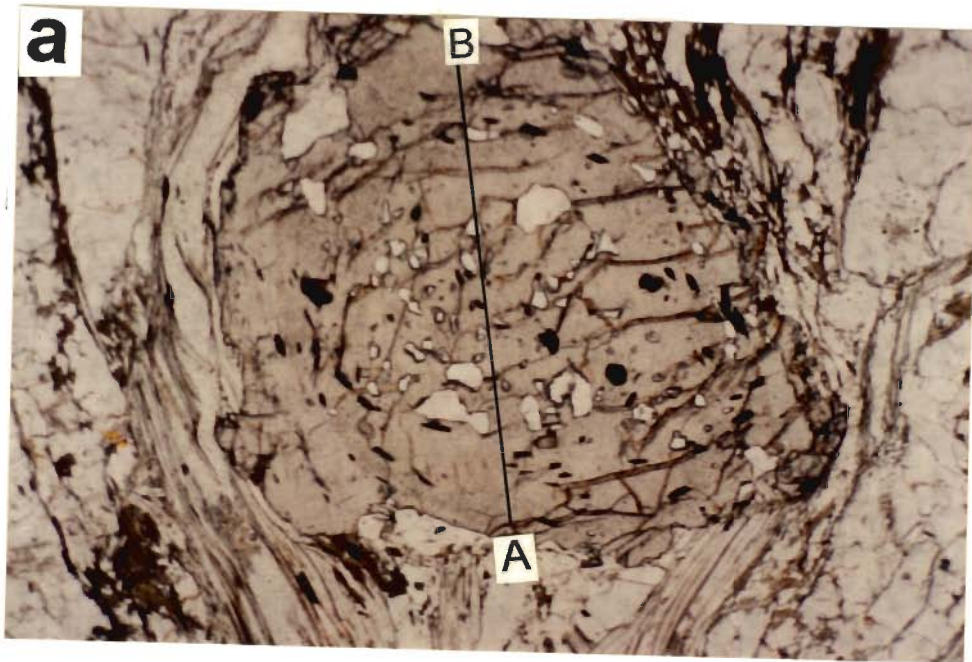
Fig.5.14

FIGURE 5.15: Mn profile (b) in pre-mylonitic (a) garnet is alomst flat. This garnet is present at the vicinity of the Chur granite. Ca also shows flat profile near the core. Staurolite Grade; Sample No. S-377; Base- 6.5 mm.
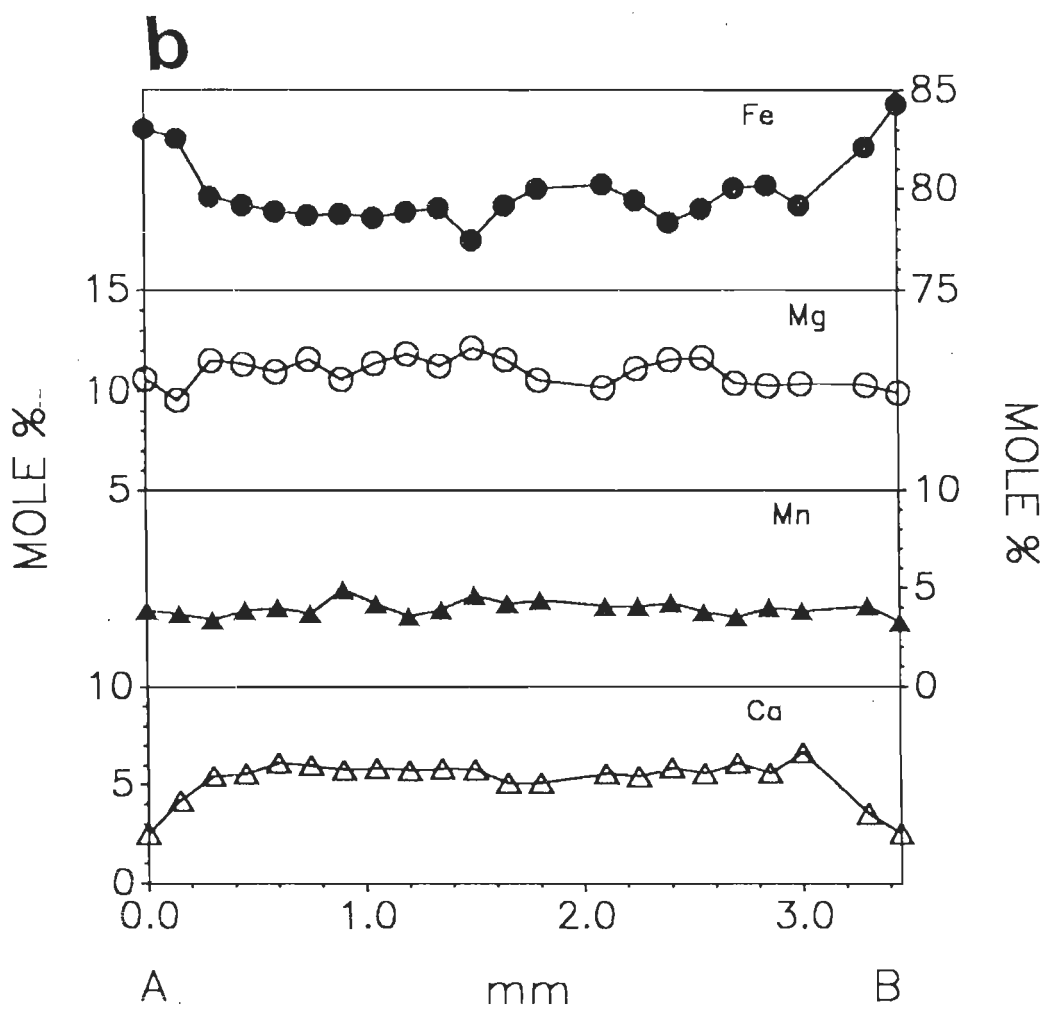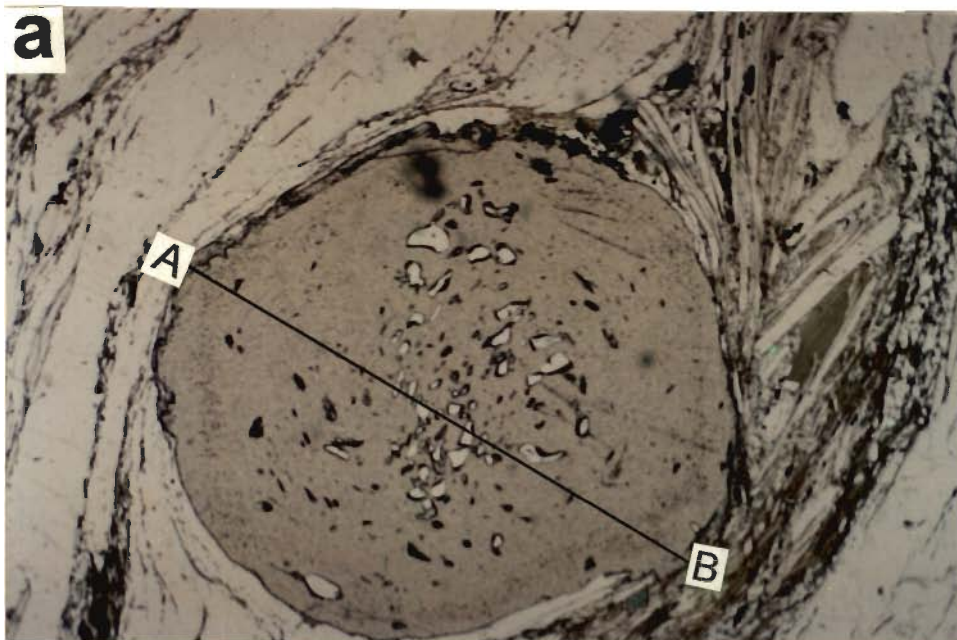
Fig. 5.15

FIGURE 5.16: Garnet in sillimanite grade (a). Reverse zoning patterns in Mg and Mn (b) are clearly observed near core. Ca shows flat trend near core. Sillimanite grade; Sample No. S-77/2; Base-
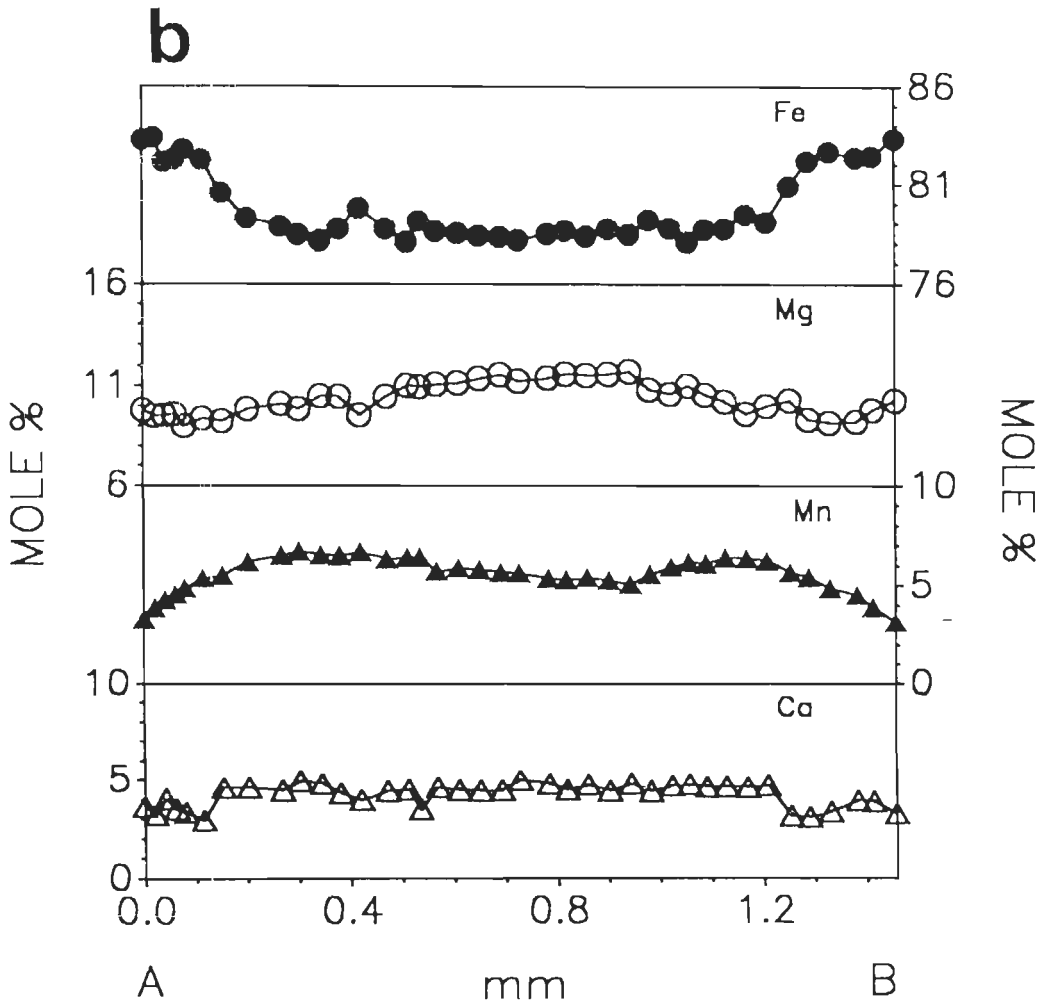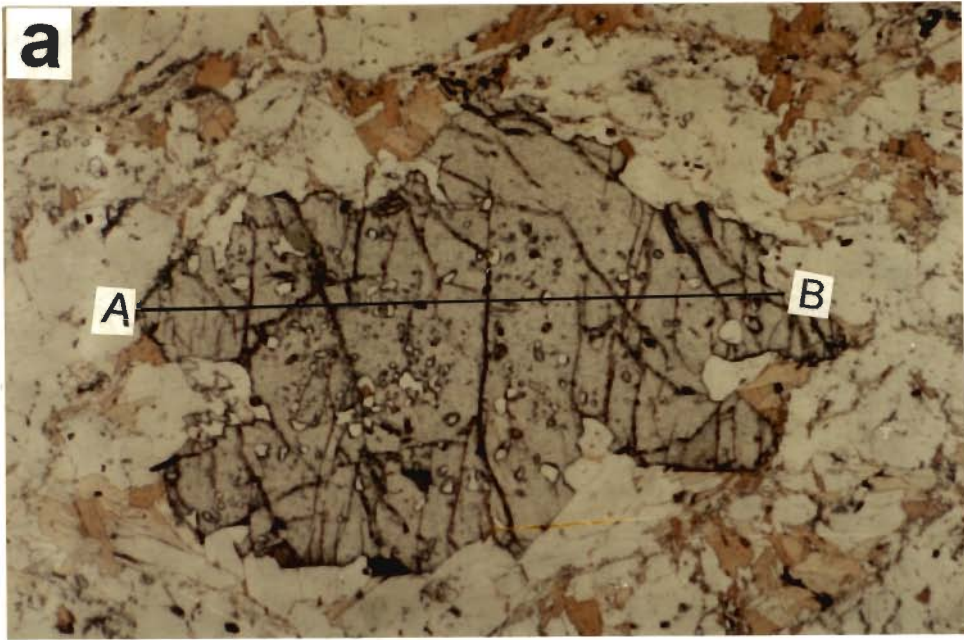
Fig.5.16

TABLE - 5.1
MINERAL ASSEMBLAGES FROM CHUR AREA

Sr. No.	SAMPLE No.	QUARTZ	PLAGIOCLASE	CHLORITE	MUSCOVITE	BIOTITE	GARNET	STAUROLITE	Al_2SiO_5	ILMENITE	OTHERS
1.	S-16	X		X	X	X	X			X	X
2.	S-38	X	X	X	X	X	X			X	X
3.	S-44	X	X		X	X	X			X	X
4.	S-46	X	X		X	X	X			X	X
5.	S-48	X			X	X	X	X		X	X
6.	S-57	X	X		X	X	X	X		X	
7.	S-59	X			X	X	X	X		X	
8.	S-62	X			X	X	X	X		X	
9.	S-77/2	X	X		X	X	X		X	X	X
10.	S-93/2	X	X	X	X	X	X			X	
11.	S-107	X	X		X	X	X	X		X	
12.	S-108	X			X	X	X			X	X
13.	S-114	X			X	X	X		X	X	X
14.	S-118	X	X	X	X	X	X			X	X
15.	S-119/2	X	X		X	X	X	X		X	X

TABLE 5.1 (Continued)

Sr. No.	SAMPLE No.	QUARTZ	PLAGIOCLASE	CHLORITE	MUSCOVITE	BIOTITE	GARNET	STAUROLITE	Al_2SiO_5	ILMENITE	OTHERS
16.	S-134	X	X	X	X	X	X	X		X	X
17.	S-148	X		X	X	X	X				
18.	S-164	X	X	X	X	X	X	X		X	
19.	S-174	X			X	X	X				
20.	S-177	X			X	X	X	X		X	
21.	S-180	X		X	X	X	X			X	
22.	S-244	X		X	X	X	X			X	X
23.	S-259	X	X	X	X	X	X			X	X
24.	S-318	X	X	X	X	X	X	X		X	X
25.	S-320	X	X		X	X	X			X	X
26.	S-321	X	X		X	X	X	X		X	X
27.	S-348	X		X	X	X	X			X	
28.	S-350	X			X	X	X			X	X
29.	S-354	X	X	X	X	X	X			X	X
30.	S-365	X	X		X	X	X			X	

TABLE 5.1 (Continued)

Sr. No.	SAMPLE No.	QUARTZ	PLAGIOCLASE	CHLORITE	MUSCOVITE	BIOTITE	GARNET	STAUROLITE	Al_2SiO_5	ILMENITE	OTHERS
31.	S-367	X	X	X	X	X	X			X	X
32.	S-377	X	X	X	X	X	X			X	X
33.	S-381	X		X	X	X	X				X
34.	S-394	X	X	X	X	X	X			X	X
35.	S-400	X		X	X	X	X			X	
36.	S-403	X		X	X	X	X			X	X
37.	S-447	X	X		X	X	X	X		X	X
38.	S-459	X		X	X	X	X			X	X
39.	S-453	X			X	X	X			X	X
40.	S-607	X	X	X	X	X	X			X	X
41.	S-616	X	X		X	X	X			X	X
42.	S-618	X	X	X	X	X	X			X	
43.	S-669	X	X		X	X	X			X	X
44.	S-675	X	X		X	X	X			X	X
45.	S-676	X	X		X	X	X			X	X

TABLE 5.1 (Continued)

Sr. No.	SAMPLE No.	QUARTZ	PLAGIOCLASE	CHLORITE	MUSCOVITE	BIOTITE	GARNET	STAUROLITE	Al$_2$SiO$_5$	ILMENITE	OTHERS
46.	S-695	X	X		X	X	X				X
47.	S-717	X			X	X	X		X	X	X
48.	S-724	X	X		X	X	X		X		X
49.	S-738	X	X	X	X	X	X			X	X
50.	S-749	X	X	X	X	X	X				
51.	S-765	X	X	X	X	X	X			X	
52.	S-812	X	X		X	X	X			X	
53.	S-833	X	X		X	X	X		X	X	X
54.	S-839	X	X	X	X	X	X				
55.	S-851	X	X		X	X	X	X		X	X
56.	S-858	X	X		X	X	X	X		X	X
57.	S-859	X	X		X	X	X			X	
58.	S-879	X			X	X	X		X		X
59.	S-881	X	X		X	X	X			X	
60.	S-882	X			X	X	X	X		X	X
61.	S-894	X	X		X	X	X		X	X	X
62.	S-897	X	X		X	X	X			X	X
63.	S-929	X			X	X	X		X	X	X

CHAPTER - 6
GEOTHERMOMETRY AND GEOBAROMETRY

6.1 BASIC THERMODYNAMIC RELATION

For any exchange and net-transfer reaction, at pressure P and temperature T of interest the change of Gibb's free energy in equilibrium condition can be expressed as

$$0 = \Delta H° + \int \Delta C_p dT - T(\Delta S° + \int (\Delta C_p/T)dT) + \int \Delta V dP + RT \ln K_{eq} \quad [R.6.1]$$

$$0 = \Delta H° + \Delta G_{(P,T)} + \int \Delta C_p dT - T(\Delta S° + \int (\Delta C_p/T)dT) + \Delta V°(P-1) + RT \ln K_{eq} \quad [R 6.1]$$

where $\Delta G_{(P,T)}$ = Change of Gibb's free energy at P,T
$\Delta H°$ = Change of enthalpy in standard state
$\Delta S°$ = Change of entropy in standard state
$\Delta V°$ = Change of volume in standard state
R = Gas constant

and

K_{eq} = Equilibrium constant.

For reaction involving only solids and assuming G= 0 equation [R 6.1] reduces to,

$$\Delta G_{(P,T)} = 0 = \Delta H° - T\Delta S° + \Delta V°(P-1) + RT \ln K_{eq}. \quad [R 6.2]$$

Activity of component i in phase j, a_i can be expressed in terms of mole fraction:

$$a_i = X_i \gamma_i, \quad [R 6.3]$$

where, X_i = mole fraction of component i in phase j.
and γ_i = activity coefficient of component i in phase j. This term may be introduced to link the non-ideal mixing behavior of a solution with that in ideal mixing.

So K_{eq} essentially becomes

$$K_{eq} = K_D \cdot K\gamma \quad [R.6.4]$$

where, K_D = Distribution constant
and $K\gamma$ = Activity constant involving activity coefficient.

For "ideal mixing" γ_i becomes 1 and equation 6.4 gives

$$RT \ln K_{eq} = RT \ln K_D, \quad [R.6.5]$$

and for "non ideal mixing" where γ_i is not equal to 1 and the equation [R 6.4] becomes

$$RT \ln K_{eq} = RT \ln (K_D K\gamma_-)$$
$$= RT \ln K_D + RT \ln K\gamma_- . \qquad [R.6.6]$$

In equation-1 and equation-2 there are two unknowns (P & T) if ΔH, ΔS and ΔV are known. Therefore ar least two independent reactions are required to solve for metamorphic pressure (P) and temperature (T) conditions.

For geothermobarmetry, equation 6.2 can be rearranged as

$$T = \frac{-\Delta H - (P-1) \Delta V}{R \ln K_{D_{eq}} - \Delta S} \qquad [R.6.7]$$

and

$$P = \frac{T(\Delta S + R \ln K_D) - \Delta H}{\Delta V} \qquad P = \frac{\Delta H - T\Delta S + RT \ln K_{eq}}{\Delta V} + 1 \qquad [R.6.8]$$

The metamorphic **temperature** is evaluated mainly from the exchange equilibria on the basis of intracrystalline distribution of elements among the sites of the same phase or intercrystalline distribution of isovalent elements present within the two or more coexisting phases (Essene 1982). The exchange reaction shows small value of ΔV and large value of ΔH. Thus it is suitable for good thermometer. In any exchange reaction redistribution of elements takes place among the phases involved in the reaction depending on the temperature suffered by the reaction (Essene 1982).

For the intracrystalline exchange thermometer, pertitioning among elements is maximized at low temperature and diminished with increasing temperature as the structures expand and consequently their entropy increases (Essene 1982). For intracrystalline exchange thermometer

feldspar and pyroxene have been examined most carefully. It is observed that intracrystalline exchange thermometer are best for calculating cooling rate, rather than for calculating temperature at the peak metamorphic condition.

In contrast, intercrystalline cation distribution does not easily reset during cooling and constitutes a potential geothermometer. Refractory phase such as garnet is less likely to reset during cooling. The intercrystalline exchange thermometer is normally described with the mutual exchange of Mg-Fe^{2+}, Ca-Mg-Fe^{2+}-Mn, Al-Fe^{3+}-Cr, Na-K, Fe-Mn etc. Among those, Fe^{2+}-Mg exchanges are the most widely used as metamorphic geothermometer. The phases include mainly garnet, biotite, clinopyroxene, orthopyroxene, spinel, ilmenite, cordierite, hornblende and cummingtonite (Essene 1982). Depending upon the mineral present in the investigated area the particular exchange reaction or reactions is/are considered for calculating temperature. However the main problem involved in the Mg-Fe^{2+} intercrystalline exchange thermometer is that the total amount of iron analyzed by microprobe is considered as Fe^{2+}. Fe^{3+} is not considered during microprobe analysis.

The metamorphic **pressure** may be calculated using net-transfer reaction which has sufficiently large value of ΔV. But in true sense, the net-transfer reactions generally have pressure as well as temperature dependence. In spite of that, those equations are more useful for calculating pressure which have sufficiently large ΔV. The phases commonly used for solid-solid reaction to calculate pressure (large ΔV) can be plagioclase, pyroxene, garnet, muscovite, sillimanite, kyanite, quartz, rutile, ilmenite etc. Since most of the minerals involved in the reactions have their complex solid solution, the pressure calculation is

dependent on standard thermodynamic and well constrained activity-composition data participating in a reaction (Essene 1982).

6.2 CHOICE OF GEOTHERMOMETER AND GEOBAROMETER

The application of geothermometry and geobarometry is based on equilibrium of co-existing mineral assemblages present in the area for which well constrained thermodynamic data and phase equilibria data are available. In the study area of investigation as mentioned in the early chapters, the rocks are mainly micaschist, quartzite, metacalc, carbonaceous schist, granite with occasional presence of amphibolite. Micaschist is chosen for thermobarometric calculation because this rock type is predominant enough in the Jutogh metasediments. Even within the quartzite unit, micaschist layers have been identified for analysis. Major minerals present within the micaschist are quartz, garnet, biotite, muscovite, plagioclase, ilmenite, chlorite, epidote, staurolite in staurolite grade, kyanite in kyanite grade and kyanite and/or sillimanite in sillimanite grade with the minor presence of sphene, apatite, zircon (see Chapter 2 & 4 also).

So, on the basis of the mineralogy, abundance of minerals and the grade from garnet to sillimanite, it is appropriate to choose garnet-biotite, biotite-muscovite, garnet-ilmenite, garnet-plagioclase, plagioclase-muscovite involving reactions for geothermometer and garnet-biotite-muscovite-plagioclase and garnet-plagioclase-Al_2SiO_5-quartz involving reactions for geobarometer. Among those above mentioned thermometers, garnet-biotite has been chosen for temperature calculation because it has been well understood, fairly well calibrated and it has yielded geologically reasonable result. For pressure calculation although garnet-plagioclase-

Al_2SiO_5-quartz gives more accurate result in high grade terrain than the other, garnet-biotite-muscovite-plagioclase assemblage has been chosen for geobarometer because except few ones (where plagioclase is not present) all mineral phases involved in this calibration were present all over the area of investigation. This calibration has also been chosen for the assemblage where Al_2SiO_5 phase is present, because, the uncertainties involved in calculation should have been same for all samples. In some samples neither plagioclase nor Al_2SiO_5 phase was~~were~~ present. For those samples, only calculation of temperature was possible assuming pressure term.

So, exchange reaction for garnet-biotite geothermometry and net transfer reaction for garnet-biotite-muscovite-plagioclase geobarometry have been chosen to calculate pressure and temperature condition. These are,

Pyrope + Annite = Almandine + Phlogopite and   [R.6.9]

Almandine + Grossular + Muscovite = 3*Anorthite + Annite
[R.6.10]
respectively.

Ilmenite is also present in fairly good amount throughout the area. As discussed earlier (Chapter 5) presence of Mn in ilmenite was in very low concentration ($X_{Mn} < 0.02$). Hence it was not appropriate to use as geothermometer as suggested by Pownceby et al. (1987).

6.3 GARNET-BIOTITE GEOTHERMOMETER

Garnet-Biotite (GB) geothermometer is widely accepted due to the wide occurrence of garnet and biotite, presence of one refractory mineral like garnet which is reset poorly during cooling except in higher grade.

The exchange reaction is

$$Fe_3Al_2Si_3O_{12} + KMgAlSi_3O_{10}(OH)_2 =$$
(Garnet)   (Biotite)
$$Mg_3Al_2Si_3O_{12} + KFe_3AlSi_3O_{10}(OH) \quad [R.6.11].$$
(Garnet)   (Biotite)
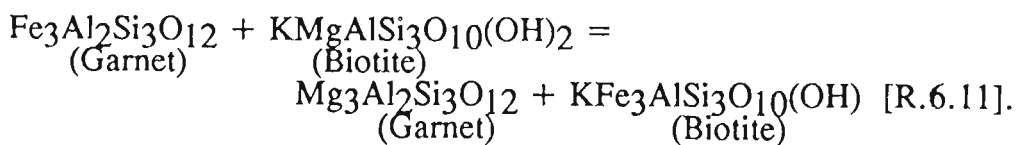
Garnet-biotite geothermometer has been proposed by Thompson (1976) and modelled experimentally as well as empirically modified by a number of workers (Goldman and Albee 1977; Ferry and Spear 1978; Pigage and Greenwood 1982; Hodges and Spear 1982; Perchuk and Lavrent'va 1983; Ganguly and Saxena 1984; Inderas and Martignole 1985; Dasgupta et al. 1991; Bhattacharyya et al. 1992). Solution models for garnet and biotite mixing alone have also been introduced (Berman 1990) with further improvement from time to time (e.g. Berman 1990; Hoisch 1990; Douce et. al. 1993). Among the various calibrations of this geothermometer, temperature has been estimated using only models of Ferry and Spear (1978), Hodges and Spear (1982) and Ganguly and Saxena (1984). Also thermodynamic data of Hodges and McKenna (1987) has been combined with Berman (1990) activity model for garnet and Hoisch (1991) activity model for biotite. Table 6.2 shows the all activity-composition relations for diferent minerals used in calculation. The thermometric equations used for calculation have been summerised in table 6.3.

6.4 GARNET - BIOTITE - MUSCOVITE - PLAGIOCLASE GEOBAROMETER

Ghent and Stout (1981) first calibrated a new but potential geobarometer using the mineral assemblage containing garnet, biotite, muscovite and plagioclase (GBMP). Gradually it became popular among petrologists not only due to the wide range of occurrence of those

minerals covering from garnet grade to lower sillimanite grade, but also due to the fact that virtually it was a potential geobarometer for rocks which lacked aluminium silicates. The end-member reactions for this assemblage are

$$Mg_3Al_2Si_3O_{12} + Ca_3Al_2Si_3O_{12} + KAl_3Si_3O_{10}(OH)_2 =$$
(Garnet)   (Garnet)   (Muscovite)
(Pyrope)
$$3CaAl_2Si_2O_8 + KMg_3(AlSi_3)O_{10}(OH)_2 \qquad [R.6.12]$$
(Plagioclase)   (Phlogopite)

Almandine + Grossular + Muscovite =
$$3 \text{ Anorthite } + \text{ Annite} \qquad [R.6.13]$$
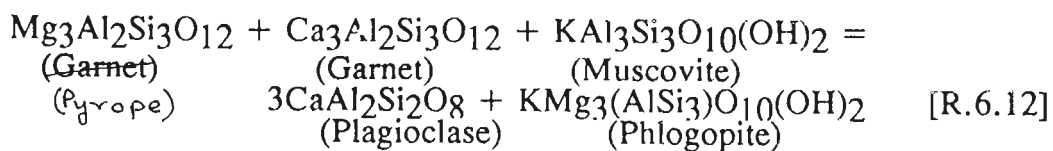
Later, several attempts have been made to improve this empirical calibration by other workers (Hodges and Crowley 1985; Hoisch 1990,1991; Applegate and Hodges 1990; Applegate and Hodges 1994). Table 6.2 and 6.3 summerise the respective activity-composition relations and barometric equation used in calculation.

6.5 VARIATIONS IN EQUILIBRIUM CONSTANTS

The variation in equilibrium constant is used to evaluate the equilibrium between mineral assemblages and the uniformity of P-T condition of the given area (Albee 1965a; Kretz 1959). Two equilibrium constants (K_D) for exchange reaction and net-transfer reaction mentioned in section 6.2 are

$$K_D(1) = [(X_{Py}) * (X_{Ann})]/[(X_{Ph}) * (X_{Alm})] \text{ and}$$

$$K_D(2) = [(X_{An})^3 * (X_{Ann})]/[(X_{Mu}) * (X_{Gr}) * (X_{Al})] \text{ respectively.}$$

If there is an ideal mixing and equilibration under uniform pressure and temperature conditions in individual grade then both the K_D values calculated from samples of different grade from the Chur area should define two straight lines for two K_Ds respectively which pass through the origins on plots of numerators versus denominators for the equations

mentioned in section 6.2 (Hodges & Royden 1984). But it is clear from Fig.6.1a that the points of corresponding distribution coefficient for exchange reaction do not define such straight line. The same situation has also been observed from Fig.6.1b which is a plot of K_D for net-transfer reaction. Albee (1965a) pointed out that significant deviation from ideal mixing would lead to a regular curved rather than straight line distribution. But such regular pattern from both the plots have not also been observed. Even in the individual grade also no such pattern is observed. So from Fig.6.1 it is concluded that the samples from the Jutogh Group of rocks could not have been reached final equilibrium under the same PT conditions throughout the area as well as in individual metamorphic grades.

6.7 RESULT

Calculation for temperature has been performed using rim compositions of garnet and coexisting biotite though in some of the samples the resorption of garnet rim has been clearly observed. Diagnostic inclusions of biotite within garnets which could store the evidence of changing parageneses during progressive metamorphism are generally absent. Where the biotite inclusions are present the analysis has been carried out. For calculation of pressure, garnet rim with coexisting biotite and muscovite have been analyzed. But plagioclase grains were not always available just at the contact of garnet. So analysis has been performed to the nearest plagioclase grain and within 0.2mm distance from garnet. Three to five points have been analyzed in each grain within 4 micron^2 area. Those points were averaged out to show the analytical error (Appendix I to IV).

6.7.1 Choice of Thermoberometric Equations for Calculation

For calculating pressure and temperature two equations, one for garnet-biotite exchange geothermometry and another for garnet-biotite-muscovite-plagioclase geobarometry, have been solved simultaneously. In some of the thin sections plagioclase was not at all available. In those cases pressure was assumed as 7Kb (Jones 1994). All calculated P-T data have been tabulated in table 6.5. Error has been estimated using the method described by Hodges and McKenna (1987).

The combination between different pressure and temperature calibrations has been thoroughly scrutinized and compared with the Al_2SiO_5 triple point as suggested by Holdaway and Mukhopadhyay (1993) (Fig.6.2, 6.3 & 6.4). It is observed that among all those combinations in Figs. 6.2a,c and Figs. 6.3a,c one P-T data from sillimanite bearing sample (S-894) lie well within the sillimanite field which is compitable with the respective assemblage. So on the basis of the mineral assemblage these four combinations have been sorted out to choose one which could give the most geologically reasonable result. Hodges (1991) informed that after attaining peak-metamorphic condition the resetting of net-transfer reaction (used for pressure calculation) to reach closure temperature is more sluggish than the exchange reaction (used for trmperature calculation). So pressure data should be considered among the different calibrations which gives highest value and consequently nearest to peak metamorphic condition. Hence, among those sorted four combinations the combination of Hodges and Crowley (1985) calibration for pressure and Hodges and McKenna (1987) calibration for temperature with Berman (1990) solution model of garnet and Hoisch

(1991) solution model fo biotite (Fig.6.3c) has been chosen which could give the most geologically reasonable result.

6.7.2 Condition of metamorphism in Chur area

It may be readily observed that pressure and temperature do not vary in systematic manner in the Chur area (Fig.6.5). Generally in garnet grade the temperature ranges from 476°C to 558°C. In the staurolite grade there is wider variation which ranges from 434°C to 588°C. In kyanite-sillimanite grade all three data show sharp rise of temperature ranging from 593°C to 614°C. The number of data is not same from one grade to another. It is also noticed that apparently the P-T data show no variation from one grade to other. So the "F" test (Spiegel 1975) has been carried out to show whether there is any actual variation in P-T dataamong different grades or not. It has been observed that the calculated F value is greater than $F_{.95}$ in case of temperature. Hence we can safely reject the hypothesis of equal means and take the mean temperature from each grade to represent the metamorphic condition of each grade from this area. The result shows that in garnet grade and staurolite grade the temperatures are 528±32°C and 545±18°C respectively. In kyanite-sillimanite grade there is a sharp increase of temperature which is 604±10°C. So according to grade increase of temperature observed. But pressure data does not clearly show any variation according to grade though from Fig.6.1b it may be concluded that the Jutogh metasediments had no uniform pressure.

As the pressure and temperature condition from Chur area shows the apperent unsystemtic variation from one place to another attempt has been made if there is any relation between P-T condition and the major

77

thrust planes present in this area. The Jutogh thrust being most pronounced thrust plane is considered to see this variation. The structural distance has been calculated with respect to the Jutogh thrust upto the vicinity of the Chur thrust. Temperature distribution pattern (Fig 6·6a) shows no systematic variation from the Jutogh thrust across the Jutogh Group.. The sudden change of temperature within very small distance is clearly observed. The highest temperature attained by the Jutogh thrust is present from the sillimanite grade at the vicinity of the Chur thrust. Fig.6.6b shows the variation of pressure across the Jutogh Group. The similar situation like tamperature is observed in case of pressure variation. It may be pointed out that all calculated data have not been plotted for the sake of clarity of the diagram.

As mentioned earlier inclusions of biotite within garnets which could store the evidence of changing paragenesis with the formation of minerals in Chur area are very few. These inclusions are present at core, middle part and also near rim within the garnets. Very few muscovite grains and no plagioclase are present as inclusions. So the pressure has been assumed to calculate temperature what has been calculated in the rim because temperature does not vary noticeably within a wide range of pressure. It has been observed that the temperature near the core gives certainly the lower temperature than the rim. But some of the cases it shows the higher temperature near rim than that at the rim. But calculated error is within the range of differences between those two data (between rim data and near-rim data), thus is not considered as a change of temperature from rim to near-rim inside the garnet. All data have been presented in Table 6.4.

6.8 DISCUSSION

From pressure temperature data it may be noticed that the pressure and temperature in the Chur area spatially vary in unsystematic manner. Structural distance versus temperature and pressure plots also show no systematic variation with respect to the reference thrust plane (Jutogh thrust). So the progressive temperature and pressure condition in the Jutogh Group is not related with the thrusting. If that is not so the presence of inverted metamorphism within the Jutogh thrust sheet has no cause or effect relationship with the thrusting. Consequently models related to thermal perturbation along the thrust planes (see Chapter-1) are not the reasons for the presence of inverted metamorphism present in this area. But an overall increase of temperature may be observed from garnet grade through staurolite grade to sillimanite grade. So it is possible that the original systematic variation of temperature and pressure condition has become unsystematic due to post-metamorphic deformation episodes which is a progressive non-coaxial ductile shearing and multiple thrusting in large scale as well as in small scale. It may be mentioned that Treloar et al. (1989) reported almost similar condition of metamorphism from south of Main Mantle Thrust, north Pakistan (Hazara region) and interpreted it as an effect of post-metamorphic stacking of thrust planes. The sudden rise of temperature from staurolite grade (514°C) to kyanite-sillimanite (604°C) grade predicts the presence of a thrust plane which is responsible to take the rocks of kyanite-sillimanite grade over the rocks of staurolite grade. But this thrust plane has been overlapped by the "Chur thrust" leaving behind virtually a sporadic occurrence of kyanite-sillimanite bearing rocks.

From the Chur area no other metamorphic phase has been recognized which might be higher than the presented peak metamorphic condition. However a low grade phase was operative during ductile shearing (Chapter 4). But it was not intense enough to obliterate the earlier pre-thrusting peak metamorphic condition.

FIGURES AND TABLES
CHAPTER - 6

FIGURE 6.1: DISTRIBUTION COEFFICIENT PLOTS FOR (a) EXCHANGE REACTION AND (b) NET TRANSFER REACTION.

(a). Distribution coefficient plot for garnet - biotite exchange reaction used for temperature calculation. Power of cube has been omitted for clarity of the figure. Symbol as in Fig.5.5 to Fig.5.8. It is noted from the figure that the data do not define a straight line passing through the origin. Even in the individual grade the data do not show such relationships.

(b). Distribution coefficient plot for garnet - biotite - muscovite - plagioclase net-transfer reaction for pressure calculation. Symbol as in Fig.5.5 to Fig.5.8. The situation similar to (a) is observed here.

NOTE: From these two distribution coefficient plots it is suggested that in individual grades rocks from the Chur area have not reached final equilibrium under the same PT condition.
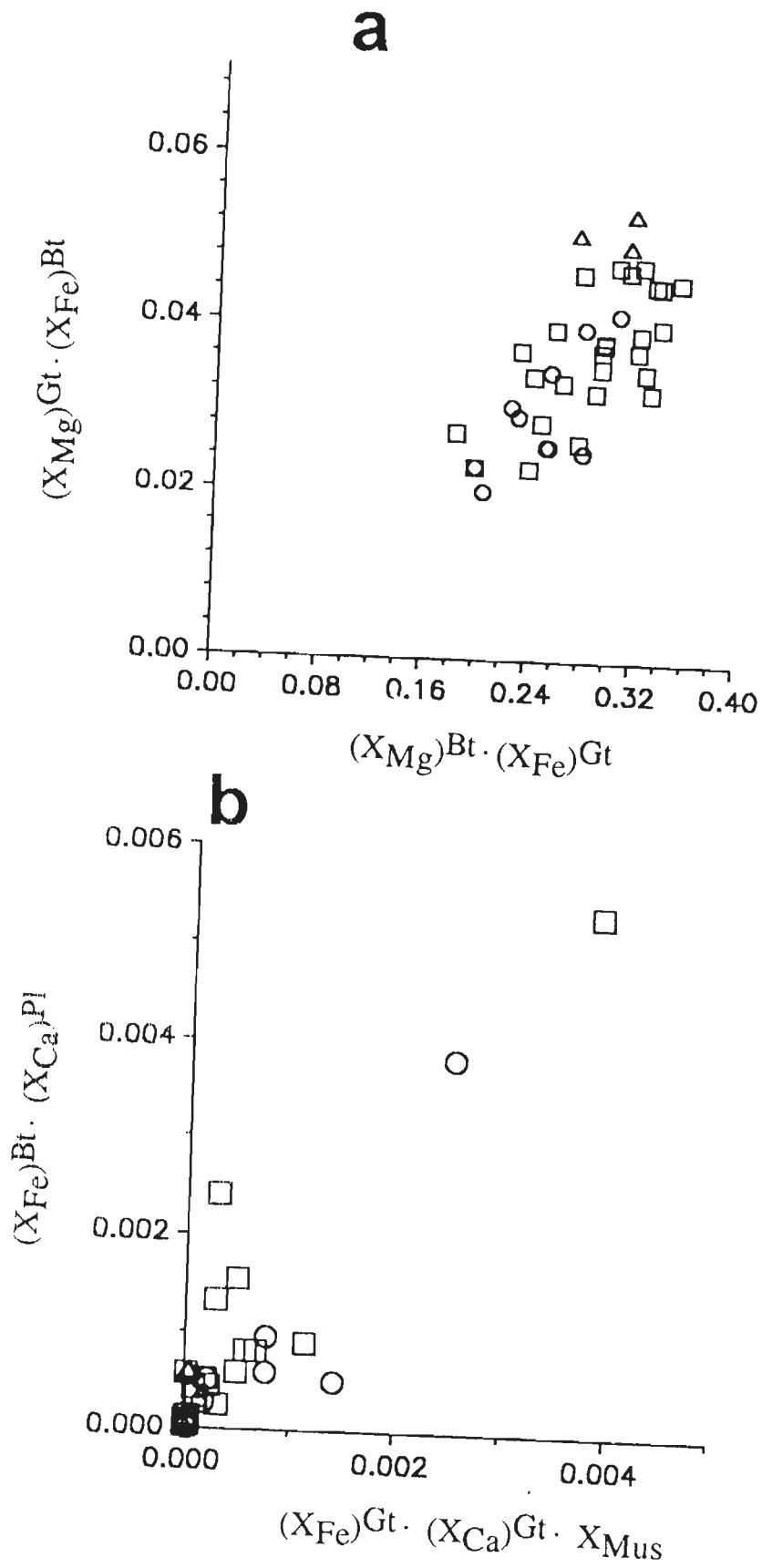
Fig.6.1

FIGURE 6.2: PRESSURE AND TEMPERATURE PLOTS USING DIFFERENT CALIBRATIONS.
Symbols as in Fig.5.5. Al_2SiO_5 triple point as suggested by Holdaway and Mukhopadhyay (1993).
r is correlation coefficient.

(a). Hodges and Crowley (1985) for pressure, Hodges and Spear (1982) for temperature.

(b). Hoisch (1991) for pressure, Hodges and Spear (1982) for temperature.

(c). Hodges and Crowley (1985) for pressure, Ferry and Spear (1978) for temperature.

(d). Hoisch (1991) for pressure, Ferry and Spear (1978) for temperature.
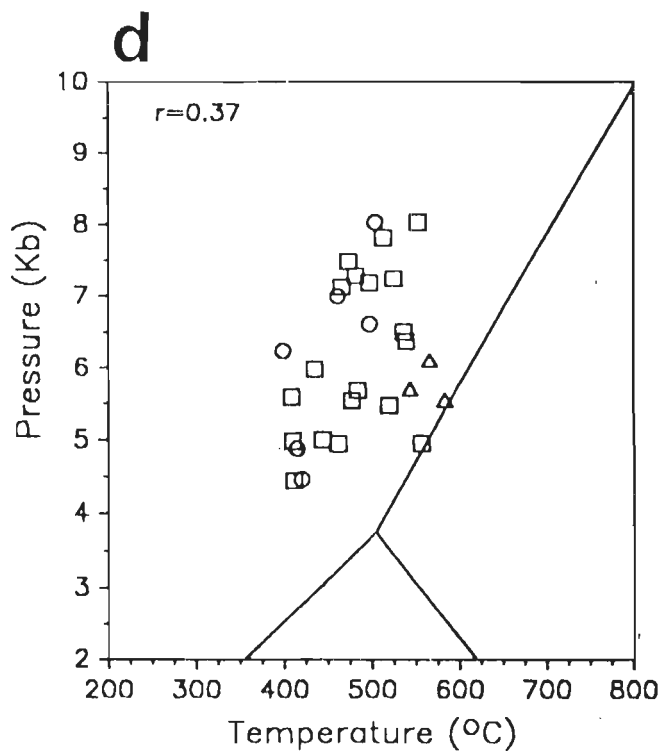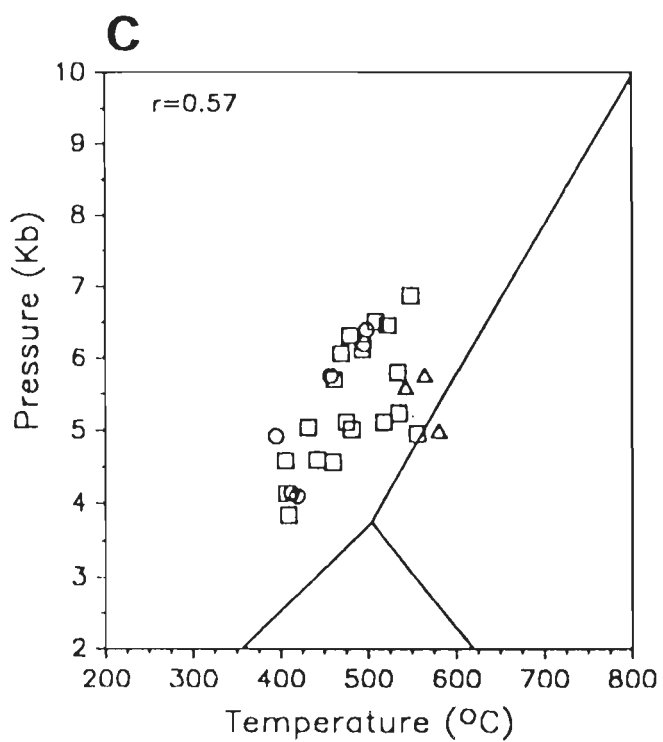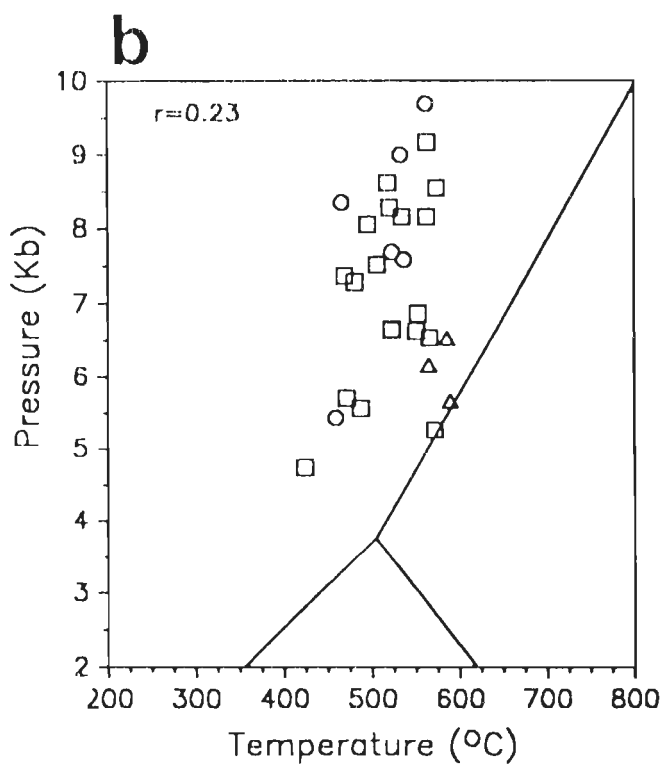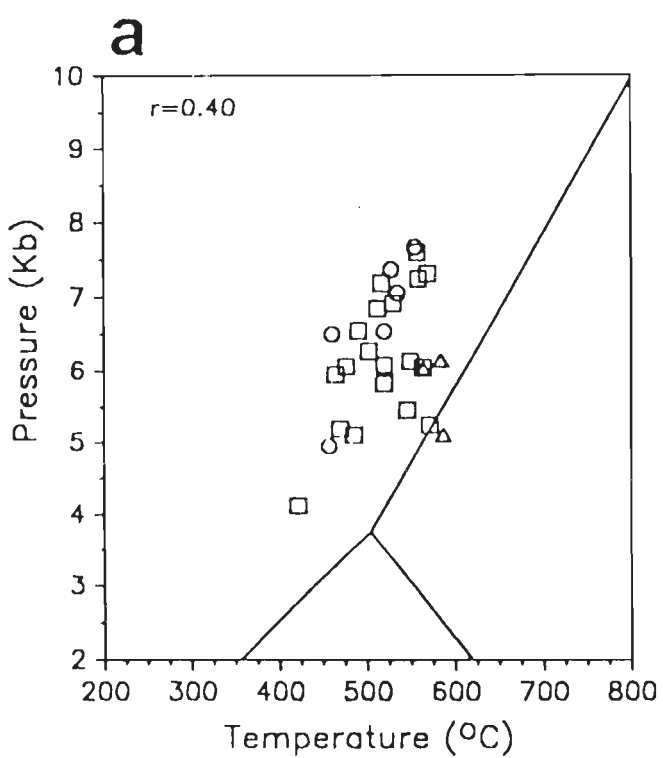
Fig.6.2

FIGURE 6.3: PRESSURE AND TEMPERATURE PLOTS USING DIFFERENT CALIBRATIONS.

Symbols as in Fig.5.5. Al_2SiO_5 triple point as suggested by Holdaway and Mukhopadhyay (1993).
r is correlation coefficient.

(a). Hodges and Crowley (1985) for pressure, Ganguly and Saxena (1984) for temperature.

(b). Hoisch (1991) for pressure, Ganguly and Saxena (1984) for temperature.

(c). Hodges and Crowley (1985) for pressure, Calibration to calculate temperature using the solution model of Berman (1990) for garnet and Hoisch(1991) model for biotite.

(d). Hoisch (1991) for pressure, Calibration to calculate temperature using the solution model of Berman (1990) for garnet and Hoisch(1991) model for biotite.
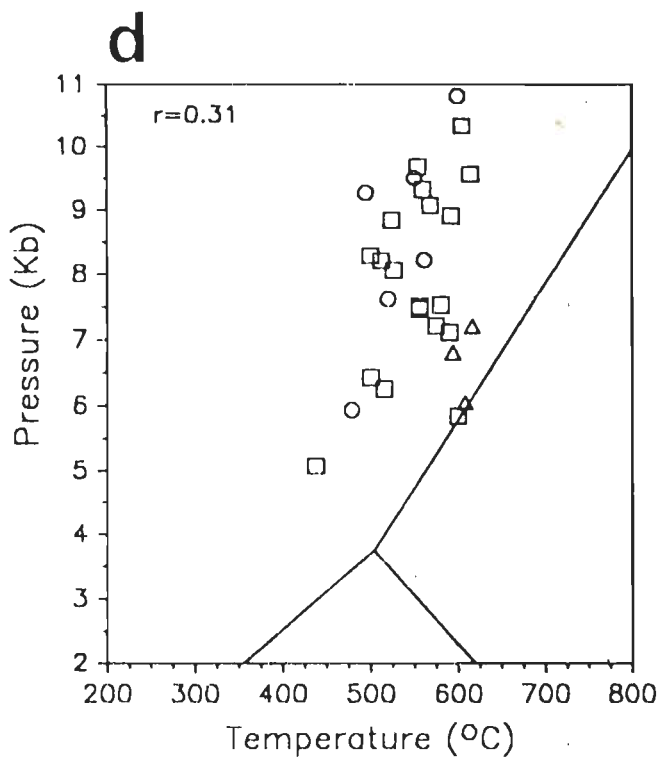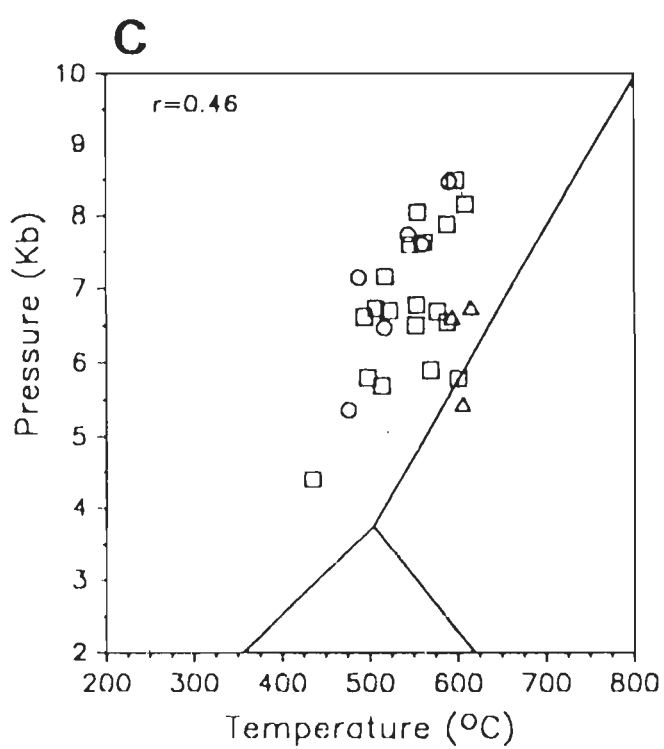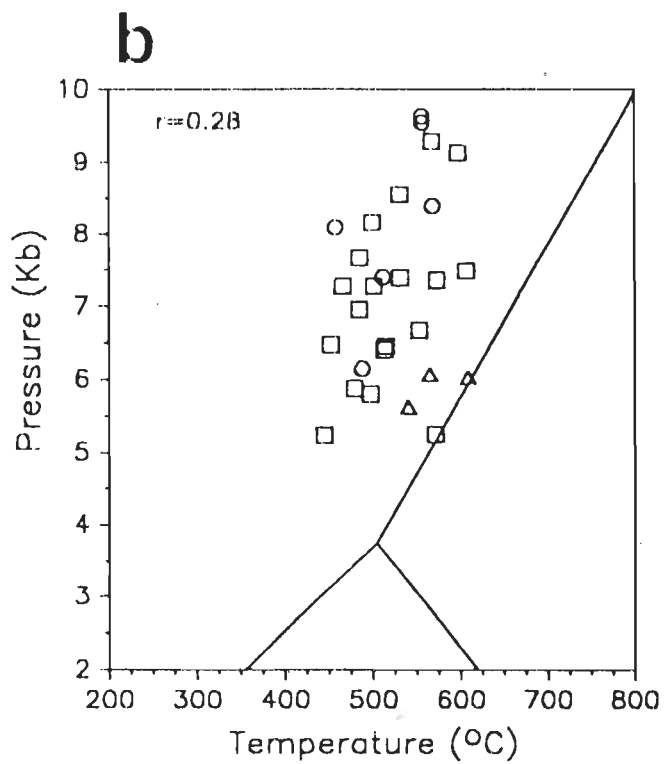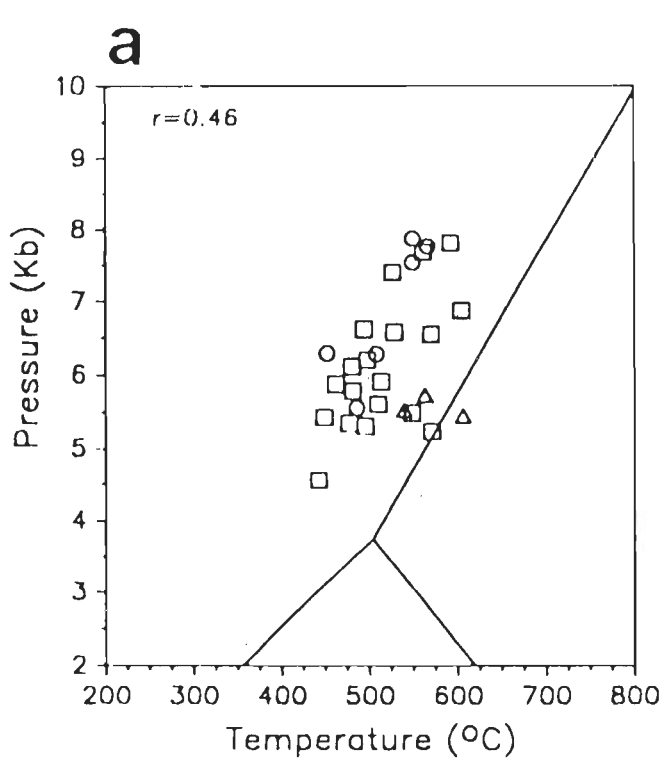
Fig.6.3

FIGURE 6.4: PRESSURE AND TEMPERATURE PLOTS USING DIFFERENT CALIBRATIONS.

Symbols as in Fig.5.5. Al_2SiO_5 triple point as suggested by Holdaway and Mukhopadhyay (1993). r is correlation coefficient.

(a)-(d). Calibration used to calculate pressure using solution models of Berman (1990) for garnet, Hoisch (1991) for biotite, Chatterjee and Flux (1986) for muscovite, Elkins and Grove (1990) for plagioclase

(a). Calibration to calculate temperature using the solution model of Berman (1990) for garnet and Hoisch(1991) model for biotite.

(b). Hodges and Spear (1982) for temperature.

(c). Ferry and Spear (1978) for temperature.

(d). Ganguly and Saxena (1984) for temperature.
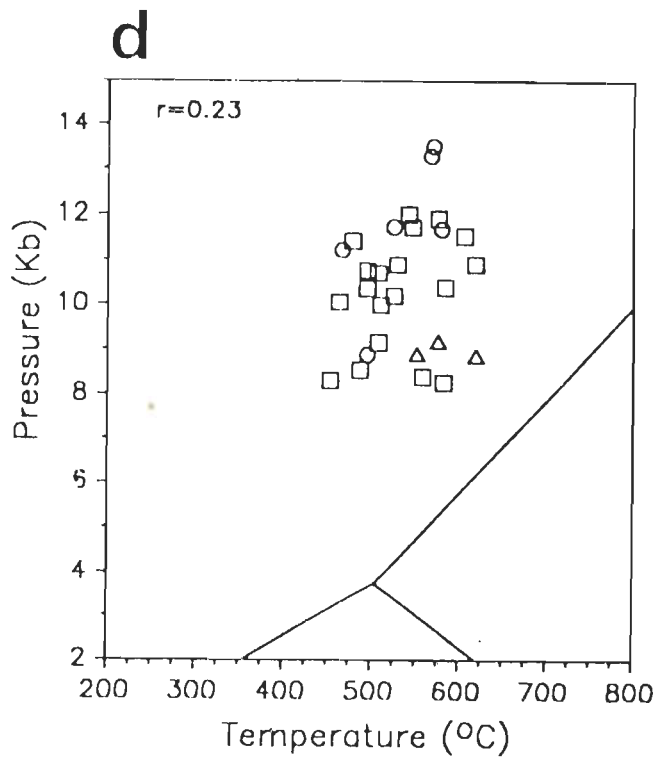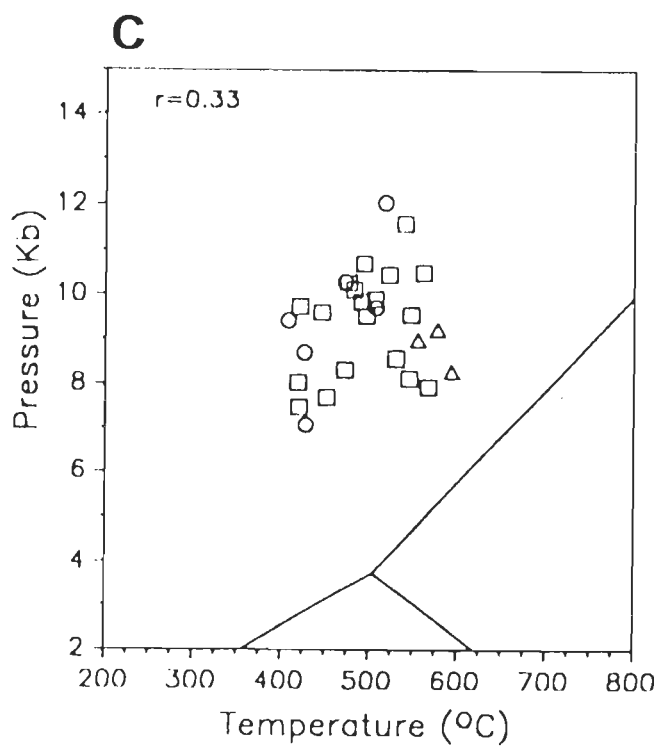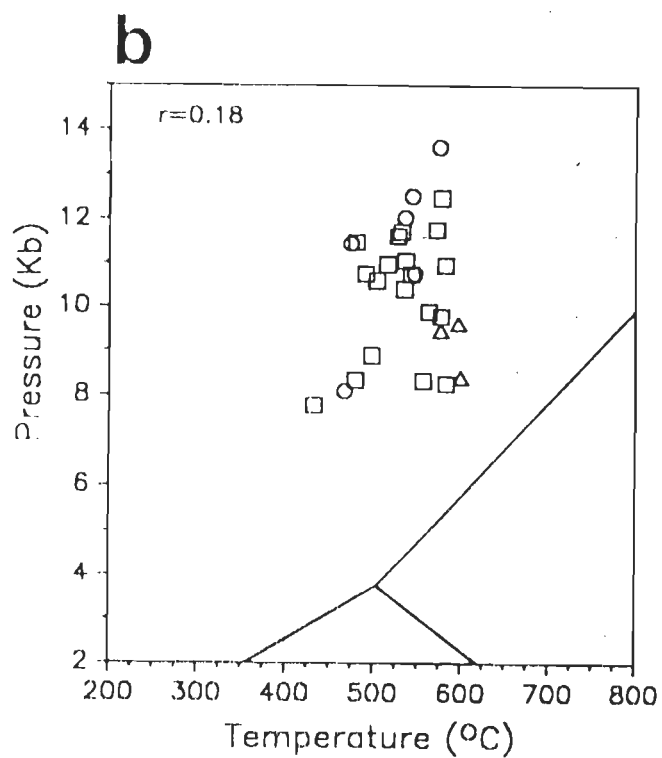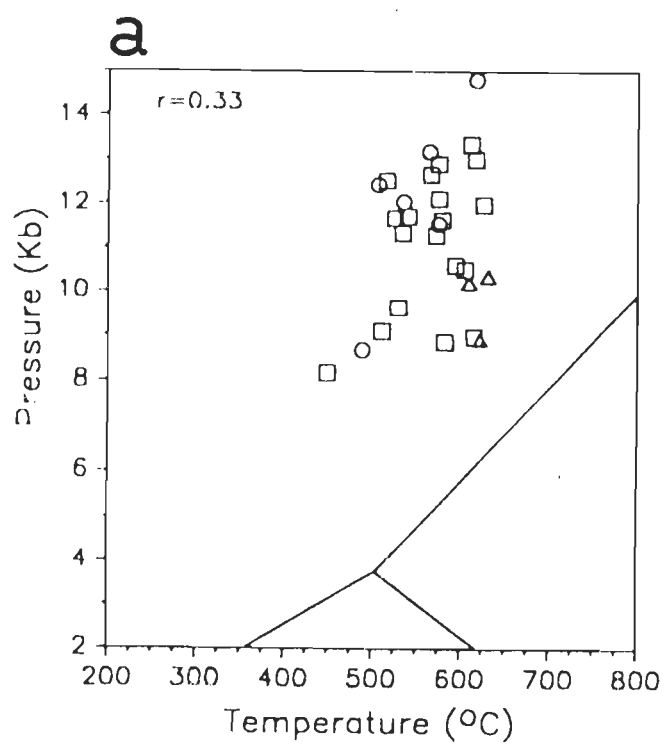
Fig.6.4

FIGURE 6.5: Pressure and temperature distribution in the Jutogh Group
from the Chur area. Note that the distribution of P-T data is rather
distributed in unsystematic manner. Temperature is in ° C and
Pressure is in Kb. Bracketed pressure terms are assumed to
calculated temperature.
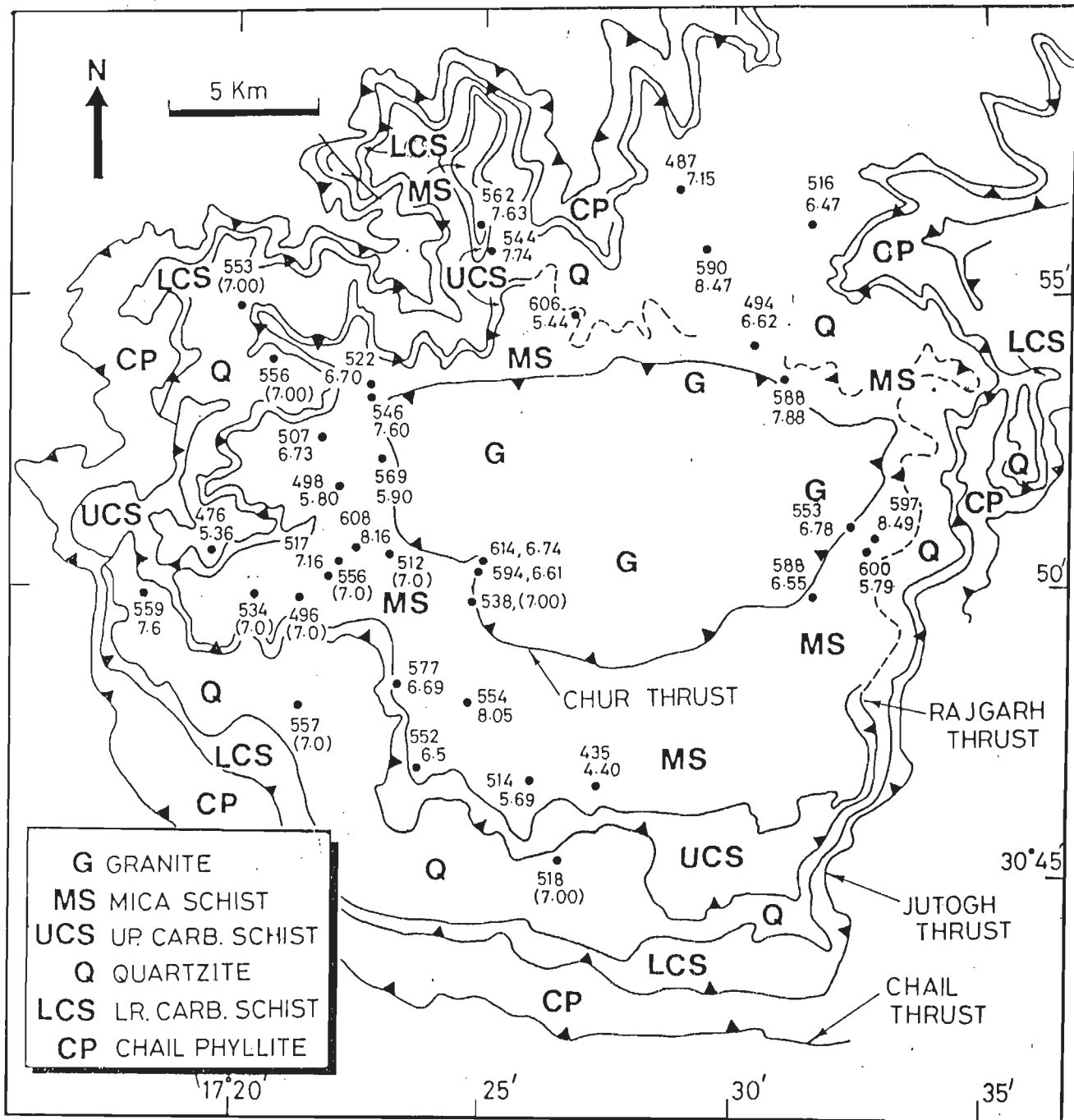
Fig. 6.5

FIGURE 6.6: Structural distance from the Jutogh thrust versus temperature (**a**), and that versus pressure (**b**), plots from the Chur area. Note that both the pressure and temperature vary in unsystematic manner from the Jutogh thrust.
JT = Jutogh thrust;

a

Temperature (^oC) vs Structural Distance from Jutogh Thrust (Km.)

JT

b

Pressure (Kb) vs Structural Distance from Jutogh Thrust (Km.)

JT
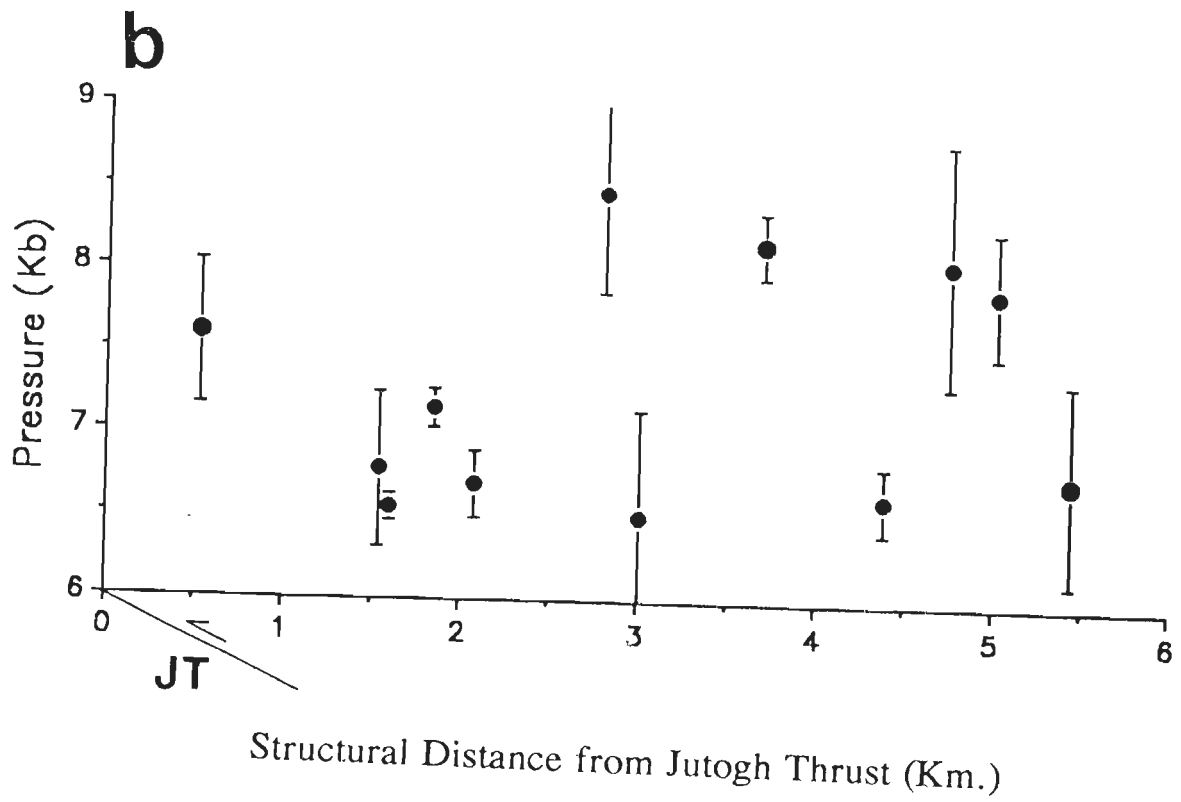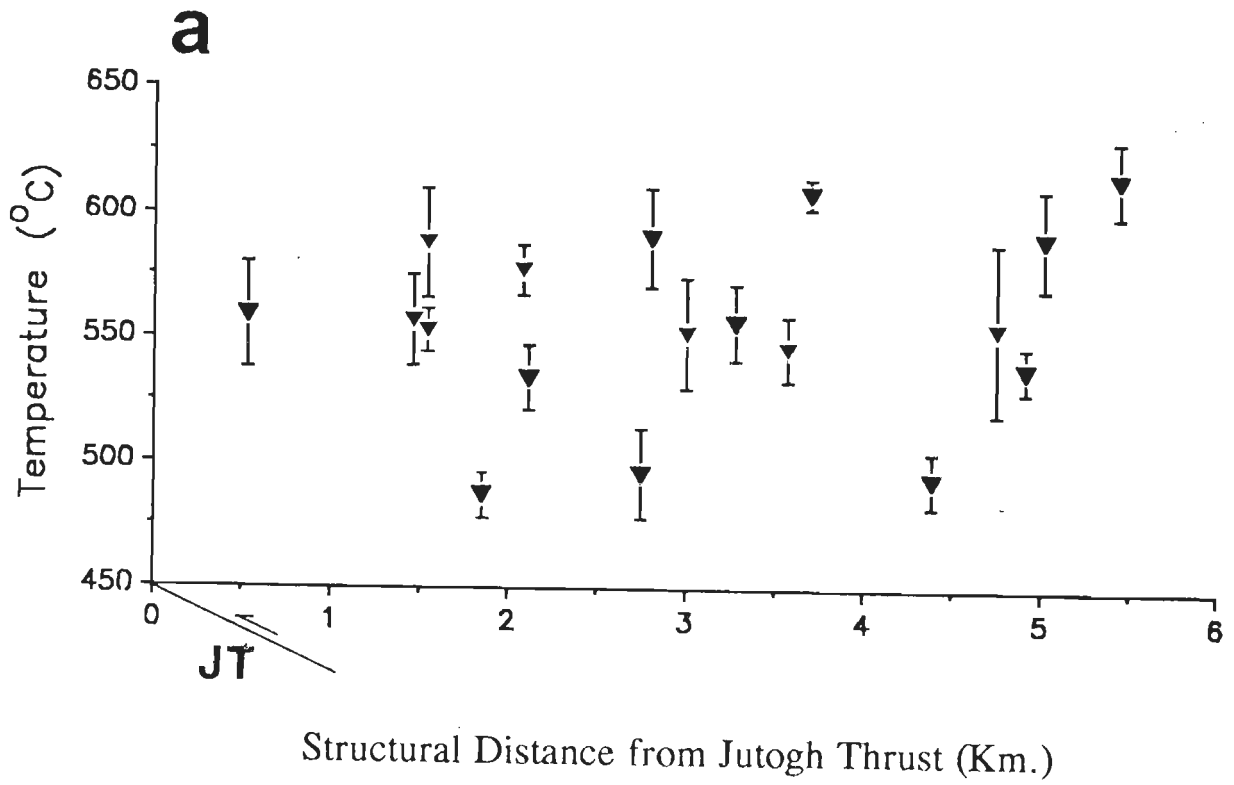
Fig.6.6

TABLE 6.1
EXPRESSIONS OF MOLE FRACTIONS FOR
GEOTHERMOBAROMETRY.

MINERALS	MOLE FRACTIONS

Garnet

$$X_{Gt} = \frac{Gt}{Fe + Mg + Mn + Ca}$$

(where Gt = Fe or Mg or Mn or Ca)

Biotite

$$X_{Bt} = \frac{Bt}{Fe + Mg + Mn + Al^{VI} + Ti}$$

(where Bt = Fe or Mg or Mn or Al^{VI} or Ti)

Muscovite

$$X_{Mu} = \frac{Mu}{Fe + Mg + Mn + Ai^{VI} + Ti}$$

(where Mu = Fe or Mg or Mn or Ai^{VI} or Ti)

Plagioclase

$$X_{Pl} = \frac{Pl}{Ca + Na + K}$$

(where Pl = Ca or Na or K)

TABLE 6.2
ACTIVITY COMPOSITION RELATIONS USED IN CALCULATION.

GARNET

(a) Hodges & Spear (1982)

$$a_{Mg} = \left[X_{Mg} \cdot \exp\left[\frac{3300\text{-}1.5T}{RT} \left(X_{Ca}^2 + X_{Fe}X_{Ca} + X_{Ca}X_{Mn} \right) \right] \right]^3$$

$$a_{Fe} = \left[X_{Fe} \cdot \exp\left[\frac{(1.5T\text{-}3300)}{RT} \cdot X_{Mg}X_{Ca} \right] \right]^3$$

$$a_{ca} = \left[X_{ca} \cdot \exp\left[\frac{(3300\text{-}1.5T)}{RT} \left(X_{Mg}^2 + X_{Fe}X_{Mg} + X_{Mg}X_{Mn} \right) \right] \right]^3$$

(P in Bar, T in Kelvin, R = 1.987 Cal)

(b) Berman (1990)

$$a_{ca} = \left[X_{Mg} \cdot \exp\left[\begin{array}{l} \left(W_{112}(2X_1X_2\text{-}2X_1^2X_2) + W_{122}(X_2^2\text{-}2X_1X_2^2) \right. \\ + W_{113}(2X_1X_3\text{-}2X_1^2X_3) + W_{133}(X_3^2\text{-}2X_1X_3^2) \\ + W_{223}(\text{-}2X_2^2X_3) + W_{233}(\text{-}2X_2X_3^2) \\ + W_{123}(X_2X_3\text{-}2X_1X_2X_3) + W_{124}(X_2X_4\text{-}2X_1X_2X_4) \\ \left. + W_{134}(X_3X_4\text{-}2X_1X_3X_4) + W_{234}(\text{-}2X_2X_3X_4) \right]/RT \end{array} \right] \right]^3$$

Table 6.2 (Continued)

$$a_{Mg} = \left[X_{Mg} \cdot \exp \left[\begin{array}{l} \left(W_{112}(X_1^2 - 2X_1^2 X_2) + W_{122}(2X_1 X_2 - 2X_1 X_2^2) \right. \\ + W_{113}(-2X_1^2 X_3) + W_{133}(-2X_1 X_3^2) \\ + W_{223}(-2X_2 X_3 - 2X_2^2 X_3) + W_{233}(X_3^2 - 2X_2 X_3^2) \\ + W_{123}(X_1 X_3 - 2X_1 X_2 X_3) + W_{124}(X_1 X_4 - 2X_1 X_2 X_4) \\ \left. + W_{134}(-2X_1 X_3 X_4) + W_{234}(X_3 X_4 - 2X_2 X_3 X_4) \right)/RT \end{array} \right] \right]^3$$

$$a_{Fe} = \left[X_{Fe} \cdot \exp \left[\begin{array}{l} \left(W_{112}(-2X_1^2 X_2) + W_{122}(-2X_1 X_2^2) \right. \\ + W_{113}(X_1^2 - 2X_1^2 X_3) + W_{133}(2X_1 X_3 - 2X_1 X_3^2) \\ + W_{223}(X_2^2 - 2X_2^2 X_3) + W_{233}(2X_2 X_3 - 2X_2 X_3^2) \\ + W_{123}(X_1 X_2 - 2X_1 X_2 X_3) + W_{124}(-2X_1 X_2 X_4) \\ \left. + W_{134}(X_1 X_4 - 2X_1 X_3 X_4) + W_{234}(X_2 X_4 - 2X_2 X_3 X_4) \right)/RT \end{array} \right] \right]^3$$

(where 1= Ca, 2= Mg, 3= Fe and 4= Mn.)
Garnet solution Properties as follows-

Parameter	W_H(J/Mol)	W_s(J/MolK)	W_v(Bar)
112	21560	18.79	0.10
122	69200	18.79	0.10
113	20320	5.08	0.17
133	2620	5.08	0.09
223	230	-	0.01
233	3720	-	0.06
123	58825	23.87	0.265
124	45424	18.79	0.100
134	11470	5.08	0.130
234	1975	-	0.035

(P in Bar, T in Kelvin)

Table 6.2 (Continued)

BIOTITE

(a) Hoisch (1991).

$$a_{Fe,\ Mg} = \left(X_{Fe,Mg}\right)^3 .exp \left[\frac{30093.8X_{Al}^2 - 10392.6 \cdot X_{Al}X_{Ti}}{RT}\right]$$

(b) Ideal

(P in Bar, T in Kelvin)

MUSCOVITE

(a) Chatterjee and Flux (1986)

$$a_{Mus} = \left(X_{Mu}\right).exp\frac{(1-X_{Mu})^2 \left[A+B(1-4X_{Mu}) + C\ (1-2X_{Mu})(1-6X_{Mu})\right]}{RT}$$

$$\left(where\ X_{Mu} = X_K^{Mu}\right)$$

(b) Hodges & Crowley (1985)

$$a_{mu} = \left(X_K X_{Al}^2\right).exp \left[\frac{(X_{Na}X_{Al}^2)^2\ (W_{Mus}+2X_K X_{Al}^2(W_{Pa}-W_{Mus})}{RT}\right]$$

(where W_{Pa} = 2923.1 + 0.1590P + 0.1698T
W_{Mus} = 4650.1 + 0.1090P + 0.3954T)
(P in Bar, T in Kelvin)

Table 6.2 (Continued)

PLAGIOCLASE

(a) Hodges and Crowley (1985)

$$a_{Ca} = X_{Ca} \cdot \exp\left[\frac{610.34}{T} - 0.3837\right]$$

(b) Elkins and Grove (1990)

$$a_{ca} = X_{ca} \cdot \exp\left[W_{OrAb}\left(X_{Na}X_K(1/2 - X_{Ca} - 2X_{Na})\right)\right.$$

$$+ W_{AbOr}\left(X_{Na}X_K(1/2 - X_{Ca} - 2X_K)\right)$$

$$+ W_{AbAn}\left(2X_{Ca}X_{Na}(1 - X_{ca}) + X_{Na}X_k(1/2 - X_k)\right)$$

$$+ W_{OrAn}\left(2X_K X_{Ca}(1 - X_{Ca}) + X_{Na}X_K(1/2 - X_{Ca})\right)$$

$$+ W_{AnOr}\left(X_K^2(1 - 2x_{Ca}) + X_{Na}X_K(1/2 - X_{Ca})\right)$$

$$\left. + W_{OrAbAn}\left(X_K X_{Na}(1 - 2X_{Na})\right)\right]/RT$$

where

	W_H(J)	W_s(J/MolK)	W_v(J/Bar)
W_{Abor}	18810	10.3	0.4602
W_{OrAb}	27320	10.3	0.3264
W_{AbAn}	7924	-	-
W_{AnAb}	00	-	-
W_{OrAn}	40317	-	-
W_{AnOr}	38974	-	0.1037
W_{AbOrAn}	12545	-	1.095

TABLE 6.3
GEOTHERMOBAROMETIC EQUATIONS USED IN CALCULATION

GEOTHREMOMETRY

1. Ferry and Spear (1978)

$$12454 - 4.662T + 0.057P + 3RT \ln K = 0$$

(where $K = (X_{Mg}/X_{Fe})^{Grt} / (X_{Mg}/X_{Fe})^{Bio}$)

R = gas constant

(T in ^{O}K, P in Bars, R = 1.987 calories)

2. Hodges and Spear (1982)

$$12454 - 4.662T + 0.057P + 3RT \ln K = 0$$

$$\text{where } K = K_D \exp \left[\frac{(3300-1.5T) \ (X_{Ca}^2 + X_{Fe}X_{Ca} + X_{Ca}X_{Mn} + X_{Mg}X_{Ca})^{Grt}}{RT} \right]$$

$$K_D = (X_{Mg}/X_{Fe})^{Grt} / (X_{Mg}/X_{Fe})^{Bio}$$

(T in ^{O}K, P in Bars, R = 1.987 calories)

Table 6.3 (Continued)

3. Ganguly & Saxena (1984)

$$T = \frac{A + \left[W_{FeMg}(X_{Fe}-X_{Mg}) + \Delta W_{Ca}X_{Ca} + \Delta W_{Mn}X_{Mn}\right]^{Grt}/R}{\ln K_D + 0.782}$$

where $A = 2089 - 0.8W_{FeMg}^{Grt}/R + 0.00956P$.

$$W_{FeMg}^{Grt} = 200\left[X_{Mg}/(X_{Mg}+X_{Fe2+})\right]^{Grt} + 2500\left[X_{Fe}^2/(X_{Mg}+X_{Fe2+})\right]^{Grt}$$

$$\Delta W_{ca} = \Delta W_{Mn} = 3000 \text{ Cal/Mol}$$

$$K_D = (X_{Fe}/X_{Mg})^{Grt}/(X_{Fe}/X_{Mg})^{Bio}$$

$$\left[T \text{ in } {}^{o}K, \ P \text{ in Bars, } R = 1.987 \text{ Calories}\right]$$

4. Using thermodynamic constants of Hodges and McKenna (1987)

$$50200 - 18.8T + 0.265p + RT \ln K = 0$$

Where $K = k_D \cdot K_\gamma$

$$K_D = (X_{Mg}/X_{Fe})^{Grt} / (X_{Mg}/X_{Fe})^{Bio}$$

$$K_\gamma = (\gamma_{Mg}/\gamma_{Fe})^{Grt} / (\gamma_{Mg}/\gamma_{Fe})^{Bio}$$

(γ values are considered for garnet as suggested by Berman (1990) and for biotite as suggested by Hoisch 1991)

(T in ${}^{o}K$, P in Bar, R = 8.3144 J)

Table 6.3 (Continued)

GEOBAROBMETRY

1. Hodges and Crowley (1985)

$$P = 1 + \cfrac{T(12.985 - R\ln K) - 5574}{0.6007 + \left[\cfrac{(X_{Pa}^2)^{Mus} \cdot (0.109 + 2\,(X_{Muss})^{Mus} * 0.268)}{3}\right]}$$

where $K = \cfrac{a_{Ca}^{Plag} \cdot a_{Fe}^{Bio}}{a_{Fe}^{Grt} \cdot a_{ca}^{Grt} \cdot (a_{Mus}^{0.33})^{Mus}}$

T in ^{O}K, P in Bar, R = 1.987 Cal

2. Hoisch (1991)

$$P = \cfrac{-51508 + 136.38T - RT\ln K}{6.35 - \Delta Vgr.}$$

where $K = \cfrac{a_{ca}^{Plag} \cdot a_{Fe}^{Bio}}{a_{Fe}^{Grt} \cdot a_{ca}^{Grt} \cdot (a_{Mus}^{0.33})^{Mus}}$

$\Delta Vgr = Vgr - 12.53$

Table 6.3 (Continued)

$$V_{gr} = 0.1 \left[V_{al} \left(\frac{X_{Fe}}{X_{Fe} + X_{Mg}} \right)^{Grt} + V_{py} \left(\frac{X_{Mg}}{X_{Fe} + X_{Mg}} \right)^{Grt} \right]$$

$$V_{al} = 125.24 + \left[1.482 * \left[1-X_{ca} \right]^2 \right] - 0.48 \left[1 + z_1 \left[\frac{1-X_{ca}}{0.066} \right] \right] \exp \left[- \frac{(Z)^2}{2} \right]$$

$$V_{py} = 125.24 + \left[0.512 * \left[1-X_{ca} \right]^2 \right] - 0.418 \left[1 + z_2 \left[\frac{1-X_{ca}}{0.083} \right] \right] \exp \left[- \frac{(Z)^2}{2} \right]$$

$$Z_1 = \frac{1- X_{ca} - 0.914}{0.066},$$

$$Z_2 = \frac{1- X_{ca} - 0.94}{0.083}$$

(T in ^{O}K, P in Bar, R = 8.3144 J)

TABLE 6.4
P-T DATA FROM CHUR AREA

The Upper One is Temperature in °C, Lower One is Pressure in Kb
Error estimated using Hodges & McKenna (1987) method.

	S-38	S-77/2	S-93/2	S-108	S-118	S-119/2	S-320	S-321
HS & HC	535 ± 21 7.06 ± .43	564 ± 4 6.02 ± .22	457 ± 24 4.94 ± .67	477 ± 12 6.06 ± 0.32	517 ± 32 7.19 ± .7	520 ± 21 5.82 ± .59	502 ± 15 6.27 ± .46	512 ± 12 6.85 ± .24
HS & H91	537 ± 21 7.59 ± 0.58	565 ± 4 6.16 ± .24	459 ± 25 5.43 ± .83	481 ± 12 7.29 ± 0.46	520 ± 33 8.28 ± .81	523 ± 21 6.66 ± .91	506 ± 15 7.52 ± .56	518 ± 13 8.62 ± .33
FS & HC	496 ± 20 6.20 ± .39	543 ± 3 5.59 ± .25	419 ± 23 4.1 ± .64	432 ± 10 5.04 ± .27	479 ± 32 6. 32 ± .69	482 ± 23 5.01 ± .49	407 ± 12 4.12 ± .37	462 ± 13 5.70 ± .25
FS & H91	497 ± 20 6.61 ± .54	543 ± 3 5.72 ± .2	420 ± 24 4.46 ± .78	435 ± 11 5.98 ± .39	482 ± 32 7.28 ± .81	484 ± 23 5.66 ± .71	410 ± 12 4.98 ± .44	466 ± 13 7.12 ± .33
GS & HC	566 ± 20 7.77 ± .42	540 ± 3 5.53 ± .17	486 ± 22 5.56 ± .62	449 ± 10 5.43 ± .26	526 ± 28 7.41 ± .61	510 ± 19 5.61 ± .52	481 ± 11 5.79 ± .36	480 ± 11 6.12 ± .21
GS & H91	568 ± 20 8.39 ± .57	540 ± 3 5.62 ± .19	488 ± 22 6.15 ± .78	452 ± 10 6.48 ± .39	530 ± 29 8.55 ± .71	513 ± 19 6.41 ± .83	485 ± 11 6.96 ± .44	485 ± 11 7.67 ± .31
BH & HC	559 ± 21 7.6 ± .44	594 ± 5 6.61 ± .24	476 ± 25 5.36 ± .7	507 ± 12 6.73 ± .33	554 ± 34 8.05 ± 0.74	552 ± 22 6.50 ± 0.64	522 ± 15 6.7 ± .45	546 ± 13 7.60 ± .25
BH & H91	561 ± 22 8.22 ± .6	594 ± 5 6.8 ± .26	479 ± 26 5.93 ± .8	513 ± 13 8.21 ± .49	559 ± 35 9.32 ± .86	556 ± 22 7.51 ± 1	527 ± 15 8.06 ± .57	554 ± 13 9.66 ± .36
BH & HR	575 ± 23 11.56 ± .69	610 ± 5 10.21 ± .21	489 ± 27 8.68 ± .95	526 ± 13 11.69 ± .52	575 ± 36 12.92 ± .96	572 ± 23 11.31 ± 1.07	540 ± 16 11.73 ± .65	566 ± 14 12.68 ± .32
HS & HR	547 ± 22 10.78 ± .66	577 ± 4 9.46 ± .28	467 ± 25 8.10 ± .9	491 ± 12 10.77 ± .49	532 ± 33 11.73 ± .8	535 ± 21 10.42 ± .97	516 ± 16 10.99 ± .65	527 ± 13 11.63 ± .3
FS & HR	508 ± 21 9.69 ± .61	555 ± 3 8.97 ± .26	428 ± 24 7.06 ± .87	446 ± 11 9.59 ± .43	494 ± 33 10.69 ± .9	497 ± 23 9.51 ± .79	419 ± 13 8.03 ± .54	476 ± 14 10.26 ± .3
GS & HR	580 ± 21 11.68 ± 0.66	552 ± 3 8.89 ± .24	496 ± 23 8.87 ± 0.84	463 ± 10 10.64 ± .4	542 ± 30 12.01 ± .79	526 ± 19 10.19 ± .9	495 ± 12 10.35 ± .51	495 ± 12 10.77 ± .27

Table 6.4 (Continued)

	S-354	S-367	S-377	S-381	S-394	S-607	S-616	S-669
HS & HC	491 ± 7 6.55 ± .94	569 ± 5 7.32 ± .18	546 ± 15 5.45 ± 0.39	470 ± 9 5.19 ± .2	486 ± 18 5.1 ± .39	550 ± 10 6.13 ± .19	422 ± 12 4.12 ± .40	520 ± 5 6.08 ± .07
HS & H91	495 ± 8 8.06 ± 1.32	574 ± 5 8.55 ± .23	550 ± 16 6.63 ± .52	471 ± 9 5.7 ± .27	487 ± 18 5.56 ± .47	552 ± 10 6.87 ± .22	424 ± 13 4.74 ± .43	522 ± 5 6.64 ± .07
FS & HC	469 ± 7 6. 06 ± .73	549 ± 5 6.87 ± .17	535 ± 15 5.23 ± .38	442 ± 8 4.59 ± .21	460 ± 17 4.56 ± .38	534 ± 10 5.8 ± .19	409 ± 11 3. 84 ± .37	475 ± 6 5.11 ± .09
FS & H91	474 ± 7 7.48 ± 1.06	553 ± 5 8.03 ± .21	539 ± 16 6.37 ± .52	444 ± 8 5 ± .25	461 ± 18 4.94 ± .46	536 ± 10 6.5 ± .22	411 ± 11 4.44 ± .53	477 ± 6 5.54 ± .08
GS & HC	494 ± 5 6.63 ± .85	593 ± 5 7.82 ± .17	548 ± 14 5.49 ± .36	477 ± 7 5.35 ± .38	496 ± 16 5.31 ± .33	570 ± 8 6.56 ± .17	443 ± 11 4.56 ± .37	513 ± 4 5.92 ± .07
GS & H91	499 ± 5 8.16 ± 1.22	597 ± 5 9.13 ± .21	553 ± 15 6.68 ± .49	479 ± 7 5.88 ± .23	497 ± 16 5.80 ± .41	573 ± 8 7.36 ± .19	445 ± 11 5.24 ± .40	515 ± 4 6.46 ± .07
BH & HC	517 ± 10 7.16 ± 1.04	608 ± 6 8.16 ± .2	569 ± 16 5.90 ± .40	498 ± 9 5.80 ± .23	514 ± 19 5.69 ± .41	577 ± 10 6.69 ± .2	435 ± 13 4.40 ± .41	553 ± 5 6.76 ± .08
BH & H91	524 ± 12 8. 84 ± 1.48	615 ± 6 9.56 ± .25	575 ± 17 7.21 ± .54	500 ± 9 6.43 ± .28	516 ± 19 6.25 ± 51	580 ± 10 7.53 ± .23	438 ± 13 5. 07 ± .44	556 ± 5 7.46 ± .08
BH & HR	535 ± 11 11.35 ± 1.43	626 ± 6 12 ± .24	582 ± 17 8.87 ± .46	511 ± 10 9.10 ± .3	530 ± 20 9.64 ± .52	594 ± 10 10.62 ± .26	449 ± 13 8.18 ± .51	575 ± 5 12.14 ±.09
HS & HR	504 ± 8 10.61 ± 1.28	582 ± 5 10.97 ± .23	557 ± 16 8.12 ± 44	480 ± 9 8.35 ± .29	498 ± 18 8.90 ± .50	563 ± 10 9.90 ± .25	433 ± 13 7.78 ± .49	537 ± 5 11.07 ± .09
HR & FS	483 ± 7 10.10 ± 1.05	562 ± 5 10.48 ± .21	546 ± 16 8.12 ± .44	452 ± 8 7.69 ± .27	472 ± 18 8.31 ± .49	547 ± 10 9.54 ± .25	420 ± 12 7.47 ± .46	491 ± 6 9.83 ± .09
GS & HR	508 ± 5 10.7 ± 1.19	606 ± 5 11.53 ± .21	559 ± 15 8.39 ± .42	487 ± 7 8.53 ± .25	508 ± 16 9.14 ± .43	584 ± 9 10.38 ± .22	454 ± 12 8.30 ± .46	530 ± 4 10.89 ± .1

Table 6.4 (Continued)

	S-675	S-676	S-695	S-738	S-749	S-765	S-812	S-833
HS & HC	572 ± 16 5.24 ± .28	558 ± 16 7.60 ± .35	564 ± 21 6.05± .45	559 ± 19 7.25 ± .36	465 ± 10 5.95 ± .21	555 ± 19 7.67 ± .57	520 ± 4 6.54 ± .06	587 ± 8 5.09± .2
HS & H91	570 ± 16 5.26 ± .29	563 ± 17 9.17 ± .47	566 ± 21 6.54 ± .52	562 ± 19 8.16 ± .44	469 ± 11 7.37 ± .28	562 ± 20 9.69 ± .71	523 ± 4 7.69 ± .09	589 ± 8 5.66 ± .2
FS & HC	556 ± 16 4.95 ± .27	509 ± 16 6.51 ± .33	518 ± 22 5.11 ± .43	522 ± 18 6. 46 ± .34	405 ± 9 4.58 ± .18	499 ± 18 6.40 ± .54	412 ± 4 4.14 ± .07	581 ± 8 4.99 ± .2
FS & H91	556 ± 16 4.95 ± .28	513 ± 16 7.81 ± .44	519 ± 22 5.47± .48	525 ± 18 7.24 ± .41	409 ± 9 5.59 ± .23	504 ± 19 8.03 ± .68	414 ± 4 4.88 ± .10	583 ± 8 5.54± .22
GS & HC	571 ± 16 5.24 ± .24	562 ± 16 7.7 ± .34	605 ± 21 6.89 ± .45	528 ± 18 6.59 ± .34	462 ± 8 5.88 ± .15	550 ± 18 7.55 ± .55	508 ± 4 6.29 ± .05	606 ± 6 5.45 ± .17
GS & H91	571 ± 14 5.25 ± .25	567 ± 16 9.29 ± .46	607 ± 21 7.49 ± .52	531 ± 18 7.39 ± .4	466 ± 8 7.28 ± .21	556 ± 8 9.55 ± .68	512 ± 4 7.4 ± .08	608 ± 6 6.03 ± .19
BH & HC	600 ± 17 5.79 ± .29	597 ± 17 8.49 ± .38	588 ± 22 6.55 ± .47	588 ± 20 7.88 ± .38	494 ± 11 6.62 ± .2	590 ± 20 8.47 ± .61	516 ± 5 6.47 ± .09	606 ± 8 5.44 ± .21
BH & H91	601 ± 17 5.84 ± .3	605 ± 18 10.34 ± .51	590 ± 22 7.11 ± .54	592 ± 20 8. 91 ± .46	500 ± 11 8.29 ± .29	600 ± 21 10.82 ± .77	520 ± 5 7.62 ± .13	609 ± 8 6.04 ± .23
BH & HR	615 ± 18 8.98 ± .4	617 ± 19 13.03 ± .58	605 ± 23 10.53 ± .7	612 ± 21 13.36 ± .52	516 ± 12 12.54 ±.39	617 ± 22 14.82 ± .91	536 ± 6 12.07 ± .16	630 ± 9 8.92 ± .28
HS & HR	583 ± 17 8.27 ± .38	572 ± 17 11.78 ± .52	577 ± 22 9.79 ± .66	577 ± 20 12.5 ± .51	481 ± 11 11.49 ± .37	574 ± 20 13.62 ± .83	535 ± 4 12.06 ± .1	600 ± 8 8.42 ± .27
GS & HR	567 ± 17 7.93 ± .37	523 ± 16 10.44 ± .47	530 ± 22 8.57 ± .61	541 ± 19 11.58 ± .48	421 ± 9 9.72 ± .3	518 ± 19 12 ± .75	426 ± 5 8.70 ± .13	593 ± 8 8.28 ± .26
GS & HR	583 ± 14 8.26 ± .2	576 ± 17 11.91 ± .51	619 ± 22 10.9 ± .68	547 ± 19 11.73 ± .47	497 ± 9 11.42 ± .28	370 ± 19 13.50 ± .80	525 ± 4 11.74 ± .09	619 ± 6 8.85 ± .23

Table 6.4 (Continued)

	S-839	S-858	S-859	S-894
HS & HC	461 ± 3 6.5 ± .12	530 ± 12 6.92 ± .23	528 ± 18 7.37 ± .31	584 ± 14 6.14 ± .5
HS & H91	466 ± 3 8.35 ± .35	534 ± 12 8.16 ± .22	533 ± 13 9 ± .38	586 ± 14 6.53 ± .64
FS & HC	395 ± 4 4. 92 ± .34	494 ± 14 6.12 ± .21	458 ± 12 5.75 ± .29	565 ± 12 5.76 ± .51
FS & H91	399 ± 4 6.24 ± .28	497 ± 14 7.18 ± .24	462 ± 12 6.99 ± .36	566 ± 12 6.1 ± .6
GS & HC	452 ± 3 6.30 ± .11	498 ± 9 6.21 ± .13	549 ± 12 7.88 ± .29	563 ± 11 5.73 ± .49
GS & H91	457 ± 4 8.09 ± .34	501 ± 9 7.28 ± .18	555 ± 12 9.64 ± .37	564 ± 12 6.07 ± .57
BH & HC	487 ± 3 7.15 ± .12	562 ± 12 7.63 ± .18	544 ± 13 7.74 ± .31	614 ± 15 6.74 ± .6
BH & H91	495 ± 4 9. 27 ± .39	568 ± 13 9.07 ± .24	550 ± 13 9.5 ± .4	617 ± 16 7.20 ± .69
BH & HR	507 ± 3 12.45 ± .18	579 ± 13 11.65 ±.19	564 ± 14 13.19 ± .48	631 ± 16 10.37 ± .71
HS & HR	475 ± 3 11.46 ± .19	543 ± 12 10.76 ± .19	544 ± 13 12.54 ± 46	597 ± 14 9.62 ± .65
GS & HR	408 ± 4 9.40 ± .19	507 ± 14 9.89 ± .22	472 ± 12 10.28 ± .43	578 ± 13 9.20 ± .6
GS & HR	467 ± 3 11.21 ± .18	511 ± 9 9.98 ± .21	567 ± 13 13.28 ± .44	573 ± 12 9.17 ± .59

Table 6.4 (Continued)

Assuming Pressure as 7Kb and Temperature is in ^{O}C

	S-16	S-46	S-59	S-62	S-180	S-348	S-350	S-400	S-882
FS	514 ± 18	458 ± 15	529 ± 15	488 ± 20	501 ± 15	482 ± 16	459 ± 18	429 ± 20	501 ± 10
GS	545 ± 15	515 ± 18	534 ± 15	487 ± 15	525 ± 12	550 ± 17	485 ± 15	488 ± 19	513 ± 8
HS	537 ± 18	506 ± 18	534 ± 12	493 ± 15	527 ± 15	534 ± 18	471 ± 18	495 ± 22	512 ± 9
BH	556 ± 18	534 ± 13	556 ± 15	512 ± 18	553 ± 15	557 ± 18	496 ± 18	518 ± 23	538 ± 9

Table 6.4 (Continued)

P-T Data from Biotite inclusions within Garnet
Pressure assumed from the Rim Data

	S-16/I1	S-16/I2	S-46	S-77/2	S-321/I1	S-321/I2	S-367	S-695	S-858
FS	477	486	488	514	490	481	518	486	494
GS	507	521	505	522	495	494	550	558	490
HS	496	509	496	528	509	502	528	541	512
BH	518	533	526	550	535	529	558	520	494

FS = Ferry & Spear (1978)
HS = Hodges & Spear (1982)
GS = Ganguly & Saxena (1984)
HC = Hodges & Crowley (1985)
H91 = Hoisch (1991)
BH = Combination of Hodges & McKenna (1987), Berman (1990), Hoisch (1991)

CHAPTER - 7
SUMMARY AND CONCLUSIONS

7.1 ROCK TYPES

The Jutogh Group of rocks from the Chur area, Himachal Himalaya constitutes the frontal part of the High Himalaya Crystalline thrust sheet. Within the Jutogh Group four main lithological units can be recognized at successively higher topographic levels. These are lower carbonaceous schist, quartzite, upper carbonaceous schist and mica schist respectively. A thin marble and calc-silicate band are also observed within the mica schist in the southern part of the Chur area (between Chauras and Haripurdhar). Also irregular patches of calc-silicate rocks and impure marble are associated with carbonaceous schist. Small lenticular bodies of amphibolite are also common within the mica schist. Above the Jutogh Group at the highest topographic and structural level a granite body called the Chur granite is present. The Jutogh Group is underlain by the phyllite and quartzite belonging to the Chail Formation.

7.2 STRUCTURES

Small-scale structures include early structures, the structures related to progressive ductile shearing and late structures. The early structures comprise two generations of foldings (F_1 and F_2) which are tight to isoclinal, recumbent to gently-plunging reclined/inclined with E or W axial trend. S_1 penetrative cleavages and S_2 crenulation cleavages are axial planer to F_1 and F_2 foldings respectively. F_1 and F_2 folds are co-axial in most of the places resulting in type 3 interference pattern. These early structures have been obliterated by a progressive ductile shearing

which has affected all rock types of this area. The most common product of ductile shearing is mylonites which vary from protomylonite through orthomylonite to ultramylonite. Mylonitic foliation is the main structure developed within the ductile shear zone. Small-scale thrusts are also developed giving imbricate or schuppen structures, particularly within the crbonaceous bands. Late structures include a set of very open and upright folds (F_3). The last episode of deformation is represented by a set of subvertical fractures cutting across all the earlier structures.

In this area four thrusts can be recognized in regional scale. These are the Chail thrust below the Chail Formation, the Jutogh thrust below the Jutogh Group, the Rajgarh thrust below upper carbonaceous schist and the Chur thrust at the contact of the Chur granite. In addition to the Chail thrust (below the Chail Formation of LHZ) other three represent an imbricate structure in the Chur area.

7.3 MICROSTRUCTURES AND TEXTURE

In the Jutogh Group of rocks index minerals of Barrovian sequence such as chlorite, biotite, garnet, staurolite, kyanite and sillimanite have been formed during early deformation (F_1-F_2) but prior to the ductile shearing. Muscovite, quartz and ilmenite have been formed during F_1 and F_2 deformations as well as during ductile shearing. Others minerals such as tourmaline and epidote group of minerals have been formed during early deformation episodes and ductile shearing also.

Two stage-growth of garnets with inclusion rich core and inclusion poor rim predicts the formation of garnet during F_1 deformation and during static phase after that. However, one low grade phase is recognized during ductile shearing when chlorite and locally biotite have

been recrystallized.

Chlorite, staurolite and sillimanite within garnet in garnet grade, staurolite grade and sillimanite grade predict the formation of garnet from chlorite, staurolite and sillimanite respectively.

7.4 METAMORPHIC ZONES

Four grades starting from garnet to sillimanite are recognized at successively higher structural and topographic levels showing the inversion of metamorphism within the Jutogh thrust sheet. Strict boundary is not possible due to post-thrusting effect on original isograd pattern. However, below the Rajgarh thrust rocks from quartzite unit and lower carbonaceous schist are considered into garnet grade. The upper carbonaceous schist and mica schist above Rajgarh thrust belong to staurolite grade. In the vicinity of the Chur granite mica schist sporadically contains kyanite or/and sillimanite, thus belongs to kyanite grade and sillimanite grade respectively.

7.5 MINERAL ASSEMBLAGES AND AFM DIAGRAMS

The mineral assemblages in garnet grade does not include garnet in pure quartzite. But within the intercalated micaceous layer of quartzite garnets with muscovite, biotite, chlorite and ilmenite and sometimes plagioclase are present. In the staurolite grade chlorite is not present with staurolite. Plagioclase is not also available from all the samples which contain staurolite. In the kyanite-sillimanite grade kyanite is present sometimes with sillimanite. Sillimanite is present as fibrolite and as needles.

AFM diagrams in garnet grade (Fig.5.2) show that garnet-biotite-

chlorite and garnet-biotite co-exist in this grade. In garnet grade Mg/Fe ratio gradually decreases from chlorite through biotite to garnet. In staurolite grade (Fig.5.3) staurolite does not co-exist with chlorite Biotite has its very wide distribution of composition. Staurolite and chlorite are not present in kyanite-sillimanite grade. The presence of crossing tie line relationships in all three grades at narrow angle is due to the analytical error.

7.6 MINERAL CHEMISTRY

Garnet from different metamorphic zones in the Jutogh Group is characterized by almandine garnet with varying proportion of spessartine, pyrope and grossular content. Fe concentration shows some decreasing trend from garnet grade (X_{Fe}=0.59-0.77) through staurolite grade (X_{Fe}=0.65-0.87) to sillimanite grade (X_{Fe}=0.76-0.83). Mn concentration decreases from garnet grade to staurolite grade. But there is no correlation of Mn concentration with sillimanite grade. Ca is more enriched in garnet grade than that in staurolite grade. In summary, from garnet grade to staurolite grade X_{Fe} increases and X_{Mn} and X_{Ca} decrease.

Biotite present in the Jutogh Group is mainly Fe rich where Fe>Mg. Mg-rich (Mg>Fe) biotites are present in minor quantity. In the garnet and staurolite grades X_{Fe} varies from 0.43-0.50 and 0.40-0.58 respectively. X_{Mg} shows no changes from garnet grade (=0.27-0.46) through staurolite grade (=0.33-0.39) to sillimanite grade (=0.36-0.38). The variation in X_{Al} and X_{Ti} has also no correlation with respect to different grades. But X_{Al} decreases with the increase of X_{Ti}.

Muscovite does not show any change in its composition from one

grade to other. But Al concentration in octahedral site decreases with the increase of Fe.

Fe rich as well as Mg rich chlorite is present in the Jutogh Group in garnet grade and staurolite grade respectively. Si, Al in octahedral site and Al in tetrahedral site do not show any changes in concentration according to grade. Plagioclase is mostly of oligoclase variety. Ilmenite is present in pure phase in the matrix and as inclusions.

7.7 GARNET ZONATION PATTERNS

Garnet zonation patterns in garnet grade show single stage growth of garnet with minor rim resorption in one sample (Fig.5.9). But two stage growth to complex growth history has been encountered in staurolite grade. Intradiffusional change in zoning profile is more extensive at successively higher topographic levels. Near the vicinity of the Chur granite Mn shows flat trend. Different Ca zonation patterns have been observed indicating complex growth history in staurolite grade because Ca retains its original zonation pattern due to its slowest diffusion rate. In sillimanite grade Mn and Mg show antithetic relationship near the core. Near the rim Fe increases with the decrease of Ca. This garnet had been nucleated in kyanite grade but continued growing in sillimanite grade also.

The garnet zonation patterns from the Jutogh Group suggest that after formation of garnets the rims of garnets have been resorbed with varying degree in garnet and staurolite grade. In staurolite grade intracrystalline diffusional modification with addition of rim resorption is more intense at successively higher topographic levels. These two suggest the increase of temperature upsection in the staurolite grade because more

the temperature suffered by the rock more the temperature range is available to reach the closure temperature, thus more easily reset the zoning profile.

7.8 METAMORPHIC REACTIONS

The normal assemblage of minerals of Barrovian sequence from different grades are present within the Jutogh Group. Chlorite continued to persist upto staurolite grade but changed the composition from Fe-rich to Mg-rich. But primary chlorite is not available with the staurolite. Rocks of kyanite grade contain no staurolite and chlorite. In sillimanite grade samples kyanite is present sometimes with the sillimanite.

The reaction responsible for the formation of garnet is

$$Chl + Mus + Qtz = Grt + Bio + H_2O \qquad [R\ 5.3]$$

with the additional Ca,Al-rich phase.

In the staurolite grade two reactions were operative. The first one became responsible for the formation of staurolite and the second one was operative at the last stage by which garnet has been formed. Both of these reactions are

$$Chl + Mus + Grt = Str + Bio + Qtz + H_2O \qquad [R\ 5.4]$$

$$\text{and } Str + Bio + Qtz + (Ca,Al)phase = Grt + Mus + H_2O \qquad [R\ 5.2]$$
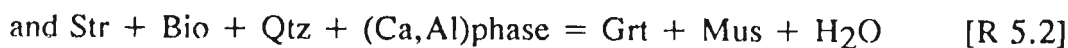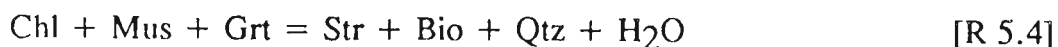
which is confirmed from garnet zonation pattern also.

In kyanite and sillimanite grade three reactions were responsible. They are

$$Str + Mus + Qtz = Al_2SiO_5 + Bio + H_2O, \qquad [R\ 5.5]$$

$$Mg\text{-rich chlorite} + Mus + Qtz = Al_2SiO_5 + Bio + H_2O \qquad [R\ 5.6]$$

$$\text{and } Bio + Al_2SiO_5 + Qtz = Grt + Mus \qquad [R\ 5.7].$$
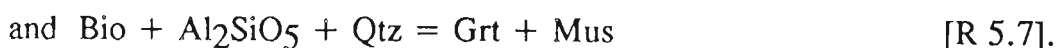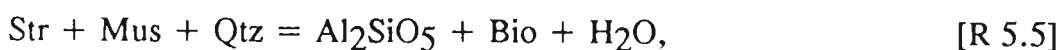
7.9 GEOTHERMOBAROMETRY

Pressure and temperature have been calculated simultaneously using different calibrations. It has been observed that combination of Berman (1990) model for garnet and Hoisch (1991) model for biotite with $\Delta H, \Delta S$ and ΔV data suggested by Hodges and McKenna (1987) to calculate temperature and Hodges and Crowley (1985) calibration for pressure calculation give the reasonable result. In garnet grade temperature ranges from 476°C to 558°C. In staurolite grade and kyanite-sillimanite grade the ranges are 434°C-588°C and 593°C-614°C although the geothermometry and geobarometry from the Chur area show an unsystematic distribution throughout the area. Sometimes calculated temperatures from rims are apparently lower than that calculated near rim inside the garnets within the limit of error estimation. Pressure estimation within the garnet could not be possible due to lack of other mineral phases except biotite required to calculate pressure. Structural distance versus temperature and that versus pressure plot suggest that there is no cause or effect relationship between the Jutogh thrust and the distribution of P-T data.

7.10 REASON BEHIND INVERTED METAMORPHISM

As mentioned earlier all Barrovian index minerals have been formed prior to the thrusting. So major progressive episode(s) in the Jutogh Group is a pre-thrusting phenomenon. In Chapter 1 different models for inverted metamorphism have been described. The hot over cold model, shear heating model (Le Fort 1975) and heat refraction model (Jaupart & Provost 1985) are readily discarded because in those cases

metamorphism should be a post thrusting phenomenon responding the transient inverted geothermal gradient near the thrust planes. The effect of intrusion of the Chur granite over the Jutogh thrust sheet (Pilgrim & West 1928) is discarded because Chur granite body is a thrust slice not an intrusive laccolith (see Chapter 3). Instead, stackings of thrust planes recognizing three major thrust planes within the Jutogh Group are present. So the overall inversion of metamorphism within the Jutogh Group of rocks is a result of the post-metamorphic stacking of already metamorphosed rocks by thrusting with high-grade rocks tectonically emplaced above lower grade ones. The unsystematic distribution of temperature and pressure was due to the thrust imbrication in large scale as well as in small scale.

7.11 REGIONAL CORRELATION

From HHCZ many workers reported (e.g. Hodges & Silverberg 1988; Inger & Harris 1992) one prograde metamorphism which is prior to the thrusting and is related to early-Himalayan orogeny (see Chapter 1). The later one (M_2) is synchronous with the MCT thrusting (e.g. Hubbard 1989) and crustal anatexis in the upper part of the HHCZ. An intermittent retrogressive phase has been identified which was overprinted by M_2. In the study area one pre-thrusting progressive phase of metamorphism and one low grade phase of metamorphism synchronous with the ductile shearing have been recognized. So the progressive phase may be synchronous with the pre-thrusting progressive metamorphism (M_1) of HHCZ. During the activation of MCT a low grade phase of metamorphism was operative during ductile shearing in the study area i.e.

at the frontal part of HHCZ. At further north near the root zone (upper part of HHCZ) during MCT thrusting second phase of metamorphism was of high grade (K-feldsper - sillimanite) wheras that phase was with very low intensity in the study area.

REFERENCES

Acharyya, S. K. 1979. Pre-Tertiary fabric and metamorphism in the eastern Himalaya. In: Metamorphic rock sequence of eastern Himalaya (edited by: Verma, P. K.), Bagchi & Co. 67-82.

Albee, A. L. 1965. Phase equilibria in three assemblages of kyanite zone pelitic schists, Lincoln Mountain Quadrangle, Central Vermont. *J. Petrol.* **6**, 246-301.

Anderson, D. E. & Olimpio, J. C. 1977. Progressive homogenization of metemorphic garnets. South Morar, Scotland: evidence for volume diffusion. *Canad. Mineral.* **15**, 205-216

Applegate, J. D. R. & Hodges, K. V. 1990. Solution model effects on the precision of an empirically calibrated geobarometer. EOS Trans. *Am. Geophy. Union* **71**, 1661.

Applegate, J. D. R. & Hodges, K. V. 1994. Empirical evalution of solution models for pelitic minerals and their applications to thermobarometry. *Contrib. Mineral Petrol.* **117**, 56-65.

Arita, K. 1983. Origin of the inverted metamorphism of the lower Himalaya, central Nepal. *Tectonophysics* **95**, 43-60.

Arita Kazunori, Gautam Pitambar & Ganzawa Yoshihiro 1990. Two metamorphic events of the Nepal Himalayas prior and posterior to India-Eurasia Collision. *J. Fac. Sci.* **22**, 519-528.

Auden, J. B. 1937. Structure of the Himalaya in Garhwal. *Geol. Soc. India Rec.* **71**, 407-433.

Banno, S., Sakai, C. & Higashino, T. 1986. Pressure-temperature trajectory of the Sanbagawa metamorphism deduced from garnet zoning. *Lithos* **19**, 51-63.

Bell, T. H. 1978. Progressive deformation and reorientation of fold axes in a ductile mylonite zone: the Woodroffe thrust. *Tectonophysics* **44**, 285-321.

Bell, T. H. & Etheridge, M. A. 1973. Microstructure of mylonites and their descriptive terminology. *Lithos* **6**, 337-348.

Bell, T. H. & Johnson, S. E. 1989. Porphyroblasts inclusion trails: The key to orogenesis. *J. Met. Geol.* **7**, 279-310.

Bell, T. H. & Rubenach, M. J. 1983. Sequential porphyroblast growth and crenulation cleavage development during progressive deformation. *Tectonophysics* **92**, 171-194.

Berman, R. G. 1988. Internally-consistent thermodynamic data for stoichiometric minerals in the system $Na_2O-K_2O-CaO-MgO-FeO-Fe_2O_3-Al_2O_3-SiO_2-TiO_2-H_2O-CO_2$. *J. Petrol.* **29**, 445-522.

Berman, R. G. 1990. Mixing properties of Ca-Mg-Fe-Mn garnets. *Am. Mineral.* **75**, 328-344.

Besse, J. & Courtillot, V. 1988, Paleogrophic maps of the continents bordering the Indian ocean since the earli Jurassic . *J. Geophys. Res.* **93**, 11791-11808.

Besse, J., Courtillot, V., Pozzi, J. P., Westphal, M., & Zhou, Y. X. 1984. Paleomagnetic estimates of crustal shortening in the Himalayan thrust and Zangbo suture. *Nature* **311**, 621-626.

Bhattacharya, A., Mohanty, L., Maji, A., Sen, S. K. & Raith, M. 1992. Non-ideal mixing in the phlogopite-annite binary:constraints from experimental data on Mg-Fe partitioning and a reformulation of the biotite-garnet thermometer. *Contrib. Mineral Petrol.* **111**, 87-93.

Bird, P. 1978. Initiation of intracontinental subduction the Himalaya. *J. Goephys. Res.* **83**, 4975-4987.

Burchfiel, D. C., Zhiliang, C., Hodges, K. V., Yuping, L., Royden, L. H., Changrong, D. & Jiene, X. 1992. The South Tibet Detachment System, Himalaya Orogeny: Extension contemporaneous with and parallel to shortening in a collision mountain belt. *Geol. Soc. Am. Spl. Papers* 260.

Carmicheal D. M. 1970. Intersecting isograds in the Whetstone Lake area, Ontario. *J. Petrol.* **11**, 147-181.

Chakravorty, S. & Ganguly, J. 1991. Compositional zoning and cation diffusion in garnets. In: Diffusion atomic ordering and mass transport- selected topics in geochemistry, *Advances in Physical Geochemistry.* Springer-Verlag.

Chatterjee, N. D. & Flux, S. 1986. Thermodynamic mixing prperties of Muscovite-Paragonite crystalline solutions at high temperatures and pressures, and their geological application. *J. Petrol.* **27**, 677-693.

Chattillon-Colinet, C., Kleppa, O. J., Newton, R. C. & Perkins III, D. 1983. Enthalpy of formation of $Fe_3Al_2Si_3O_{12}$ (almandine) by high temperature alkaly borate solution calorimetry. *Geochim. Cosmochi. Acta.* **47**, 439-444.

Cobbold, P. R. & Quinquis, H. 1980. Development of seath folds in shear regimes. *J. Struct. Geol* **2**, 119-126.

Crawford, M. L. 1977. Calcium zoning in almandine garnet, Wissahickon Formation, Philadelphia, Pennsylvania. *Canad. Mineral.* **15**, 243-249.

Das, B. K & Rastogi, R. 1988. Ptrology of the Jutogh metapelites near Chur, Himachal Himalaya, India. *J. Geol. Soc. Ind.* **31**, 251-266.

Dasgupta, S., Sengupta, P., Guha, D. & Fukuoka, M. 1991. A refined garnet-biotite Fe-Mg exchange geothermonmeter and its application in amphibolites and granulites. *Contrib. Mineral. Petrol.* **109**, 130-137.

Davis, G. H. 1984. Structural geology of rocks and regions. John Wiley & Sons.

Dennis, A. J. & Secor, D. T. 1987. A model for the development of crenulations in shear zones with applications from the Southern Apalachian Piedmont. *J. Struct. Geol.* **9**, 109-117.

Dennis, A. J. & Secor, D. T. 1990. On resolving shear direction in foliated rocks deformed by simple shear. *Geol. Soc. Am. Bull.* **102**, 1257-1267.

Douce, Patino A. E., Johnston, A. D. & Rice, J. M. 1993. Octahedral excess mixing properties in biotite: a working model with applications to geobarometry and geothermometry. *Am. Mineral.* **78**, 113-131.

Dubey, A. K. & Bhat, M. I. 1991. Structural evolution of the Simla area, NW Himalaya : Implications for crustal thickening. *J. Southeast Asian earth Sci.* **6**, 41-53.

Elkins, L. T. & Grove, T. L. 1990. Ternary feldsper experiments and thermodynamic models. *Am. Mineral.* **75**, 544-559.

England, P. C. & Thompson, A. B. 1984. Pressure-temperature-time paths of regional metamorphism I. Heat transfer during the evolution of regions of thickened continental crust. *J. Petrol* **25**, 894-928.

Essene, E. J. 1982. Geologic thermometry and barometry. In: Characterization of metamorphism through Mineral Equilibria (edited by: Ferry, J. M.), *Reviews of Mineralogy* **10**, 153-206

Eugster, H. P., Albee, A. L., Bence, A. E., Thompson, J. B. & Waldbaum, D. R. 1972. The two phase region and excess mixing properties of paragonite-muscovite crystalline solutions. *J. Petrol.* **13**, 147-179.

Ferry, J. M. & Spear, F. S. 1978. Experimental calibration of partitioning of Fe and Mg between biotite and garnet. *Contrib. Mineral. Petrol.* **66**, 113-117.

Florence, F. P. & Spear, F. S. 1991. Effects of diffusional modification of garnet growth zoning on P-T path calculation. *Contrib. Mineral. Petrol.* **107**, 487-500.

Frank, W., Thoni, M. & Purtscheller, F. 1977. Geology and petrology of Kulu-south-Lahul area. *Colloques internat. C. N. R. C.*, No. **268**, 147-172.

Frost, B. R. & Tracy, R. J. 1991. P-T paths from zoned garnets: some minimum criteria. *Am. J. Sci.* **291**, 917-939.

Fuchs, G. 1981. Outline of the geology of the Himalaya. *Mitt. Osterr. Geol. Ges.* **74/75**, 101-127.

Fuhrman, M. L. & Lindsley, D. H. 1988. Ternary feldspar modeling and thermometry. *Am. Mineral.* **73**, 201-215.

Gairola, V. K. & Ackermand, D. 1988. Geothermobarometry of the Central Crystallines from the Garhwal Himalaya. *J. Geol. Soc. Ind.* **30**, 230-242.

Ganguly, J. 1978. Energetics of some ferromagnesium silicate solid solutions derive from compositional relations between coexisting phases. *Phy. and Chem. Min.* **3**, 301-302.

Ganguly, J. 1979. Garnet and clinopyroxenes solid solutions, and geothermometry based on Fe-Mg distribution coefficient. *Geochim. Cosmochim. Acta* **43**, 101-29.

Ganguly, J. & Saxena, S. K. 1984. Mixing properties of aluminosilicate garnets: constraints from natural and experimental data, and applications to geothermo-barometry. *Am. Mineral.* **69**, 88-97.

Gansser, A. 1964. Geology of the Himalaya. Interscience, New York.

Gansser, A. 1974. Himalaya. In: Mesozoic-Cenozoic Orogenic Belts (edited by Spencer, A. M.), *Geol. Soc. London Spl. Publ.* **4**, 267-278.

Ghent, E. D. & Stout, M. Z. 1981. Geobarometry and geothermometry of Plagioclase-Biotite-Garnet-Muscovite assemblages. *Contrib. Mineral. Petrol.* **76**, 92-97.

Ghosh, S. K. 1975. Distortion of planar structres around rigid spherical bodies. *Tectonophysics* **28**, 185-208.

Ghosh, S. K. 1977. Drag patterns of planar structures around rigid inclusions. In: *Energitics of Geological processes* (edited by Saxena, S. K. & Bhattacharji, S.), 98-120. Springer-Verlag.

Ghosh, S. K. & Ramberg, H. 1976. Reorientatuion of inclusions by combination of pure shear and simple shear. *Tectonophysics* **34**, 1-70.

Ghosh, S. K. & Sengupta, S. 1984. Successive development of plane noncylindrical folds in progressive deformation. *J. Struct. Geol.* **6**, 703-709.

Ghosh, S. K. & Sengupta, S. 1987. Progressive development of structures in a ductile shear zones. *J. Struct. Geol.* **9**, 277-288.

Goldman, D. S. & Albee, A. L. 1977. Correlation of Mg/Fe pertitioning between garnet and biotite with O/O partitioning between quartz and magnetite. *Am. J. Sci.* **277**.750-767.

Graham, C. M. & England, P. C. 1976. Thermal regimes and regional metamorphism in the vicinity of overthrust faults: An example of shear heating and inverted metamorphic zonation from southern California. *Earth. Planet. Sci. Lett.* **31**, 142-152.

Gray, D. R. 1977a. Morphological classification of crenulation cleavage. *J. Geology* **85**, 229-235.

Gray, D. R. 1977b. Differentiation associated with a discrete crenulation cleavages. *Lithos* **10**, 89-101.

Guggenheim, E. A. 1967. Thermodynamics. North Holland.

Heim, A. & Gansser, A. 1939. Central Himalaya. Geological observations of the swiss expedition 1939. *Soc. Hev. Sci. Nat. Mem.* **73**, 1-245. (Reprinted by Hindustan Pub. corp., New delhi, 1975).

Helgeson, H. C., Delany, J. M., Nesbitt, H. W. & Bird, D. K. 1978. Summary and critique of the thermodynamic properties of rock forming minerals. *Am. J. Sci.* **278-A**.

Hobbs, B. E., Means, W. D. & Williams, P. F. 1976. Outline structural geology. Wiley & Sons.

Hodges, K. V. 1991. Pressure-Temperature-Time paths. *Annu. Rev. Earth Planet. Sci.* **19**, 207-236.

Hodges, K. V. & Crowley, P. D. 1985. Error estimation and empirical geothermobarometry for pelitic systems. *Am. Mineral.* **70**, 702-709.

Hodges, K. V., Hubbard, S. M. & Silverberg, D. S. 1988. Metamorphic constraints on the thermal evolution of the central Himalayan Orogen. *Phil. Trans. R. Soc. London* **A326**, 257-280.

Hodges, K. V., Le Fort, P. & Pecher, A. 1988. Possible thermal buffering by crustal anatexis in collision orogens: Thermobarometric evidence from the Nepalese Himalaya. *Geology* **16**, 707-710.

Hodges, K. V. & McKenna, L. W. 1987. Realistic propagation of uncertainities in geologic thermobarometry. *Am. Mineral.* **72**, 671-680.

Hodges, K. V. & Royden, L. R. 1984. Geologic thermobarometry retrograded metamorphic rocks: an indication of the uplift trajectory of a portion of the Northern Scandinavian Caledonides. *J. Geophys. Res.* **89**, 7077-7090.

Hodges, K. V. & Silverberg, D. S. 1988. Thermal evolution of the Greater Himalaya, Garhwal, India. *Tectonics* **7**, 583-600.

Hodges, K. V. & Spear, F. S. 1982. Geothermometry, geobarometry and the Al_2SiO_5 tripple point at Mt. Moosilauke, New Hampshire. *Am. Mineral.* **67**, 1118-1134.

Hoisch, T. D. 1990. Empirical calibration of six geobarometers for the mineral assemblage quartz + muscovite + biotite + plagioclase garnet. *Contrib. Mineral. Petrol.* **104**, 225-234.

Hoisch, T. D. 1991. Equilibria within the mineral assemblage quartz + muscovite + biotite + garnet + plagioclase, and implications for the mixing properties of octahedrally-coordinated cations ain muscovite and biotite. *Contrib. Mineral. Petrol.* **108**, 43-54.

Hollister, L. S. 1966. Garnet zoning: An interpretation based on the Rayleigh fractionation model. *Science* **154**, 1647-1651.

Honegger, K., Le Fort, P., Mascle, G. & Zimmermann, J. -L. 1989. The blueschist along the Indus Suture Zone in Ladakh, NW Himalaya. *J. Met. Geol.* **7**, 57-72.

Hubbard, M. S. 1989. Thermobarometric constraints on the thermal history of the Main Central Thrust Zone and Tibetan Slab, eastern Nepal Himalaya. *J. Met. Geol* **7**, 19-30.

Hubbard, M. S. & Harrison, T. M. 1989. 40Ar/39Ar age constraints on deformation and metamorphism in the Main Central Thrust Zone and Tibetan Slab, Eastern Nepal Himalaya. *Tectonics* **8** 865-880.

Indares, A. & Martignole, J. 1985. Biotite-garnet geothermometry in the granulite facies: the influence of Ti and Al in biotite. *Am. Mineral.* **70**, 270-278.

Inger, S. & Harris, N. B. W. 1992. Tectonothermal evolution of the High Himalayan Crystalline Sequence, Langtang Valley, northern Nepal. *J. Met. Geol.* **10**, 439-452.

Jain, A. K. & Manickavasgam, R. M. 1993. Inverted metamorphism in the intracontinental ductile shear zone during Himalayan collision tectonics. *Geology* **21**, 407-410.

Jaupart, C. & Provost, A. 1985. Heat foccussing, granite genesis and inverted metamorphic gradients in continental collision zones. *Earth and Planet. Sci. Lett.* **73**, 385-397.

Jiang, J. & Lasaga, A. C 1990. The effect of post-growth thermal event on growth-zoned garnet: implications for metamorphic P-T history calculations. *Contrib. Mineral. Petrol.* **105**, 454-459.

Jones, K. A. 1994. Progressive metamorphism in a crustal-scale shear zone: an example from the Leon region, north-west Brittany, France. *J. Met. Geol.* **12**, 69-88.

Kanwar, R. C. & Singh, I. 1979. Structural history of the Jutogh metasediments, SW of Chur mountain, Sirmur district, Himachal Pradesh. In : *Structural Geology of the Himalaya* (edited by Saklani, P. S.), Today and Tomorrow's Publishers, New Delhi, 183-200.

Karabinos, P. 1983. Polymetamorphic garnet zoning from southeastern Vermont. *Am. J. Sci.* **284**, 1008-1025.

Kishore, N. & Kanwar, R. C. 1984a. Petrography, Petrochemistry, Origin and emplacement of Chor granites. *Bull. Indi. Geol. Asson.* **17**, 1-27.

Kishore, N. & Kanwar, R. C. 1984b. Structural history of the granitic rocks of the Nohra-Haripurdhar area of Chor pluton. *Bull. Ind. Geol. Asson.* **17**, 195-205.

Klootwijk, C.T., Gee, J.S., Peirce, J.W., Smith, G.M. & Mcfadden, P.L. 1992. An early India-Asia Contact: Paleomagnetic Constraints from Ninetyeast Ridge, ODP Leg 121. *Geology* **20**, 395-398.

Koziol, A. M. & Newton, R. C. 1988. Redetermination of the anorthite breakdown reaction and improvement of the plagioclase-garnet-Al_2SiO_5-quartz barometer. *Am. Mineral.* **73**, 216-223.

Kretz, R. 1959. Chemical study of garnet, biotite, and hornblende from geisses of southwestern Quebec, with emphasis on distribution of element in coexisting minerals. *J. Geol.* **67**, 371-403.

Kundig, R. 1989. Domal structures and hogh-grade metamorphism in the Higher himalayan Crystalline, Zanskar region, north-western Himalaya, India. *J. Met. Geol.* **7**, 43-55.

Lal, R. K., Ackermand, D. & Singh, J. B. 1987. Geothermobarometry in Barrovin type of metamorphism of Pelitic schist, Sinai, District Singhbhum, Bihar. *Recent Res. In Geol.* **33**, 125-142.

Lal, R.K., Mukerji, S. & Ackermand, D. 1981. Deformation and Barrovian Metamorphism at Tadakh, Darjeeling (Eastern Himalaya). In: *Metamorphic Tectonics of the Himalaya* (ed.Saklani, P.S.) Today and Tommorow Publisher, New Delhi, 238-278.

Le Fort, P. 1986. Metamorphism and magmatism during the Himalayan collision. In: Collision Tectonics (Edited by Coward, M. P. & Ries, A. C.) *Geol. Soc. Lond. Spl. Publ.* **19**, 159-172.

Le Fort, P. 1975. Himalayas : the collidal range. Present knowledge of the continental arc. *Am. J. Sci.* **275A**, 1-44.

Le Fort, P. 1986. Metamorphism and Magmatism during Himalayan collision. In: Collision Tectonics (eds. Coward, M.P. & Ries, A.C.). *Geol. Soc. London Spl. Publ.* **19**, 159-172.

Loomis, T.P. 1972. Contact metamorphism of pelitic rocks by the Ronda ultramafic intrusion, southern Spain. *Geol. Soc. Am. Bull.* **83**, 2449-2474.

Loomis, T. P. 1983. Compositional zoning of crystals: a record of growth and reaction history. In: *Kinetics and equilibrium in mineral reactions* (edited by: Saxena, S. K.). Advances in Physical Geochemistry, **3**, Springer-Verlag, New York.

Loomis, T. P., Ganguly, J. & Elphick, S. C. 1985. Experimental determination of cation diffusivities in alumina silicate garnets: II. Multicomponent simulation and tracer diffusion coefficients. *Contrib. Mineral. Petrol.* **90**, 45-51.

Matcalfe, R.P. 1993. Pressure, temperature and time constraints across the Main Central Thrust Zone and High Himalayan Slab in the Garhwal Himalaya. In: Himalayan Tectonics (eds. Treolar, P.J. & Searle, M.P.) *Geol. Soc. Spl. Publ.* **74**, 485-509.

Misch, P. 1971. Paracrystalline microboudinage in a metamorphic reaction sequence. *Geol. Soc. Am. Bull.* **81**, 2484-2485.

Misch, P. 1972. Porphyroblasts and "crystallisation force": Some textural criteria: A reply. *Geol. Soc. Am. Bull.* **83**, 921-922.

Miyashiro, A. 1953a. Progressive metamorphism of the calcium-rich rocks of the Gosaisyo-Takanuki district, Abu-Kuma Plateau, Japan. *J. Geol. Geogr.* **23**, 83-107.

Miyashiro, A. 1953b. Calcium-poor garnet in relation to metamorphism. *Geochim. Cosmochim. Acta.* **4**, 179-208.

Mohan, A., Windley, B.F. & Searle, M.P. 1989. Geothermobarometry and development of inverted metamorphism in the Darjeeling and Sikkim region of the eastern Himalaya. *J. Met. Geol.* **7**, 95-110.

Molnar, P. & England, P. 1990. Temperatures, heat flux and frictional stress near major thrust faults. *J. Geophys. Res.* **95**, 4833-4856.

Molnar, P. & Tappnnier, P. 1975. Cenozoic tectonics of Asia: Effects of a continental collision. *Science* **189**, 419-426.

Mukhopadhyay, D. K. 1989. Significance of a small scale structures in the Kolar Schist Belt, South India. *J. Geol. Soc. India* **33**, 291-308.

Mueller, G. & Schneider, A. 1971. Chemistry and genesis of garnets in metamorphic rocks. *Contrib. Mineral. Petrol.* **31**, 178-182.

Mueller, R. F. 1972. Stability of biotite: a discussion. *Am. Mineral.* **57**, 300-316.

Mueller, R. F. & Saxena. S. K. 1977. Chemical Petrology. Springer-Verlag.

Naha, K. & Ray, S. 1970. Metamorphic history of the Jutogh Series in the Simla Klippe, Lower Himalayas. *Contrib. Mineral. Petrol.* **28**, 147-164.

Naha, K. & Ray, S. 1971. Evidence of overthrusting in the metamorphic terrain of the Simla Himalyas. *Am. J. Sci.* **270**, 30-42.

Naha, K. & Ray, S. 1972. Structural evolution of Simla Klippe in the Lower Himalayas. *Geol. Rund.* **61**, 1050-1086.

Newton, R. C., Charlu, T. V. & Kleppa, O. J. 1980. Thermochemistry of the high structural state plagioclases. *Geochim. Cosmochim. Acta* **44**, 933-941.

Newton, R. C. & Haselton, H. T. 1981. Thermodynamics of the garnet-plagioclase-Al_2SiO_5-quartz geobarometer. In: *Advances in physical geochemistry I* (edited by Newton, R. C., Navrotsky, A. & Wood, B. J.) Springer Verlag.

Oldham, R.D. 1883. Note on the Geology of Jaunsar and the lower Himalayas. *Rec. Geol. Surv. India* **16**, 193-198.

Olimpio, J. C. & Anderson, D. E. 1978. The relationship between chemical and textural (optical) zoning in metamorphic garnets, South Morar, Scotland. *Am. Mineral.* **63**, 677-689.

Oxburgh, E.R., & Turcotle, D. 1974. Thermal gradients and regional metamorphism in overthrusts terrains with special reference to the eastern Alps. Schweiz. *Mineral. Petrogr. Mitt.* **54**, 641-662.

Patriarch, P.E., & Achache, J. 1984. India-Eurasia collision chronology has implications for crustal shortening and driving mechanism of plates. *Nature* **311**, 615-621.

Pecher, A. 1975. The Main Central Thrust in the Nepal Himalaya and the related Metamorphism in the Modi-Khola cross section (Annapurna range). *Him. Geol.* **5**, 115-131.

Pecher, A. 1977. Geology of the Nepal Himalaya: deformation and petrography in the MCT zone. In: Himalaya, Sciences de la Terre, CNRS, Paris, 301-318.

Pecher, A. 1989. The metamorphism of the Central Himalaya. *J. Met. Geol.* **7**, 31-41.

Perchuk, L. L. & Lavrenteva IV 1983. Experimental investigation of exchange equilibria in the system cordierite - garnet - biotite. In: *Kinetics and equilibrium in mineral reactions* (edited by Saxena, S. K.) Springer Berlin, Heidelberg, New York.

Pigage, L. C. & Greenwood, H. J. 1982. Internally consistent estimates of pressure and temperature: the straulolite problem. *Am. J. Sci.* **282**, 943-969.

Pilgrim, G. E. & West, W. D. 1928. The structure and correlation of Simla rocks. *Mem. Geol. Surv. India* **53**, 1-150.

Platt, J. P. 1983. Progressive refolding in ductile shear zones. *J. Struct. Geol.* **5**, 619-622

Platt, J. P. & Vissers, R. L. M. 1980. Extensional structures in anisotropic rocks. *J. Struct. Geol.* 2, 397-410.

Pognante, U. & Lombardo, B. 1989. Metmorphic evolution of the High Himalayan Crystalline in South-East Zanskar, India. *J. Met. Geol.*7, 9-17.

Powell, C. McA. & Conaghan, P. J. 1973. Plate tectonics and the Himalayas. *Earth. Planet. Sci. Lett.*20, 1-12.

Pownceby, M. I., Wall, V. J. & O'Neill H (1987) Fe-Mn Partitioning between garnet and ilmenite experimental calibration and applications. *Contrib. Mineral. Petrol* 97, 116-126.

Purohit, K. K., Islam, R. & Thakur, V. C. Metamorphism of psammo-Pelitic rocks - Bhagirathi valley, Garhwal Himalaya. *J. Him. Geol.*1, 167-174.

Ramsay, J. G. 1967. Folding and fracturing of rocks. McGraw Hill.

Ramsay, J. G. 1980. Shear zone geometry: A review. *J. Struct. Geol.*2, 83-99.

Ramsay, J. G. & Allison, I 1979. Structural analyʒis of shear zones in an alpinised Hercinian granite. *Schweiz. Mineral. Petrogr. Mitt.*59, 251-279.

Ramsay, J. G. & Graham, R. H. 1970. Strain variation in shear belts. *Cann. J. Earth. Sci.*7, 786-813.

Ramsay, J. G. & Huber, M. 1. 1983. The techniques of modern structural geology. 1 Strain Analysis. Academic Press.

Ray, S. 1947. Zonal metamorphism in the Eastern Himalaya and some aspects of local geology. *Quart. J. Geol. Met. Soc. India* 19, 117-138.

Robinson, P. 1991. The eye of the petrographer, the mind of the petrologist. *Am. Mineral.* 76, 1781-1810.

Roy, M. K. & Mukherjee, A. B. 1976. The relationship between the metamorphic and movement episodes in the Jutogh Series, rest of the Chor granite near Rajgarh, Himachal Pradesh. *Him. Geol.*6, 240-246.

Royden, L. & Hodges, K. V. 1984. A technique for analyzing the thermal and uplift histories of eroding orogeny belts: A Scandinavian example. *J. Geophys. Res.* 89, 7091-7106.

Saxena, S. K. 1982. Computation of multicomponent phase equilibria. In: *Advances in Physical Geochemistry* (edited by Saxena, S. K.). Springer Verlag. 226-249.

Saxena, S. K. & Ribbe, P. H. 1972. Activity-composition relations in feldspars. *Contrib. Mineral. Petrol.* 37, 131-138.

Scholz, C.H. 1980. Shear heating and the state of stress on faults. *J. Geophys. Res.* 85, 6174-6184.

Schulien, S. 1975. Determination of the equilibrium constant and the enthalpy of the reaction for Mg^{2+}-Fe^{2+} exchange between biotite and salt solution. *Fortsch. der Mineral.* 52, 133-139.

Searle, M. P. 1986. Structural evolution and sequence of thrusting in the High Himalayan, Tibetan-Tethys and Indus Suture Zones of Zanskar and Ladakh, western Himalaya. *J. Struct. Geol.*8, 923-936.

Searle, M. P., Cooper, D. J. W. & Rex, A. J. 1988. Collision tectonics of the Ladakh Zanskar Himalaya. *Phil. Trans. R. Soc. Lond.*A326, 117-150.

Searle, M.P. & Rex, A.J. 1989. Thermal model for the Zanskar Himalaya. *J. Metamorphic Geol.* 7, 127-134.

Searle, M. P., Metcalfe, R. P., Rex, A. J. & Norry, M. J. 1993. Field relations, petrogenesis and emplacement of the Bhagirathi leucogranite, Garhwal Himalaya. In: Himalayan Tectonics (edited by Treloar, P. J. & Searle, M. P.). *Geol. Soc. Spl. Publ.*74, 429-444.

Shi, Y. & Wang, C. Y. 1987. Two dimensional modelling of the P-T-t paths of regional metamorphism in simple overthrust terrains. *Geology* 15, 1048-1051.

Sibson, R. H. 1977. Fault rocks and fault mechanisms. *J. Geol. Soc. Lond.*133, 191-233.

SinhaRoy, S. & Bhargava, O. N. 1989. Metamorphism and magmatism in the Himalaya. *Geol. Surv. Ind. Spl. Publ.* 26, 61-83.

Sinha Roy, S. 1981a. Metamorphic facies and inverted metamorphic sequences of the eastern Himalayan crystalline rocks. In: Today and Tomorrow's Publ. New Delhi, 279-302.

Sinha Roy, S. 1982a. Himalayan Main Central Thrust and its Implications for Himalayan inverted metamorphism. *Tectonophysics* **84**, 197-224.

Spear, F. S. 1988. Metamorphic fractional crystallization and internal metasomatism by diffusional homogenization of zoned garnets. *Contrib. Mineral. Petrol.* **99**, 507-517.

Spear, F. S. 1991. On the interpretation of peak metamorphic temperatures in light of garnet diffusion during cooling. *J. Met. Geol.* **9**, 379-388.

Spear, F. S. & Selverstone, J. 1983. Quantitative P-T paths from zoned minerals: theory and tectonic applications. *Contrib. Mineral. Petrol.* **83**, 348-357.

Spry, A. H. 1969. Meatamorphic Textures. Pergamon Press.

Spigel, M. R. 1982. Probanility and Statistics. McGraws-Hill.

Srikantia, S. V. & Bhargava, O. N. 1985. Chail series of the Himachal Himalaya. *J. Geol. Soc. India.* 26, 350-355.

Srikantia, S. V., Jangi, B. L. & Reddy, K. P. 1975. The lithistratigraphic classification of the Jutogh Formation of the Chaur mountain. *Geol. Surv. Ind. Misc. Publ.*24, 1-10.

Staubli, A. 1989. Polyphase metamorphism and the development of the Main Central Thrust. *J. Met. Geol.* 7,73-93.

Stöcklin, J. 1980. Geology of Nepal and its regional frame. *J. Geol. Soc. London* 137, 1-34.

St-Onge, M. R. 1987. Zoned poikiloblastic garnets: P-T paths and syn-metamorphic uplift through 30 Km of structural depth, Wopmay Orogen, *Canad. J. Petrol.* 28, 1-21.

Thakur, V. C. 1980. Tectonics of the Central Crystallines of Western Himalaya. *Tectonophysics* 62, 141-154.

Thakur, V. C. 1981. An overview of the thrusts and nappes of Western Himalaya. In : Thrust and nappe tectonics (edited by Mc. Clay, K. R. & Price, N. J.), *Geol. Soc. London Spl. Publ.* 9, 381-392.

Thompson, J. B. Jr. 1957. The graphical analysis of mineral assemblages in pelitic schist. *Am. Mineral.* 42, 842-858.

Thompson, J. B. Jr. & Norton, S. A. 1968. Paleozoic regional metamorphism in New England and adjacent areas. In: Studies of Appalachian Geology: Northern and Maritime (edited by: Zen, E-A., white, w. S., Hadley, B. J. & Thompson, J. B. Jr). John Wiley and Sons, 319-327.

Tracy, R. J. 1982. Compositional zoning and inclusion in metamorphic minearls. Characterization of metamorphism through mineral equilibria (edited by Ferry, J. M.). *Reviews in Mineralogy.* **10**, 355-397.

Treloar, P. J., Broughton, R. D., Williams, M. P., Coward, M. P. & Windley, B. F. 1989. Deformation, metamorphism and imbrication of the Indian plate, South of the Main Central Thrust, North Pakistan. *J. Met. Geol.*7, 111-125.

Trzcienski W. E. (Jr.) 1977. Garnet zoning - product of a continuous reaction. *Canad. Mineral.* **15**, 250-256.

Valdiya, K. S. 1980a. The two intracrustal boundary thrust of the Himalaya. *Tectonophysics* **66**, 323-348.

Valdiya, K. S. 1980b. Geology of Kumaun Lesser Himalaya. Wadia Institute of Himalayan Geology, Dehradun , India.

Vernon, R. H. 1978. Porphyloblast-matrix microstructural relationships in deformed metamorphic rocks. *Geol. Rund.* **67**, 288-305.

Vernon, R. H. 1989. Porphyroblast-matrix microstructural relationships: Recent approaches and problems. In: Evolution of metamorphic belts (edited by Daly, J. S., Cliff, R. A. & Yardley, B. W. D.), *Geol. Soc. Spl. Publ.* **43**, 83-102.

Virdi, N. S. 1979. A status of the Chail Formation vis-a-vis Jutogh-Chail relationship in the Himachal Lesser Himalaya. *Him. Geol.*9, 111-125.

Virdi, N. S. 1981. Chail Metamorphics of the Himachal Lesser Himalaya. In: Metamorphic tectonics of the Himalaya.(Edited by. Saklani. P. S.), Today & Tomorrow's Publication, New Delhi, 89-100.

White, S. H., Burrows, S. E., Carreras, J., Shaw, N. D. & Humphreys, F. J. 1980. On mylonites in ductile shear zones. *J. Struct. Geol.*2, 175-187.

William, P. F. & Price, G. P. 1990. Origin of kink bands and shear-band cleavage in shear zones: an experimental study. *J. Struct. Geol.*12, 145-164.

Windley, B. F. 1983. Metamorphism and tectonics of the Himalaya. *J. Geol. Soc. London* **140**, 849-865.

Windley, B.F. 1988. Tectonic Framework of the Himalaya, Karakoram and Tibet and problems of thir evolution. *Phil. Trans. R. Soc. London* A326, 3-16.

Winkler, H. G. F. 1979. Petrogenesis of metamorphic rocks. Springer-Verlag.

Wones, D. K. 1972. Stability of biotite: a reply. *Am. Mineral.* **57**, 316-317.

Yardley, B. W. D. 1989. An introduction to metamorphic petrology. Longman (ELBS).

Zwart, H. J. 1962. On the determinatiom of polymetamorphic mineral associations, and its implications to the Bosot area (Coastal Pyrenees). *Geol. Rund.* **52**, 38-65.

APPENDIX

N.A. = Not Analysed
Error (in bracket) estimated as standard deviation

APPENDIX - IA
REPRESENTATIVE MICROPROBE ANALYSIS OF GARNET (RIM)

SAMPLE NO. -	S-16	S-38	S-46	S-59	S-62	S-77/2	S-93/2
NO OF POINTS AVERAGED -	4	5	5	5	5	5	5
WEIGHT %							
SiO_2	36.706(.259)	36.748(.296)	36.781(.183)	37.000(.173)	37.192(.196)	36.673(.095)	37.434(.193)
Al_2O_3	20.805(.189)	20.957(.132)	20.753(.120)	20.924(.099)	21.167(.048)	20.573(.089)	20.991(.136)
FeO	33.887(.324)	29.436(.571)	32.000(.665)	37.709(.302)	38.291(.336)	36.829(.130)	29.980(.427)
MgO	2.131(.123)	1.505(.069)	1.407(.027)	2.463(.121)	2.599(.072)	2.548(.092)	1.443(.135)
MnO	3.924(.164)	7.234(.268)	3.434(.107)	1.102(.082)	0.441(.042)	1.705(.138)	7.533(.401)
CaO	1.736(.016)	3.241(.155)	4.581(.182)	0.428(.037)	0.393(.062)	1.098(.095)	3.479(.087)
Cr_2O_3	N.A.	N.A.	N.A.	N.A.	N.A.	N.A.	N.A.
TiO_2	N.A.	0.047(.029)	N.A.	N.A.	N.A.	N.A.	N.A.
Total	99.189(.530)	99.168(.846)	98.956(.634)	99.626(.352)	100.083(.293)	99.426(.190)	100.860(.727)
CATION (12 O BASIS)							
Si	2.9979(.008)	2.9982(.015)	3.0040(.014)	3.0082(.010)	3.0054(.010)	2.9949(.004)	3.0085(.008)
Al	2.0032(.008)	2.0154(.010)	1.9978(.006)	2.0052(.010)	2.0161(.007)	1.9804(.006)	1.9885(.005)
Fe	2.3152(.023)	2.0083(.026)	2.1856(.038)	2.5641(.021)	2.5878(.022)	2.5154(.010)	2.0151(.028)
Mg	0.2594(.014)	0.1830(.008)	0.1712(.003)	0.2985(.014)	0.3130(.009)	0.3102(.012)	0.1729(.016)
Mn	0.2716(.013)	0.4999(.018)	0.2376(.007)	0.0759(.005)	0.0301(.003)	0.1179(.010)	0.5128(.026)
Ca	0.1520(.002)	0.2834(.015)	0.4009(.017)	0.0373(.003)	0.0340(.005)	0.0961(.008)	0.2996(.007)
Cr	N.A.	N.A.	N.A.	N.A.	N.A.	N.A.	N.A.
Ti	N.A.	0.0029(.002)	N.A.	N.A.	N.A.	N.A.	N.A.
Total	7.9993(.009)	7.9911(.013)	7.9971(.013)	7.9892(.011)	7.9864(.009)	8.0149(.004)	7.9974(.009)

APPENDIX IA (Continued)

SAMPLE NO.	- S-108	S-118	S-119/2	S-180	S-320	S-321	S-348
NO OF POINTS AVERAGED	- 5	3	5	3	3	5	5
WEIGHT %							
SiO_2	36.754(.160)	36.816(.189)	37.517(.218)	36.724(.129)	37.479(.247)	36.895(.203)	37.670(.211)
Al_2O_3	21.129(.076)	20.623(.090)	21.542(.260)	20.500(.286)	20.970(.112)	20.854(.109)	20.809(.146)
FeO	34.477(.286)	35.693(.091)	34.341(1.012)	33.817(.160)	30.421(.070)	34.255(.409)	28.898(.309)
MgO	2.520(.092)	1.576(.150)	2.152(.165)	2.280(.103)	1.154(.152)	2.515(.047)	1.449(.053)
MnO	0.551(.029)	1.218(.062)	1.399(.070)	2.783(.073)	1.006(.092)	0.201(.027)	6.121(.135)
CaO	4.035(.226)	3.202(.036)	3.236(.642)	2.390(.030)	8.962(.267)	4.480(.253)	4.855(.107)
Cr_2O_3	N.A.	N.A.	N.A.	N.A.	N.A.	N.A.	N.A.
TiO_2	N.A.	N.A.	N.A.	0.003(.003)	N.A.	N.A.	0.022(.017)
Total	99.466(.689)	99.128(.220)	100.187(.825)	98.497(.446)	99.992(.654)	99.200(.606)	99.824(.367)
CATION (12 O BASIS)							
Si	2.9751(.010)	3.0104(.008)	3.0074(.010)	3.0123(.008)	3.0054(.003)	2.9909(.016)	3.0363(.013)
Al	2.0160(.007)	1.9877(.007)	2.0353(.013)	1.9819(.017)	1.9820(.006)	1.9926(.005)	1.9770(.014)
Fe	2.3340(.014)	2.4409(.011)	2.3020(.060)	2.3199(.013)	2.0402(.016)	2.3229(.023)	1.9480(.021)
Mg	0.3041(.010)	0.1921(.019)	0.2571(.019)	0.2788(.012)	0.1379(.017)	0.3039(.005)	0.1741(.007)
Mn	0.0378(.002)	0.0843(.004)	0.0950(.004)	0.1934(.006)	0.0684(.007)	0.0138(.002)	0.4179(.009)
Ca	0.3499(.018)	0.2806(.003)	0.2782(.056)	0.2100(.002)	0.7699(.018)	0.3891(.021)	0.4193(.008)
Cr	N.A.	N.A.	N.A.	N.A.	N.A.	N.A.	N.A.
Ti	N.A.	N.A.	N.A.	0.0002(.000)	N.A.	N.A.	0.0013(.001)
Total	8.0169(.013)	7.9960(.010)	7.9750(.012)	7.9965(.002)	8.0038(.004)	8.0127(.018)	7.9739(.010)

APPENDIX IA (Continued)

SAMPLE NO.	S-350	S-354	S-367	S-377	S-381	S-394	S-400
NO OF POINTS AVERAGED	3	3	4	3	3	3	5

	WEIGHT %						
SiO_2	37.153(.168)	36.402(.139)	36.587(.121)	36.540(.099)	36.440(.161)	36.708(.033)	36.718(.319)
Al_2O_3	20.952(.136)	20.722(.099)	21.095(.046)	20.758(.067)	20.660(.108)	20.781(.106)	21.053(.129)
FeO	37.898(.256)	35.179(.230)	37.931(.214)	35.351(.413)	35.926(.171)	35.355(.161)	30.198(.343)
MgO	1.890(.098)	2.183(.070)	1.642(.039)	2.480(.075)	1.909(.045)	1.897(.094)	1.470(.111)
MnO	1.248(.127)	2.506(.263)	1.310(.081)	2.794(.070)	2.169(.169)	2.456(.184)	2.861(.241)
CaO	1.083(.021)	1.801(.676)	1.686(.069)	0.892(.019)	2.421(.029)	2.181(.065)	6.518(.293)
Cr_2O_3	N.A.	N.A.	N.A.	N.A.	N.A.	N.A.	N.A.
TiO_2	N.A.	N.A.	N.A.	N.A.	N.A.	N.A.	0.033(.019)
Total	100.224(.390)	98.793(.213)	100.251(.312)	98.815(.543)	99.525(.334)	99.378(.224)	98.851(.382)

	CATION (12 O BASIS)						
Si	3.0108(.019)	2.9884(.004)	2.9755(.007)	2.9958(.016)	2.9802(.009)	2.9971(.005)	2.9859(.013)
Al	2.0013(.009)	2.0053(.005)	2.0221(.007)	2.0060(.006)	1.9916(.013)	2.0000(.010)	2.0180(.010)
Fe	2.5685(.013)	2.4154(.028)	2.5798(.011)	2.4239(.021)	2.4572(.010)	2.4142(.009)	2.0538(.015)
Mg	0.2283(.012)	0.2672(.009)	0.1990(.004)	0.3031(.008)	0.2327(.006)	0.2309(.012)	0.1782(.013)
Mn	0.0856(.008)	0.1743(.019)	0.0903(.006)	0.1940(.004)	0.1502(.011)	0.1698(.013)	0.1971(.017)
Ca	0.0940(.002)	0.1583(.059)	0.1469(.006)	0.0783(.002)	0.2122(.003)	0.1908(.006)	0.5681(.028)
Cr	N.A.	N.A.	N.A.	N.A.	N.A.	N.A.	N.A.
Ti	N.A.	N.A.	N.A.	N.A.	N.A.	N.A.	0.0020(.001)
Total	7.9885(.015)	8.0089(.007)	8.0136(.008)	8.0011(.016)	8.0241(.004)	8.0028(.006)	8.0031(.013)

APPENDIX IA (Continued)

SAMPLE NO. -	S-453	S-607	S-616	S-669	S-675	S-676	S-695
NO OF POINTS AVERAGED -	3	4	3	3	5	4	5
WEIGHT %							
SiO_2	37.359(.080)	36.642(.055)	37.362(.187)	37.116(.251)	37.107(.163)	37.397(.495)	37.236(.138)
Al_2O_3	21.680(.080)	21.185(.196)	21.124(.114)	21.056(.070)	20.894(.134)	20.902(.253)	20.678(.083)
FeO	34.075(.290)	34.950(.115)	31.842(.153)	33.961(.633)	37.781(.258)	37.874(.447)	29.545(.443)
MgO	2.097(.120)	1.963(.081)	2.145(.061)	1.982(.105)	2.438(.092)	1.884(.102)	1.252(.077)
MnO	3.969(.270)	3.654(.067)	6.533(.232)	1.657(.293)	1.571(.060)	2.158(.085)	8.162(.552)
CaO	2.052(.020)	1.275(.018)	1.115(.097)	3.867(.145)	1.270(.071)	0.977(.052)	3.933(.354)
Cr_2O_3	N.A.	N.A.	N.A.	N.A.	N.A.	0.007(.008)	N.A.
TiO_2	N.A.	N.A.	N.A.	N.A.	N.A.	0.023(.021)	N.A.
Total	101.232(.200)	99.669(.550)	100.121(.351)	99.639(.254)	101.061(.159)	100.222(1.250)	100.806(.816
CATION (12 O BASIS)							
Si	2.9841(.010)	2.9840(.004)	3.0166(.010)	3.0020(.017)	2.9869(.008)	3.0258(.005)	3.0042(.013)
Al	2.0412(.010)	2.0334(.007)	2.0103(.015)	2.0074(.005)	1.9824(.011)	1.9935(.004)	1.9665(.008)
Fe	2.2763(.020)	2.3804(.010)	2.1501(.005)	2.2973(.045)	2.5435(.021)	2.4952(.011)	1.9937(.036)
Mg	0.2497(.010)	0.2382(.009)	0.2582(.008)	0.2389(.013)	0.2925(.011)	0.2270(.010)	0.1506(.010)
Mn	0.2685(.020)	0.2520(.005)	0.4467(.015)	0.1135(.020)	0.1071(.004)	0.1479(.006)	0.5576(.035)
Ca	0.1757(.002)	0.1113(.002)	0.0965(.008)	0.3351(.012)	0.1096(.006)	0.0848(.005)	0.3398(.029)
Cr	N.A.	N.A.	N.A.	N.A.	N.A.	0.0005(.001)	N.A.
Ti	N.A.	N.A.	N.A.	N.A.	N.A.	0.0014(.001)	N.A.
Total	7.9955(.007)	7.9993(.004)	7.9784(.012)	7.9942(.015)	8.0220(.007)	7.9761(.007)	8.0124(.015)

APPENDIX IA (Continued)

SAMPLE NO.	S-738	S-749	S-765	S-812	S-833	S-839	S-858
NO OF POINTS AVERAGED =	4	3	5	3	3	3	5

WEIGHT %							
SiO_2	37.779(.384)	36.784(.243)	37.094(.168)	37.041(.254)	36.794(.104)	37.593(.241)	37.599(.251)
Al_2O_3	21.582(.246)	20.647(.097)	20.586(.136)	21.121(.111)	21.029(.155)	21.420(.216)	21.183(.137)
FeO	32.524(.177)	33.632(.267)	32.406(.241)	23.264(.556)	32.560(.082)	31.908(.348)	36.351(.191)
MgO	2.938(.069)	1.464(.051)	1.760(.059)	1.080(.031)	2.514(.093)	1.462(.041)	2.821(.104)
MnO	2.212(.196)	1.735(.098)	2.039(.071)	5.955(.462)	5.057(.170)	1.871(.051)	1.129(.119)
CaO	3.032(.128)	5.512(.189)	4.766(.234)	10.079(.166)	0.461(.024)	6.105(.273)	1.567(.123)
Cr_2O_3	0.006(.010)	N.A.	N.A.	N.A.	N.A.	N.A.	0.006(.008)
TiO_2	0.036(.020)	N.A.	0.063(.052)	N.A.	N.A.	N.A.	0.020(.020)
Total	100.109(.775)	99.774(.120)	98.714(.265)	98.540(.391)	98.415(.161)	100.359(.360)	100.676(.340)

CATION (12 O BASIS)							
Si	3.0126(.004)	2.9873(.008)	3.0232(.010)	2.9966(.008)	3.0134(.005)	3.0065(.005)	3.0093(.010)
Al	2.0286(.009)	1.9765(.005)	1.9776(.012)	2.0140(.013)	2.0300(.011)	2.0191(.012)	1.9984(.009)
Fe	2.1694(.027)	2.2844(.027)	2.2088(.022)	1.5739(.031)	2.2302(.010)	2.1343(.033)	2.4333(.011)
Mg	0.3493(.006)	0.1773(.006)	0.2138(>007)	0.1302(.003)	0.3069(.011)	0.1743(.006)	0.3366(.012)
Mn	0.1493(.012)	0.1194(.007)	0.1407(.005)	0.4082(.033)	0.3508(.013)	0.1268(.004)	0.0765(.008)
Ca	0.2590(.010)	0.4796(.015)	0.4161(.019)	0.8737(.016)	0.0404(.002)	0.5231(.021)	0.1344(.011)
Cr	0.0004(.001)	N.A.	N.A.	N.A.	N.A.	N.A.	0.0004(.001)
Ti	0.0022(.001)	N.A.	0.0038(.003)	N.A.	N.A.	N.A.	0.0012(.001)
Total	7.9707(.005)	8.0245(.009)	7.9840(.007)	7.9966(.008)	7.9717(.009)	7.9841(.011)	7.9901(.008)

APPENDIX IA (Continued)

SAMPLE NO. - S-859	S-882	S-894
NO OF POINTS AVERAGED - 3	3	5

WEIGHT %

	S-859	S-882	S-894
SiO_2	36.741(.085)	36.685(.117)	37.972(.172)
Al_2O_3	20.901(.047)	20.778(.124)	21.105(.242)
FeO	26.276(.523)	37.283(.125)	36.307(.309)
MgO	1.148(.046)	2.274(.010)	2.764(.149)
MnO	8.168(.143)	1.453(.051)	0.671(.154)
CaO	6.279(.075)	0.648(.032)	1.561(.142)
Cr_2O_3	N.A.	0.009(.009)	N.A
TiO_2	N.A.	0.025(.024)	0.006(.007)
Total	99.513(.511)	99.155(.230)	100.386(.604)

CATION (12 O BASIS)

	S-859	S-882	S-894
Si	2.9837(.012)	3.0018(.010)	3.0379(.010)
Al	2.0007(.002)	2.0040(.011)	1.9901(.012)
Fe	1.7845(.031)	2.5515(.005)	2.4292(.012)
Mg	0.1390(.006)	0.2774(.012)	0.3297(.018)
Mn	0.5619(.010)	0.1007(.004)	0.0455(.011)
Ca	0.5464(.007)	0.0568(.003)	0.1338(.012)
Cr	N.A.	0.0015(.001)	N.A.
Ti	N.A.	0.0006(.001)	0.0003(.001)
Total	8.0162(.012)	7.9943(.007)	7.9665(.006)

SAMPLE NO. -	S-16/I1	S-16/I2	S-46	S-77/2	S-321/I1	S-321/I2	S-367
NO OF POINTS AVERAGED -.	4	4	4	5	5	5	4
WEIGHT %							
SiO_2	36.243(.137)	36.601(.147)	37.185(.445)	36.673(.095)	37.024(.145)	37.424(.309)	36.550(.046)
Al_2O_3	20.635(.096)	20.851(.056)	20.875(.312)	20.573(.089)	21.182(.116)	20.913(.144)	20.813(.053)
FeO	33.494(.343)	32.498(.078)	32.921(.070)	36.829(.130)	36.386(.293)	37.382(.385)	38.453(.256)
MgO	2.112(.054)	2.028(.077)	1.607(.101)	2.548(.092)	2.624(.148)	2.459(.149)	1.768(.059)
MnO	4.142(.195)	4.547(.202)	3.349(.100)	1.705(.138)	1.012(.058)	1.052(.123)	1.522(.067)
CaO	1.739(.045)	2.110(.075)	3.545(.178)	1.098(.095)	1.688(.095)	1.959(.095)	0.900(.059)
Cr_2O_3	N.A.	N.A.	N.A.	N.A.	N.A.	N.A.	N.A.
TiO_2	0.022(.011)	0.068(.062)	N.A.	N.A.	N.A.	N.A.	N.A.
Total	98.387(.316)	98.703(.359)	99.482(.752)	99.426(.190)	99.916(.392)	101.189(.801)	100.006(.253)
CATION (12 O BASIS)							
Si	2.9884(.010)	2.9984(.009)	3.0182(.007)	2.9949(.004)	2.9917(.007)	2.9991(.014)	2.9848(.002)
Al	2.0056(.008)	2.0134(.005)	1.9971(.013)	1.9804(.006)	2.0174(.005)	1.9754(.014)	2.0034(.008)
Fe	2.3097(.022)	2.2266(.007)	2.2350(.021)	2.5154(.010)	2.4589(.022)	2.5053(.013)	2.6262(.014)
Mg	0.2596(.007)	0.2477(.001)	0.1944(.012)	0.3102(.012)	0.3161(.017)	0.2937(.017)	0.2152(.007)
Mn	0.2893(.014)	0.3155(.013)	0.2302(.007)	0.1179(.010)	0.0692(.004)	0.0714(.008)	0.1053(.0050)
Ca	0.1536(.004)	0.1852(.007)	0.3084(.016)	0.0961(.008)	0.1462(.008)	0.1682(.008)	0.0788(.0050)
Cr	N.A.	N.A.	N.A.	N.A.	N.A.	N.A.	N.A.
Ti	0.0014(.001)	0.0042(.004)	N.A.	N.A.	N.A.	N.A.	N.A.
Total	8.0076(.012)	7.9910(.004)	7.9833(.012)	8.0149(.004)	7.9996(.007)	8.0131(.016)	8.0137(.005)

APPENDIX IB (Continued)

SAMPLE NO.	– S-695	S-858
NO OF POINTS AVERAGED	– 5	5

WEIGHT %		
SiO_2	37.002(.265)	37.935(.413)
Al_2O_3	20.434(.186)	21.144(.220)
FeO	30.718(.485)	36.031(.745)
MgO	1.318(.130)	2.578(.052)
MnO	8.016(.653)	1.251(.067)
CaO	3.158(.059)	1.549(.049)
Cr_2O_3	N.A.	0.009(.011)
TiO_2	N.A.	0.008(.011)
Total	100.646(.612)	100.505(1.034)

CATION (12 O BASIS)		
Si	3.0010(.012)	3.0354(.022)
Al	1.9534(.010)	1.9941(.005)
Fe	2.0837(.041)	2.4111(.043)
Mg	0.1593(.016)	0.3075(.008)
Mn	0.5505(.043)	0.0848(.004)
Ca	0.2745(.006)	0.1329(.005)
Cr	N.A.	0.0006(.001)
Ti	N.A.	0.0005(.001)
Total	8.0224(.009)	7.9669(.023)

SAMPLE NO. –	S-16	S-38	S-46	S-59	S-62	S-77/2	S-93/2
NO OF POINTS AVERAGED –	5	5	3	2	4	4	5

WEIGHT %

	S-16	S-38	S-46	S-59	S-62	S-77/2	S-93/2
SiO_2	35.753(.220)	35.130(.280)	35.857(.184)	36.196(.066)	35.743(.321)	35.704(.335)	35.870(.180)
Al_2O_3	18.086(.205)	17.007(.240)	17.790(.095)	18.428(.028)	18.048(.076)	19.539(.278)	18.557(.127)
FeO	20.495(.248)	21.374(.321)	22.271(.196)	20.830(.159)	19.658(.613)	19.849(.028)	20.210(.358)
MgO	9.107(.098)	8.165(.101)	8.584(.079)	9.147(.043)	9.987(.251)	9.730(.133)	9.643(.088)
MnO	0.133(.071)	0.238(.053)	0.113(.030)	0.032(.032)	0.026(.016)	0.044(.022)	0.156(.058)
CaO	0.051(.035)	0.309(.105)	1.130(.113)	0.518(.182)	0.143(.069)	0.214(.090)	0.831(.139)
K_2O	8.406(.180)	8.587(.208)	7.965(.156)	9.221(.074)	8.314(.218)	8.496(.161)	7.922(.117)
Na_2O	0.213(.015)	0.039(.016)	0.112(.013)	0.292(.036)	0.444(.047)	0.245(.021)	0.081(.055)
TiO_2	1.258(.085)	2.632(.154)	1.880(.164)	1.681(.142)	1.036(.129)	2.247(.153)	1.515(.027)
Cr_2O_3	N.A.	0.016(.010)	0.014(.014)	0.039(.019)	0.011(.011)	0.012(.021)	N.A.
ZnO	N.A.	0.059(.048)	0.163(.032)	N.A.	0.024(.023)	0.028(.028)	N.A.
BaO	N.A.	N.A.	N.A.	N.A.	N.A.	N.A.	N.A.
Total	93.502(.409)	93.556(.535)	95.879(.400)	96.384(.285)	93.434(.367)	96.108(.521)	94.785(.414)

CATION (22 O BASIS)

	S-16	S-38	S-46	S-59	S-62	S-77/2	S-93/2
Si	5.5459(.030)	5.5018(.029)	5.4790(.009)	5.4805(.005)	5.5325(.025)	5.4348(.031)	5.4704(.034)
Al	3.3067(.024)	3.1393(.033)	3.2050(.016)	3.2885(.016)	3.2190(.015)	3.4782(.052)	3.3357(.014)
Fe	2.6587(.024)	2.7995(.041)	2.8457(.013)	2.6395(.026)	2.4950(.034)	2.4830(.019)	2.5775(.040)
Mg	2.1061(.025)	1.9061(.021)	1.9523(.022)	2.0655(.015)	2.3415(.033)	2.2076(.019)	2.1921(.022)
Mn	0.0175(.009)	0.0316(.007)	0.0120(.004)	0.0045(.005)	0.0023(.004)	0.0054(.004)	0.0202(.007)
Ca	0.0086(.006)	0.0520(.018)	0.1870(.017)	0.0820(.027)	0.0233(.010)	0.0362(.019)	0.1357(.022)
K	1.6636(.040)	1.7158(.046)	1.5483(.028)	1.7835(.012)	1.6418(.049)	1.6820(.032)	1.5414(.024)
Na	0.0641(.100)	0.0117(.005)	0.0180(.000)	0.0410(.004)	0.1350(.008)	0.0580(.007)	0.0239(.0160)
Ti	0.1468(.010)	0.3100(.017)	0.2157(.019)	0.1910(.018)	0.1210(.014)	0.1548(.010)	0.1738(.003)
Cr	N.A.	0.0020(.001)	–	–	–	–	N.A.
Zn	N.A.	0.0057(.004)	0.0150(.004)	N.A.	0.0023(.004)	0.0036(.004)	N.A.
Ba	N.A.	N.A.	N.A.	N.A.	N.A.	N.A.	N.A.
Total	15.5180(.037)	15.4755(.037)	15.4780(.003)	15.5760(.002)	15.5857(.061)	15.5436(.016)	15.4707(.039)

SAMPLE NO.	S-108	S-118	S-119/2	S-180	S-320	S-321	S-348
NO OF POINTS AVERAGED	3	3	3	5	3	5	5
			WEIGHT %				
SiO_2	37.639(.482)	34.742(.043)	35.547(1.097)	36.024(.523)	34.710(.104)	35.147(.582)	36.205(.346)
Al_2O_3	19.658(.281)	18.244(.128)	19.010(.318)	18.450(.130)	17.489(.140)	18.457(.354)	17.522(.086)
FeO	15.445(.148)	23.094(.157)	20.045(.581)	20.742(.658)	21.654(.338)	18.648(.420)	22.633(.267)
MgO	10.712(.173)	8.123(.144)	9.743(.572)	10.354(.346)	8.747(.186)	11.587(.170)	9.017(.190)
MnO	0.012(.011)	0.025(.018)	0.010(.015)	0.080(.051)	0.006(.004)	0.036(.031)	0.189(.061)
CaO	0.686(.121)	0.177(.026)	0.508(.133)	0.029(.021)	0.025(.021)	0.110(.026)	0.178(.082)
K_2O	6.511(.279)	9.304(.1570	6.037(.599)	8.633(.306)	9.682(.171)	7.342(.286)	8.227(.239)
Na_2O	0.152(.011)	0.199(.024)	0.148(.045)	0.110(.037)	0.133(.027)	0.074(.018)	0.146(.076)
TiO_2	1.000(.061)	1.093(.036)	1.795(.232)	1.473(.097)	1.714(.023)	1.800(.135)	1.619(.210)
Cr_2O_3	0.025(.008)	N.A.	0.023(.004)	N.A.	N.A.	0.016(.000)	0.031(.022)
ZnO	0.051(.042)	N.A.	0.050(.061)	N.A.	N.A.	-	0.087(.031)
BaO	N.A.	N.A.	N.A.	N.A.	N.A.	0.029(.033)	0.114(.048)
Total	91.891(.851)	95.001(.364)	92.916(.829)	95.895(.632)	94.160(.331)	93.246(.407)	95.968(.641)
			CATION (22 O BASIS)				
Si	5.6897(.013)	5.4151(.011)	5.4562(.117)	5.4513(.058)	5.4387(.024)	5.3891(.068)	5.5266(.022)
Al	3.5025(.012)	3.3517(.015)	3.4406(.080)	3.2910(.019)	3.2300(.023)	3.3362(.072)	3.1526(.025)
Fe	1.9531(.038)	3.0103(.013)	2.5740(.082)	2.6251(.083)	2.8376(.043)	2.3915(.055)	2.8895(.032)
Mg	2.4137(.015)	1.8875(.037)	2.2308(.147)	2.3360(.085)	2.0432(.043)	2.6489(.051)	2.0517(.037)
Mn	0.0015(.002)	0.0033(.002)	0.0013(.020)	0.0103(.007)	0.0009(.001)	0.0046(.004)	0.0245(.008)
Ca	0.1114(.020)	0.0296(.004)	0.0833(.021)	0.0047(.004)	0.0042(.004)	0.0180(.004)	0.0292(.014)
K	1.2553(.040)	1.8501(.027)	1.1825(.117)	1.6667(.056)	1.9356(.031)	1.4361(.052)	1.6021(.038)
Na	0.0444(.004)	0.0602(.007)	0.0440(.013)	0.0323(.011)	0.0403(.008)	0.0221(.005)	0.0433(.023)
Ti	0.1135(.008)	0.1282(.004)	0.2071(.026)	0.1676(.011)	0.2020(.003)	0.2076(.014)	0.1859(.024)
Cr	0.0030(.001)	N.A.	0.0028(.001)	N.A.	N.A.	0.0019(.000)	0.0038(.003)
Zn	0.0058(.005)	N.A.	0.0058(.007)	N.A.	N.A.	0.0064(.004)	0.0082(.003)
Ba	N.A.	N.A.	N.A.	N.A.	N.A.	0.0017(.002)	0.0068(.003)
Total	15.0939(.008)	15.7360(.017)	15.2283(.070)	15.5850(.034)	15.7325(.037)	15.4641(.025)	15.5242(.009)

SAMPLE NO. -	S-350	S-354	S-367	S-377	S-381	S-394	S-400
NO OF POINTS AVERAGED -	3	3	5	3	3	4	4

WEIGHT %

SiO_2	35.378(.199)	34.774(.112)	35.110(.213)	36.220(.180)	37.085(.152)	36.353(.142)	36.672(.768)
Al_2O_3	18.242(.169)	17.455(.050)	18.917(.103)	17.947(.200)	18.906(.118)	18.963(.111)	17.896(.161)
FeO	22.005(.261)	19.107(.223)	25.358(.238)	19.731(.220)	18.772(.215)	21.007(.682)	18.908(.339)
MgO	9.539(.054)	9.781(.004)	6.912(.088)	12.228(.243)	9.000(.032)	9.451(.162)	9.093(.210)
MnO	0.006(.009)	0.014(.020)	0.028(.027)	-	0.030(.034)	0.080(.032)	0.094(.073)
CaO	0.035(.042)	0.106(.032)	0.022(.023)	0.027(.027)	0.410(.043)	0.016(.002)	0.703(.130)
K_2O	9.592(.062)	9.771(.047)	8.939(.064)	9.187(.193)	7.590(.338)	8.646(.120)	7.769(.127)
Na_2O	0.279(.030)	0.313(.019)	0.220(.057)	0.200(.013)	0.157(.034)	0.261(.026)	0.102(.021)
TiO_2	1.200(.014)	1.203(.034)	1.456(.064)	0.694(.058)	1.822(.011)	1.277(.051)	2.125(.123)
Cr_2O_3	N.A.	N.A.	N.A.	N.A.	N.A.	N.A.	0.021(.019)
ZnO	N.A.	N.A.	N.A.	N.A.	N.A.	N.A.	0.056(.020)
BaO	N.A.	N.A.	N.A.	N.A.	N.A.	N.A.	N.A.
Total	96.276(.532)	92.524(.185)	96.962(.336)	96.234(.632)	93.772(.308)	96.054(.499)	93.439(.950)

CATION (22 O BASIS)

Si	5.4099(.016)	5.4864(.019)	5.3891(.028)	5.4569(.018)	5.6302(.019)	5.4906(.028)	5.6204(.043)
Al	3.2880(.015)	3.2461(.009)	3.4225(.018)	3.1870(.011)	3.3831(.014)	3.3759(.024)	3.2335(.019)
Fe	2.8142(.028)	2.5211(.028)	3.2552(.027)	2.4860(.020)	2.3834(.024)	2.6533(.081)	2.4246(.067)
Mg	2.1745(.017)	2.3003(.002)	1.5814(.020)	2.7459(.034)	2.0367(.003)	2.1278(.034)	2.0774(.021)
Mn	0.0008(.001)	0.0019(.003)	0.0036(.003)	-	0.0039(.004)	0.0102(.004)	0.0123(.008)
Ca	0.0057(.007)	0.0180(.006)	0.0037(.004)	0.0043(.004)	0.0667(.007)	0.0026(.003)	0.1155(.021)
K	1.8714(.002)	1.9668(.009)	1.7505(.013)	1.7662(.050)	1.4702(.068)	1.6660(.026)	1.5195(.027)
Na	0.0828(.009)	0.0957(.006)	0.0655(.017)	0.0585(.004)	0.0461(.010)	0.0765(.008)	0.0302(.001)
Ti	0.1379(.001)	0.1428(.005)	0.1681(.008)	0.0786(.006)	0.2080(.002)	0.1450(.006)	0.2450(.015)
Cr	N.A.	N.A.	N.A.	N.A.	N.A.	N.A.	0.0025(.002)
Zn	N.A.	N.A.	N.A.	N.A.	N.A.	N.A.	0.0053(.002)
Ba	N.A.	N.A.	N.A.	N.A.	N.A.	N.A.	N.A.
Total	15.7852(.025)	15.7791(.013)	15.6396(.028)	15.7834(.028)	15.2283(.059)	15.5479(.020)	15.2862(.040)

SAMPLE NO. –	S-607	S-616	S-669	S-675	S-676	S-695	S-738
NO OF POINTS AVERAGED –	4	3	3	5'	5	5	5
WEIGHT %							
SiO_2	34.026(.248)	35.799(.548)	35.393(.091)	35.097(.283)	35.534(.669)	35.689(.245)	36.048(.540)
Al_2O_3	20.176(.350)	18.765(.167)	18.043(.161)	17.958(.198)	17.530(.109)	17.159(.065)	17.828(.438)
FeO	22.484(.231)	17.434(.411)	20.753(.165)	21.176(.459)	23.340(.459)	24.194(.183)	18.081(.378)
MgO	8.237(.027)	11.799(.190)	9.636(.095)	8.213(.154)	7.701(.181)	6.993(.156)	11.158(.044)
MnO	0.086(.023)	0.068(.056)	0.020(.011)	0.037(.048)	0.007(.013)	0.145(.033)	0.109(.044)
CaO	1.211(.218)	0.371(.059)	0.024(.017)	0.086(.057)	0.405(.062)	0.004(.005)	0.268(.133)
K_2O	6.645(.382)	7.953(.293)	9.800(.052)	8.937(.103)	7.391(.101)	9.303(.092)	7.927(.2940)
Na_2O	0.204(.094)	0.150(.032)	0.153(.021)	0.157(.049)	0.110(.053)	0.086(.030)	0.080(.029)
TiO_2	0.325(.026)	1.253(.049)	1.898(.019)	2.800(.040)	1.556(.045)	3.351(.064)	1.964(.204)
Cr_2O_3	N.A.	N.A.	N.A.	N.A.	0.034(.023)	N.A.	0.012(.011)
ZnO	N.A.	N.A.	N.A.	N.A.	0.049(.042)	N.A.	0.029(.040)
BaO	N.A.	N.A.	N.A.	N.A.	0.086(.038)	N.A.	0.070(.089)
Total	93.394(.312)	93.592(.812)	95.720(.304)	94.461(.607)	93.743(.530)	96.924(.562)	93.574(.521)
CATION (22 O BASIS)							
Si	5.3052(.037)	5.4503(.026)	5.4184(.012)	5.4343(.036)	5.5518(.053)	5.4693(.023)	5.5103(.040)
Al	3.7077(.045)	3.3675(.006)	3.2558(.022)	3.2773(.025)	3.2288(.020)	3.0995(.023)	3.2121(.061)
Fe	2.9320(.030)	2.2205(.076)	2.6569(.019)	2.7422(.056)	3.0507(.085)	3.1008(.016)	2.3122(.067)
Mg	1.9146(.009)	2.6775(.016)	2.1992(.024)	1.8956(.030)	1.7937(.032)	1.5975(.032)	2.5430(.097)
Mn	0.0114(.003)	0.0087(.007)	0.0027(.002)	0.0049(.006)	0.0009(.002)	0.0188(.004)	0.0141(.006)
Ca	0.2020(.036)	0.0606(.010)	0.0039(.003)	0.0143(.010)	0.0679(.011)	0.0006(.001)	0.0440(.022)
K	1.3223(.083)	1.5443(.041)	1.9141(.011)	1.7654(.017)	1.4734(.009)	1.8189(.016)	1.5461(.058)
Na	0.0617(.029)	0.0444(.010)	0.0454(.006)	0.0472(.015)	0.0333(.016)	0.0255(.009)	0.0236(.009)
Ti	0.0381(.003)	0.1435(.005)	0.2185(.003)	0.3260(.005)	0.1828(.006)	0.3862(.006)	0.2257(.023)
Cr	N.A.	N.A.	N.A.	N.A.	0.0042(.003)	N.A.	0.0015(.001)
Zn	N.A.	N.A.	N.A.	N.A.	0.0048(.004)	N.A.	0.0027(.004)
Ba	N.A.	N.A.	N.A.	N.A.	0.0053(.002)	N.A.	0.0042(.005)
Total	15.4950(.052)	15.5173(.015)	15.7149(.006)	15.5072(.031)	15.3976(.043)	15.5171(.022)	15.4395(.599)

SAMPLE NO. —	S-749	S-765	S-812	S-833	S-839	S-858	S-859
NO OF POINTS AVERAGED —	4	5	3	3	3	5	3

WEIGHT %

	S-749	S-765	S-812	S-833	S-839	S-858	S-859
SiO_2	36.330(.110)	35.644(.238)	35.825(.306)	35.668(.618)	36.247(.090)	37.206(.431)	34.898(.035)
Al_2O_3	18.654(.110)	18.039(.224)	16.296(.218)	18.070(.177)	18.911(.035)	19.010(.230)	17.323(.066)
FeO	20.771(.153)	21.477(.306)	20.317(.281)	22.827(.368)	19.337(.3860	18.812(.285)	22.225(.215)
MgO	9.588(.177)	8.657(.238)	9.636(.087)	8.960(.192)	9.929(.096)	11.370(.166)	8.358(.098)
MnO	0.118(.084)	0.049(.029)	0.207(.055)	0.102(.035)	0.021(.029)	0.004(.008)	0.138(.006)
CaO	0.050(.063)	0.102(.044)	0.052(.074)	0.038(.053)	0.159(.101)	0.145(.070)	0.081(.051)
K_2O	8.628(.081)	8.561(.110)	9.217(.239)	8.342(.048)	8.625(.246)	7.579(.123)	9.040(.094)
Na_2O	0.108(.066)	0.106(.045)	0.152(.046)	0.059(.016)	0.094(.031)	0.261(.046)	0.100(.048)
TiO_2	1.395(.020)	1.880(.116)	2.116(.076)	2.505(.134)	1.278(.005)	1.467(.143)	1.724(.004)
Cr_2O_3	N.A.	N.A.	N.A.	N.A.	N.A.	0.008(.012)	N.A.
ZnO	N.A.	N.A.	N.A.	N.A.	N.A.	0.014(.019)	N.A.
BaO	N.A.	N.A.	N.A.	N.A.	N.A.	0.084(.078)	N.A.
Total	95.642(.358)	94.515(.652)	93.818(.274)	96.571(.204)	94.601(.499)	95.960(.854)	93.887(.334)

CATION (22 O BASIS)

	S-749	S-765	S-812	S-833	S-839	S-858	S-859
Si	5.5059(.014)	5.4995(.020)	5.5794(.020)	5.4111(.066)	5.5145(.023)	5.5226(.020)	5.4788(.006)
Al	3.3322(.009)	3.2805(.019)	2.9914(.028)	3.2314(.026)	3.3913(.012)	3.3259(.029)	3.2057(.008)
Fe	2.6327(.026)	2.7713(.038)	2.6466(.048)	2.8967(.061)	2.4603(.044)	2.3353(.030)	2.9180(.023)
Mg	2.1660(.030)	1.9908(.044)	2.2371(.016)	2.0268(.053)	2.2518(.017)	2.5157(.016)	1.9561(.027)
Mn	0.0152(.011)	0.0064(.004)	0.0273(.007)	0.0131(.004)	0.0026(.004)	0.0005(.001)	0.0184(.001)
Ca	0.0081(.010)	0.0168(.007)	0.0087(.012)	0.0061(.009)	0.0259(.017)	0.0230(.011)	0.0136(.009)
K	1.6683(.020)	1.6851(.019)	1.8316(.053)	1.6148(.015)	1.6739(.004)	1.4353(.024)	1.8107(.0150
Na	0.0315(.019)	0.0318(.014)	0.0461(.014)	0.0173(.005)	0.0279(.009)	0.0750(.013)	0.0306(.015)
Ti	0.1590(.002)	0.2182(.015)	0.2478(.009)	0.2860(.017)	0.1463(.001)	0.1638(.016)	0.2036(.001)
Cr	N.A.	N.A.	N.A.	N.A.	N.A.	0.0009(.002)	N.A.
Zn	N.A.	N.A.	N.A.	N.A.	N.A.	0.0013(.002)	N.A.
Ba	N.A.	N.A.	N.A.	N.A.	N.A.	0.0049(.032)	N.A.
Total	15.5189(.014)	15.5004(.030)	15.6160(.054)	15.5033(.059)	15.4945(.041)	15.4042(.032)	15.6355(.015)

SAMPLE NO. –	S-882	S-894
NO OF POINTS AVERAGED –	5	4

WEIGHT %		
SiO_2	35.723(.122)	34.497(.234)
Al_2O_3	17.283(.072)	18.240(.106)
FeO	20.904(.326)	22.076(.528)
MgO	10.646(.175)	9.937(.140)
MnO	0.016(.024)	0.017(.029)
CaO	0.024(.029)	0.173(.222)
K_2O	8.420(.149)	8.293(.088)
Na_2O	0.204(.020)	0.147(.014)
TiO_2	2.529(.036)	1.691(.147)
Cr_2O_3	0.034(.011)	N.A.
ZnO	0.011(.019)	N.A.
BaO	N.A.	N.A.
Total	95.794(.396)	95.071(.720)

CATION (22 O BASIS)		
Si	5.4267(.007)	5.3198(.008)
Al	3.0947(.016)	3.3148(.016)
Fe	2.6558(.040)	2.8463(.056)
Mg	2.4108(.030)	2.2840(.039)
Mn	0.0020(.003)	0.0022(.004)
Ca	0.0039(.005)	0.0287(.037)
K	1.6320(.032)	1.6312(.009)
Na	0.0602(.006)	0.0439(.004)
Ti	0.2890(.004)	0.1962(.018)
Cr	0.0040(.001)	N.A.
Zn	0.0010(.002)	N.A.
Ba	N.A.	N.A.
Total	15.5801(.020)	15.6656(.017)

REPRESENTATIVE MICROPROBE ANALYSIS OF BIOTITE (INCLUSIONS IN GARNET)

SAMPLE NO. –	S-16/I1	S-16/I2	S-46	S-77/2	S-321/I1	S-321/I2	S-367
NO OF POINTS AVERAGED –	5	5	3	4	5	5	5
WEIGHT %							
SiO$_2$	35.685(.277)	36.033(.274)	35.985(.232)	35.262(.187)	35.552(.145)	36.139(.285)	35.164(.245)
Al$_2$O$_3$	18.267(.201)	18.122(.198)	17.526(.130)	18.965(.177)	17.687(.182)	18.213(.206)	18.704(.200)
FeO	19.265(.278)	19.846(.346)	21.516(.090)	19.247(.574)	19.319(.303)	19.574(.261)	24.374(.282)
MgO	9.843(.186)	9.702(.060)	8.607(.096)	9.361(.070)	10.825(.163)	10.355(.162)	7.929(.189)
MnO	0.098(.033)	0.110(.029)	0.095(.013)	0.033(.025)	0.011(.014)	0.053(.048)	0.063(.048)
CaO	0.113(.070)	0.107(.097)	0.469(.139)	0.092(.054)	0.016(.014)	0.027(.027)	–
K$_2$O	8.367(.163)	8.244(.110)	8.329(.231)	8.515(.084)	7.401(.064)	7.635(.075)	8.722(.119)
Na$_2$O	0.240(.039)	0.242(.021)	0.181(.007)	0.269(.018)	0.122(.012)	0.202(.070)	0.280(.070)
TiO$_2$	1.732(.107)	2.056(.043)	2.575(.071)	2.619(.073)	2.494(.122)	1.722(.074)	1.575(.068)
Cr$_2$O$_3$	0.010(.011)	0.002(.002)	0.009(.005)	0.004(.007)	0.009(.012)	N.A.	N.A.
ZnO	0.040(.037)	0.033(.029)	0.060(.074)	0.055(.062)	0.028(.035)	N.A.	N.A.
BaO	N.A.	N.A.	N.A.	N.A.	0.083(.053)	N.A.	N.A.
Total	93.660(.901)	94.497(.330)	95.352(.645)	94.422(.607)	93.547(.460)	93.920(.490)	96.811(.658)
CATION (22 O BASIS)							
Si	5.4930(.017)	5.5049(.019)	5.5117(.005)	5.4648(.026)	5.4556(.020)	5.5207(.048)	5.4051(.013)
Al	3.3150(.009)	3.2634(.031)	3.1643(.017)	3.4380(.020)	3.1991(.028)	3.2794(.038)	3.5080(.030)
Fe	2.4807(.018)	2.5356(.040)	2.7553(.013)	2.4858(.024)	2.4794(.036)	2.5006(.026)	3.1712(.073)
Mg	2.2588(.026)	2.2096(.018)	1.9637(.022)	2.1588(.020)	2.4762(.030)	2.3579(.030)	1.6153(.088)
Mn	0.0127(.004)	0.0143(.004)	0.0120(.004)	0.0045(.005)	0.0015(.002)	0.0068(.006)	0.0038(.004)
Ca	0.0188(.012)	0.0175(.016)	0.0737(.023)	0.0160(.010)	0.0026(.002)	0.0044(.005)	0.0096(.007)
K	1.6437(.031)	1.6070(.028)	1.6260(.035)	1.7190(.028)	1.4490(.015)	1.4880(.012)	1.7499(.004)
Na	0.0716(.012)	0.0717(.006)	0.0273(.001)	0.0743(.001)	0.0364(.006)	0.0597(.021)	0.0466(.022)
Ti	0.2005(.012)	0.2362(.006)	0.2977(.008)	0.1865(.001)	0.2878(.0140)	0.1979(.009)	0.1148(.005)
Cr	0.0012(.001)	0.0002(.001)	–	–	0.0012(.002)	N.A.	N.A.
Zn	0.0038(.004)	0.0031(.003)	0.0060(.009)	0.0068(.008)	0.0026(.003)	N.A.	N.A.
Ba	N.A.	N.A.	N.A.	N.A.	0.0050(.003)	N.A.	N.A.
Total	15.4998(.024)	15.4635(.031)	15.4377(.013)	15.5545(.046)	15.3964(.009)	15.4154(.039)	15.6243(.015)

APPENDIX IIB (Continued)

SAMPLE NO. -	S-695	S-858
NO OF POINTS AVERAGED -	5	3

WEIGHT %		
SiO_2	34.799(.121)	37.276(.106)
Al_2O_3	16.795(.079)	17.954(.232)
FeO	22.785(.199)	20.941(.357)
MgO	7.606(.201)	11.490(.117)
MnO	0.251(.078)	0.066(.059)
CaO	0.015(.021)	0.019(.017)
K_2O	9.118(.103)	7.653(.202)
Na_2O	0.122(.019)	0.252(.036)
TiO_2	2.327(.117)	0.122(.015)
Cr_2O_3	N.A.	0.005(.007)
ZnO	N.A.	0.017(.025)
BaO	N.A.	0.028(.035)
Total	93.818(.360)	95.823(.429)

CATION (22 O BASIS)		
Si	5.4940(.007)	5.6031(.025)
Al	3.1253(.021)	3.1809(.037)
Fe	3.0084(.024)	2.6324(.039)
Mg	1.7900(.042)	2.5747(.027)
Mn	0.0335(.011)	0.0084(.008)
Ca	0.0026(.004)	0.0030(.003)
K	1.8365(.021)	1.4675(.008)
Na	0.0373(.006)	0.0735(.010)
Ti	0.2763(.014)	0.0138(.002)
Cr	N.A.	0.0006(.001)
Zn	N.A.	0.0016(.002)
Ba	N.A.	0.0016(.002)
Total	15.6039(.026)	15.5611(.029)

APPENDIX - III
REPRESENTATIVE MICROPROBE ANALYSIS OF MUSCOVITE

SAMPLE NO. —	S-38	S-77/2	S-93/2	S-108	S-118	S-119/2
NO OF POINTS AVERAGED —	4	3	5	2	3	5
WEIGHT %						
SiO_2	48.982(.394)	48.505(.171)	48.244(.183)	47.998(.355)	47.656(.792)	47.697(.159)
Al_2O_3	33.151(.333)	35.961(.382)	36.060(.262)	35.924(.016)	34.540(.588)	35.700(.345)
FeO	2.120(.066)	1.156(.012)	1.579(.064)	0.913(.019)	2.240(.139)	1.363(.118)
MgO	0.988(.050)	0.858(.069)	0.754(.031)	0.549(.032)	0.641(.035)	0.583(.018)
MnO	0.028(.021)	0.017(.024)	0.018(.019)	—	0.032(.045)	0.010(.015)
CaO	0.026(.031)	0.010(.014)	0.010(.009)	0.210(.148)	0.018(.026)	0.069(.044)
K_2O	9.730(.110)	9.837(.017)	9.552(.146)	8.363(.290)	8.587(1.96)	8.732(.042)
Na_2O	0.523(.058)	0.839(.029)	0.778(.070)	1.345(.103)	0.738(.251)	1.337(.027)
TiO_2	0.485(.048)	0.369(.022)	0.345(.024)	0.416(.004)	0.394(.021)	0.196(.017)
Cr_2O_3	0.008(.008)	N.A	N.A.	0.014(.013)	N.A.	0.009(.007)
ZnO	0.004(.007)	N.A	N.A.	0.029(.016)	N.A.	N.A.
BaO	N.A.	N.A	N.A.	N.A.	N.A.	N.A.
Total	96.045(.616)	97.552(.356)	97.340(.379)	95.761(.562)	94.846(.852)	95.696(.512)
CATION (22 O BASIS)						
Si	6.4401(.020)	6.2586(.027)	6.2404(.020)	6.2623(.017)	6.3139(.059)	6.2545(.015)
Al	5.1375(.033)	5.4690(.047)	5.4979(.028)	5.5248(.023)	5.3939(.052)	5.5176(.024)
Fe	0.2331(.007)	0.1248(.001)	0.1708(.007)	0.0997(.002)	0.2483(.017)	0.1494(.013)
Mg	0.1935(.010)	0.1651(.013)	0.1454(.006)	0.1067(.007)	0.1285(.006)	0.1139(.004)
Mn	0.0031(.002)	0.0019(.002)	0.0020(.002)	—	0.0036(.005)	0.0011(.002)
Ca	0.0037(.004)	0.0014(.002)	0.0015(.001)	0.0294(.021)	0.0025(.004)	0.0096(.006)
K	1.6321(.020)	1.6193(.003)	1.5762(.019)	1.3919(.052)	1.4539(.340)	1.4607(.004)
Na	0.1333(.015)	0.2099(.007)	0.1952(.018)	0.3402(.024)	0.1900(.066)	0.3398(.008)
Ti	0.0479(.005)	0.0358(.002)	0.0335(.002)	0.0408(.001)	0.0392(.002)	0.0195(.002)
Cr	0.0008(.001)	N.A	N.A.	0.0014(.001)	N.A.	0.0009(.001)
Zn	0.0005(.001)	N.A.	N.A.	0.0028(.001)	N.A.	N.A.
Ba	N.A.	N.A	N.A.	N.A.	N.A.	N.A.
Total	13.8256(.012)	13.8858(.003)	13.8629(.020)	13.8000(.029)	13.7718(.289)	13.8670(.007)

APPENDIX III (Continued)

SAMPLE NO.	S-320	S-321	S-354	S-367	S-377	S-381
NO OF POINTS AVERAGED	3	3	3	5	3	3
			WEIGHT %			
SiO_2	47.508(.168)	48.629(.177)	46.768(.168)	48.123(.199)	48.433(.283)	48.474(.121)
Al_2O_3	33.082(.580)	36.339(.164)	35.009(.175)	36.379(.187)	34.739(.287)	36.250(.189)
FeO	2.025(.084)	0.692(.052)	1.940(.082)	1.647(.101)	2.405(.009)	0.987(.092)
MgO	1.062(.048)	0.574(.032)	0.483(.013)	0.454(.035)	0.712(.076)	0.623(.020)
MnO	0.019(.023)	0.063(.089)	0.018(.025)	0.049(.033)	–	–
CaO	0.020(.014)	0.035(.050)	0.010(.014)	0.001(.003)	0.001(.001)	0.008(.011)
K_2O	10.627(.082)	8.932(.064)	9.300(.018)	9.224(.098)	8.652(.173)	8.680(.040)
Na_2O	0.501(.040)	1.454(.017)	1.722(.058)	1.263(.035)	1.795(.093)	1.245(.092)
TiO_2	0.398(.042)	0.458(.052)	0.387(.006)	0.443(.033)	0.254(.037)	0.460(.016)
Cr_2O_3	N.A.	N.A.	N.A.	N.A.	N.A.	N.A.
ZnO	N.A.	N.A.	N.A.	N.A.	N.A.	N.A.
BaO	N.A.	N.A.	N.A.	N.A.	N.A.	N.A.
Total	95.242(.889)	97.176(.492)	93.637(.114)	97.583(.259)	96.991(.899)	96.727(.219)
			CATION (22 O BASIS)			
Si	6.3469(.038)	6.2627(.007)	6.1987(.016)	6.2117(.014)	6.3050(.016)	6.2643(.007)
Al	5.2087(.044)	5.5162(.008)	5.4693(.024)	5.5349(.018)	5.3303(.002)	5.5218(.019)
Fe	0.2263(.010)	0.0745(.006)	0.2151(.009)	0.1779(.011)	0.2619(.002)	0.1067(.010)
Mg	0.2114(.009)	0.1101(.006)	0.0954(.002)	0.0874(.007)	0.1380(.014)	0.1200(.004)
Mn	0.0022(.003)	0.0068(.009)	0.0020(.003)	0.0054(.003)	–	–
Ca	0.0028(.002)	0.0049(.007)	0.0014(.002)	0.0002(.0004)	0.0001(.0001)	0.0011(.001)
K	1.8111(.005)	1.4676(.010)	1.5726(.005)	1.5190(.013)	1.4369(.020)1	1.4310(.004)
Na	0.1236(.009)	0.3630(.026)	0.4425(.015)	0.3160(.009)	0.4530(.020)	0.3119(.023)
Ti	0.0400(.004)	0.0443(.005)	0.0385(.001)	0.0430(.003)	0.0248(.003)	0.0447(.001)
Cr	N.A.	N.A.	N.A.	N.A.	N.A.	N.A.
Zn	N.A.	N.A.	N.A.	N.A.	N.A.	N.A.
Ba	N.A.	N.A.	N.A.	N.A.	N.A.	N.A.
Total	13.979(.019)	13.8501(.019)	14.0355(.012)	13.8955(.003)	13.9500(.027)	13.8015(.009)

SAMPLE NO.	S-394	S-607	S-616	S-669	S-675	S-676	S-695
NO OF POINTS AVERAGED	4	3	3	3	3	3	2
WEIGHT %							
SiO_2	48.747(.405)	47.337(.317)	46.653(.373)	47.431(.227)	48.161(.306)	49.325(.273)	47.717(.360)
Al_2O_3	35.474(.437)	36.504(.289)	34.740(.252)	34.635(.091)	35.236(.238)	34.454(.178)	34.003(.207)
FeO	1.297(.161)	1.281(.276)	1.602(.188)	1.392(.014)	1.253(.077)	1.881(.146)	1.792(.046)
MgO	0.656(.035)	0.513(.017)	0.753(.055)	0.852(.016)	0.694(.065)	0.777(.090)	0.816(.036)
MnO	0.018(.031)	0.009(.009)	0.042(.014)	-	0.037(.035)	0.013(.019)	0.020(.032)
CaO	0.070(.061)	0.036(.026)	0.022(.025)	0.016(.022)	0.059(.045)	0.021(.024)	0.027(.020)
K_2O	9.221(.085)	9.032(.077)	9.887(.110)	10.813(.058)	9.872(.162)	9.035(.040)	10.437(.113)
Na_2O	1.175(.050)	1.050(.046)	0.879(.030)	0.564(.066)	0.609(.041)	1.030(.063)	0.367(.064)
TiO_2	0.319(.014)	0.235(.046)	0.351(.011)	0.632(.012)	0.682(.046)	0.308(.020)	0.520(.033)
Cr_2O_3	N.A.	N.A.	N.A.	N.A.	N.A.	0.002(.003)	N.A.
ZnO	N.A.	N.A.	N.A.	N.A.	N.A.	0.054(.062)	N.A.
BaO	N.A.	N.A.	N.A.	N.A.	N.A.	0.325(.107)	N.A.
Total	96.977(.758)	95.997(.751)	94.929(.423)	96.335(.205)	96.603(.494)	97.225(.210)	95.699(.447)
CATION (22 O BASIS)							
Si	6.3135(.010)	6.1905(.020)	6.2227(.016)	6.2505(.019)	6.2804(.010)	6.3924(.021)	6.3198(.029)
Al	5.4153(.031)	5.6268(.031)	5.4618(.028)	5.3798(.019)	5.4158(.016)	5.2632(.035)	5.3083(.033)
Fe	0.1406(.018)	0.1400(.029)	0.1788(.022)	0.1534(.002)	0.1366(.008)	0.2039(.016)	0.1984(.006)
Mg	0.1267(.007)	0.1000(.004)	0.1497(.011)	0.1674(.003)	0.1349(.013)	0.1500(.017)	0.1611(.007)
Mn	0.0020(.003)	0.0011(.001)	0.0047(.002)	-	0.0042(.004)	0.0015(.002)	0.0022(.004)
Ca	0.0097(.008)	0.0050(.004)	0.0032(.004)	0.0024(.003)	0.0082(.006)	0.0030(.003)	0.0038(.003)
K	1.5236(.013)	1.5071(.021)	1.6825(.020)	1.8179(.007)	1.6423(.028)	1.4939(.010)	1.7635(.012)
Na	0.2950(.011)	0.2660(.013)	0.2274(.007)	0.1440(.017)	0.1541(.011)	0.2588(.016)	0.0943(.016)
Ti	0.0310(.001)	0.0231(.004)	0.0352(.001)	0.0626(.001)	0.0669(.005)	0.0300(.002)	0.0518(.003)
Cr	N.A.	N.A.	N.A.	N.A.	N.A.	0.0003(.001)	N.A.
Zn	N.A.	N.A.	N.A.	N.A.	N.A.	0.0043(.005)	N.A.
Ba	N.A.	N.A.	N.A.	N.A.	N.A.	0.0165(.005)	N.A.
Total	13.8574(.014)	13.8596(.012)	13.9660(.017)	13.9780(.014)	13.8434(.021)	13.8178(.005)	13.9032(.016)

SAMPLE NO.	–	S-738	S-749	S-765	S-812	S-833	S-839	S-858
NO OF POINTS AVERAGED	–	3	4	5	3	3	3	5

WEIGHT %

SiO_2		49.053(.362)	48.214(.642)	48.421(.318)	47.586(.130)	47.658(.262)	48.230(.311)	48.581(.312)
Al_2O_3		35.045(.231)	34.878(.534)	34.259(.625)	31.598(.132)	35.349(.145)	34.908(.538)	35.199(.128)
FeO		1.026(.061)	1.449(.536)	1.481(.154)	2.791(.187)	1.101(.052)	1.658(.100)	0.909(.460)
MgO		0.721(.098)	0.836(.117)	0.783(.105)	1.183(.112)	0.722(.045)	1.037(.156)	0.548(.019)
MnO		–	0.116(.080)	0.010(.013)	0.053(.043)	–	0.039(.034)	0.023(.025)
CaO		0.083(.056)	0.029(.026)	0.174(.073)	0.080(.056)	0.005(.007)	0.034(.030)	0.008(.007)
K_2O		8.300(.148)	9.432(.123)	9.211(.218)	10.276(.122)	10.230(.116)	9.616(.177)	8.517(.082)
Na_2O		0.611(.101)	1.021(.083)	1.152(.210)	0.338(.024)	0.370(.016)	1.146(.224)	1.510(.068)
TiO_2		0.580(.038)	0.254(.011)	0.247(.034)	0.484(.018)	0.796(.024)	0.185(.020)	0.440(.120)
Cr_2O_3		0.016(.020)	N.A.	N.A.	N.A.	N.A.	N.A.	0.019(.019)
ZnO		–	N.A.	N.A.	N.A.	N.A.	N.A.	0.040(.031)
BaO		0.325(.722)	N.A.	N.A.	N.A.	N.A.	N.A.	0.199(.062)
Total		95.760(.403)	96.229(.783)	95.738(.436)	94.389(.266)	96.231(.394)	96.853(.573)	95.993(.415)

CATION (22 O BASIS)

Si		6.3857(.023)	6.3109(.019)	6.3644(.044)	6.4274(.007)	6.2447(.025)	6.2896(.030)	6.3350(.034)
Al		5.3775(.030)	5.3812(.050)	5.3074(.079)	5.0306(.026)	5.4596(.020)	5.3654(.057)	5.4103(.021)
Fe		0.1117(.007)	0.1592(.061)	0.1629(.018)	0.3153(.021)	0.1206(.005)	0.1809(.012)	0.0992(.050)
Mg		0.1399(.019)	0.1632(.023)	0.1535(.021)	0.2382(.023)	0.1410(.001)	0.2017(.031)	0.1066(.004)
Mn		–	0.0130(.009)	0.0012(.002)	0.0061(.005)	–	0.0043(.004)	0.0025(.003)
Ca		0.0116(.066)	0.0042(.004)	0.0245(.010)	0.0116(.008)	0.0007(.001)	0.0047(.004)	0.0011(.001)
K		1.3786(.029)	1.5751(.011)	1.5446(.036)	1.7708(.018)	1.7103(.020)	1.5999(.028)	1.4170(.016)
Na		0.1543(.026)	0.2590(.020)	0.2934(.053)	0.0884(.006)	0.0940(.004)	0.2896(.056)	0.3819(.017)
Ti		0.0568(.004)	0.0250(.001)	0.0244(.003)	0.0492(.002)	0.0785(.002)	0.0182(.002)	0.0431(.012)
Cr		0.0016(.002)	N.A.	N.A.	N.A.	N.A.	N.A.	0.0019(.002)
Zn		–	N.A.	N.A.	N.A.	N.A.	N.A.	0.0032(.0020)
Ba		0.0166(.004)	N.A.	N.A.	N.A.	N.A.	N.A.	0.0102(.003)
Total		13.6343(.024)	13.8908(.024)	13.8763(.029)	13.9376(.016)	13.8494(.026)	13.9543(.017)	13.8120(.025)

APPENDIX III (Continued),

SAMPLE NO.	–	S-859	S-894
NO OF POINTS AVERAGED	–	3	5

WEIGHT %

SiO_2	47.419(.062)	48.308(.114)
Al_2O_3	32.140(.109)	34.884(.184)
FeO	3.872(.097)	0.908(.439)
MgO	1.013(.134)	0.553(.024)
MnO	0.003(.0050	0.008(.011)
CaO	0.051(.014)	0.025(.023)
K_2O.	9.750(.058)	9.205(.106)
Na_2O	0.517(.009)	1.003(.081)
TiO_2	0.367(.027)	0.710(.054)
Cr_2O_3	N.A.	0.026(.032)
ZnO	N.A.	0.023(.029)
BaO	N.A.	0.388(.117)
Total	95.132(.079)	96.041(.680)

CATION (22 O BASIS)

Si	6.3711(.002)	6.3249(.024)
Al	5.0899(.014)	5.3834(.015)
Fe	0.4351(.011)	0.0992(.048)
Mg	0.2028(.027)	0.1079(.005)
Mn	0.0004(.001)	0.0009(.001)
Ca	0.0074(.002)	0.0036(.003)
K	1.6713(.010)	1.5377(.018)
Na	0.1347(.002)	0.2545(.020)
Ti	0.0371(.003)	0.0700(.006)
Cr	N.A.	0.0023(.003)
Zn	N.A.	0.0018(.002)
Ba	N.A.	0.0199(.006)
Total	13.9498(.009)	13.8061(.025)

REPRESENTATIVE MICROPROBE ANALYSIS OF PLAGIOCLASE

SAMPLE NO. -	S-38	S-77/2	S-93/2	S-108	S-118	S-119/2	S-320
NO OF POINTS AVERAGED -.	5	5	5	5	3	5	3
WEIGHT %							
SiO_2	64.774(1.225)	64.869(.240)	64.119(.477)	62.894(.181)	65.654(.618)	62.984(.467)	59.487(.229)
Al_2O_3	22.166(.341)	22.656(.144)	22.334(.143)	23.280(.109)	20.888(.113)	23.688(.142)	25.114(.068)
CaO	2.665(.188)	4.088(.092)	3.635(.275)	5.210(.050)	2.550(.079)	5.221(.037)	7.509(.091)
Na_2O	9.275(.581)	9.253(.094)	9.172(.173)	8.917(.113)	10.118(.105)	8.534(.179)	7.522(.017)
K_2O	0.696(.513)	0.114(.010)	0.077(.017)	0.061(.010)	0.148(.099)	0.049(.018)	0.087(.002)
FeO	0.048(.095)	N.A.	N.A.	N.A.	N.A.	N.A.	N.A.
BaO	N.A.	N.A.	0.018(.023)	N.A.	N.A.	N.A.	N.A.
TiO_2	N.A	N.A.	N.A.	N.A.	N.A.	N.A.	N.A.
Total	99.624(1.182)	100.980(.451)	99.355(.595)	100.362(.173)	99.358(.257)	100.476(.705)	99.719(.202)
CATION (8 O BASIS)							
Si	2.8616(.018)	2.8324(.005)	2.8407(.009)	2.7766(.004)	2.9038(.013)	2.7723(.002)	2.6620(.004)
Al	1.1547(.031)	1.1660(.004)	1.1663(.006)	1.2114(.004)	1.0890(.009)	1.2290(.004)	1.3247(.005)
Ca	0.1261(.007)	0.1912(.004)	0.1726(.014)	0.2464(.003)	0.1209(.004)	0.2462(.003)	0.3601(.005)
Na	0.7941(.040)	0.7834(.007)	0.7879(.011)	0.7633(.011)	0.8678(.010)	0.7283(.011)	0.6527(.002)
K	0.0396(.030)	0.0064(.001)	0.0044(.001)	0.0034(.001)	0.0084(.005)	0.0027(.001)	0.0050(.000)
Fe	0.0018(.003)	N.A.	N.A.	N.A.	N.A.	N.A.	N.A.
Ba	N.A.	N.A.	0.0003(.001)	N.A.	N.A.	N.A.	N.A.
Ti	N.A.	N.A.	N.A.	N.A.	N.A.	N.A.	N.A.
Total	4.9779(.007)	4.9794(.007)	4.9722(.009)	5.0011(.009)	4.9899(.016)	4.9785(.006)	5.0045(.003)

APPENDIX IV (Continued)

SAMPLE NO.	- S-321	S-354	S-367	S-377	S-381	S-394	S-607
NO OF POINTS AVRARGED	- 3	3	5	3	3	3	5
WEIGHT %							
SiO_2	63.149(.329)	66.980(.137)	66.429(.317)	66.868(.240)	64.879(.285)	65.407(.030)	66.346(.981)
Al_2O_3	23.034(.095)	19.702(.207)	20.986(.146)	20.660(.062)	22.020(.244)	22.103(.039)	21.264(.280)
CaO	4.781(.152)	1.097(.021)	1.965(.059)	2.084(.049)	3.450(.046)	3.423(.149)	2.164(.077)
Na_2O	8.634(.099)	11.010(.372)	10.684(.148)	11.216(.297)	9.658(.207)	9.649(.117)	10.546(.317)
K_2O	0.115(.092)	0.132(.103)	0.072(.018)	0.073(.011)	0.096(.017)	0.065(.020)	0.147(.119)
FeO	N.A.	N.A.	N.A.	N.A.	N.A.	N.A.	N.A.
BaO	0.044(.028)	N.A.	0.028(.048)	N.A.	N.A.	N.A.	0.011(.017)
TiO_2	0.007(.014)	N.A.	N.A.	N.A.	N.A.	N.A.	N.A.
Total	99.763(.488)	98.921(.297)	100.164(.347)	100.901(.513)	100.103(.596)	100.647(.220)	100.478(.364)
CATION (8 O BASIS)							
Si	2.7969(.002)	2.9649(.005)	2.9122(.003)	2.9166(.004)	2.8548(.008)	2.8600(.005)	2.9015(.005)
Al	1.2026(.005)	1.0279(.011)	1.0844(.005)	1.0621(.002)	1.1420(.006)	1.1392(.001)	1.0962(.005)
Ca	0.2269(.007)	0.0521(.001)	0.0923(.003)	0.0974(.003)	0.1627(.001)	0.1604(.007)	0.1014(.004)
Na	0.7415(.005)	0.9450(.030)	0.9083(.015)	0.9485(.022)	0.8240(.017)	0.8181(.009)	0.8942(.020)
K	0.0065(.005)	0.0075(.006)	0.0040(.001)	0.0040(.001)	0.0054(.001)	0.0036(.001)	0.0083(.007)
Fe	N.A.	N.A.	N.A.	N.A.	N.A.	N.A.	N.A.
Ba	0.0008(.001)	N.A.	0.0005(.001)	N.A.	N.A.	N.A.	0.0002(.001)
Ti	0.0002(.003)	N.A.	N.A.	N.A.	N.A.	N.A.	N.A.
Total	4.9754(.003)	4.9974(.017)	5.0017(.011)	5.0286(.019)	4.9889(.014)	4.9813(.009)	5.0018(.013)

APPENDIX IV (Continued)

SAMPLE NO.	- S-616	S-669	S-675	S-676	S-695	S-738	S-749
NO OF POINTS AVRARGED	- 3	3	5	5	5	3	4
WEIGHT %							
SiO_2	66.578(.283)	62.020(.227)	64.146(.179)	63.750(.237)	64.022(.506)	65.140(.925)	63.868(.096)
Al_2O_3	20.164(.049)	23.111(.012)	22.242(.117)	23.391(.168)	23.384(.240)	22.198(.749)	23.049(.198)
CaO	1.772(.017)	5.319(.014)	3.585(.207)	3.782(.116)	5.297(.159)	4.162(.054)	4.684(.072)
Na_2O	10.834(.043)	8.730(.254)	9.428(.147)	9.615(.143)	8.833(.198)	9.037(.387)	9.496(.214)
K_2O	0.049(.014)	0.114(.012)	0.182(.020)	0.121(.073)	0.286(.013)	0.064(.019)	0.094(.003)
FeO	N.A.	N.A.	N.A.	N.A.	N.A.	N.A.	N.A.
BaO	N.A.	N.A.	0.045(.052)	0.027(.044)	0.028(.034)	N.A.	N.A.
TiO_2	N.A.	N.A.	N.A.	N.A.	N.A.	0.023(.011)	N.A.
Total	99.397(.381)	99.294(.469)	99.628(.519)	100.686(.388)	101.850(.577)	100.624(.629)	101.191(.250)
CATION (8 O BASIS)							
Si	2.9388(.001)	2.7697(.001)	2.8394(.005)	2.7973(.005)	2.7863(.011)	2.8504(.037)	2.7955(.008)
Al	1.0491(.002)	1.2166(.005)	1.1604(.006)	1.2098(.007)	1.1996(.013)	1.1449(.038)	1.1892(.008)
Ca	0.0838(.001)	0.2545(.002)	0.1700(.009)	0.1780(.005)	0.2470(.008)	0.1952(.003)	0.2197(.003)
Na	0.9273(.001)	0.7559(.019)	0.8092(.010)	0.8181(.012)	0.7453(.013)	0.7667(.033)	0.8059(.018)
K	0.0028(.001)	0.0065(.001)	0.0103(.001)	0.0068(.004)	0.0159(.001)	.0.0036(.001)	0.0053(.001)
Fe	N.A.	N.A.	N.A.	N.A.	N.A.	N.A.	N.A.
Ba	N.A.	N.A.	0.0008(.001)	0.0005(.001)	0.0005(.001)	N.A.	N.A.
Ti	N.A.	N.A.	N.A.	N.A.	N.A.	0.0007(.001)	N.A.
Total	5.0018(.001)	5.0032(.012)	4.9901(.010)	5.0105(.008)	4.9946(.006)	4.9615(.035)	5.0156(.013)

APPENDIX IV (Continued)

SAMPLE NO.	S-765	S-812	S-833	S-839	S-858	S-859	S-894
NO OF POINTS AVRARGED	5	3	3	5	5	3	5
				WEIGHT %			
SiO_2	63.697(.328)	60.247(.053)	67.111(.133)	63.870(.309)	63.780(.236)	65.421(.231)	62.183(.289)
Al_2O_3	23.465(.496)	25.212(.122)	20.563(.081)	22.110(.205)	23.663(.133)	22.098(.066)	23.326(.105)
CaO	4.270(.368)	7.195(.071)	1.562(.041)	3.913(.201)	4.017(.099)	3.597(.044)	3.703(.091)
Na_2O	9.092(.211)	7.695(.075)	10.748(.414)	9.377(.104)	9.320(.102)	9.919(.036)	9.558(.127)
K_2O	0.088(.017)	0.119(.017)	0.154(.026)	0.081(.018)	0.062(.008)	0.099(.012)	0.089(.025)
FeO	N.A.	N.A.	N.A.	N.A.	N.A.	N.A.	N.A.
BaO	0.008(.011)	N.A.	N.A.	N.A.	0.038(.030)	N.A.	0.017(.017)
TiO_2	N.A.	N.A.	N.A.	N.A.	N.A.	N.A.	N.A.
Total	100.620(.589)	100.468(.089)	100.138(.642)	99.351(.156)	100.880(.224)	101.134(.237)	99.876(.459)
				CATION (8 O BASIS)			
Si	2.7949(.023)	2.6729(.004)	2.9375(.008)	2.8360(.011)	2.7914(.006)	2.8530(.002)	2.7941(.001)
Al	1.2135(.021)	1.3185(.006)	1.0609(.001)	1.1572(.011)	1.2207(.007)	1.1359(.001)	1.2159(.002)
Ca	0.2007(.017)	0.3420(.004)	0.0733(.002)	0.1862(.010)	0.1884(.005)	0.1681(.002)	0.1755(.004)
Na	0.7735(.017)	0.6619(.006)	0.9121(.031)	0.8074(.010)	0.7909(.009)	0.8387(.005)	0.8196(.011)
K	0.0049(.001)	0.0067(.001)	0.0086(.001)	0.0046(.001)	0.0034(.001)	0.0055(.001)	0.0050(.001)
Fe	N.A.	N.A.	N.A.	N.A.	N.A.	N.A.	N.A.
Ba	0.0001(.000)	N.A.	N.A.	N.A.	0.0006(.001)	N.A.	0.0003(.000)
Ti	N.A.	N.A.	N.A.	N.A.	N.A.	N.A.	N.A.
Total	4.9876(.015)	5.0020(.005)	4.9924(.023)	4.9914(.003)	4.9954(.007)	5.0012(.005)	5.0104(.007)